CANADIAN THESES

THÈSES CANADIENNES

NOTICE

The quality of this microfiche is heavily dependent upon the quality of the original thesis submitted for microfilming. Every effort has been made to ensure the highest quality of reproduction possible.

If pages are missing, contact the university which granted the degree.

Some pages may have indistinct print especially if the original pages were typed with a poor typewriter ribbon or if the university sent us an inferior photocopy.

Previously copyrighted materials (journal articles, published tests, etc.) are not filmed.

Reproduction in full or in part of this film is governed by the Canadian Copyright Act, R.S.C. 1970, c. C-30.

AVIS

La qualité de cette microfiche dépend grandement de la qualité de la thèse soumise au microfilmage. Nous avons tout fait pour assurer une qualité supérieure de reproduction.

S'il manque des pages, veuillez communiquer avec l'université qui a conféré le grade.

La qualité d'impression de certaines pages peut laisser à désirer, surtout si les pages originales ont été dactylographiées à l'aide d'un ruban usé ou si l'université nous a fait parvenir une photocopie de qualité inférieure.

Les documents qui font déjà l'objet d'un droit d'auteur (articles de revue, examens publiés, etc.) ne sont pas microfilmés.

La reproduction, même partielle, de ce microfilm est soumise à la Loi canadienne sur le droit d'auteur, SRC 1970, c. C-30.

THIS DISSERTATION
HAS BEEN MICROFILMED
EXACTLY AS RECEIVED

LA THÈSE A ÉTÉ
MICROFILMÉE TELLE QUE
NOUS L'AVONS REÇUE

THERMODYNAMIC AND COMBUSTION MODEL OF A TWO-STROKE DIESEL ENGINE WITH "OFF-SPECIFICATION" FUELS

BY

YING-QI XIA

A THESIS PRESENTED TO
THE SCHOOL OF GRADUATE STUDIES
UNIVERSITY OF OTTAWA
IN PARTIAL FULFILLMENT OF
THE REQUIREMENTS FOR THE DEGREE OF
DOCTOR OF PHILOSOPHY
IN
THE MECHANICAL ENGINEERING DEPARTMENT

OTTAWA, ONTARIO, CANADA.
JANUARY, 1987

ISBN 0-315-36553-6

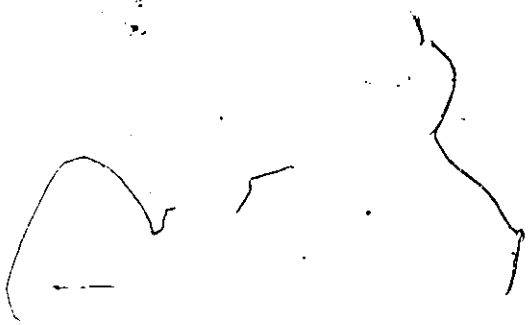

UNIVERSITÉ D'OTTAWA
UNIVERSITY OF OTTAWA

ACKNOWLEDGEMENTS

I am pleased to take this opportunity to express my deep sense of gratitude to my supervisor Dr. R.C. Flanagan for his outstanding supervision throughout this research. His extremely valuable instructions, suggestions and helpfulness during the writing of this thesis was always greatly appreciated.

The financial supports for the present study provided by the Department of National Defense of Canada under contract number 2SV84–00185 and in part by NSERC Grant are gratefully acknowledged.

My appreciation is also expressed to the professors, staff members and colleagues of the Department, especially Mr. Luc Menard, Mrs. Susan Flanagan and Mr. Don Seaman for their co-operations and kind suggestions.

Sincere thanks are also due to the State Education Commission of China and Beijing Institute of Technology for the initial scholarships and support during the study.

Finally, I would like to express my special thanks to those who are very dear to me — my family, my parents and my wife. I have been deeply indebted to my beloved but much–neglected son. I will never forget their sacrifices and encouragements over my six-year study in Canada.

ABSTRACT

This thesis consists of two parts:

Part I: Model Development and Evaluation

Part II: Engine/Fuel Analysis

In Part I, a thermodynamic and combustion model was developed for a two-stroke, turbocharged, compression ignition engine. The model was fitted to the AVGP-GM6V53T engine through direct correlation with experimental data.

Considerable attention was given to the combustion model and involved the development of an ignition delay, fuel-air mixing rate, fuel-air reaction rate and equilibrium combustion submodels. Combustion is based on fundamental chemical kinetics and assumes that equilibrium of seven chemical reactions is reached at each calculation step. Thus, the history of combustion products/emissions is traced throughout the cycle.

An extensive model evaluation study was performed. It was found that the model can accurately predict both engine performance and combustion characteristics over the complete speed/load range of the engine and for all three test fuels. Thus, the fundamental objective of developing a model that could simulate the AVGP engine when burning off-specification fuels was realized.

In Part II, engine/fuel interaction studies provided considerable insight into the behavior, combustion and ignition delay of the off-specification fuels. A number of parametric studies were conducted and focused on both engine performance and combustion parameters, in particular: indicated power, thermal efficiency, maximum cylinder pressure and maximum cylinder pressure rate. Intercooling was seen as the single most promising parameter for improving engine performance and could be coupled with increased mass of injected fuel and/or tuned injection timing. Also, of the

standard engine variables, injection timing was seen to be the most attractive approach for controlling the high pressure rates associated with the low-cetane fuels; however, losses in thermal efficiency also result. On the other hand, it was predicted that an optimized dual injection (pilot plus main) could reduce the pressure rates of Fuels 3 and 4 to the level of Fuel 1 without any appreciable loss in engine thermal efficiency or rated engine power.

TABLE OF CONTENTS

LIST OF FIGURES

LIST OF TABLES

LIST OF SYMBOLS

aTDC	— After top dead center
A	— Area
A_i	— Number of moles of reactant i
A_{in}	— Intake port opening area
A_{out}	— Exhaust valve opening area
bTDC	— Before top dead centre
B_i	— Number of moles of product i
c	— Specific heat
CA	— Crank angle
C_F	— Fuel Concentration
C_{vi}	— Specific heat at constant volume for species i (J/Mole/K)
C_{vp}	— Average specific heat of total mass of combustion products (J/K)
C/H	— Carbon/Hydrogen ratio
CN	— Cetane number
$C(N)$	— Function in fuel-air mixing rate model
CR	— Compression ratio
D	— Cylinder bore
$Delay$	— Ignition delay
DP	— Cylinder pressure rate
E	— Activation energy
FA	— Fuel/Air ratio
h	— Heat transfer coefficient
Δh_f°	— Enthalpy of formation at standard reference state
H	— Total enthalpy
H_{in}, H_{out}	— Enthalpy into and out of the cylinder respectively

ΔH — Enthalpy of reaction

IHP — Indicated horsepower

IMEP — Indicated mean effective pressure

ISFC — Indicated specific fuel consumption

k_c — Equilibrium constant based on concentration

k_p — Equilibrium constant based on partial pressure

K_n — Specific reaction rate constant

K_{bp} — Back pressure coefficient

m — Order of reaction of fuel

$m(N)$ — Function in fuel-air mixing rate model

M_c — Cylinder mass based on airbox condition

M_d — Mass of delivered air to cylinder

M_{dt} — Initial trapped mass of air

M_i — Mass of injected fuel

M_{in}, M_{out} — Mach number of inflow and outflow respectively

MR — Fuel–air mixing rate

M_u — Mass of unburned fuel

n — Order of reaction of air

N — Engine speed

N_u — Nusselt number

P — Pressure

P_{ab} — Airbox pressure

P_e — Exhaust pressure

P_o — Motored cylinder pressure

P_g — Gas pressure

P_{in} — Initial cylinder pressure

PR — Fuel-air preparation rate

P_{O_2} — Partial pressure of oxygen

q	— Heat flux
Q	— Heat
R	— Universal gas constant
R_e	— Reynolds number
R_s	— Scavenging ratio
RR	— Fuel-air reaction rate
S	— Piston stroke
t	— Time
t_{fi}	— Fuel injection timing
T	— Temperature
T_{ab}	— Airbox temperature
T_c	— Cylinder temperature
T_{cr}	— Critical autoignition temperature
T_g	— Gas temperature
T_{in}	— Initial cylinder temperature
T_L	— Local temperature
T_w	— Combustion chamber wall temperature
U	— Internal energy
V_{ct}	— Total cylinder volume
V_g	— Instantaneous gas velocity
V_{in}	— Initial cylinder volume
V_P	— Mean piston velocity
$\dot{W}$	— Reaction rate
W	— Molecular weight
W_k	— Work
$W_{k,T}$	— Total work
W_{in}	— Inflow mass
W_{out}	— Outflow mass

α	— Crank angle
ς	— Mixing coefficient
η_{ch}	— Charging efficiency
η_t	— Indicated thermal efficiency
μ	— Viscosity
ρ	— Density
ϕ	— Fuel/air equivalence ratio
Λ	— Reaction rate frequency factor

PART I

MODEL DEVELOPMENT AND EVALUATION

CHAPTER 1

INTRODUCTION

1.1 BACKGROUND AND OBJECTIVE

While Canadian Tar Sands crude oil market penetration forecasts vary, it is clear that these vast reserves will eventually provide a significant portion of Canadian oil demand. It is projected that such penetration will result in off-specification diesel fuels, especially their aromatic content and cetane number. In this regard, the CGSB* fuels panel, through a nation wide survey of the oil industry, concluded that a 35 cetane fuel with high end points (to 380 °C) could result in the 1990-2000 time frame. It is now generally accepted that this fuel is more likely to see penetration in Canada after the year 2000 and the 1990 fuel will most likely be a 37 cetane with no significant changes in the end products [1]. One important step towards the utilization of the middle distillate and tar sands crude is clearly the identification of engines tolerant of broader or more relaxed fuel properties.

The development of such an engine is yet in an early stage. The research follows three principle paths: engine testing, bench studies and numerical modeling. Bench studies lend well to R&D directed at injector spray characteristics, ignition delay and combustion pressure rates. Engine tests can provide extensive evaluation of engine performance characteristics, emissions characteristics and combustion characteristics subject to controlled input variables. It is also important to guide the experimental research by developing predictive analytical models and theory applicable to the fuels of the 1990's.

The thermodynamic and combustion modeling program is seen to have several principal benefits. First, the simulation model, once tested for accuracy, can be used

* Canadian General Standerd Board

to predict performance trends in terms of fundamental design parameters. In this regard, the following are of specific interest to the overall R&D objectives:

a) to analyze engine-fuel interaction, especially when burning off-specification fuels;

b) to model early combustion parameters such as ignition delay and maximum cylinder pressure rate;

c) to evaluate engine performance trends subject to engine parameter variations; and

d) to conduct pressure rate analyses and gain insight into controlling parameters related to knock and rough combustion.

Such results can then be used to shorten and direct specific experimental investigation, and to aid the designer in a better understanding of the effects of various design changes. Second, the compilation and ordering of existing knowledge helps to determine those areas in which knowledge is inadequate, thus identifying important areas for future research. Further, modeling in general provides considerable insight and understanding of the physical test results and phenomenon.

1.2 MODELING/LITERATURE OVERVIEW

The use of modern computers for engine cycle analysis makes more complex and realistic cycle calculations possible. As a result, interest in combustion modeling has been growing since the 1970's. In general, a diesel engine thermodynamic simulation consists of a series of sub-models such as cycle processes, heat transfer, fuel injection, ignition delay, combustion, gas exchange process, etc.

Cycle process models are typically based on the air standard cycle calculations by solving the first law of thermodynamics. These techniques can be easily found in most thermodynamic textbooks such as Obert [2], Wark [3] and Eastop [4]. In the

compression ignition engine cycle, the combustion model is referred to as a heat release model; this is discussed in detail by Benson and Whitehouse [5]. In a combustion chamber, the basic method to calculate the cycle processes is to solve the first law of thermodynamics and the mass continuity equation.

Heat transfer processes in a combustion chamber are very complex, involving rapidly varying gas pressure and temperature and local fluid velocities. Heat flux into the walls varies throughout the engine cycle from a small negative value to a large positive value and also varies due to differences in local gas temperatures and velocity. Up to now, an adequate theoretical analysis of heat transfer under these conditions has not been achieved. The heat transfer calculations usually performed are semi-empirical. These models are all dependent on an estimate of the instantaneous conditions in the engine combustion chamber. Numerous investigators have reported on work of this kind [6-11]. Annand's paper [12] gives a critical examination of much of the earlier published work. Few of the multitude of formulae referred to are now of much more than historical interest. Three have been used in cycle calculations at various time, these are by Eichelberg [8], Annand [12] and Woschni [13]. Eichelberg's model has the virtues of simplicity and explicitness. There are no unknown or variable constants so it is easy to use. The Annand and Woschni expressions, although different in form, are both based largely on turbulent convection considerations.

Ignition delay is a critical model in thermodynamic calculations. For this analytical work, a precise ignition delay model that would represent not only the engine operating point (speed and load) but also fuel quality was required. From a broad survey of the literature, a number of ignition delay models were identified and evaluated. The work done by Wolfer [14], Faeth [19], Hardenberg [20] and Pedersen [21] are commonly used. (Model details are given in Appendix 'A'). None of the models, however, included a correlation of ignition delay with both engine speed/load and fuel quality.

The combustion model is of primary interest to the R&D program. The nature and the complexity of the combustion model depends on the type and purpose of the cycle calculation. Thus, they can be classified as Diagnostic Models or Prediction Models.

Diagnostic models are used to better understand an engine's behavior. Heat release calculations are at the heart of most diagnostic applications. In this technique, measured engine cylinder pressure data are analyzed to determine how fast energy was released in order to create the measured pressure. Schweitzer [22] described a heat release model for diesel engines more than 50 years ago. He lumped heat transfer losses with the energy addition from combustion to derive a simple equation for the energy release rate. This equation could be evaluated completely with data from a pressure-volume ($P - V$) diagram. Diagnostic models produced all of the important features of the diesel heat-release diagram, as shown by Obert [23], Amann [24], Foster [25] and Blumberg [26]. The step to digital-computer codes to carry out heat release calculations was taken by Austen and Lyn [27] and Krieger and Borman [28] for direct-injected diesel engines. Their diesel heat-release model considered a single-zone and assumed that injected fuel was immediately mixed and burned within the cylinder. A paper presented by Gupta and Sharma [29] provided an excellent method to calculate the mass burning rate (or heat release rate) in a diesel engine taking into account dissociation and heat transfer effects.

In the literature, diagnostic heat-release models have been used: (1) to convert experimental data into a more fundamental form, (2) to provide a means of computing or estimating quantities which are difficult to measure, and (3) to evaluate the effects of cyclic variations.

Prediction models, for the most part, are the inverse of diagnostic models. Prediction requires a deep understanding of the strengths and weaknesses of a model as well as an understanding of the range over which the model is valid. Good predictions

have been achieved by modest improvements on the air standard cycle by using small steps and assuming spatially uniform cylinder conditions (i.e. composition, pressure and temperature) and considering combustion as a "heat-release" process. This may be called a "single-zone" model. In some cases the model has been made more complex by considering the way in which fuel and air mix inside the cylinder and expressing the result as if the cylinder contents consist of a volume of air and a volume of air, fuel and combustion products. This is referred to as a two-zone combustion model.

Single-zone combustion models are represented by Austen and Lyn [30] and Whitehouse and Way [31], [32]. Lyn's method emphasizes the importance of the rate of fuel injection and also indicates how the various stages of the combustion process may be dealt with mathematically. The Whitehouse-Way model assumes droplet diffusion in the combustion chamber and allows for the effect of oxygen available on mixing. This method provides two-governing equations: a reaction rate model and a preparation rate model with implicit ignition delay. This latter approach was examined in detail [49,50,51,52] and will be the subject of further discussions in Chapter 4.

Two-zone combustion models divide the combustion chamber contents into two parts and assume uniformity within each part. Such two-zone models have been developed both for quiescent combustion chamber engines by Whitehouse and Sareen [33] and for the case of an engine with air swirl by Whitehouse and Abughres [34]. The temperature and composition of the "burning zone" is obtained from the masses, combustion rates and energy balance, and results in a pressure/volume relationship. The other " non-burning zone" consists of that part of the gases originally trapped, mainly pure air, that has not yet been incorporated into the burning zone. The first law of thermodynamics, the ideal gas law and the volume/time relationship for the engine are used to determine the pressure, temperature and volume relationships. Multi-zone combustion models are at early stages of development and can be used to explore chemistry and obtain emission data. Some of the work published in this area is by Shahed [35], Hodgetts [36], Bedran [37] and Amsden [38].

1.3 THERMODYNAMIC AND COMBUSTION MODEL OVERVIEW

The objective of the thermodynamic and combustion modeling was to achieve an acceptable simulation of the 6V53T engine with specified fuels, thus allowing numerical engine-fuel parametric studies to be performed. Clearly, with the current state-of-the-art as evidenced from the literature overview, this can only be reasonably approached through direct correlations of semi-empirical predictive models with experimental data. Further, it is also clear that new models, especially those that correlate with fuel properties and engine operating point (speed, load), will have to be developed if the R&D objectives are to be met. Fundamentally, the requirement is to predict the instantaneous gas state in the cylinder, namely: the temperature, pressure and species concentrations (reactants and combustion products). The overall simulation program is structured as a number of sub-models which include:

a) engine geometry and design,

b) fuel properties and simulation,

c) heat transfer,

d) fuel injection rate and timing (functions of engine speed and load),

e) initial state for the start of cycle calculations,

f) ignition delay,

g) fuel-air mixing rate,

h) mixed fuel-air reaction rate,

i) thermochemical calculations for combustion processes,

j) blowdown and scavenging processes and cycle closure,

k) calculation of engine indicated performance, and

l) calculation of combustion characteristics.

Of all the submodels, those that integrate to make-up the combustion process of the engine are seen to be the key for accurate simulation and reliable predictive capability of the model. The combustion process, though lasting only several milliseconds, houses all key combustion characteristics (eg. maximum pressure rates and cylinder

pressures, etc.) and determines the performance of the engine. Furthermore, it is during this period when fuel properties manifest themselves with regard to engine-fuel interaction and combustion/engine behavior. Additionally, the engine operating point is subtly integrated with this interaction and behaviour and changes their character with every speed and load setting.

The philosophy used in this research for modeling the combustion process is depicted in Fig. 1.1. Here, four models, namely: ignition delay, fuel-air mixing rate, fuel-air reaction rate and thermochemical calculation, control the process. It should be noted that each of these models, either explicitly or implicitly, involve both fuel properties and engine operating speed/load parameters. Of particular interest is the combustion model. Here, rather than using the heating value of the fuel, fundamental thermochemics is used. This permits, through a fuel simulation of C/H ratio, density and aromatic content, these properties to be involved directly in the combustion process. Seven chemical equilibrium reactions, resulting in eleven species, are used. Through an iterative procedure, using the enthalpies of formation and the total enthalpies of each species, the instantaneous thermodynamic state and species concentrations can be determined.

Figure 1.2 shows the operating concept of the overall simulation program. Initially, data specifying the engine design, fuel properties and simulation point are read. Thereafter, a computer generated simulated fuel and injection schedule are established. To start cycle calculations, initial conditions (temperature, pressure and mass of trapped gases) at the start of compression are selected and correlated with the test point of interest.

The main body of the program evaluates the instantaneous gas state in the cylinder (temperature, pressure and species concentrations) as a function of crank angle position. This involves a large iteration of six major submodels (heat transfer, fuel injection, ignition delay, fuel-air mixing rate, fuel-air reaction rate and chemical equi-

librium) together with the cycle process calculations. The incremented 'calculation step' is set at 1 °CA except from 30 °bTDC to 10 °aTDC, where a step size of 0.1 °CA is used. This high precision step size is used during the critical, and rapidly changing, combustion process region.

Following blowdown and scavenging, the cycle is closed and engine indicated performance and combustion characteristic data are determined.

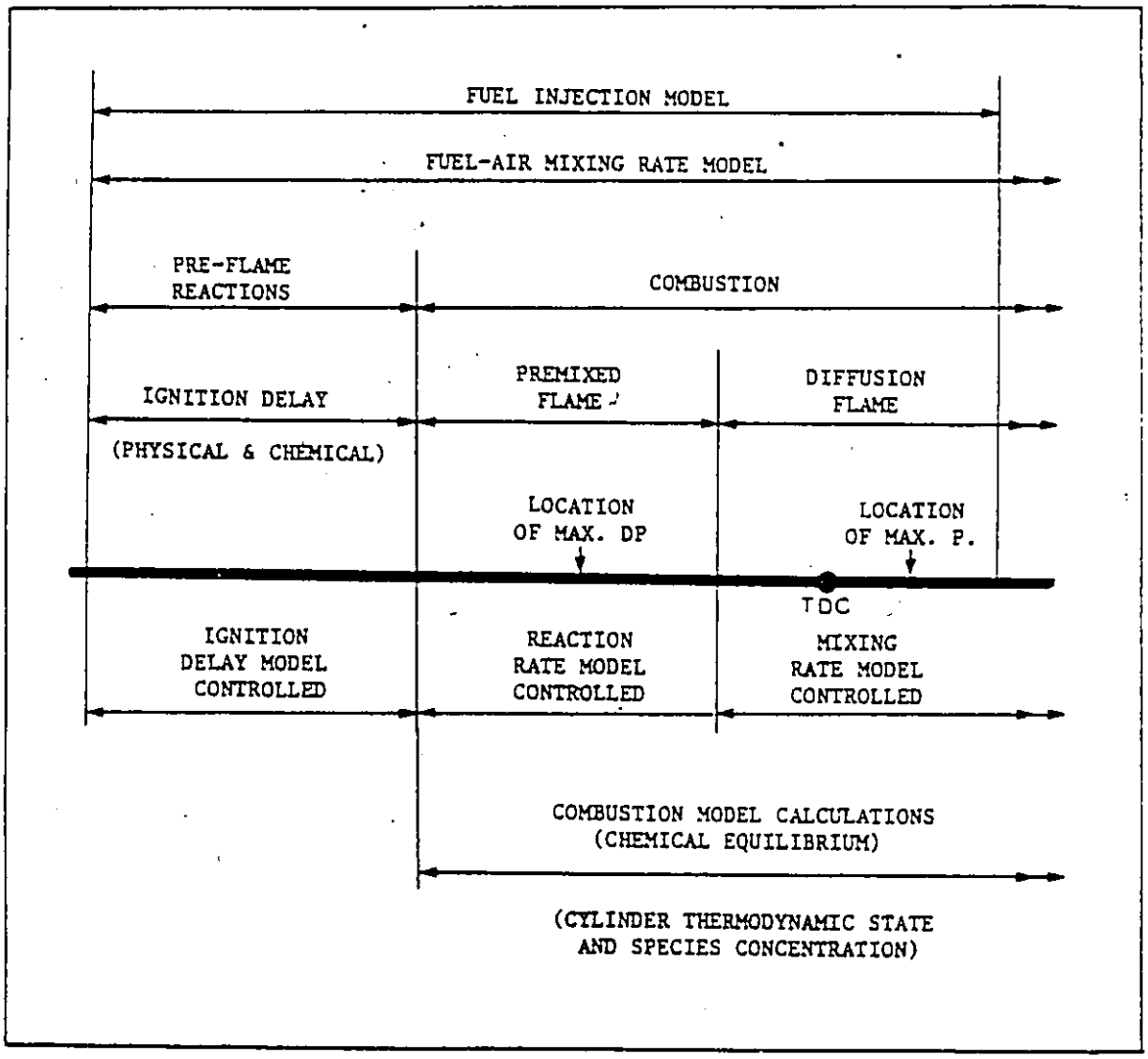

Fig. 1.1: Combustion Event Sequence and Modeling Structure

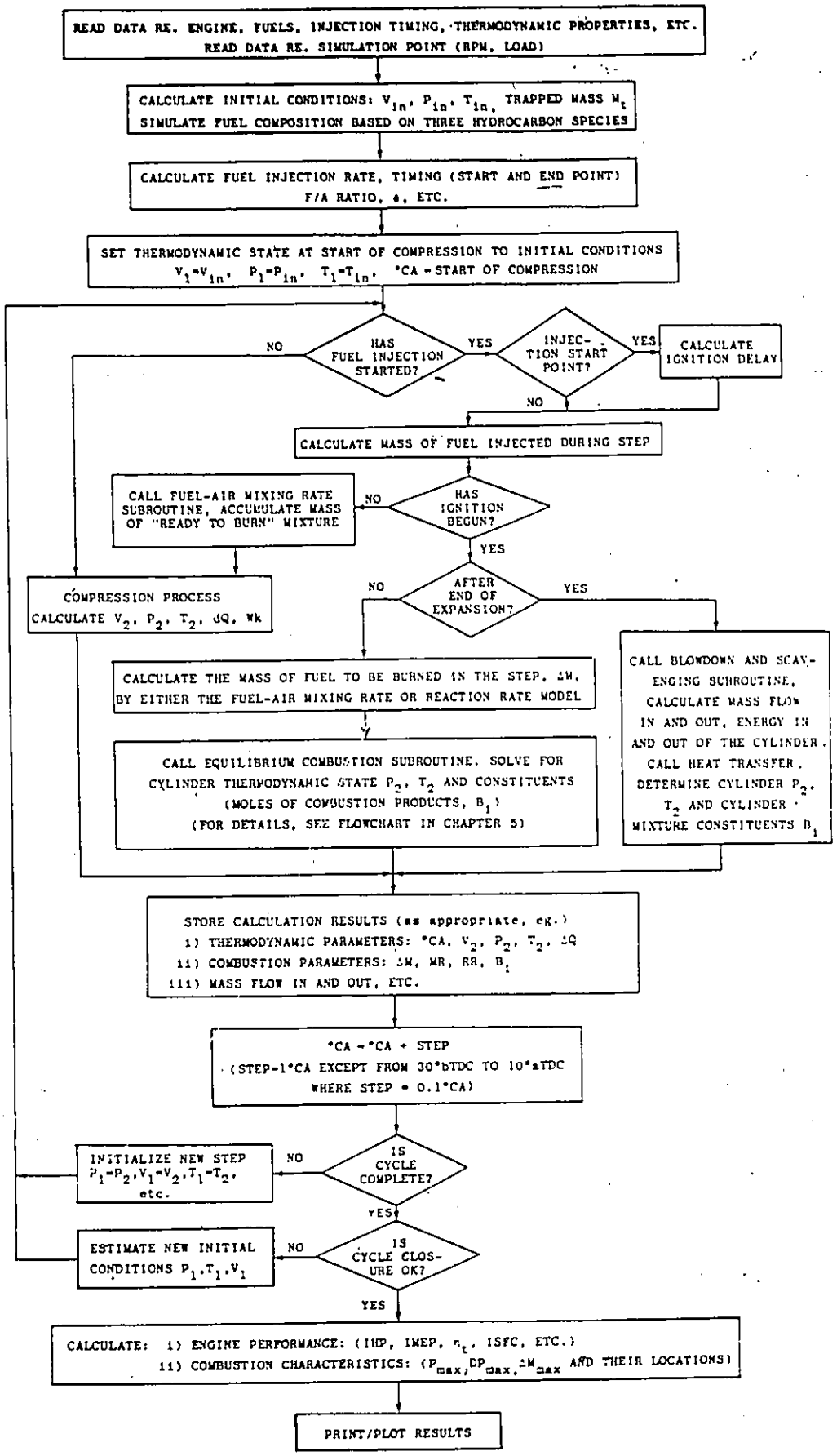

Fig. 1.2: Flowgraph of the Simulation Program

CHAPTER 2

BASIC SUB-MODEL DEVELOPMENT

2.1 INTRODUCTION

The thermodynamic model is structured as a system of sub-models as detailed in Section 1.3. This chapter deals with what has been termed the basic sub-models. These models, in general, relate to and distinguish the engine being studied with respect to both its design concepts; eg. water cooled vs. air cooled, two-stroke vs four-stroke, direct vs. indirect injection, etc. and its physical characteristics; eg. cylinder displacement, valve and port opening areas as functions of crank angle position; valve, port and injection timing, etc.

It should be noted that although these models correlate with an actual engine (6V53T) and fuels being used in the R&D program, no loss in generality results. Indeed the inverse can be argued. For example, the fuel simulation model is quite unique and provides the combustion model with a simulated hydro-carbon structure based on the diesel fuel's specification test data, in particular the C/H ratio, fuel density and aromatic content. This, in turn, affects not only species concentrations but also the cylinder thermodynamic state and thus, engine indicated performance. Further, any pure fuel or combination could be used. Likewise, the fuel injection model which accurately simulates the 6V53T engine fuel injection timing and flow rate, also allows any injection profile and rate to be specified. This is the essence of the parametric and pilot injection studies conducted in the thesis Part II.

2.2 ENGINE MODEL

For this R&D program, the engine being investigated is the Canadian Forces AVGP-GM6V53T. It is a V-6, water cooled, direct injected (unit injectors), two-stroke, turbocharged diesel engine with specification as listed in Table 2–1. For the purpose of analyzing the gas exchange process (blowdown and scavenging), Fig. 2.1 gives the valve and port timing. The data set giving the exhaust valve and inlet port opening areas, as a function of crank angle position, was obtained from GM-DDA [39]. This data is listed in Table 2–2 and plotted in Fig. 2.2. Also cylinder volume as a function of engine geometry (Table 2–1) and crank angle position can be written as:

$$V_c = \frac{\pi D^2 S}{4(CR-1)} + \frac{\pi D^2}{4}\left[\frac{S}{2}(1-\cos\alpha) + \frac{S^2}{8L}\sin^2\alpha\right], \qquad (2\text{–}1)$$

where:

V_c	— Cylinder volume (m^3)
D	— Cylinder diameter (m)
S	— Stroke (m)
CR	— Compression ratio
L	— Connecting rod length (m)
α	— Crank angle (degree from TDC)

The above data is sufficient to characterize an engine for the purpose of thermodynamic modeling.

TABLE 2-1

TEST ENGINE SPECIFICATIONS

Manufacturer	Detroit Diesel Allison Division (GMDDA)
Model	6V53T (5063-5394), Turbocharged
Type	Two cycle; compression ignition
Compression ratio	17.5:1
Compression pressure	525 psi @600 rpm
Idle speed	500-600 rpm
Governed speed	2800 rpm
Number of cylinders	6
Firing order	1L-3R-3L-2R-2L-1R
Rotation	Right hand (clockwise)
Bore	3.875 in (98.4 mm)
Stroke	4.500 in (114.3 mm)
Connecting rod length	8.81 in (223.5 mm)
Piston displacement	318 cu.in. (5.22 l)
Gross horsepower	275 @2800 rpm (nominal)
Valve clearance	cold - 0.026 in. hot - 0.024 in.
Coolant temperature	160 - 180°F (72-82°C)

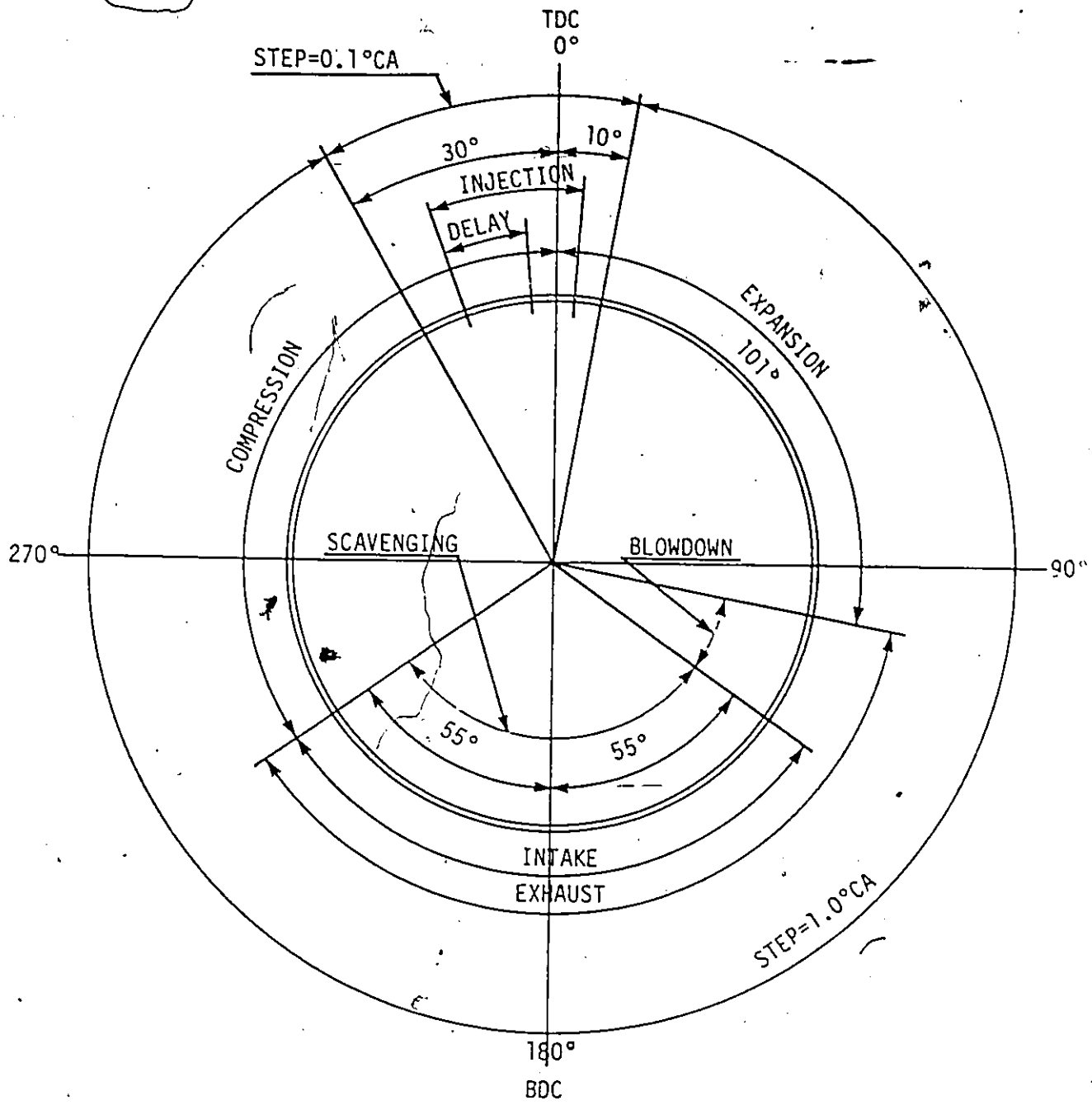

Fig. 2.1: AVGP-GM6V53T Engine Valve and Port Timing

TABLE 2-2

GM DATA FOR OPENING AREA OF INTAKE PORT

AND EXHAUST VALVES OF THE AVGP-GM 6V53T ENGINE

CRANK ANGLE (Degree) from TDC	PISTON TRAVEL (in) from TDC	EXHAUST VALVE AREA (in^2)	INTAKE PORT AREA (in^2)
101.00	2.96100	0.001	0.0
105.00	3.10493	0.199	0.0
110.00	3.27731	0.530	0.0
115.00	3.44041	0.918	0.0
120.00	3.59344	1.326	0.0
125.00	3.73572	1.721	0.009
126.00	3.76283	1.796	0.103
127.00	3.78950	1.870	0.243
128.00	3.81570	1.942	0.410
129.00	3.84144	2.012	0.595
130.00	3.86672	2.081	0.792
131.00	3.89152	2.148	0.996
135.00	3.98600	2.397	1.830
140.00	4.09326	2.408	2.795
145.00	4.18823	2.408	3.650
150.00	4.27076	2.408	4.393
155.00	4.34072	2.408	5.022
160.00	4.39802	2.408	5.526
165.00	4.44262	2.408	5.893
170.00	4.47449	2.408	6.130
175.00	4.49362	2.408	6.259
180.00	4.50000	2.408	6.300
185.00	4.49362	2.408	6.259
190.00	4.47449	2.408	6.130
195.00	4.44262	2.408	5.893
200.00	4.39802	2.264	5.526
205.00	4.34072	1.910	5.022
210.00	4.27076	1.511	4.393
215.00	4.18823	1.091	3.650
220.00	4.09326	0.691	2.795
225.00	3.98601	0.358	1.830
229.00	3.89152	0.166	0.996
230.00	3.86672	0.130	0.792
231.00	3.84144	0.097	0.595
232.00	3.81570	0.069	0.410
233.00	3.78950	0.044	0.243
234.00	3.76284	0.024	0.103
235.00	3.73572	0.005	0.009
236.00	3.70815	0.0	0.0
237.00	3.68013	0.0	0.0

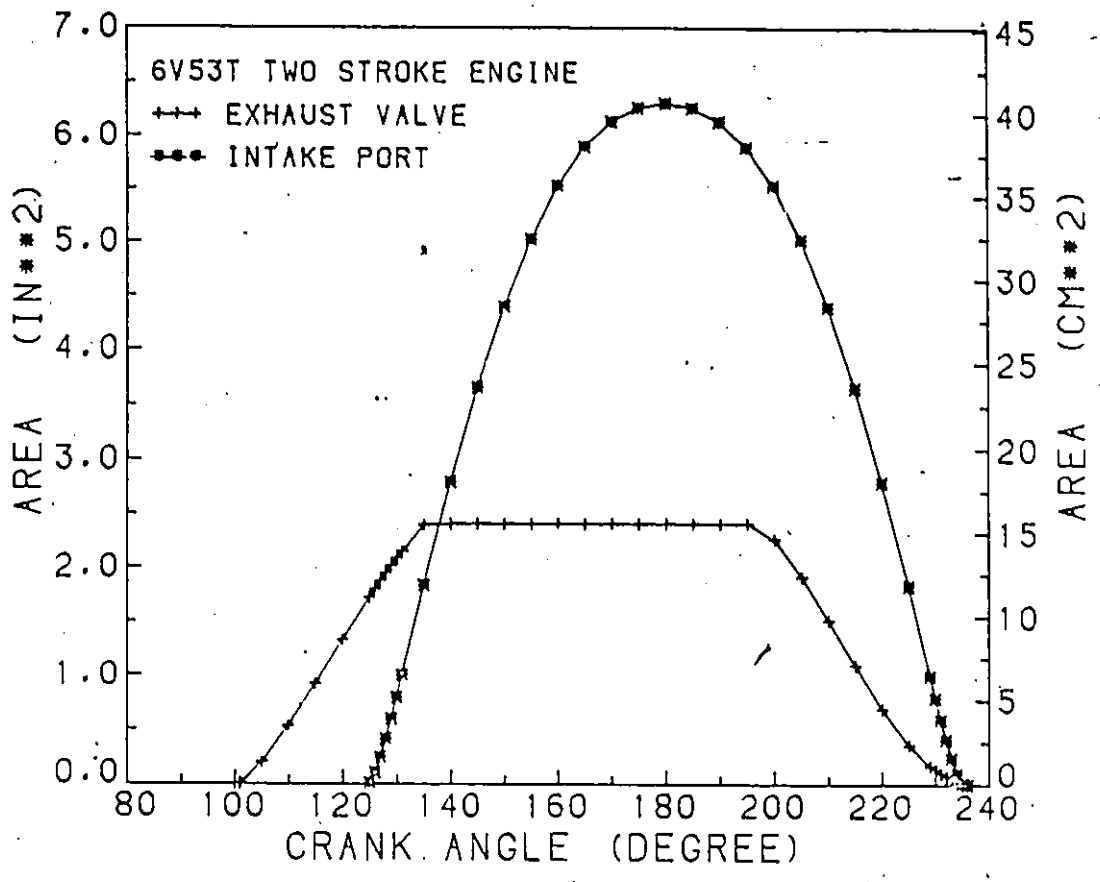

Fig. 2.2: Opening Areas of Intake Port and Exhaust Valves vs. Crank Angle

2.3 FUEL MODEL

2.3.1 FUEL SPECIFICATION

For the R&D program, three fuels were of particular interest, namely: a high quality reference fuel used to establish 'baseline' engine performance and combustion characteristics and two off-specification fuels, both being representative of possible fu-

ture Canadian fuels. * Fuel specifications, taken from Webster [40], are listed in Table 2–3 while the following provides a summary of each fuel.

a) Fuel 1: This fuel meets the Canadian General Standards Board (CGSB), 3-GP-30 standard for high stability diesel and was selected as the reference fuel. Key specifications are: Cetane No. = 46.7, Total Aromatic = 21.3%, Distillation Range = 173—351°C and Density = 0.8403.

b) Fuel 3: A blend comprising 40% of a distillate cut from western Canadian tar sands crude, with 60% from conventional western crude both from the St. Boniface Refinery. This fuel provided an example of a best case 1990 fuel with a substantial percentage of tar sands derived products. Key specifications are: Cetane No. = 36.9, Total Aromatics = 39.4%, Distillation Range = 171—306°C, and Density = 0.8463.

c) Fuel 4: A blend comprising 78% of a distillate cut from a 50/50 mixture of conventional western Canadian and tar sands crude and 22% of hydrogen treated cracked stock. This provided a fuel containing a substantial level of aromatics and cracked components and is typical of diesel fuel quality predicted for the 1990-2000 time frame. Key specifications are: Cetane No. = 35.9, Total Aromatics = 42.35%, Distillation Range = 164—381°C, and Density = 0.8783.

* All fuels were supplied by the National Research Council of Canada, Fuels and Lubricants Laboratory under the coordination of Mr. G.D. Webster.

TABLE 2-3

FUEL SPECIFICATION

PROPERTY	FUEL 1	FUEL 3	FUEL 4
Density @15°C, kg/L (D1298)	.8403	.8463	.8783
Distillation (D86)			
I.B.P., °C	173	171	164
10% recovered, °C	203	196	196
50% recovered, °C	257	236	268
90% recovered, °C	323	287	354
F.B.P. °C	351	306	381
Recovered % vol.	98.0	98.0	98.3
Carbon Residual, % mass (D524)	1.9	1.6	1.8
Cloud Point, °C (D2500)	-12	-43	-8
Pour Point, °C (D97)	-18	-54	-39
Kinematic Viscosity @40°C, mm2/S (D445)	2.41	1.90	2.78
Ash, % mass (D482)	0.000	0.000	0.002
Water and Sediment, % vol. (D1796)	0.000	0.000	0.000
Sulphur, % mass (D1552)	0.21	0.21	0.53
Nitrogen Content (chemiluminescent) ppm by wt	-	30	-
Flash Point, °C (D93)	57	60	60
Total Acid No. mg KOH/g (D974)	0.03	0.01	-0.03
Corrosion, 3 hr. @100°C (D130)	1a	1a	1a
Cetane Number (D613)	46.7	36.9	35.9
Cetane Index, ASTM (D976) CGSB	48.0	40.0	40.0
Aniline Point, °C (D611)	64.4	49.8	46.9
Carbon (By Difference) % mass	86.6	86.39	87.83
Hydrogen Content, % mass (D3701)	13.4	12.08	12.17
C/H Ratio	6.6	7.15	7.2
Smoke Point, mm (D1322)	17.0	14.7	12.1
Heat of Combustion, MJ/kg (23.4M)	45.63	45.54	44.94
Hydrocarbon Type Analysis			
Saturates and Olefins, %	77.8	60.4	56.02
Poly-Aromatics and Polar Compounds, %	0.9	0.2	1.63
Total Aromatics %	21.3	39.4	42.35

2.3.2 FUEL MODEL

Experimental investigations have revealed that the off-specification fuels (Fuels 3 and 4) give rise to high pressure rates during the early combustion period resulting in diesel knock and/or pressure waves throughout the expansion stroke [47, 48, 49]. Thus, one of the principal objectives of the thermodynamic model was to investigate this phenomenon and to perform analytical analysis aimed at reducing pressure rates while maintaining engine performance. Such a demand from a thermodynamic model is unique and requires sub-models which correlate with fuel properties.

The three experimental or test fuels, as is the case for all diesel fuels, are comprised of many hydrocarbon species, the composition of which is unknown. As such, information on their basic thermodynamic properties is unknown (eg. specific heat, enthalpy, etc.) but rather, what is known or can be determined is simply overall fuel specification data as listed in Table 2–3.

In this analysis, one approach used to integrate fuel properties into the analysis was the establishment of a fuel model. Here, three pure fuels, the basic thermodynamic properties of which are well known, are blended to simulate the test fuels. In particular, to simulate the key specification data of C/H ratio, aromatics content and fuel density. The three pure fuels (or basic species) selected were:

SPECIES	FORMULA	DENSITY (Kg/m^3)
n-Octane	C_8H_{18}	707.1
Benzene	C_6H_6	884.0
Dodecane	$C_{12}H_{26}$	828.5

These species were selected on the basis that n-Octane is representative of gasoline, dodecane is representative of diesel fuel and benzene is a high density aromatic. In general, not all of the three key specification data can be matched; however, for the species selected, good approximations were achieved.

If X_1, X_2 and X_3 are the mass fractions of the species, then, for a unit mass of test fuel:

$$X_1 + X_2 + X_3 = 1 \tag{2-2}$$

It is important to match, exactly, the C/H ratio of the simulated fuel with that of the test fuel since C/H ratio is used in the combustion model. Now, defining 'm_i' as the number of carbon atoms and 'n_i' as the number of hydrogen atoms in each species 'i', then their molecular weights 'W_i' can be written as:

$$W_1 = 12.010m_1 + 1.008n_1 = 114.22 \qquad \text{for } C_8H_{18},$$
$$W_2 = 12.010m_2 + 1.008n_2 = 78.110 \qquad \text{for } C_6H_6,$$
$$W_3 = 12.010m_3 + 1.008n_3 = 170.33 \qquad \text{for } C_{18}H_{26}.$$

Further, for a unit mass of fuel, it follows that the number of moles of each species is given by: X_i/W_i. Thus, the C/H ratio becomes:

$$C/H = \frac{12.01}{1.008} \cdot \frac{\frac{m_1}{W_1}X_1 + \frac{m_2}{W_2}X_2 + \frac{m_3}{W_3}X_3}{\frac{n_1}{W_1}X_1 + \frac{n_2}{W_2}X_2 + \frac{n_3}{W_3}X_3} \tag{2-3}$$

Equation (2-3) can be simplified by letting $k = (1.008/12.01)C/H$, $a_i = m_i/W_i$ and $b_i = n_i/W_i$. Thus, the C/H ratio Equation (2-3) becomes:

$$(a_1 - kb_1)X_1 + (a_2 - kb_2)X_2 + (a_3 - kb_3)X_3 = 0 \tag{2-4}$$

The third equation can be established from either aromatic content or fuel density, viz:

Aromatic content:

$$X_2 = \text{total aromatics} \tag{2-5}$$

Fuel density:

$$X_1(1 - \frac{\rho}{\rho_1}) + X_2(1 - \frac{\rho}{\rho_2}) + X_3(1 - \frac{\rho}{\rho_3}) = 0 \tag{2-6}$$

As stated, all specification data cannot be matched, thus an approximation to Equations (2-5) and (2-6) must be made. Table 2–4 lists the simulated fuels selected together with a comparison of the specification data from the three test fuels.

TABLE 2-4

COMPOSITION AND SPECIFICATION OF SIMULATED FUELS

FUEL	Mass Fraction (%)			Volume Fraction (%)			Comparison With Specification Data								
							Density Kg/m³)			Aromatics (%)			C/H Ratio		
	X_1 C_8H_{18}	X_2 C_6H_6	X_3 $C_{12}H_{26}$	Z_1 C_8H_{18}	Z_2 C_6H_6	Z_3 $C_{12}H_{26}$	Spec. Data	Model	Diff. (%)	Spec. Data	Model	Diff. (%)	Spec. Data	Model	Diff. (%)
Fuel #1 CN=46.7	5.76	26.50	67.74	6.79	25.01	68.20	840.3	834.1	-0.7	21.3	26.5	+24	6.46	6.46	0
Fuel #3 CN=36.9	4.72	41.20	54.08	5.63	39.31	55.06	846.3	843.5	-0.3	39.4	41.2	+4.6	7.15	7.15	0
Fuel #4 CN=35.9	0.45	41.9	57.65	0.54	40.30	59.16	878.3	850.2	-3.2	42.4	41.9	-1.2	7.20	7.20	0

2.4 INITIAL STATE

To begin a cycle analysis, an initial state must be determined wherein cylinder contents and thermodynamic properties (P_{in},T_{in}) are known or can be accurately estimated. In general, this can most easily be achieved at the onset of compression.

For the 6V53T engine, the air mass trapped in the cylinder at the end of the scavenging process (or onset of compression) can be calculated from the charging efficiency formula developed by GM-DDA [39] as:

$$\eta_{ch} = 0.9 - (1.0 - 0.34R_s)\exp(-1.11R_s), \qquad \text{for} \qquad 0.3 < R_s < 1.8 \tag{2–7}$$

where R_s is the scavenging ratio defined as:

$$R_s = \frac{M_d}{M_c} = \frac{\text{Delivered Air}}{\text{Ideal Cylinder Mass Based On Airbox Density}}$$

and:

$$M_c = 28.96\frac{P_{ab} \cdot V_{ct}}{R_{mol} \cdot T_{ab}}, \qquad (kg).$$

where P_{ab} and T_{ab} are airbox pressure and temperature respectively, V_{ct} is the total cylinder volume.

Further, from a survey of experimental $P - CA$ data, it can be seen that the initial pressure (P_{in}) at the onset of compression is characteristically 1.5 *psi* higher than airbox pressure (P_{ab}) for the 6V53T engine. Thus, for the onset of compression (55° aBDC, Fig. 2.1), the initial state can be accurately estimated as:

a) Trapped mass in the cylinder;

$$M_{dt} = \eta_{ch} \cdot M_c, \tag{2–8}$$

b) Initial cylinder pressure;

$$P_{in} = P_{ab} + 1.5\,\text{psi}, \quad \text{and} \tag{2–9}$$

c) Initial cylinder temperature;

$$T_{in} = \frac{P_{in} \cdot V_{in}}{R \cdot M_{dt}}, \tag{2-10}$$

where cylinder volume at the start of compression (V_{in}) can be obtained from Equation (2-1).

2.5 HEAT TRANSFER

2.5.1 LITERATURE OVERVIEW

Heat transfer between the cylinder gases and the variable geometry combustion space boundary is a complex process. Further, it is important for thermodynamic cycle analysis to establish the instantaneous heat transfer throughout the complete cycle, as this affects the instantaneous cylinder thermodynamic state (P,T). This, in turn, controls the combustion process.

For most practical purposes, the instantaneous gas temperature (T_g) may be considered uniform throughout the combustion space (i.e. single zone), and further, the combustion space boundary temperature at a fixed location may be considered constant over the cycle. These "steady-state" boundary temperatures do vary widely from point-to-point. Thus, the boundary is normally divided into common areas, typically: the exhaust valve, head, cylinder wall and piston crown areas.

In the literature, the three most common heat transfer correlations are those by Eichelberg [9], Annand [12] and Woschni [13]; viz:

a) Eichelberg's model:

$$\frac{q}{A} = 10.47 \times 10^{-3} V_P^{\frac{1}{3}} (PT)^{\frac{1}{2}} (T_g - T_w) \tag{2-11}$$

b) Annand's model:

$$\frac{q}{A} = a\frac{K}{D}(R_e)^b(T_g - T_w) + c(T_g^4 - T_w^4) \qquad (2\text{–}12)$$

c) Woschni's model:

$$\frac{q}{A} = 110D^{-0.2}P_g^{0.8}T_g^{-0.53}\left[C_1V_P + C_2\frac{V_{ct}T_{in}}{P_{in}V_{in}}(P_g - P_0)\right]^{0.8}(T_g - T_w) \qquad (2\text{–}13)$$

where the subscript 'g' refers to cylinder gases and 'w' to the combustion space boundary.

In general, heat transfer in an IC engine results from both convection and radiation, which are influenced by the rapid changes in gas temperatures and the high gas velocities in the cylinder. Thus, forced turbulent fluid flow is considered and the convective heat transfer coefficient is expressed as a correlation between Reynolds number (R_e) and Nusselt number (N_u) of the form:

$$N_u = C \cdot R_e^b. \qquad (2\text{–}14)$$

Here, 'C' and 'b' are constants and the Reynolds number can be written as:

$$R_e = \frac{\rho V_g D}{\mu} \qquad (2\text{–}15)$$

where 'V_g' is the instantaneous gas velocity and 'D' is the cylinder bore.

The Annand and Woschni expressions, although different in form, are both largely based on turbulent convection considerations. This gives the first term in Annand's correlation while the second is a standard radiation term.

In Woschni's equation, the index 'b' (Eq. 2-14) is taken as 0.8 for turbulent flow in pipes, and 'C' is taken as 0.035 from Hausen's equation for turbulent flow in pipes. Further, if the density, viscosity and thermal conductivity of the gas in the cylinder are expressed as functions of cylinder gas temperature (T_g) and pressure (P_g), then Equation (2-14) leads directly to Woschni's Equation (2-13) where gas velocity is written as:

$$V_g = C_1V_P + C_2\left[\frac{V_{ct}T_{in}}{P_{in}V_{in}}\right](P_g - P_o). \qquad (2\text{–}16)$$

Here, V_P is the mean piston velocity; V_{ct} is the cylinder displacement; P_{in},T_{in} and V_{in} are the pressure, temperature and volume at the beginning of compression and $(P_g - P_0)$ is the pressure differential between fired and motored curves. It could be noted that $(P_g - P_0) = 0$ except during combustion and expansion, and thus accounts for radiation and additional combustion - induced turbulence.

Both the Annand and Woschni equations have constants which may be adjusted to give reasonable overall heat transfer values.

2.5.2 HEAT TRANSFER MODEL

In this analysis, the combustion chamber of the 6V53T engine was represented by four heat transfer surfaces, namely: piston crown, cylinder sleeve (variable), valve area and cylinder head; with the following assumptions:

a) each surface has a uniform temperature,

b) surface temperatures are constant with time,

c) surface deposits are neglected, and

d) the heat transfer coefficient is the same and uniform for all the surfaces.

Thus, the instantaneous heat transfer rate from the cylinder gases to the boundary can be written as:

$$\frac{dQ}{dt} = h \sum_{i=1}^{4} A_i (T_g - T_{w_i}), \qquad (Kcal/h) \tag{2–16a}$$

where:

h — instantaneous heat transfer coefficient.

A_i — area of surface 'i' (m^2),
available from 6V53T engine geometry.

T_{w_i} — temperature of surface 'i'.

T_g — instantaneous cylinder gas temperature.

The temperatures of the four surfaces selected were based on values recommended by GM-DDA [42]:

Piston crown temperature	$T_{w_1} = 616\ ^\circ K$,	
Cylinder sleeve temperature	$T_{w_2} = 422\ ^\circ K$,	(2-16b)
Valves temperature	$T_{w_3} = 616\ ^\circ K$,	
Cylinder head temperature	$T_{w_4} = 560\ ^\circ K$.	

Then the instantaneous heat transfer coefficient can be calculated according to Woschni's correlation,viz:

$$h = 110 D^{-0.2} P_g^{0.8} T_g^{-0.53} \left[C_1 V_P + C_2 \frac{V_{ct} T_{in}}{P_{in} V_{in}} (P_g - P_0) \right]^{0.8} \qquad (2\text{–}16c)$$

where:

h	—	instantaneous heat transfer coefficient $(Kcal/m^2 \cdot h \cdot ^\circ C)$,
D	—	cylinder diameter (m),
P_g, T_g	—	instantaneous cylinder pressure (Kg/cm^2) and temperature $(^\circ K)$,
V_P	—	mean piston velocity (m/s),
V_{ct}	—	cylinder displacement (m^3),
P_0	—	instantaneous cylinder pressure for a motored cycle (Kg/cm^2),
P_{in}, T_{in}, V_{in}	—	initial cylinder pressure (Kg/cm^2), temperature $(^\circ K)$ and volume (m^3) at the beginning of compression.

A series of numerical/analytical experiments were conducted to assess the values

of the constants C_1 and C_2 relative to the 6V53T engine. It was found, for the operating range of the engine (1500 to 2800 RPM), that the constants recommended by Woschni [23] gave good overall heat transfer values. Thus, Woschni's recommended values were used, viz:

$$C_1 = 2.28 \text{ during compression and expansion,}$$
$$= 6.18 \text{ during scavenging, and}$$
$$C_2 = 3.24 \times 10^{-3} \quad (m/s^\circ K).$$

2.6 FUEL INJECTION MODEL

The start, duration and mass rate of fuel injection are critical to the thermodynamic model. Since these injection parameters vary with both engine load and speed, it was necessary to develop an injection map covering the complete operating range of the 6V53T engine with N65 unit injectors and cam profile of the AVGP unit.

This objective was reviewed with the GM-DDA Division [42] and a set of injection data covering each 20% rack position for every 100 RPM (1500-2800 RPM) was produced. The map of data was entered into the computer and an interpolation scheme established to provide the fuel injection profile for any experimental test point based on experimental fuel flow rate and engine speed.

Thus, for any experimental test point, the fuel injection model will predict the start, end and duration of injection; the injection rate and the total mass of fuel injected as a function of crank angle position. Figure 2.3 gives typical injection schedules for full load and two part load operating points (250 and 100 ft-lb. brake torque) at 1500, 2200 and 2800 RPM respectively.

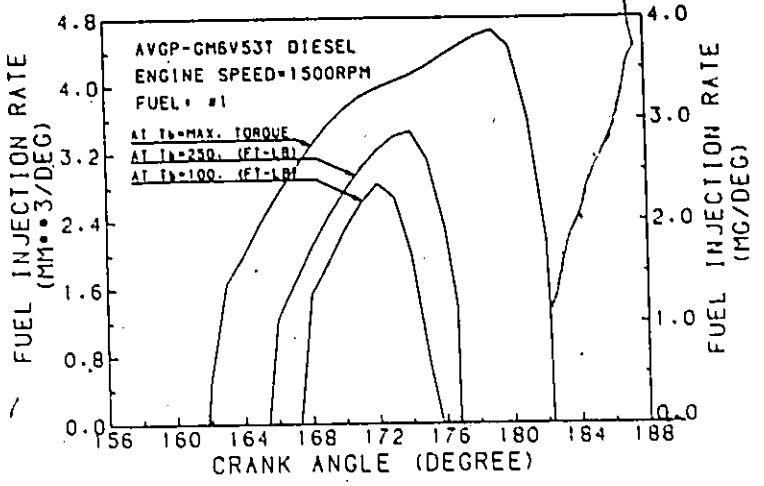

(a) 1500 RPM

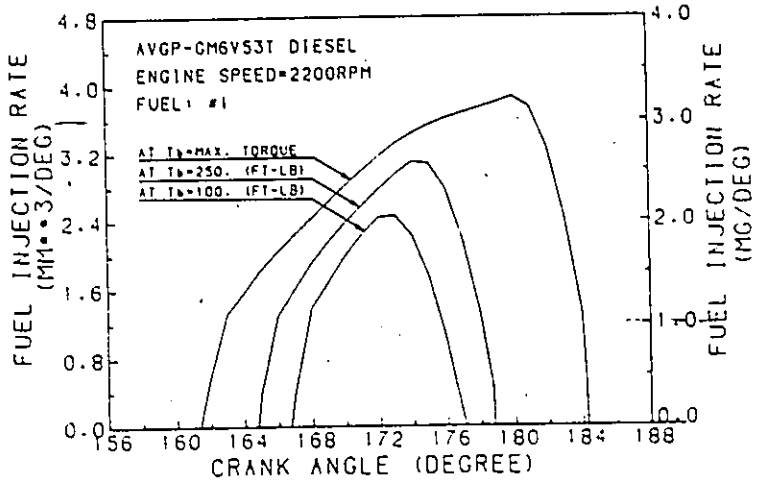

(b) 2200 RPM

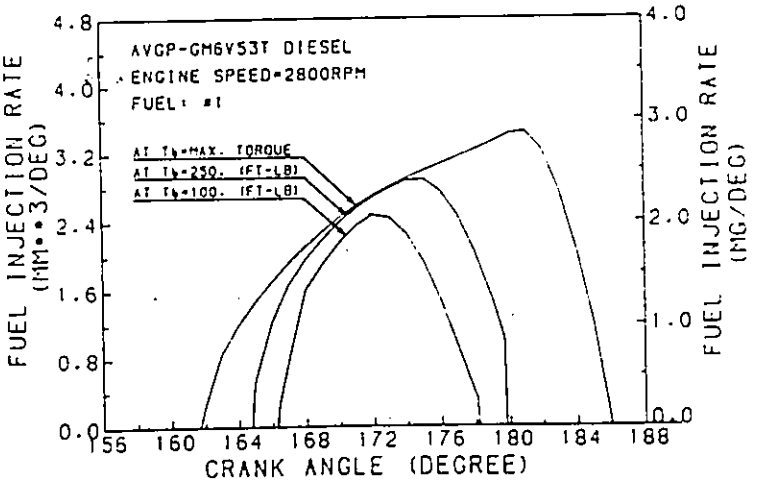

(c) 2800 RPM

Fig. 2.3: Injection Schedules from the Fuel Injection Model

It should be noted that the model allows complete flexibility in choosing injection timing and rates, that is, timing can be varied while the above rate is preserved or both timing and rate may be altered including multiple injection. Such is required for parametric and pilot injection studies.

CHAPTER 3

IGNITION DELAY MODEL

3.1 OVERVIEW

In high speed diesel engines,the combustion process lasts about 4-5 ms. However, the initial phase of the process, that of ignition delay, lasts only about 1 ms or less. Ignition delay has historically been an area of intense analytical and experimental investigation. It is this period which characterizes not only diesel fuel quality but also the combustion characteristics and, to a considerable degree, the thermodynamic performance of the engine.

During the ignition delay period, a complex set of physical and chemical phenomena must occur before sustained chemical reaction (or autoignition) occurs. These include: liquid fuel injection, penetration, atomization and/or distribution, vaporization and mixing with air; heat, mass and momentum transfer between the liquid fuel and surrounding air; localized, heterogeneous heat release by chemical pre-flame reactions; etc. It is common to visualize ignition delay as a physical plus chemical delay; however, virtually all analytical models simulate ignition delay as an integrated or single process.

From preliminary model investigation [49, 50, 51], it was recognized that an explicit ignition delay model would be required in order to simulate, over the full operating range of the engine, the early (or rapid) combustion phase common to diesel engines. This was particularly important since experimental data [45, 46, 47, 48] revealed abnormal combustion with the off-specification fuels, resulting in a very high pressure rise rate during this period.

From a broad survey of the literature [14-21], a number of ignition delay models were identified and evaluated (Appendix 'A'). None of the models tested gave satisfac-

tory results when compared with the 6V53T experimental ignition delay measurements and further, none of the models incorporated both a load and fuel property dependency which was of particular importance to the research objective. Thus, an ignition delay model was mathematically developed that reflects both engine operating conditions, i.e. fuel/air ratio, cylinder temperature and pressure, as well as fuel cetane number.

3.2 MODEL DEVELOPMENT

Several definitions are considered valuable before proceeding with the model development, namely:

a) **Ignition Delay** is defined as the time period from the start of fuel injection to the onset of combustion. For the physical measurements, onset of combustion is taken to be synonymous with a sustained and measurable temperature/pressure rise in the cylinder due to combustion or chemical heat release.

b) **Order of Reaction** is the number of atoms or molecules whose concentrations determine the rate of the reactions. In a hydrocarbon combustion, the order with respect to each reagent must be found experimentally and can not be predicted or deduced from the equation for the reaction. Some experimental values of the order of reaction, taken from Kanury [43] are given in Table 3-1.

c) **Activation Energy** is the energy needed to raise the system from initial reactants to the activated complex. In other words, in order to undergo a chemical reaction, molecules need not only collide with one another but must do so with sufficient energy so as to break the weakest of the bonds. The activated complex is the transient state of the reactants which can spontaneously decompose into products at a constant rate. The activation energy is the energy of formation of the activated complex state. Some values of activation energy are also given in Table 3–1.

TABLE 3-1

ORDER OF REACTION AND ACTIVATION ENERGY

FUEL	FORMULA	OXIDANT	ORDER OF REACTION	ACTIVATION ENERGY (Kcal/lb-mole)
PROPANE	C_3H_8	Air	1.60	31.0
METHANE	CH_4	Air	1.60	29.0
HEXANE (n)	C_6H_{14}	Air	-	50.7
DECANE (n)	$C_{12}H_{26}$	Air	1.62	51.0
OCTANE (iso)	C_8H_{18}	Air	1.52	32.4
OCTANE (n)	C_8H_{18}	Air	1.80	40.0
OCTANE (n)	C_8H_{18}	O_2	1.80	40.0
BENZENE	C_6H_6	Air	-	47.2
HYDROGEN	H_2	Air	2.17	57.0
CARBON MONOXIDE	CO	-	-	78.0

Conceptually, the ignition delay model assumes a near stoichiometric mixing zone between the fuel-lean mixture in the cylinder and the fuel-rich injection stream. For the development, either a plume or a heterogeneous family of such zones can be postulated. While pressure is taken to be constant throughout the combustion space, temperature differences exist between the three zones. Pre-ignition reactions take place in the mixing zone at regions near stoichiometric conditions. These pre-flame reactions

raise the local temperatures, T_L. When the local temperatures reach a critical value, T_{cr}, a sustained reaction or flame will result, giving rise to the rapid combustion of the neighboring mixed gasses in the cylinder. Further, the model also postulates that the activation energy is a function of fuel cetane number, CN, and in this development, a linear relationship is used. This assumption is supported by the work of Henein [18] and Hardenberg [20] who present correlations as follows, respectively:

$$E = 15500 - 230(CN - 15), \qquad (\text{BTU/lb} - \text{mole}), \text{ and} \qquad (3-1)$$

$$E = 618840/(CN + 25), \quad . \quad (\text{J/mole}). \qquad (3-2)$$

Thus, the heat released by the preflame reactions is used to increase the internal energy of the local mixture. If ρ is the density, c is the specific heat of the mixture and ΔH is the enthalpy of reaction, then:

$$\rho\ c\ \frac{\Delta T_L}{\Delta t} = \Delta H \cdot \dot{W}, \qquad (3\text{–}3)$$

where the pre-flame reaction rate $\dot{W}$ is given by the Arrhenius law of reaction [43]:

$$\dot{W} = K_n \cdot C_F^{n'} \cdot e^{-\frac{E}{RT}}, \qquad (3\text{–}4)$$

Here K_n is the specific reaction rate constant, C_F is the concentration of fuel and superscript n' is the overall order of reaction.

Equation (3-3) then becomes:

$$\rho\ c\ \Delta T_L = \Delta H \cdot K_n \cdot C_F^{n'} \cdot e^{-\frac{E}{RT}} \Delta t. \qquad (3\text{–}5)$$

Now based on the modeling concept, ignition delay is taken as the time required to vaporize and raise the local temperature of the fuel-air mixture, T_L, from the initial gas temperature at the start of injection, T, to the critical temperature T_{cr}. Thus, $\Delta T = T_{cr} - T$ when $\Delta t = t_i$, the ignition delay. Substituting into Equation (3-5) yields:

$$t_i = \frac{\rho\ c\ (T_{cr} - T) \cdot e^{\frac{E}{RT}}}{\Delta H\ K_n\ C_F^{n'}}. \qquad (3\text{–}6)$$

Now t_i can be readily expressed in crank angle degrees by introducing the engine speed N. Thus, the ignition delay takes the form:

$$Delay = \frac{\rho\ c\ N\ (T_{cr} - T) \cdot e^{\frac{E}{RT}}}{\Delta H\ K_n\ C_F^{n'}}. \qquad (^\circ CA) \qquad (3\text{-}7)$$

Ignition delay can be presented in a more workable form by applying the following relations:

$$\rho = \frac{P}{RT}, \qquad \text{and} \qquad (3-8)$$

$$C_F^{n'} = (X_F \cdot \frac{P}{RT})^{n'}, \qquad (3-9)$$

where X_F is the mole fraction of fuel. Thus:

$$X_F = \frac{n_F}{n_F + n_A} = \frac{M_F/W_F}{M_F/W_F + M_A/W_A} \qquad (3\text{-}10)$$

where:

$n_F,\ n_A$ — numbers of moles of fuel and air respectively,

$M_F,\ M_A$ — masses of fuel and air respectively,

$W_F,\ W_A$ — molecular weights of fuel and air respectively,

Now, in diesel engines:

$M_F \ll M_A$ since $M_F/M_A = F/A$ ratio $\ll 1$, and

$W_F \gg W_A$ since $W_F = 170.33$ for diesel fuel

$W_A = 28.96$ for air.

Thus, $M_F/W_F \ll M_A/W_A$.

Therefore, Equation (3-10) can be simplified by dropping M_F/W_F from the denominator.

$$X_F \simeq \frac{M_F/W_F}{M_A/W_A} = FA \cdot (W_A/W_F)$$

where FA is fuel/air ratio, or

$$X_F \simeq \frac{28.96}{170.33} \cdot (FA). \qquad (3\text{-}11)$$

Now Equation (3-9) takes the form:

$$C_F^{n'} \simeq (\frac{28.96}{170.33})^n \cdot (FA)^m \cdot (\frac{P}{RT})^n \qquad (3\text{–}12)$$

where n – order of reaction for air, and

m – order of reaction for fuel.

Finally, the activation energy is taken as a linear function of cetane number, viz:

$$E = a(CN) + b \qquad (3\text{–}13)$$

Substituting these relations back into Eq. (3-7) and collecting terms, ignition delay takes the final form of:

$$\text{Delay} = C \cdot N \cdot \frac{(T_{cr} - T) \cdot T^{n-1}}{(FA)^m \cdot P^{n-1}} \cdot \exp\left[\frac{a(CN) + b}{RT}\right], \qquad (^\circ\text{CA}) \qquad (3\text{–}14)$$

$$\text{where } C = \frac{c \cdot R^{n-1}}{\Delta H \cdot K_n \cdot [\frac{28.96}{170.33}]^n} = \text{constant.}$$

In the equation, P and T are the pressure (atm) and temperature $(^\circ K)$ of the cylinder gases at the start of injection, in practice, these will be known from the thermodynamic model. For the 6V53T engine, temperatures at the start of injection are in the range of 875-1075 $(^\circ K)$ while pressures are about 32-48 (atm).

3.3 MODEL CONSTANTS

In order to determine the constants in the model, Equation (3-14), a non-linear multi-variable optimization program was developed. It uses the conjugate direction technique [44] to minimize the average error between the model prediction and the experimental data which is considered correct. Table 3-2 lists the data used to evaluate the model constants and includes measured delays for each fuel type at specified engine load/speed setting together with nominal values for the parameters P, T and FA.

TABLE 3-2

DATA FOR DETERMINING COEFFICIENTS OF IGNITION DELAY MODEL

TORQUE (Ft-lbs)		N (RPM)	Nominal Values			Measured Ignition Delay (°CA)		
			T (°K)	P (atm)	FA (Kg/Kg)	FUEL 1 CN=46.7	FUEL 3 CN=36.9	FUEL 4 CN=35.9
FULL LOAD	585	1500	876	32.1	0.057	7.7	9.0	9.0
	578	2200	968	38.8	0.046	8.0	9.1	8.8
	499	2800	1069	47.4	0.038	7.7	8.3	8.0
PART LOAD	250	1500	933	33.1	0.028	8.7	10.2	10.3
	250	2200	1004	37.8	0.027	9.3	11.1	11.0
	250	2800	1076	44.6	0.026	8.2	9.6	9.2

As stated earlier in Chapter 2, data from a two-stroke turbocharged diesel engine (GM6V53T) is used together with three fuels: a high quality reference diesel fuel (Fuel 1: CN=46.7) and two off-specification fuels (Fuel 3: CN=36.9 and Fuel 4: CN=35.9). A description of the experimental program and complete specifications of both the engine and fuels are given in references [45-46]. For the evaluation, a completely unconstrained optimization procedure was used which yielded the following values:

$$a = -119.5 \qquad T_{cr} = 1454.7$$
$$b = 21022 \qquad m = 0.495$$
$$C = 2.23 \times 10^{-8} \qquad n = 1.736$$

Using these constants, the average error between the experiment and model predicted values is only 0.21 $°CA$, which corresponds exactly with the accuracy of the experimental measurements. Thus, for the 6V53T diesel engine, ignition delay is written as:

$$\text{Delay} = 2.23 \times 10^{-8} N \frac{(1454.7 - T)T^{0.736}}{(FA)^{0.495} P^{0.736}} \cdot \exp\left[\frac{21022 - 119.5(CN)}{RT}\right], \qquad (°\text{CA}). \tag{3-15}$$

where N — engine speed (RPM)

T — cylinder temperature at injection start ($°K$)

P — cylinder pressure at injection start (atm, abs.)

FA — fuel/air ratio (kg/kg)

CN — cetane number of fuel

R — gas constant (8.314 kj/kg-mole $°K$)

To what extent model constants will vary with engine type is an area of current interest.

3.4 MODEL EVALUATION

The ignition delay model developed is a function of engine thermodynamic state (cylinder pressure and temperature at start of injection, P and T), engine operating point (speed and load, N and FA) and fuel quality (cetane number). This range of parameters makes the model very attractive for thermodynamic simulation and parametric analyses of engine-fuel behavior. In assessing the model, it is particularly interesting to reflect on the model constants determined by the unconstrained numerical optimization technique.

(a). The critical temperature T_{cr} was defined as the local temperature in the mixing zone at which ignition occurs. Optimization placed T_{cr} at a value of 1454.7 ($°K$). This value is in the lower range of flame temperatures for most hydrocarbon fuels ($1400 - 2500\ °K$). T_{cr} is not to be confused with cylinder thermodynamic state, flame temperature or auto-ignition temperature, but rather, as postulated, is the local temperature in the near-stoichiometric mixing zone (raised through pre-flame reactions) at which the local radicals have enough energy to sustain combustion. Physically T_{cr} appears to be well placed.

(b). The orders of reaction; 'm' for fuel and 'n' for air, as stated, are ex-

perimentally determined parameters. Numerical optimization placed these values at: $m = 0.495$ and $n = 1.736$. Based on the work of Westbrook and Dryer [54], the order of reaction for octine is 0.25 and for oxygen is 1.5. Thus, 'm' and 'n' are physically well placed.

(c). Activation energy 'E', Equation (3-13), assumed to be linear with fuel cetane number, is given by the optimization program as:

$$E = 21022 - 119.5(CN), \qquad \text{KJ/Kg} - \text{mole}. \tag{3-16}$$

Activation energy vs. cetane number, Equation (3-16), is plotted in Fig. 3.1 together with that from Henein's [18] and Hardenberg's [20] models. Again,it would appear that the numerically determined values (a and b in Eq.(3-16)) are well placed, giving 'E' the correct order of magnitude and characteristics.

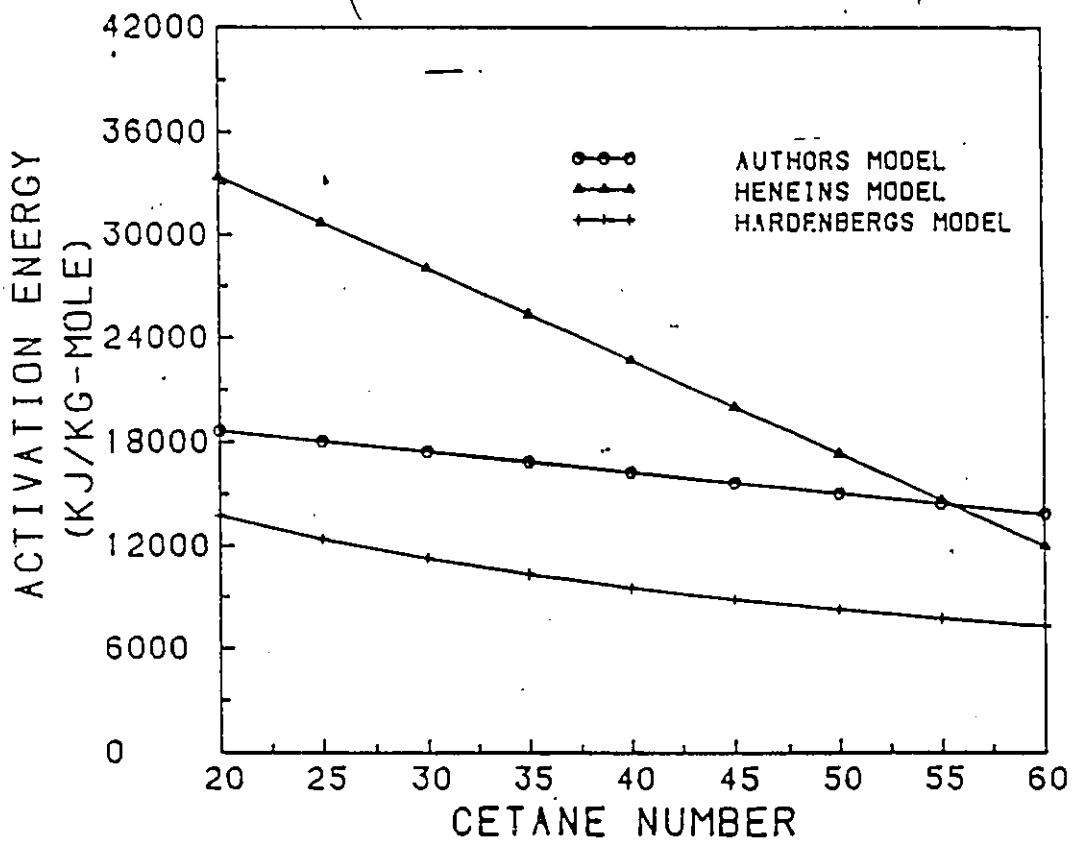

Fig. 3.1: Correlation of Cetane Number with Activation Energy

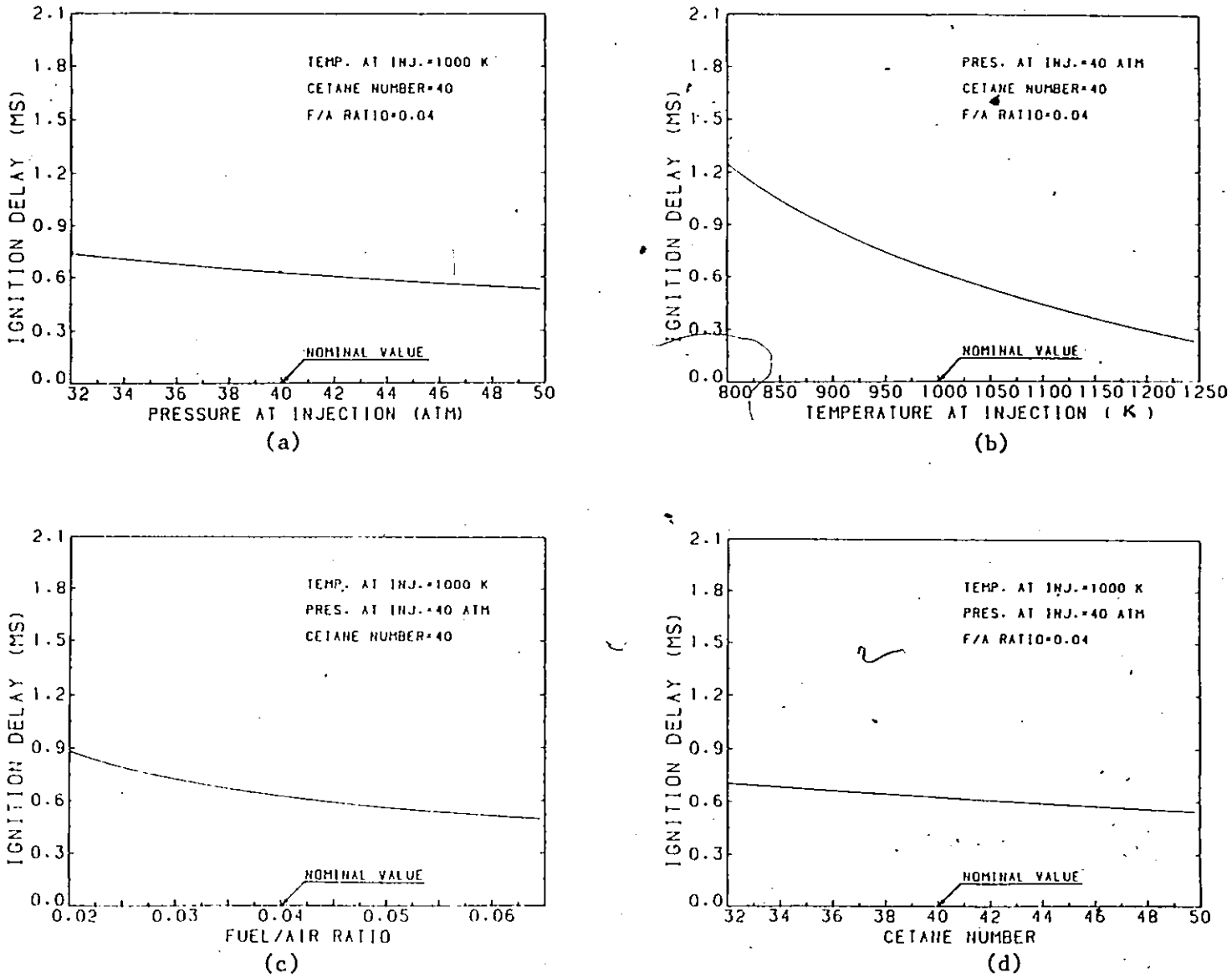

Fig. 3.2: Effect of Individual Parameters on Ignition Delay

(a) I.D. vs. Pressure at Start of Injection
(b) I.D. vs. Temperature at Start of Injection
(c) I.D. vs. F/A Ratio
(d) I.D. vs. Fuel Cetane Number

(d). No direct comparisons can be made with the remaining two constants in the equation, namely: the fuel/air ratio index 'm' determined as 0.495, and the collection of other constants 'C' determined as 2.23×10^{-8}. However, it is speculated that these values may be engine dependent, eg: piston geometry or turbulence; two stroke vs. four stroke; naturally aspirated vs. turbocharged, etc.

A general evaluation of ignition delay and comparison with experimental data requires operation of the complete thermodynamic/combustion model in order to account for the integrated effect of the parameters (pressure, temperature, F/A ratio and fuel cetane number). Such a comparison is conducted in Chapter 7, however it is of value at this time to investigate the individual parameter effects on ignition delay. For this study, ignition delay is presented in milliseconds so as to eliminate engine speed dependency and nominal values of P=40 atm, T=1000 °K, FA=0.04 and CN=40.0 were chosen. Further, the parametric range used in the plots are typical of those encountered with the 6V53T engine. Figure 3.2 gives the variation of ignition delay with each of the individual parameters. Further insight can be gained from a parameter sensitivity study as presented in Table 3-3. Here the nominal values of the parameters are varied by ±10% and the corresponding percent of variation in ignition delay is calculated. It is interesting to note the nearly linear correlation between fuel cetane number and ignition delay predicted by the model. Also the variation of ignition delay with cetane number is less pronounced than anticipated. Indeed, the effects of fuel/air ratio and pressure on ignition delay are similar to that of cetane number while temperature at the start of injection is the dominant parameter.

TABLE 3-3

IGNITION DELAY - PARAMETER SENSITIVITY ANALYSIS

(Nominal Values: P=40 atm, T=1000°K, F/A=0.04, CN=40)

PARAMETER	TEST CONDITION		PREDICTED IGNITION DELAY	
			VALUE(ms)	DEVIATION
Pressure at Injection (atm)	Nominal	40	0.6264	-
	+10%	44	0.5840	-6.8%
	-10%	36	0.6769	+8.1%
Temperature at Injection (°K)	Nominal	1000	0.6264	-
	+10%	1100	0.4389	-29.9%
	-10%	900	0.8786	+40.3%
F/A Ratio	Nominal	0.04	0.6264	-
	+10%	0.044	0.5976	-4.6%
	-10%	0.036	0.6600	+5.4%
Cetane Number	Nominal	40	0.6264	-
	+10%	44	0.5914	-5.6%
	-10%	36	0.6635	+5.9%

3.5 CLOSURE

The salient features of the analysis can be summarized as follows:

(a). An analytical ignition delay model which incorporates engine thermodynamic state (P,T at start of injection); engine operating conditions (speed and load or F/A ratio) and fuel quality (cetane number) has been developed.

(b). The generalized model Equation (3-14) may be used for any diesel engine and diesel fuel. However experimental data on ignition delay may be required so as to establish/adjust the model constants. In this regard, it is projected that the index 'm' and general constant 'C' may show variability with engine type.

(c). Model constants were evaluated for the 6V53T engine (two stroke, tur-

bocharged diesel) using an unconstrained, non-linear, multivariable numerical optimization technique with experimental data from three fuel types, three engine speeds and two load settings. The constants so determined were shown to be physically realistic values.

(d). Based on the model, ignition delay was seen to have a near linear variation with fuel cetane number. However the sensitivity of ignition delay to cetane number is similar to that of F/A ratio and pressure with temperature being the dominant parameter.

CHAPTER 4

FUEL-AIR MIXING RATE AND REACTION RATE MODELS

4.1 INTRODUCTION

For preliminary thermodynamic model development, the Whitehouse-Way model [5] was selected as a starting point due to its relative simplicity and widely accepted use in the literature. It can be summarized as follows:

Preparation Rate:

$$PR = K\ M_i^{1-x}\ M_u^{x}\ P_{O_2}^{m}, \tag{4-1}$$

Reaction Rate:

$$RR = \frac{K' \cdot P_{O_2}}{N \cdot \sqrt{T}} \cdot \exp\left(-\frac{E}{RT}\right) \cdot \int (PR - RR)\ d\alpha, \tag{4-2}$$

Where:

K, K', x, m	— constants,
M_i, and M_u	— mass of injected and unprepared fuel respectively,
T	— gas temperature,
N	— engine speed,
E	— activation energy of the fuel,
α	— crank angle degree,
P_{O_2}	— partial pressure of oxygen.

Evaluation of equations (4-1) and (4-2) by direct correlation with experimental data taken from two two-stroke engines (Foden FD6 and Rolls-Royce K60) reports the constants in the equations to be [5]:

$$\begin{aligned} K &= 0.0175 \\ x &= 1 \\ m &= 0.4 \\ K' &= 1.2 \times 10^{10} \\ E/R &= 1.5 \times 10^{4} \end{aligned} \qquad (4\text{-}3)$$

The above model was analytically investigated, for the 6V53T engine running on both Fuel 1 and No. 2-D, at a wide range of engine operating points. The general conclusions were as follows [49, 50, 51]:

a) Using the literature recommended values for the preparation and reaction rate constants (Eq. 4-3), no acceptable correlation between the predicted P-CA curve and the experimentally derived data, for either Fuel 1 or No. 2-D, could be found.

b) By manipulating the constants of Equation (4-3), high precision matching of the P-CA curves could be achieved. However, the point-to-point variation of these 'constants' eliminated any possible predictive capability of the model. That is, it could be made to simulate a known (experimental) solution, but not to predict.

Further evaluation of the model revealed two concerns. Firstly, in order to arrive at Equation (4-1), it is necessary for the number of droplets of injected fuel to be identical to the number of droplets of unprepared fuel for all time from the start of injection to the end of combustion. This does not allow for fuel to be progressively consumed or conversely requires all the fuel to be instantaneously injected at the beginning of the combustion process. Secondly, the preparation rate was not correlated with time or engine operating speed. Although it is agreed that once combustion is established, progression of combustion apparently correlates with CA, not time, concern still exists for CI engines since: (a) fuel injection rates are variable with engine speed for a fixed rack setting and this fuel mass is critical in the preparation rate equation; and (b) the sensitivity of both the correlation and calculations of indicated engine parameters requires very high precision.

Based on the above analysis and observations, a fuel-air mixing rate model was developed and the reaction rate model (4-2) was modified. The developed models are both functions of : (a) engine operating conditions (speed and load), (b) cylinder thermodynamic state (P and T), and (c) available fuel in the cylinder. These features make the simulation program more realistic and enable simulation of the engine, over its complete operating range, with considerable accuracy.

4.2 FUEL-AIR MIXING RATE MODEL

4.2.1 MODEL DEVELOPMENT

Fuel-air mixing relates to the physical processes involved from the start of liquid fuel injection to the time when a combustible fuel-air vapor mixture exists. Such processes can be expected to be a function of (1) time, (2) fuel vaporization and heating, (3) oxygen availability and entrainment, and (4) species transport.

Thus, the following are proposed:

1) Time (t) is inversely proportional to engine speed.

   Thus: $t \propto 1/N$.

2) Fuel vaporization and heating (fv) is taken directly proportional to the instantaneous environment temperature (T) and the mass of fuel unprepared (M_{fu}) plus a function of droplet size and penetration. The latter two terms are related to injector geometry and injection pressure. These in turn, can be related to a geometric constant plus a function of engine speed.

   Thus: $fv \propto C_1 \, f(N) \, T \, M_{fu}$.

3) Oxygen availability (O_a) is assumed proportional to the instantaneous oxygen density (P_{O_2}/T). It is also clear that not all oxygen becomes available for

combustion as it is limited due to the transport processes. Hence, P_{O_2} must incorporate an engine speed dependency.

Thus: $O_a \propto C_2 \, P_{O_2}^{m(N)}/T.$

4) Species transport (S_t) is again related to jet penetration and distribution plus cylinder turbulence. Thus, it is logical to assume a direct relationship with engine speed and an inverse relationship with engine load, or fuel-air equivalence ratio.

Thus: $S_t \propto C_3 g(N)/\phi^{K(N)}$.

Combining terms, the fuel-air mixing rate (MR) takes the form:

$$MR \propto C_1 C_2 C_3 \cdot \frac{f(N) \cdot g(N)}{N} \cdot \phi^{-K(N)} \cdot M_{fu} \cdot P_{O_2}^{m(N)},$$

$$\text{or :} \qquad MR = C(N) \cdot \phi^{-K(N)} \cdot M_{fu} \cdot P_{O_2}^{m(N)}. \qquad (4\text{–}4)$$

4.2.2 EVALUATION OF MODEL FUNCTIONS

A series of numerical experiments were performed, at both full and part loads for each of five engine speeds, so as to evaluate the functional relationships in Equation (4-4). For ease of execution, Equation (4-4) can, at any discrete test point 'i', be represented by:

$$MR_i = F_i \cdot M_{fu} \cdot P_{O_2}^{m_i(N)}$$

where: $F_i = C(N) \cdot \phi_i^{-K(N)}$

Thus, it is a direct matter to vary the numerical values of F_i and $m_i(N)$ so as to obtain the best numerical fit with the experimental data at each test point. Table 4–1 lists the results of the experiments conducted.

TABLE 4-1

VALUE OF MIXING RATE FUNCTIONS
FROM EXPERIMENTAL/ANALYTICAL COMPARISON

ENGINE SPEED (RPM)	$m_i(N)$	$F_i = C(N).\phi_i^{-K(N)}$		EQUIVALANCE RATIO ϕ_i	
		FULL LOAD	PART LOAD	FULL LOAD	PART LOAD
1500	1.91	0.00031	0.00051	0.824	0.401
1800	1.64	0.00059	0.00092	0.743	0.389
2200	1.33	0.00133	0.00196	0.662	0.386
2500	1.08	0.00239	0.00325	0.602	0.380
2800	0.84	0.00401	0.00520	0.549	0.379

Now, knowing the value of the function $F_i = C(N) \cdot \phi_i^{-K(N)}$ the fuel/air equivalence value ϕ_i from the thermodynamic program at two operating points (as given in Table 4-1), the value of $K(N)$ and $C(N)$ can be solved directly for any given RPM, viz:

$$F_1 = C(N)/\phi_1^{K(N)} \qquad \text{and} \qquad F_2 = C(N)/\phi_2^{K(N)} \tag{4-5}$$

rearranging:

$$K(N) = \frac{\ln(F_1/F_2)}{\ln(\phi_2/\phi_1)} \tag{4-6}$$

Using Equation (4-6) and the values of F_i from Table 4-1 together with the values of ϕ_i, the values of $K(N)$ can be solved directly as:

RPM	1500	1800	2200	2500	2800
$K(N)$	0.691	0.687	0.719	0.668	0.701

From the data, it is clear that $K(N)$ is not a function of RPM, but rather a

constant, as could have been implicated in the development, with an average value of 0.69.

Using $K(N) = 0.69$, the value of C(N) vs. RPM can be calculated from Equation (4-5) as:

RPM	1500	1800	2200	2500	2800
$C(N)$	0.00027	0.00048	0.00100	0.00168	0.00265

From the numerical experiments, it is interesting to note that engine indicated power was dominantly controlled by the functional parameter $C(N)$ while $m(N)$ affected maximum cylinder pressure. Using a least squares curve fit, $m(N)$ was found to be best represented by a linear function and $C(N)$ by a cubic polynomial. Thus, the fuel-air mixing rate model takes the general form:

$$MR = C(N) \cdot \phi^{-K} \cdot M_u \cdot P_{O_2}^{m(N)}, \qquad (kg/deg), \qquad (4\text{–}7)$$

where:

ϕ — fuel/air equivalence ratio,
M_u — mass of unburned fuel in the cylinder (Kg),
P_{O_2} — partial pressure of oxygen (bar),
N — engine speed (RPM),
K — model constant,
$C(N), m(N)$ — model functions.

For the 6V53T engine, the model parameters were found by direct comparison with experimental data as:

$$K = 0.69,$$
$$m(N) = 3.12 - 0.000815\ N,$$
$$C(N) = -0.00197 + 0.361 \times 10^{-5}\ N - 0.223 \times 10^{-8}\ N^2 + 0.546 \times 10^{-12}\ N^3.$$

Values of the model function $C(N)$ and $m(N)$ versus engine speed are calculated and plotted in Fig. 4.1.

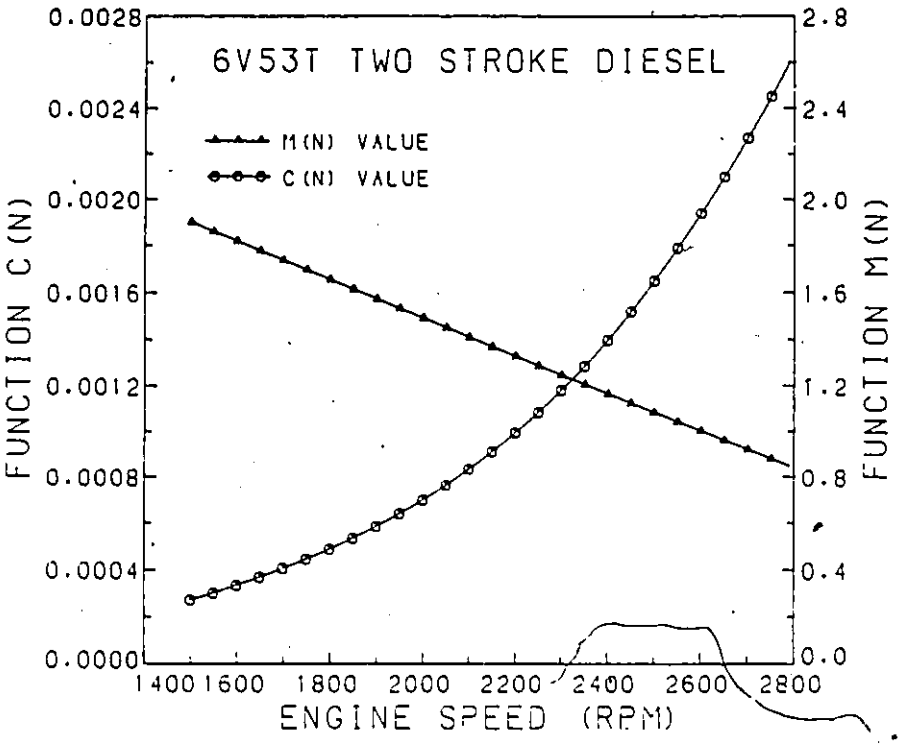

Fig. 4.1: Values of the Mixing Rate Model Function vs. Engine Speed

4.3 REACTION RATE MODEL

Once a mixture of fuel and air is formed in the cylinder, the rate of reaction/combustion will depend on the cylinder thermodynamic state (P and T) and the concentration of the premixed fuel. Arrhenius [43] postulated that reaction rate takes the form:

$$-\frac{dC_A}{dt} = K_n \cdot C_A^n \quad = \Lambda \cdot e^{-\frac{E}{RT}} \cdot C_A^n, \tag{4-8}$$

Where 'Λ' is called the frequency factor and 'E' is the activation energy. Of the many molecules present in a reacting system, Arrhenius assumed that there exist some special

molecules which have the ability to take part in a chemical reaction, by virtue of their energy. The energy of these special molecules is the activation energy,'E', and the term $e^{(-E/RT)}$ indicates the fraction of molecules that are special (i.e., energetic) and capable of participating in the reaction. The factor 'A' is a large number indicating the number of collisions between molecules in the reacting system.

Based on the Arrhenius law of reaction rate, Whitehouse and Way [5] proposed a chemical reaction rate for engine combustion of the following form:

$$\text{Rate} \sim \text{(velocity of gas molecules)(oxygen density)(mass of unburned fuel)}\ e^{(-E/RT)}.$$

Assuming that: (i) velocity of gas molecules is proportional to the square root of the temperature, (ii) the density of oxygen is proportional to the partial pressure divided by the temperature and (iii) the unburned fuel is given by $\int (PR - RR)\ d\alpha$ where PR is the preparation rate and RR is the reaction rate per degree crank angle, then the above expression can be written in the form:

$$RR = \frac{K'\ P_{O_2}}{N \cdot \sqrt{T}} \cdot \exp\left(-\frac{E}{RT}\right) \cdot \int (PR - RR)\ d\alpha. \qquad (4\text{–}9)$$

From numerical experiments conducted with the simulation program, it was found that early combustion in the diesel engine (i.e., the 3-4 crank angle degrees immediately following ignition delay) is controlled by the reaction rate of the reacting system, that is, the fuel-air mixture in the cylinder. Although it was also found that this early combustion period does not significantly affect maximum cylinder pressures or engine indicated performance, as these are primarily controlled by the fuel-air mixing rate, reaction rate does control maximum cylinder pressure rates which occur within 1-2 crank angle degrees following onset of combustion. Thus, the reaction rate model was found to be very important to the simulation in that, for the off-specification fuels, maximum cylinder pressure rates were a major concern [46,47,48].

Recognizing that K'(Eq. 4-9) correlates with 'A' (Eq. 4-8), that is, the number

of collisions between molecules in the reacting system, one can expect K' to be a function of engine load (or equivalence ratio ϕ) and engine speed (N). Thus, K' can be expected to be of the form:

$$K' = f(N) \cdot \phi^a. \tag{4-10}$$

Thus, the model parameters can be evaluated by using the same solution procedure outlined for the mixing-rate model (section 4.2.2). Table 4–2 lists the values of K' found to give a best match with experimental data for two load settings at each of five operating speeds.

TABLE 4–2

K' VALUE VS ENGINE SPEED/LOAD

ENGINE SPEED (RPM)	$K'_i = f(N)\phi_i^a$ ($\times 10^{12}$)		EQUIVALANCE RATIO ϕ_i	
	FULL LOAD	PART LOAD	FULL LOAD	PART LOAD
1500	0.860	0.265	0.824	0.401
1800	0.305	0.127	0.743	0.389
2200	0.118	0.057	0.662	0.386
2500	0.079	0.037	0.602	0.380
2800	0.060	0.030	0.549	0.379

It follows from Equation (4-10) that 'a' can be resolved for each engine speed as:

$$a = \ln\left\{\frac{K_1'}{K_2'}\right\} \Big/ \ln\left\{\frac{\phi_1}{\phi_2}\right\}. \tag{4-11}$$

Thus, from Table 4-2:

RPM	1500	1800	2200	2500	2800
a	1.63	1.35	1.34	1.65	1.87

Now, using a nominal value of $a = 1.47$, the values of $f(N)$ can be calculated from Equation (4-10) as listed in Table 4-3.

TABLE 4-3

CALCULATED f(N) VALUE

ENGINE SPEED (RPM)	f(N) VALUE ($\times 10^{13}$)		
	FULL LOAD	PART LOAD	AVERAGE
1500	0.1144	0.1020	0.1082
1800	0.0473	0.0511	0.0492
2200	0.0217	0.0233	0.0225
2500	0.0167	0.0154	0.0161
2800	0.0145	0.0125	0.0135

Also the average value of $f(N)$ can be best represented by a power function, viz:

$$f(N) = C \cdot N^{-b}, \tag{4-12}$$

where: $C = 4.66 \times 10^{22}$

$b = 3.37$

Thus, the reaction rate model can be written in a general form as:

$$RR = C \cdot \frac{\phi^a}{N^{b+1}} \cdot \frac{P_{O_2}}{\sqrt{T}} \cdot e^{-\frac{E}{RT}} \cdot \int (MR - RR)\, d\alpha, \tag{4-13}$$

where:

RR — reaction rate (Kg/deg),

MR — mixing rate (Kg/deg),

ϕ — fuel/air equivalance ratio,

P_{O_2} — partial pressure of oxygen (Bar),

T — gas temperature (K),

N — engine speed (RPM),

E — activation energy of fuel ($Kj/Kg-mole$),

R — gas constant (8.314 $Kj/Kg-mole\,^{\circ}K$),

α — crank angle degree,

$a,\ b,\ C$ — model constants.

For the 6V53T engine, the model constants were found by direct comparison with experimental data as:

$$a = 1.47$$

$$b = 3.37$$

$$C = 4.66 \times 10^{22}$$

4.4 CLOSURE

The fuel-air mixing rate model and reaction rate model represented by Equations (4-7) and (4-13) were used in the general thermodynamic and combustion simulation program. Incorporated with all other submodels, engine performance was predicted for a wide range of operating points and compared with experimental data as listed in Tables 4–4 and 4–5.

From the Tables, it can be observed that: a) model predictions of IHP, maximum pressure, pressure rate and their locations all show excellent trends over the complete engine speed range and two load settings; b) numerically, the prediction errors for indicated horsepower, maximum cylinder pressure and pressure rate are within 1% and c) the locations of maximum cylinder pressure and pressure rate are within one crank angle degree.

TABLE 4-4

MODEL PREDICTIONS AND COMPARISON WITH EXPERIMENTAL MEASUREMENTS AT FULL LOAD CONDITIONS, FUEL #1

ENGINE SPEED	INDICATED POWER (IHP)		MAXIMUM PRESSURE (psia)		MAX. P LOCATION (deg. aBDC)		MAXIMUM PRESSURE RATE (psi/deg)		MAX. DP LOCATION (deg. aBDC)	
(RPM)	M	E	M	E	M	E	M	E	M	E
1500	177.1	176.4	1656.5	1648.2	186.4	185.6	115.4	134.6	169.5	170.4
1600	192.9	190.9	1688.3	1666.0	186.4	185.7	119.6	126.3	169.7	170.3
1700	205.3	204.9	1689.6	1696.9	186.5	186.1	117.3	113.3	169.8	170.3
1800	218.3	219.4	1701.4	1668.6	186.5	186.0	121.8	118.0	169.9	170.3
1900	234.5	233.8	1735.1	1671.3	186.5	186.2	117.0	111.4	169.7	170.4
2000	243.6	245.5	1716.8	1677.4	186.5	186.3	118.1	105.5	169.9	170.6
2100	258.6	260.1	1736.3	1699.4	186.6	186.7	114.8	106.3	169.6	169.9
2200	271.4	272.8	1761.0	1728.5	186.6	186.7	110.0	101.0	169.3	169.6
2300	283.7	282.3	1784.0	1734.7	186.6	186.9	110.2	101.5	169.2	169.6
2400	291.3	291.0	1757.2	1721.5	186.6	186.8	106.5	103.0	169.3	169.6
2500	301.7	299.2	1772.5	1736.2	186.5	187.1	102.4	104.0	169.1	169.5
2600	307.2	306.7	1754.0	1745.2	186.5	187.0	96.4	99.7	169.0	169.4
2700	314.2	311.4	1756.3	1707.9	186.4	186.7	90.5	96.5	168.8	169.5
2800	320.7	322.7	1755.1	1716.2	186.3	186.8	82.0	92.1	168.5	169.5

Note: M - model prediction
E - experiment measurement

TABLE 4-5

MODEL PREDICTIONS AND COMPARISON WITH EXPERIMENTAL MEASUREMENTS AT PART LOAD CONDITIONS, FUEL #1

ENGINE SPEED (RPM)	INDICATED POWER (IHP)		MAXIMUM PRESSURE (psia)		MAX. P LOCATION (deg. aBDC)		MAXIMUM PRESSURE RATE (psi/deg)		MAX. DP LOCATION (deg. aBDC)	
	M	E	M	E	M	E	M	E	M	E
1500	91.8	91.1	1173.1	1159.3	184.7	183.3	192.3	207.3	174.2	174.8
1600	100.1	97.8	1199.3	1178.5	184.6	183.0	198.7	207.8	174.4	175.3
1700	108.1	105.6	1202.5	1194.2	184.8	183.3	195.3	199.0	174.7	175.4
1800	113.1	109.5	1189.6	1194.3	184.9	183.8	186.7	193.9	175.0	175.6
1900	122.4	122.9	1222.9	1206.8	184.8	184.1	183.8	195.7	174.7	175.7
2000	129.4	131.2	1233.1	1225.0	184.8	184.5	175.9	169.3	174.6	175.3
2100	135.7	137.4	1240.1	1218.8	184.8	184.7	167.1	161.2	174.6	175.4
2200	147.5	145.3	1273.6	1227.5	184.8	184.8	161.1	152.5	174.3	174.9
2300	155.8	154.2	1295.1	1253.8	184.8	184.9	154.1	139.0	174.1	174.6
2400	164.0	163.3	1314.6	1263.2	184.8	185.2	148.5	131.7	174.0	174.4
2500	173.2	174.4	1321.9	1282.6	184.8	185.3	139.4	136.9	173.9	174.1
2600	181.7	180.5	1347.5	1264.7	184.8	184.8	129.0	133.4	173.3	174.1
2700	188.3	189.2	1343.8	1265.1	184.8	184.7	120.2	135.7	173.3	174.2
2800	200.6	199.3	1374.8	1319.6	184.8	184.9	114.2	122.9	173.2	173.5

Note: M - model prediction
E - experiment measurement

CHAPTER 5

COMBUSTION MODEL

5.1 INTRODUCTION

This chapter describes the calculation procedure used to determine the thermodynamic state (pressure and temperature) as well as the concentration of species (reactants and products of combustion) which occur in a cylinder throughout the combustion period (see Fig. 1.2). The basic assumptions used in the combustion model are as follows.

1) Temperature and pressure are uniform throughout the cylinder.

2) Chemical reactions have reached equilibrium at the end of each calculation step. A step size of $1°CA$ is used throughout the cycle except during the ignition delay/rapid combustion/peak cylinder pressure region (30° bTDC to 10° aTDC) where a $0.1°CA$ step is used in order to more accurately trace the thermodynamic state and species concentrations during this rapidly changing period.

3) The products of combustion of a hydrocarbon-air fuel mixture can be represented by:

   a) major products – CO_2 and H_2O (plus excess air, O_2 and N_2);

   b) minor products – CO, H_2, CH_4, OH, O, H, and NO.

At the beginning of each step, the cylinder temperature and pressure (T_1, P_1) are known together with the reaction products accumulated from previous steps. During this step, fuel may be injected at temperature T_F as determined by the fuel injection model and additional fuel may be prepared for combustion as given by the fuel-air mixing rate model, however, the amount of fuel that reacts during the step is controlled by

either the reaction rate model (Eq. 4-12) or by the fuel-air mixing rate model itself (Eq. 4-7), depending on the combustion regime (see Fig. 1.2). Thus, the reactants for each step consist of the products from the previous step plus the fuel to be consumed which can be expressed as the number of moles of each of the three species: C_8H_{18}, C_6H_6 and $C_{12}H_{26}$ in accord with the proportions determined by the fuel simulation model (Section 2.3.2). At the end of each step, a new chemical equilibrium state is reached which will correlate with a new thermodynamic state, T_2 and P_2.

Now, if 'A_i' is defined as the number of moles of reactants and 'B_i' as the number of moles of products, then the overall chemical reaction formula can be written as:

$$A_1C_{m_1}H_{n_1} + A_2C_{m_2}H_{n_2} + A_3C_{m_3}H_{n_3} + A_4O_2 + A_5N_2 + A_6CO_2 + A_7H_2O$$
$$+A_8CO + A_9H_2 + A_{10}CH_4 + A_{11}OH + A_{12}O + A_{13}H + A_{14}NO$$
$$= B_4O_2 + B_5N_2 + B_6CO_2 + B_7H_2O + B_8CO + B_9H_2$$
$$+B_{10}CH_4 + B_{11}OH + B_{12}O + B_{13}H + B_{14}NO \qquad (5\text{–}1)$$

In Equation (5-1), any hydrocarbon fuel or combination of fuels could be used in the model development. In this analysis, the subscripts m_1, m_2, m_3 indicate the number of carbon atoms and n_1, n_2, n_3 indicate the number of hydrogen atoms in C_8H_{18}, C_6H_6 and $C_{12}H_{26}$ respectively. To solve, the eleven (11) unknowns in Equation (5-1) must be determined, namely the number of moles of each product (B_4 to B_{14}) together with the thermodynamic state T_2, P_2. In the following sections, twelve equations are developed, namely; four conservation equations for atomic species; the energy equation from the first law of thermodynamics for a closed system and seven equilibrium equations for the chemical reactions. These, together with the equation of state, allow a general solution for each calculation step.

5.2 MASS AND ENERGY CONSERVATION

5.2.1 CONSERVATION EQUATIONS FOR ATOMIC SPECIES

In the case of hydrocarbon fuels which burn in air, there are four atomic species: C, H, O and N. From Equation (5-1), the mass conservation of these species can be written as: (1) balance of carbon, C:

$$B_6 + B_8 + B_{10} = m_1 A_1 + m_2 A_2 + m_3 A_3 + A_6 + A_8 + A_{10} \qquad (5\text{–}2)$$

(2) balance of hytrogen, H:

$$2B_7 + 2B_9 + 4B_{10} + B_{11} + B_{13}$$
$$= n_1 A_1 + n_2 A_2 + n_3 A_3 + 2A_7 + 2A_9 + 4A_{10} + A_{11} + A_{13} \qquad (5\text{–}3)$$

(3) balance of oxygen, O:

$$2B_4 + 2B_6 + B_7 + B_8 + B_{11} + B_{12} + B_{14}$$
$$= 2A_4 + 2A_6 + A_7 + A_8 + A_{11} + A_{12} + A_{14} \qquad (5\text{–}4)$$

(4) balance of nitrogen, N:

$$2B_5 + B_{14} = 2A_5 + A_{14} \qquad (5\text{–}5)$$

5.2.2 ENERGY EQUATION

By definition, the internal energy of a gas mixture may be expressed as:

$$U = H - PV = H - NRT \qquad (5\text{–}6)$$

where the ideal gas equation of state: $PV = NRT$ is used. Thus, the first law of thermodynamics for a closed system, undergoing combustion in a cylinder, can be expressed as:

$$(H_2 - RN_2T_2) - (H_1 - RN_1T_1) = Q_{trans} - Q_{vap} - W_k \qquad (5\text{–}7)$$

where:

H_1	—	Total enthalpy of reactants (lefthand side of Eq 5-1) at T_1,
H_2	—	Total enthalpy of products (rihgthand side of Eq 5-1) at T_2,
N_1, N_2	—	Total numbers of moles at the start and end,
T_1, T_2	—	Temperatures at start and end respectively,
Q_{trans}	—	Heat added to the mixture by heat transfer through the boundary,
Q_{vap}	—	Heat reqiered to vaporize the fuel that reacts during the step and raise the temperature from T_F to T_1,
W_k	—	Work done by the system.

The enthalpies H_1 and H_2 used in Equation (5-7) are the total enthalpies which include the enthalpy of formation and relative enthalpies for each chemical species. Thus, Equation (5-7) is a general energy equation applicable to either reacting or non-reacting mixtures.

5.3 EQUILIBRIUM EQUATIONS OF CHEMICAL REACTIONS

5.3.1 EQUILIBRIUM CONSTANTS

When a mixture of reactants (hydrocarbon fuel, air and accumulated products) are allowed to react in an engine cylinder, a state of chemical equilibrium will be reached. The composition or concentration of species, at equilibrium, depends upon the temperature and pressure of the mixture. Chemical equilibrium is 'dynamic' in nature rather than 'static'; that is, at equilibrium the forward and backward reaction rates are equal. If 'k_f' and 'k_b' are the forward and backward specific reaction rate constants respectively, then in general, a chemical reaction at equilibrium can be written as:

$$a\,A + b\,B \underset{k_b}{\overset{k_f}{\rightleftharpoons}} c\,C + d\,D \tag{5-8}$$

Now, the law of mass action states that the rate at which a reaction takes place is proportional to the product of the reactant concentrations, the constant of proportionality being the specific reaction rate. Thus, if 'C_j' represents the concentration of component 'j', then for Equation (5-8), the law of mass action gives:

$$k_f\,C_A^a\,C_B^b = k_b\,C_C^c\,C_D^d, \qquad \text{or}$$

$$\frac{k_f}{k_b} = \frac{C_C^c\,C_D^d}{C_A^a\,C_B^b} = k_c, \tag{5-9}$$

where 'k_c' is called the equilibrium constant, the subscript 'c' indicates that its definition is based upon component concentrations. Now, component concentrations 'C_j' can be written in terms of partial pressures 'P_j', viz:

$$C_j = \frac{N_j}{V} = \frac{P_j}{RT}$$

Therefore,

$$\begin{aligned} k_c &= \left(\frac{P_C}{RT}\right)^c \left(\frac{P_D}{RT}\right)^d \Big/ \left(\frac{P_A}{RT}\right)^a \left(\frac{P_B}{RT}\right)^d \\ &= \frac{P_C^c\,P_D^d}{P_A^a\,P_B^b} \left\{\frac{1}{RT}\right\}^{(c+d)-(a+b)} \\ &= k_p \left\{\frac{1}{RT}\right\}^{(c+d)-(a+b)} \end{aligned} \tag{5-10}$$

where 'k_p' is the equilibrium constant based on partial pressures. Now, the term $(c + d) - (a + b)$ is the change in the number of moles (ΔN_R) due to the reaction and by definition of partial pressures, $P_j = (N_j/N_m)P$ where 'N_m' is the total number of moles in the mixture and 'P' is the total pressure. Thus, 'k_p' can be expressed as:

$$k_p = \frac{N_C^c\,N_D^d}{N_A^a\,N_B^b} \left(\frac{P}{N_m}\right)^{\Delta N_R} \tag{5-11}$$

It could be noted that values of 'k_p', as a function of temperature, are tabulated in the literature.

5.3.2 EQUILIBRIUM EQUATIONS

Based on the assumption (Sect. 5.1) that diesel engine combustion results in the following species: CO_2, H_2O, CO, H_2, CH_4, OH, O, H, and NO; seven equilibrium reactions can be written:

$$
\begin{array}{lrcl}
(1) & & CO_2 \rightleftharpoons & CO + \frac{1}{2}O_2 \\
(2) & CO_2 + & H_2 \rightleftharpoons & CO + H_2O \\
(3) & CO + & 3H_2 \rightleftharpoons & CH_4 + H_2O \\
(4) & & H_2O \rightleftharpoons & \frac{1}{2}H_2 + OH \\
(5) & & \frac{1}{2}O_2 \rightleftharpoons & O \\
(6) & & \frac{1}{2}H_2 \rightleftharpoons & H \\
(7) & \frac{1}{2}O_2 + & \frac{1}{2}N_2 \rightleftharpoons & NO
\end{array}
\qquad (5\text{–}12)
$$

For each of the chemical reactions (Eq. 5-12), the equilibrium constant (k_p, Eq. 5–11) can now be written. Referring to the overall chemical reaction formula (Eq. 5–1), the seven equilibrium equations at the end of the calculation step (i.e. at T_2 and P_2) take the form:

$$(1) \qquad k_{p_1} = \frac{B_8 \cdot B_4^{\frac{1}{2}}}{B_6} \cdot \left(\frac{P_2}{B_T}\right)^{\frac{1}{2}} \qquad (5\text{–}13)$$

$$(2) \qquad k_{p_2} = \frac{B_2 \cdot B_7}{B_6 \cdot B_9} \qquad (5\text{–}14)$$

$$(3) \qquad k_{p_3} = \frac{B_{10} \cdot B_7}{B_6 \cdot B_9^3} \left(\frac{P_2}{B_T}\right)^{-2} \qquad (5\text{–}15)$$

$$(4) \qquad k_{p_4} = \frac{B_9^{\frac{1}{2}} \cdot B_{11}}{B_7} \left(\frac{P_2}{B_T}\right)^{\frac{1}{2}} \qquad (5\text{–}16)$$

$$(5) \qquad k_{p_5} = \frac{B_{12}}{B_4^{\frac{1}{2}}} \left(\frac{P_2}{B_T}\right)^{\frac{1}{2}} \qquad (5\text{–}17)$$

$$(6) \qquad k_{p_6} = \frac{B_{13}}{B_9^{\frac{1}{2}}} \left(\frac{P_2}{B_T}\right)^{\frac{1}{2}} \qquad (5\text{–}18)$$

$$(7) \qquad k_{p_7} = \frac{B_{14}}{B_4^{\frac{1}{2}} \cdot B_5^{\frac{1}{2}}} \qquad (5\text{–}19)$$

where: $B_T = \sum_{i=4}^{14} B_i$

5.4 EVALUATION OF CYLINDER EQUILIBRIUM STATE

The established equations can now be used to determine the cylinder equilibrium state at each step in the calculation, namely: the species concentrations and thermodynamic state, T_2 and P_2. Figure 5.1 gives a flowchart of the evaluation procedure while the following provides the details of each of the steps used.

STEP 1: Estimate T_2, P_2

To begin the procedure, the thermodynamic state at the end of the calculation step can be estimated using basic polytropic equations, viz:

$$T_2 = T_1\left(\frac{V_1}{V_2}\right)^{n-1}$$
$$P_2 = P_1\left(\frac{V_1}{V_2}\right)^{n} \qquad (5\text{–}20)$$

STEP 2: Determine Equilibrium Constants

For each of the seven chemical reactions, the equilibrium constant (k_{p_i}, i = 1 to 7) can be determined from Table 5–1. A computer subroutine is used to search and interpolate the value of k_{p_i} at temperature T_2 from the tabulated data.

STEP 3: Evaluate Species Concentrations

The products of combustion are divided into two groups, namely: the major products CO_2, H_2O, O_2 and N_2, and the minor products CO, H_2, CH_4, OH, O, H and NO.

(i) By assuming that the concentrations of minor species do not change during the step, a first estimate of major species concentrations can be determined from the mass conservation Equations (5–2, 5–3, 5–4 and 5–5) as:

$$B_6 = m_1A_1 + m_2A_2 + m_3A_3 + A_6$$
$$B_7 = \tfrac{1}{2}(n_1A_1 + n_2A_2 + n_3A_3) + A_7$$
$$B_4 = A_4 - (B_6 - A_6) - \tfrac{1}{2}(B_7 - A_7) \qquad (5\text{–}21)$$
$$B_5 = A_5$$

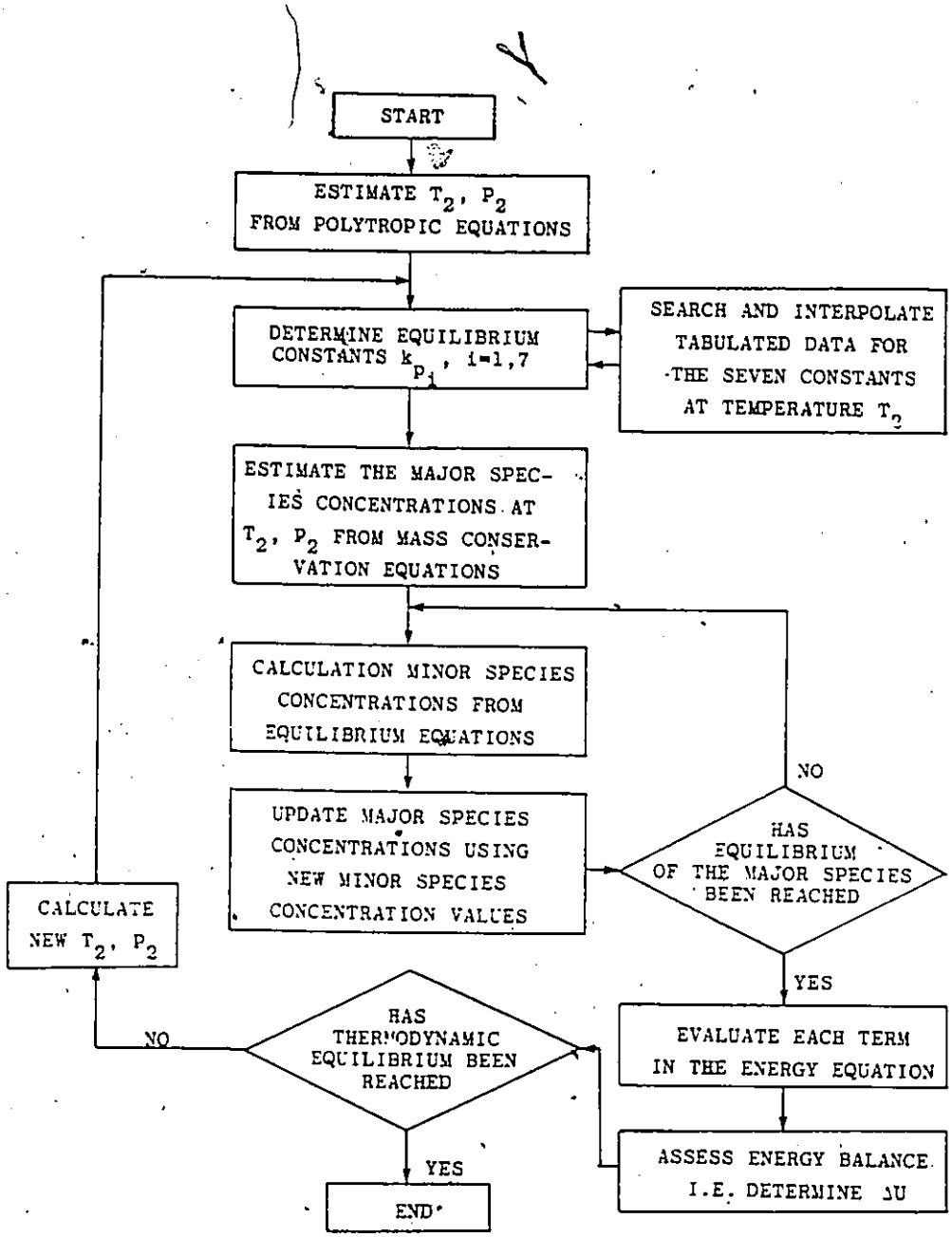

Fig. 5.1: Flow Graph of Combustion Model Equilibrium Calculation

TABLE 5-1

EQUILIBRIUM CONSTANTS FOR SEVEN REACTIONS

T°K	$Log_{10}K_p$ for Reactions						
	1	2	3	4	5	6	7
298.2		-4.50	27.02				-15.04
400.0		-2.09	16.77				-11.07
500.0		-2.02	10.70				-8.74
600.0	-20.11	-1.43	6.60				-7.20
700.0	-16.59	-1.00	3.71	-16.60			-6.07
800.0	-13.93	-0.67	1.51	-14.06			-5.22
900.0	-11.86	-0.41	-0.20	-12.07	-11.06	-9.95	-4.58
1000.0	-10.23	-0.22	-1.53	-10.50	-9.67	-8.65	-4.06
1100.0	-8.89	-0.07	-2.64	-9.22	-8.45	-7.55	-3.62
1200.0	-7.79	0.06	-3.59	-8.14	-7.46	-6.66	-3.29
1300.0	-6.81	0.17	-4.37	-7.22	-6.60	-5.90	-2.99
1400.0	-6.01	0.27	-5.06	-6.45	-5.91	-5.25	-2.71
1500.0	-5.33	0.35	-5.64	-5.78	-5.29	-4.69	-2.47
1600.0	-4.73	0.42	-6.15	-5.20	-4.75	-4.19	-2.27
1700.0	-4.19	0.48	-6.61	-4.66	-4.25	-3.75	-2.09
1800.0	-3.71	0.54	-7.00	-4.21	-3.83	-3.37	-1.94
1900.0	-3.27	0.59	-7.37	-3.79	-3.44	-3.02	-1.82
2000.0	-2.88	0.64	-7.69	-3.41	-3.10	-2.74	-1.70
2100.0	-2.54	0.69	-7.97	-3.07	-2.78	-2.44	-1.58
2200.0	-2.24	0.73	-8.23	-2.79	-2.53	-2.20	-1.47
2300.0	-1.96	0.76	-8.47	-2.52	-2.29	-1.97	-1.38
2400.0	-1.69	0.79	-8.70	-2.27	-2.06	-1.75	-1.29
2500.0	-1.43	0.82	-8.91	-2.03	-1.84	-1.55	-1.21
2600.0	-1.21	0.85	-9.10	-1.81	-1.63	-1.36	-1.14
2700.0	-1.00	0.87	-9.27	-1.60	-1.44	-1.19	-1.07
2800.0	-0.81	0.89	-9.43	-1.41	-1.26	-1.03	-1.01
2900.0	-0.63	0.91	-9.57	-1.24	-1.09	-0.89	-0.95
3000.0	-0.46	0.93	-9.72	-1.07	-0.93	-0.76	-0.90

The reactions and the corresponding numbers:

1. $CO_2 \rightleftharpoons CO + \frac{1}{2} O_2$
2. $CO_2 + H_2 \rightleftharpoons CO + H_2O$
3. $CO + 3H_2 \rightleftharpoons CH_4 + H_2O$
4. $H_2O \rightleftharpoons \frac{1}{2}H_2 + OH$
5. $\frac{1}{2} O_2 \rightleftharpoons O$
6. $\frac{1}{2} H_2 \rightleftharpoons H$
7. $\frac{1}{2}O_2 + \frac{1}{2}N_2 \rightleftharpoons NO$

(ii) Having an estimate of the major species and the values of the equilibrium constants at temperature T_2, the minor species can now be calculated from the equilibrium Equations (5–13) through (5–19) as:

$$\begin{aligned}
B_8 &= B_6 \cdot k_{p_1}/(B_4^{-\frac{1}{2}} \cdot Z^{-\frac{1}{2}}) \\
B_9 &= B_8 \cdot B_7/(B_6 \cdot k_{p_2}) \\
B_{10} &= B_8 \cdot B_9^3 \cdot Z^2 \cdot k_{p_3}/B_7 \\
B_{11} &= B_7 \cdot k_{p_4}/(B_9 \cdot Z)^{\frac{1}{2}} \\
B_{12} &= B_4^{\frac{1}{2}} \cdot k_{p_5}/Z^{\frac{1}{2}} \\
B_{13} &= B_9^{\frac{1}{2}} \cdot k_{p_6}/Z^{\frac{1}{2}} \\
B_{14} &= B_4^{\frac{1}{2}} \cdot B_5^{\frac{1}{2}} \cdot k_{p_7}
\end{aligned} \qquad (5\text{–}22)$$

where: $Z = P_2/B_T$

(iii) Again, by applying the mass conservation equations together with the calculated minor species (Eq. 5–22), an improved estimate of the major species can be made, viz:

$$\begin{aligned}
B_6 &= m_1 A_1 + m_2 A_2 + m_3 A_3 \\
&\quad + A_6 + A_8 + A_{10} - B_8 - B_{10} \\
B_7 &= \tfrac{1}{2}(n_1 A_1 + n_2 A_2 + n_3 A_3) + A_7 + A_9 + 2A_{10} \\
&\quad - B_9 - 2B_{10} + \tfrac{1}{2}(A_{11} + A_{13} - B_{11} - B_{13}) \\
B_4 &= A_4 + A_6 - B_6 \\
&\quad + \tfrac{1}{2}(A_7 + A_8 + A_{11} + A_{12} + A_{14} - B_7 - B_8 - B_{11} - B_{12} - B_{14}) \\
B_5 &= A_5 + \tfrac{1}{2}(A_{14} - B_{14})
\end{aligned} \qquad (5\text{–}23)$$

(iv) An iterative solution of Equations (5–22) and (5–23) can now be entered into until equilibrium of the major species is achieved thus giving the concentration of all species (major and minor) at the estimated thermodynamic state T_2, P_2.

STEP 4: Evaluate the Energy Equation

Having established chemical equilibrium at T_2, P_2 and knowing the overall equilibrium in the cylinder at the start (T_1, P_1), it is now possible to calculate each term in

the energy Equation (5–7).

(i) The total enthalpies H_1 and H_2 in the energy Equation (5–7) can be calculated based on the number of moles for each species and their corresponding equilibrium temperatures T_1 and T_2. Denoting the total enthalpy of any component 'i' at temperature 'T' by $h_{i,T}$, then:

$$h_{i,T} = \Delta h^{\circ}_{f,i} + (h_T - h_{298})_i \tag{5-24}$$

where Δh°_f is the enthalpy of formation at the standard reference state ($298^{\circ}K$, $1\ atm$), h_T is the enthalpy at the specified temperature T, and h_{298} is the enthalpy at the reference temperature of $298^{\circ}K$. The enthalpy of formation Δh°_f for each of the fourteen species in Equation (5–1) is listed in Table 5–2. Further, the enthalpy change $(h_T - h_{298})_i$ for each species at temperature T can be determined by interpolating the data in Table 5–3.

Thus, the total enthalpies at the beginning and end of each step can be written as:

$$H_1 = \sum_{i=1}^{14} A_i \cdot h_{i,T_1},$$
$$H_2 = \sum_{i=4}^{14} B_i \cdot h_{i,T_2}. \tag{5-25}$$

TABLE 5–2

ENTHALPY OF FORMATION

Δh°_f in Cal/g-mole

FORMULA	Δh°_f	FORMULA	Δh°_f
C_8H_{18}	-49820	CO	-26420
C_6H_6	+19820	H_2	0
$C_{12}H_{26}$	-69520	CH_4	-17890
O_2	0	OH	+10060
N_2	0	O	+59159
CO_2	-94050	H	+52089
H_2O	-57800	NO	+21600

TABLE 5-3

RELATIVE ENTHALPIES

(All relative enthalpies have been adjusted to be zero at 298°K)

Temp. °K	$h_T - h_{298}$ in Cal/g-mole													
	C_8H_{18}	C_6H_6	$C_{12}H_{26}$	O_2	N_2	CO_2	H_2O	CO	H_2	CH_4	OH	O	H	NO
300	82	31	116	13	13	17	16	13	13	17	13	9	9	14
310	519	199	790	83	82	108	96	82	81	105	84	59	59	86
320	965	385	1523	154	152	199	173	152	150	193	155	109	109	158
330	1421	589	2306	224	221	292	257	222	219	281	226	159	159	231
350	2392	1077	3894	367	361	481	423	362	358	466	367	258	258	376
400	4903	2365	7984	726	711	961	832	712	706	940	720	507	507	738
450	7652	3785	12545	1091	1062	1463	1244	1064	1055	1441	1073	755	755	1099
500	10637	5336	17507	1460	1415	1985	1660	1419	1405	1977	1427	1003	1003	1462
600	17377	8842	28517	2214	2127	3088	2508	2138	2105	3163	2135	1500	1500	2190
700	25066	12801	40665	2990	2855	4250	3383	2870	2808	4484	2843	1996	1996	2935
800	33701	17152	53840	3788	3597	5458	4292	3622	3514	5932	3554	2493	2493	3709
900	43284	21825	67954	4604	4355	6707	5231	4394	4225	7502	4272	2990	2990	4507
1000	53815	26750	82925	5431	5130	7994	6195	5183	4941	9184	4999	3486	3486	5320
1100	65352			6270	5921	9310	7186	5986	5666	10971	5735	3983	3983	6143
1200				7119	6724	10649	8207	6798	6403	12842	6479	4479	4479	6972
1300				7976	7537	12010	9258	7619	7152	14782	7237	4976	4976	7810
1400				8838	8356	13387	10331	8449	7909	16781	8012	5473	5473	8657
1500				9707	9184	14779	11428	9287	8675	18831	8802	5969	5969	9511
1600				10588	10021	16186	12548	10132	9450	20927	9598	6466	6466	10371
1700				11475	10867	17605	13693	10983	10234	23062	10402	6962	6962	11234
1800				12366	11720	19036	14860	11838	11029	25235	11213	7459	7459	12109
1900				13259	12575	20475	16048	12700	11834	27444	12029	7956	7956	12976
2000				14155	13432	21922	17252	13566	12650	29688	12852	8452	8452	13852
2100				15060	14293	23376	18472	14436	13473	31961	13684	8949	8949	14730
2200				15971	15158	24836	19703	15310	14302	34257	14522	9445	9445	15612
2300				16889	16027	26303	20944	16186	15136	36574	15367	9942	9942	16496
2400				17812	16898	27778	22197	17063	15980	38910	16221	10438	10438	17383
2500				18739	17771	29259	23463	17941	16829	41266	17082	10935	10935	18272
2600				19669	18846	30746	24740	18820	17687	43640	17951	11431	11431	19164
2700				20604	19524	32237	26025	19701	18641	46026	18822	11928	11928	20057
2800				21545	20406	33732	27318	20586	19419	49329	19697	12425	12425	20952
2900				22494	21291	35230	28619	21472	20287		20576	12921	12921	21851
3000				23446	22178	36732	29928	22360	21162		21458	13418	13418	22758

(ii) In the 'NRT' terms, N_1 and N_2 are the total number of moles in the cylinder at T_1 and T_2 respectively, thus:

$$N_1 = \sum_{i=1}^{14} A_i, \qquad \text{and}$$
$$N_2 = \sum_{i=4}^{14} B_i. \tag{5–26}$$

(iii) Q_{trans} is the heat transferred through the boundary and calculated using Woschni's model as detailed in Section 2.5,

(iv) Q_{vap} is the heat required to vaporize and raise the temperature of the liquid fuel from injection temperature T_F to cylinder gas temperature T_1 for each calculation step, the mass of fuel 'ΔM' is that determined by the fuel-air mixing rate model. Thus:

$$Q_{\text{vap}} = \Delta M[L + C_F(T_1 - T_F)] \tag{5–27}$$

where: L — Latent heat of vaporization,

C_F — Specific heat of fuel.

(v) The work done by the gases in the cylinder is directly evaluated from the mean cylinder pressure as:

$$W_k = (\frac{P_1 + P_2}{2})(V_2 - V_1) \tag{5–28}$$

STEP 5: Assess Energy Balance

The energy equation will be satisfied only at thermodynamic equilibrium. Thus, an energy balance, namely:

$$\Delta U = [(H_2 - RN_2T_2) - (H_1 - RN_1T_1)] - [Q_{\text{trans}} - Q_{\text{vap}} - W_k] \tag{5–29}$$

will establish the overall state of equilibrium. In practice, overall equilibrium was assumed to have been reached when the final temperature T_2 did not vary by more than half a degree Kelvin, viz:

$$\Delta T_2 = \left|\frac{\Delta U}{C_{vp}}\right| < 0.5 \qquad (^\circ K). \tag{5–30}$$

where C_{vp} is the average specific heat of total combustion products in the cylinder, and if C_{vi} is specific heat of product 'i', then

$$C_{vp} = \sum_{i=4}^{i=14} B_i C_{vi}$$

If equilibrium has not been achieved, then new estimates of T_2 and P_2 can be made, namely:

$$T_{2,\text{new}} = T_{2,\text{old}} - \frac{\Delta U}{C_{vp}}$$
$$P_{2,\text{new}} = P_1 \left(\frac{N_2}{N_1}\right)\left(\frac{T_{2,\text{new}}}{T_1}\right)\left(\frac{V_1}{V_2}\right) \qquad (5\text{–}31)$$

and an iterative solution, going back to Step 2, can be executed until equilibrium is achieved.

CHAPTER 6

BLOWDOWN AND SCAVENGING MODEL

6.1 INTRODUCTION

The period during which the combustion products in a cylinder are replaced by a fresh charge is referred to as the gas exchange period. This period, in a two-stroke engine, consists of two processes: (a) the blowdown process in which the exhaust valves open near the end of the expansion stroke, thus allowing cylinder pressure to drop quickly to the exhaust pressure, and (b) the scavenging process during which both intake ports and exhaust valves are open.

During the gas exchange period, the cylinder thermodynamic state and contents are determined by the blowdown and scavenging model. The model developed assumes that the flow through the cylinder intake ports and exhaust valves is isentropic in a converging nozzle. The mass flow of fresh air into the cylinder depends on the airbox pressure P_{ab} and temperature T_{ab}, cylinder pressure P_c and the intake port opening area A_{in}, while the mass flow out of the cylinder depends on the cylinder pressure P_c and temperature T_c, exhaust back pressure P_e and the exhaust valve opening area A_{out}. Fig. 6.1 shows a schematic of the gas exchange model. Airbox conditions T_{ab} and P_{ab} are treated as known parameters from experimental data and P_e is assumed to be a function of airbox pressure, viz: $P_e = K_{bp}P_{ab}$ while K_{bp} is referred to as the exhaust back pressure coefficient. Alternatively, P_{ab}, T_{ab} and P_e could be determined from a simulation of the turbocharger and blower. The timing and area, as a function of crank angle position, for both the exhaust valves and intake ports are based on engine design. This data is given, for the 6V53T engine, in Chapter 2, Figures 2.1 and 2.2 and Table 2–2.

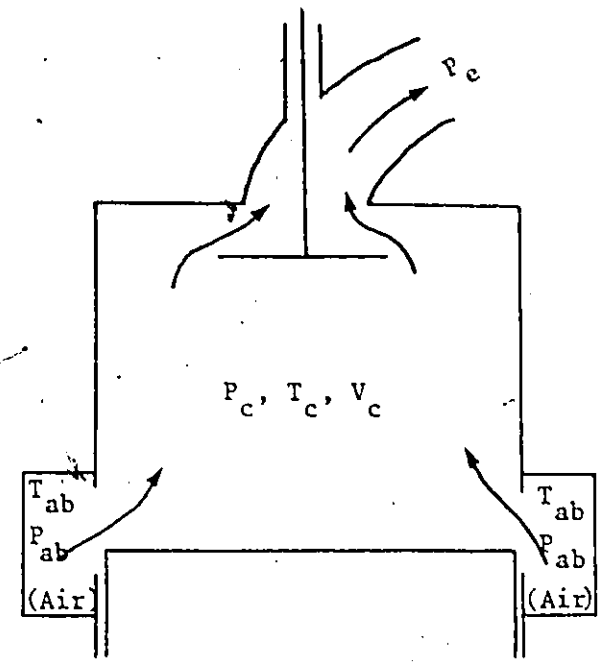

(a) Engine Simulation

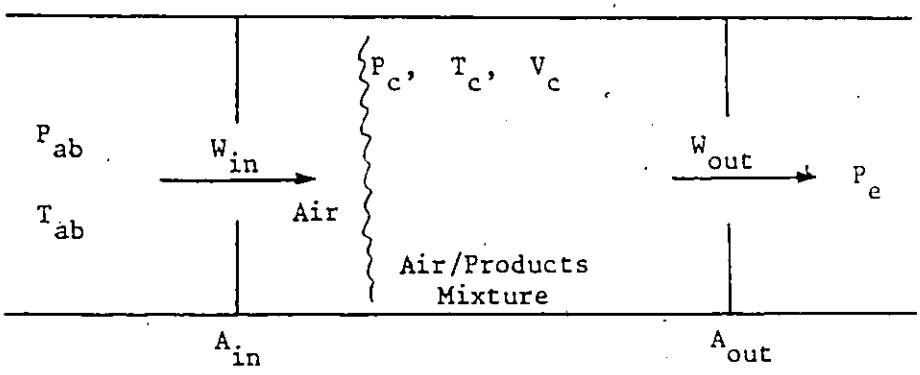

(b) Equivalent System

Fig. 6.1: Gas Exchange System Schematic

During scavenging, the mixing pattern of fresh air and cylinder gases is a complicated process. This can be reasonably well evaluated by using multidimensional techniques. In this model, a mixing coefficient 'ς' is introduced so as to allow some flexibility in selecting the mixing pattern. When $\varsigma = 0$, there is no mixing in the cylinder and fresh air accumulates; at the other extreme, when $\varsigma = 1$, the fresh charge is completely mixed with the cylinder gasses. In reality ς should lie between the two extremes.

Thus, the model developed simulates the cylinder thermodynamic state (T and P) and contents (mass and constituents) as a function of crank angle position and given airbox conditions (P_{ab} and T_{ab}).

6.2 MASS FLOW THROUGH THE CYLINDER

6.2.1 FLOW INTO THE CYLINDER

As outlined, the intake process is modeled as isentropic air flow in a converging section with upstream airbox pressure P_{ab} and temperature T_{ab}, downstream cylinder pressure P_c and intake port opening area A_{in}. From gas dynamic theory, in a converging section, the Mach number 'M' cannot increase beyond unity for isentropic flow. If P^* is the critical pressure at the throat for $M = 1.0$, then the critical pressure ratio 'P_{cr}' for the fresh intake air is given by:

$$P_{cr} = \frac{P^*}{P_{ab}} = \left(\frac{2}{K+1}\right)^{\frac{K}{K-1}}. \qquad (6\text{–}1)$$

For intake air at $300 - - - 350°K$, the specific heat ratio $K = 1.4$. Then, $P_{cr} = 0.528$ and three possible flow patterns exist.

CASE I:

if: $\frac{P_c}{P_{ab}} < 0.528$, then the flow is choked and;

$M_{in} = 1.0,$

$P_{in} = P^* = 0.528\ P_{ab}.$

CASE II:

if: $1.0 > \frac{P_c}{P_{ab}} > 0.528$, then the flow is not choked and;

$P_{in} = P_c,$

$$M_{in} = \left\{ \left[\left(\frac{P_{ab}}{P_{in}} \right)^{\frac{K-1}{K}} - 1 \right] \frac{2}{K-1} \right\}^{\frac{1}{2}}.$$

CASE III:

if: $\frac{P_c}{P_{ab}} > 1.0$, then inverse flow occurs and

$P_{in} = P_{ab},$

$$M_{in} = \left\{ \left[\left(\frac{P_c}{P_{in}} \right)^{\frac{K-1}{K}} - 1 \right] \frac{2}{K-1} \right\}^{\frac{1}{2}}.$$

In practice, Cases I and III will not occur during a normal scavenging process. Now, having identified the flow pattern, the mass flow of fresh air into the cylinder (W_{in}) during a time step 'dt' is given by:

$$W_{in} = \dot{W}_{in}\ dt \tag{6-2}$$

where:

Flow Rate :	$\dot{W}_{in} = \rho_{in}\ M_{in}\ C_{in}\ A_{in}$	
Density:	$\rho_{in} = \frac{P_{in}/g}{R\ T_{in}}$	
Speed of Sound:	$C_{in} = \sqrt{K\ g\ R\ T_{in}}$	
Temperature:	$T_{in} = \frac{T_{ab}}{1+\frac{K-1}{2}M_{in}^2}$	(Cases I and II)
	$T_{in} = \frac{T_c}{1+\frac{K-1}{2}M_{in}^2}$	(Case III)

6.2.2 MASS FLOW OUT OF THE CYLINDER

For flow out of the cylinder, the gas specific heat ratio is taken as $K = 1.36$. Thus, the critical pressure ratio, from Equation (6–1), is 0.535 and the three possible flow patterns can be summarized as follows:

CASE I:

if: $\frac{P_e}{P_c} < 0.535$, then the flow is choked and;

$M_{out} = 1.0$

$P_{out} = P^* = 0.535\ P_c$

CASE II:

if: $1.0 > \frac{P_e}{P_c} > 0.535$, then the flow is not choked and;

$P_{out} = P_e$

$$M_{out} = \left\{ \left[\left(\frac{P_c}{P_{out}} \right)^{\frac{K-1}{K}} - 1 \right] \frac{2}{K-1} \right\}^{\frac{1}{2}}$$

CASE III:

if: $\frac{P_e}{P_c} > 1.0$, then inverse flow occurs and;

$P_{out} = P_c$

$$M_{out} = \left\{ \left[\left(\frac{P_e}{P_{out}} \right)^{\frac{K-1}{K}} - 1 \right] \frac{2}{K-1} \right\}^{\frac{1}{2}}$$

For most of the blowdown period, Case I will apply due to the high cylinder pressure. Thus, the mass flow out of the cylinder during a time step 'dt' can be written as:

$$W_{out} = \dot{W}_{out}\ dt \qquad (6\text{–}3)$$

where:

Flow Rate: $\dot{W}_{out} = \rho_{out}\ M_{out}\ C_{out}\ A_{out}$

Density: $\rho_{out} = \frac{P_{out}/g}{R \cdot T_{out}}$

Speed of Sound: $C_{out} = \sqrt{K\ g\ R\ T_{out}}$

Temperature: $T_{out} = \frac{T_c}{1 + \frac{K-1}{2} M_{out}^2}$ (Cases I and II)

$T_{out} = \frac{T_e}{1 + \frac{K-1}{2} M_{out}^2}$ (Case III)

6.2.3 CYLINDER CONTENTS

It is now a direct matter to establish the cylinder contents for each step by applying Equations (6-2) and (6-3) together with the mixing coefficient 'ς'. At the beginning of each step, the cylinder contents are known and consist of two parts, namely: (i) the mass of fresh air, $W_{1,\text{fresh}}$, and (ii) the mass of mixed air and products, $W_{1,\text{mixed}}$. Thus, at the beginning of each step;

$$W_1 = W_{1,\text{fresh}} + W_{1,\text{mixed}}$$

and, at the end of each step;

$$W_2 = W_{2,\text{fresh}} + W_{2,\text{mixed}} = W_1 + W_{in} - W_{out} \qquad (6\text{–}4)$$

where:

$$W_{2,\text{fresh}} = W_{1,\text{fresh}} + (1 - \varsigma)W_{in}$$

$$W_{2,\text{mixed}} = W_{1,\text{mixed}} + \varsigma\, W_{in} - W_{0ut}$$

The number of moles of each species (B_i, $i = 4, 14$; see Chapter 5, Eq. 5–1) can now be readily established. Details of this calculation are presented in the following section.

6.3 CYLINDER THERMODYNAMIC STATE

The thermodynamic state in the cylinder during blowdown and scavenging is governed by the first law for open systems, viz:

$$Q_{in} - W_k = U_2 - U_1 - H_{in} + H_{out}$$

or

$$U_2 = U_1 + H_{in} - H_{out} + Q_{in} - W_k \qquad (6\text{–}5)$$

where:

U_2 — final internal energy in the system at T_2

U_1 — initial internal energy in the system at T_1

H_{in} — incoming enthalpy of W_{in}

H_{out} — outflowing enthalpy of W_{out}

Q — heat transfer into the system

W_k — work done by the system

Further, by definition;

$$U = H - PV = H - NRT \tag{6–6a}$$

and the total enthalpy per unit mole of species is:

$$h = \Delta h_f^\circ + (h_T - h_{298}) \tag{6–6b}$$

where:

Δh_f° — enthalpy of formation

$(h_T - h_{298})$ — relative enthalpy (tabulated)

Thus, if N_i is the number of moles of each species 'i', then U takes the form:

$$U = \sum_{i=1}^{n} N_i \cdot h_i - NRT \tag{6–6c}$$

The cylinder thermodynamic state at the end of each step must satisfy the energy Equation (6-5). Having established the cylinder contents, (Section 6.2.3), an iterative solution can be directly applied as outlined below.

STEP 1: Estimate T_2, P_2

$$T_2 = T_1\left[\left(\frac{W_2}{W_1}\right)\left(\frac{V_1}{V_2}\right)\right]^{k-1}, \tag{6–7a}$$

$$P_2 = P_1\left(\frac{W_2}{W_1}\right)\left(\frac{T_2}{T_1}\right)\left(\frac{V_1}{V_2}\right). \tag{6–7b}$$

STEP 2: Calculate U_1

$$U_1 = \sum_{i=4}^{14} A_i \cdot h_i - W_1 R T_1 \tag{6–8}$$

where:

A_i — number of moles of each of the eleven species in the cylinder at the beginning of each step,

h_i — total enthalpy per mole of each species per Equation (6–6).

STEP 3: Calculate H_{in}

$$H_{in} = N_{O_2} \cdot h_{O_2} + N_{N_2} \cdot h_{N_2} \qquad (6\text{–}9)$$

where:

$N_{O_2} = 0.21(W_{in}/28.96)$, the number of moles of oxygen in the inflowing mass W_{in},

$N_{N_2} = 0.79(W_{in}/28.96)$, the number of moles of nitrogen in the inflowing mass W_{in},

h_{O_2}, h_{N_2} are the total enthalpies per unit mole of O_2 and N_2 at airbox temperature T_{ab} as per Equation (6–6).

STEP 4: Calculate H_{out}

There are two possible cases for the calculation of H_{out} depending on mixture availability.

(i) If the mass of the cylinder mixture of fresh air and exhaust gases, W_2, is greater than the outflow W_{out}, then all of the outflow mass is from the mixture at an average temperature of $(T_1 + T_2)/2$.

Thus, the enthalpy out of the cylinder is:

$$H_{out} = \sum_{i=4}^{14} \left(\frac{W_{out}}{W_{1,\text{mixed}}}\right) \cdot A_i \cdot h_i \qquad (6\text{–}10a)$$

Further, the number of moles at the end of the step can now be determined as:

$$\text{for} \quad O_2 \; : \quad B_4 = (1 - \frac{W_{out}}{W_{1,\text{mixed}}}) \cdot A_{4,\text{mixed}} + A_{4,\text{fresh}} + N_{O_2}$$

$$\text{for} \quad N_2 \; : \quad B_5 = (1 - \frac{W_{out}}{W_{1,\text{mixed}}}) \cdot A_{5,\text{mixed}} + A_{5,\text{fresh}} + N_{N_2}$$

where $A_{4,\text{mixed}}$ and $A_{5,\text{mixed}}$ are the number of moles of O_2 and N_2 in the mixture respectively, and $A_{4,\text{fresh}}$ and $A_{5,\text{fresh}}$ are those in the fresh air.

For the remaining species; CO_2, H_2O, CO, H_2, CH_4, OH, O, H and NO (i=6 to 14), then

$$B_i = \left(1 - \frac{W_{out}}{W_{1,mixed}}\right) \cdot A_i.$$

(ii) If the outflow mass, W_{out}, is greater than the mass of available mixture, then the model assumes that all of the outflow is from the accumulated air. Thus, the enthalpy out at average cylinder temperature $(T_1 + T_2)/2$ is:

$$H_{out} = \sum_{i=4}^{14} \left(\frac{W_{out}}{W_{1,fresh}}\right) \cdot A_i \cdot h_i \qquad (6\text{–}10b)$$

and the number of moles at the end of the step can be written as:

$$\text{for} \quad O_2 \; : \quad B_4 = (1 - \frac{W_{out}}{W_{1,fresh}}) \cdot A_4 + N_{O_2},$$
$$\text{for} \quad N_2 \; : \quad B_5 = (1 - \frac{W_{out}}{W_{1,fresh}}) \cdot A_5 + N_{N_2},$$

and for the remaining species numbered from 6 to 14:

$$B_i = \left(1 - \frac{W_{out}}{W_{1,fresh}}\right) \cdot A_i.$$

STEP 5: Determine Q_{in}

Q_{in} is calculated by the heat transfer model established in Chapter 2, Section 2.4.

STEP 6: Determine W_k

$$W_k = (\frac{P_1+P_2}{2}) \; (V_2 - V_1) \qquad (6\text{–}11)$$

STEP 7: Assess Thermodynamic State

The accuracy of the estimated thermodynamic state in the cylinder (T_2, P_2) can now be assessed by invoking the energy Equation (6-5) since the total internal energy 'U_2' can now be calculated directly as:

$$U_2 = \sum_{i=4}^{14} B_i \cdot h_i - W_2 R T_2 \qquad (6\text{–}12)$$

Now, Equation (6-5) can be written as an energy balance where $\Delta U \rightarrow 0$, viz:

$$\Delta U = U_2 - (U_1 + H_{in} - H_{out} + Q_{in} - W_k) \qquad (6\text{–}13)$$

Now ΔU can be used to improve T_2 and P_2:

$$T_{2,new} = T_{2,old} - \frac{\Delta U}{C_{vp}}$$

$$P_{2,\text{new}} = P_1\left(\frac{W_2}{W_1}\right)\left(\frac{T_{2,\text{new}}}{T_1}\right)\left(\frac{V_1}{V_2}\right)$$

where C_{vp} is the average specific heat for total mass of cylinder mixture as expressed in Chapter 5.

STEP 8: Iterate

Using the new values of T_2 and P_2, steps 2—7 can be repeated to reduce the unbalanced internal energy ΔU. In practice, this iteration is repeated until:

$$\Delta T_2 = \left|\frac{\Delta U}{C_{vp}}\right| < 0.5 \qquad °K.$$

6.4 EVALUATION OF THE MODEL

In developing the blowdown and scavenging model, two parameters were introduced to add generality, namely: (i) the mixing rate coefficient 'ς', and (ii) the exhaust back pressure coefficient 'K_{bp}'.

The mixing rate coefficient does not have any significant impact on cylinder thermodynamic state nor on scavenging flow rates or trapped mass. In the model, it correlates with the residual gases (combustion products) remaining in the cylinder at the end of the scavenging period. For the 6V53T engine, no data was available in this regard, thus a nominal value of 0.5 was chosen.

On the other hand, the exhaust back pressure coefficient strongly affects scavenging flow rates (Table 6–1) which were also experimentally measured over the full operating range of the engine. Through a series of numerical experiments and correlation with available data, a value of $K_{bp} = 0.9$ was selected.

TABLE 6-1

EFFECT OF BACK PRESSURE COEFFICIENT K_{bp} ON FLOW RATE

ENGINE SPEED (RPM)	2200	2200	2200	2200	2200
BACK PRESSURE COEF. K_{bp}	0.86	0.88	0.90	0.92	0.94
FLOW RATE (Kg/Cyl/Cyc.)$\times 10^{-3}$	0.236	0.221	0.203	0.183	0.161

CHAPTER 7

MODEL EVALUATION

7.1 INTRODUCTION

The thermodynamic and combustion model developed in Chapters 2 through 6 consists of a number of sub-models, principal among them being: fuel simulation; initial conditions; heat transfer; fuel injection schedule; ignition delay; fuel-air mixing rate; reaction rate; equilibrium combustion; blowdown and scavenging; cylinder thermodynamic state; etc. The empirical constants and functions in these sub-models were evaluated for the 6V53T engine operating at discrete test points. Further, many of the sub-models are not only original but unique in the respect that they reflect not only engine speed and load characteristics but also fuel specification data.

The objective of this chapter is to thoroughly investigate the ability (and accuracy) of this model to simulate the behavior of the 6V53T engine at all speed/load conditions for each of the three test fuels; in particular, to assess (i) sub-model integration and interaction; (ii) behavioral trends and numerical accuracy; and (iii) the subtleties of fuel-to-fuel characteristics. This is accomplished through direct comparisons with an extensive experimental base established as part of the overall program [45, 46, 47, 48], which includes both indicated and combustion characteristics for all three test fuels, and through comparisons with the open literature.

7.2 OVERALL MODEL EVALUATION

All indicated and combustion characteristic data are derived from the cylinder pressure curve. Thus, a general comparison of the pressure–crank angle (P-CA) curves

provide an important overall assessment of the model. Numerical accuracy of the model is best judged by indicated performance characteristics (i.e. the integrated P-CA curve) and subtleties of the model by specific characteristics of the P-CA curve, such as maximum cylinder pressures and pressure rates and their locations. This section assesses all of these aspects for the complete engine speed/load range and for all three test fuels. *

7.2.1 $P - CA$ COMPARISON

Figures 7.1 through 7.9 plot cylinder pressure vs. crank angle for the complete cycle together with the experimentally measured values. The complete engine speed range (1500, 2200 and 2800 RPM), at both full load and part load, * for each of the test fuels is presented. All of the curves show excellent correlation with the experimental data for all of the cycle processes, namely: compression, heat transfer, injection, ignition delay, rapid combustion, main combustion, expansion and tail combustion, blowdown and scavenging.

It could be noted that compression is initial condition model controlled, start of combustion is ignition delay model controlled, early combustion is reaction rate model controlled, main combustion is fuel-air mixing rate model controlled and the gas exchange process is blowdown and scavenging model controlled. Further, the cylinder gas thermodynamic state (pressure and temperature) and constituents (combustion product species and concentrations) are determined by the equilibrium combustion model together with the integrated effects of a number of sub-models principal among which are the fuel simulation and heat transfer models.

Several pertinent observations from the P-CA plots can be made: (i) the sub-

* Throughout this report, the general term 'part-load' implies a brake torque output of 250 ft-lbs. unless otherwise specified.

model integration is effective; (ii) the model moves from fuel-to-fuel and from test point-to-point (engine speed and load) with considerable accuracy, (iii) the subtle differences of early combustion (rapid pressure rise at the start of combustion) are reflected between fuel and engine test points, and (iv) fuel property effects on the pressure curves are evident.

7.2.2 MAXIMUM CYLINDER PRESSURE

Maximum cylinder pressure and location on the P-CA diagram are both critical parameters that relate to engine combustion analysis and design, especially at full load operating conditions. The values of maximum cylinder pressure are important for engine mechanical design and the maximum pressure location will strongly affect the thermodynamic performance of the engine. With respect to the model, these values are the integrated effect of many sub-models, including such key models as fuel injection timing and rate, ignition delay, fuel-air mixing and reaction rates and combustion.

Figure 7.10 plots maximum cylinder pressure vs. engine speed, at both full and part loads, for each of the three fuels. The experimental data points, at each 100 RPM. are also shown. The location of maximum pressure, together with the experimental data, is shown in Fig. 7.11 for all three fuels. From a study of these plots, several items are noted.

i) Excellent correlation between the model and experimental data exists at all engine speed/load settings and for each fuel. Maximum pressures are typically within several percent and locations within one crank angle degree.

ii) Model trending is accurate. Subtle changes in maximum cylinder pressure and its location due to engine speed, engine load and fuel properties are all correctly interpreted by the model.

7.2.3 MAXIMUM PRESSURE RATE

In a diesel engine, a period of 'rapid combustion' lasting only several crank angle degrees (typically less than half a milli-second), always directly follows ignition delay (or onset of combustion). It is during this period when diesel knock may occur and can be identified (experimentally) as large pressure rate fluctuations. From the experimental program, knock was one of the key concerns identified when burning Fuels 3 and 4. Thus, when developing the thermodynamic/combustion model, the early combustion period was given special consideration. In this simulation, early combustion is directly controlled by the reaction rate model and indirectly through fuel property correlations, the ignition delay and fuel-air mixing rate models.

Figure 7.12 shows maximum pressure rate as a function of engine speed at two load settings for each of the three fuels. The corresponding experimental data points are also plotted. It is clear from the plots that this rapid combustion period, at least with respect to maximum pressure rates, is fairly accurately simulated. Pressure rate trends as a function of fuel properties, engine speed and engine load are correct (eg. high pressure rates are associated with low speed, low load engine operation and with low cetane fuels) and the numerical values predicted are accurate. The model does tend to predict the location of maximum pressure rate (Fig. 7.13) about one crank angle degree early for the off-specification fuels. This, however, is not a significant variation.

It could be noted that this early combustion period does not significantly affect maximum cylinder pressures nor engine indicated performance. This could account for the almost total lack of attention given it in the literature. However, for engine-fuel studies, pressure rates are one of the key parameters to be evaluated.

7.2.4 ENGINE INDICATED PERFORMANCE

When the cycle is closed by the simulation program, the cylinder pressure curve can be used to generate the indicated engine performance. Basically, the indicated mean effective pressure ($IMEP$), indicated horsepower (IHP), indicated thermal efficiency (η_{th}) and indicated specific fuel consumption ($ISFC$) are of general interest. The total work done during the cycle can be obtained by summing the work of each step, viz:

$$W_{k,T} = \sum_i (\frac{P_i + P_{i+1}}{2})(V_{i+1} - V_i) \ , \qquad (N - M). \tag{7-1}$$

Thus, the indicated mean effective pressure can be expressed as:

$$\text{IMEP} = W_{k,T}/V_h \qquad (N/M^2) \tag{7-2}$$

where V_h is the cylinder displacement and indicated power for the engine becomes:

$$\text{Power} = i \cdot W_{k,T} \cdot N/60 \ , \qquad (W) \tag{7-3}$$

where 'i' is the number of cylinders and 'N' is the engine speed (RPM), or:

$$\text{IHP} = 2.235 \times 10^{-5} \cdot i \cdot W_{k,T} \cdot N. \qquad (HP) \tag{7-4}$$

Indicated thermal efficiency is:

$$\eta_{th} = -\frac{W_{k,T}}{\Delta H_R \cdot M_t} \times 100\% \tag{7-5}$$

Where the minus sign allows for the sign of the heat of reaction ΔH_R and M_t is the total mass of fuel injected into a cylinder.

The model predictions for the 6V53T engine indicated performance, i.e. IHP, IMEP, ISFC and η_{th} are plotted in Figures 7.14 to 7.17 for the three fuels as a function of engine speed. Experimental results, under the same operating conditions, are also given on each plot and excellent correlation exists at all engine speeds and loads and for each fuel. This is not surprising since these parameters are based on cylinder

pressure simulation and the P-CA curve was shown to reflect all phases of the cycle with considerable accuracy. IHP is considered to be the key engine performance 'measure' and, in this regard, the model trends are vary accurate (re. engine speed, engine load and fuel type). Numerically, only slight variations from experimental data exist for Fuels 3 and 4, at full load with Fuel 3 being 1–2% higher and Fuel 4 being 2–3% lower than the experimental value.

7.2.5 SUMMARY

In this section, the overall model behavior was evaluated by focusing on engine performance criterion (IHP, etc.); cylinder thermodynamic simulation (maximum cylinder pressure and location); fuel combustion characteristics (maximum cylinder pressure rate and location) as well as overall P-CA comparisons. It was shown that the model exhibits exact trending as well as considerable numerical accuracy at all engine speed/load settings and for all test fuels. In the following section specific areas of interest are examined including: ignition delay, cycle closure or the blowdown and scavenging process, heat transfer and combustion products/emissions.

7.3 SPECIFIC EVALUATIONS

7.3.1 IGNITION DELAY

From model analyses [49, 50, 51], it was shown that ignition delay was a key factor affecting early combustion behavior in a diesel engine and that the need for an explicit ignition delay model was clear. The model in Chapter 3 represents ignition delay as a direct function of engine operating speed and load, fuel cetane number, temperature and pressure at the start of injection. Thus, indirectly, ignition delay is a complex inte-

gration of fuel properties, engine operation and engine design and, in very subtle ways, involves virtually all the thermodynamic and combustion sub-models. For example, ignition delay is directly dependent on temperature at the start of injection. Thus, the value of this variable alone will depend on the engine operating point (speed and load), engine design (turbocharger characteristics and scavenging process, fuel injection timing, compression ratio, etc.), fuel properties (eg. fuel density/ heat value, etc., will affect engine output and thus turbocharger characteristics), heat transfer and so on. These extensive but subtle interactions are not explicit and their integrated affect on ignition delay cannot be easily understood; however, they will be reflected by the thermodynamic/combustion simulation program.

Thus, ignition delay predictions require the general simulation program to be used. Figure 7.18 plots ignition delay vs. engine speed at full and part load for each of the three test fuels. In the plots, the experimental data points are also shown. In the experimental program [45, 46, 47, 48], two delays were measured and termed 'ignition delay' and 'combustion delay'. These are both measures of the onset of combustion, the difference between the two being that combustion delay represents a higher heat release rate while ignition delay represents the first measurable (and sustained) deviation of the fired pressure curve from the motored curve. These conditions usually occurred within a fraction of a crank angle degree and were often the same point. For model analysis, the average of these values was considered to be the most representative point and is used in the comparison.

A study of the plots (Fig. 7.18) again reveals accurate ignition delay predictions, especially considering the complex interplay of parameters and sub-models. Not only are engine load, speed and fuel type trends correct, but the subtle fuel-to- fuel differences in ignition delay measured in the experimental program (and yet remain unexplained) are also reflected by the model. Such engine/fuel analyses are not the subject of this chapter and will be treated later.

7.3.2 CYCLE CLOSURE

The gas exchange process is controlled by the blowdown and scavenging submodel which also closes the cycle. This section examines, in detail, the gas exchange process using Fuel 1 data only since differences due to fuel type during this period are not significant.

Table 7-1 presents the model values of scavenging air mass flow rate and cycle closure parameters (i.e., initial conditions of trapped mass, temperature and pressure). Initial conditions at the start of the cycle are determined as outlined in Section 2.4 while the flow rate is compared with experimental data. Overall, excellent cycle closure is achieved, in particular:

(i) At the end of the scavenging process, model predicted trapped masses in the cylinder agree to within 3% with those determined from the GM model, (see Section 2.4).

(ii) Model predicted final pressure and temperature at the end of scavenging are also well matched with the initial estimated pressure P_{in} and temperature T_{in} at the beginning of compression. The pressure difference is less than 1% while the temperature difference is less than 6%.

Figures 7.19 and 7.20 plot pressure vs. crank angle during blowdown (and scavenging, in part) at part load and full load respectively, for three engine speeds. Again, excellent correlation with experimental data exists.

TABLE 7-1

BLOWDOWN AND SCAVENGING MODEL EVALUATION

6V53T TWO-STROKE ENGINE, FULL LOAD, FUEL 1

50% MIXING PATTERN, BACK PRESSURE = 90% OF AIRBOX PRESSURE

ENGINE SPEED (RPM)	MASS FLOW RATE (KG/CYL/CYC)		CYCLE CLOSURE PARAMETERS					
			TRAPPED MASS (Kg/Cyl)		PRESSURE (psia)		TEMPERATURE (°K)	
	MEASURED $x10^{-2}$	MODEL $x10^{-2}$	INITIAL VALUE $x10^{-2}$	MODEL CLOSURE $x10^{-2}$	INITIAL CONDITION	MODEL CLOSURE	INITIAL CONDITION	MODEL CLOSURE
1500	0.197	0.240	0.103	0.102	21.21	20.74	375	386
1600	0.200	0.232	0.105	0.103	21.96	21.55	381	396
1700	0.198	0.223	0.106	0.103	22.46	22.09	386	405
1800	0.194	0.216	0.107	0.105	23.21	22.90	394	412
1900	0.196	0.214	0.110	0.107	24.21	23.97	402	422
2000	0.193	0.206	0.110	0.107	24.71	24.51	410	432
2100	0.195	0.204	0.113	0.109	25.71	25.58	417	442
2200	0.196	0.203	0.115	0.112	26.96	26.92	428	452
2300	0.197	0.203	0.118	0.115	28.21	28.25	438	462
2400	0.197	0.197	0.119	0.115	28.71	28.80	444	471
2500	0.198	0.196	0.121	0.117	29.96	30.14	454	481
2600	0.198	0.193	0.122	0.118	30.71	31.00	462	491
2700	0.200	0.192	0.123	0.121	31.96	32.29	472	501
2800	0.201	0.191	0.126	0.123	33.21	33.63	481	510

7.3.3 HEAT TRANSFER

For each step of the cycle, the instantaneous heat transfer is calculated using Woschni's model and the heat transfer rate is calculated as detailed in Section 2.5.2. Although no direct comparison of these values with experimental data can be made, some comparisons with the open literature are of value.

Figure 7.21 plots the heat transfer coefficient vs. crank angle for two load settings at 2200 RPM. The plots also show the coefficient of the motored curve so as to see the effect of combustion. Compared with the literature (Fig. 7.22), the heat transfer coefficient is clearly of the correct magnitude and character. Also the instantaneous heat transfer rate ($Kcal/s$) per cylinder is shown in Fig. 7.23 as a function of crank angle position at the same engine operating point. Such data is of value for the design of the engine cooling system.

Cylinder gas temperature is the key parameter upon which the above calculations are based. Figure 7.24 shows the cylinder gas temperatures at the 2200 RPM test point. The cylinder thermodynamic state (gas temperature and pressure) is evaluated at each step of the cycle. Through direct comparison with experimental data, pressures have been shown to reflect all phases of the cycle (rapid or early combustion, main combustion, blowdown and scavenging, etc.) with considerable accuracy. Thus, it follows that predicted gas temperatures will also accurately reflect the cylinder thermodynamic condition.

At 2200 RPM, full load, maximum cylinder temperature reaches 2134 $^{\circ}K$ at about 15 $^{\circ}CA$ aTDC. This is about 8–9 $^{\circ}CA$ later than that of maximum cylinder pressure. At the beginning of blowdown, gas temperatures are still in the order of 1300 $^{\circ}K$. Two typically steps occur in the temperature curve. The first is always at the 56$^{\circ}CA$ position as this is the point where the simulation program closes the cycle (i.e. start of compression) as discussed in the previous section. The second step occurs at about 10 $^{\circ}CA$ bTDC at full load ($\simeq$ 5$^{\circ}CA$ bTDC part load) and corresponds to the

early or rapid combustion phase of the diesel cycle.

7.3.4 COMBUSTION PRODUCTS/EMISSIONS

The combustion sub-model (Chapter 5) is based on the equilibrium of seven chemical reactions which represent eleven species, namely: O_2, N_2, CO_2, H_2O, CO, H_2, CH_4, OH,O, H, and NO. Thus, the simulation program evaluates the number of moles of each species at each calculation step and hence, traces the history of combustion products, assuming chemical equilibrium, throughout the cycle. Although in an operating engine, chemical equilibrium will not normally be reached, especially that of CO and NO, the analysis does provide some insight into the behavior of the combustion products as well as engine emissions. It could be noted that no attempt was made to develop an emission model, nor was such a model required to meet the research objective.

Figure 7.25 shows a typical history of combustion products development throughout a cycle. Here, Fuel 1 at 2200 RPM, full load is used and species percent-by-volume vs. crank angle position are plotted. For the test case shown, several observations can be made.

(i) N_2, of course, is the major species representing 78.7% by volume at the end of expansion while available oxygen (excess air) is 7.1%.

(ii) CO_2 and H_2O are major products of combustion and represent 7.4% and 6.8% respectively by the end of expansion.

(iii) The volume percentages of the minor species all maximize about 16—18°CA aTDC with the exception of NO which peaks slightly sooner. All minor species show moderately rapid dissociation curves during expansion.

(iv) Of the minor species, NO and OH show the highest formations reaching maximum values of 0.85% and 0.30% respectively. Further, their dissociation rates

are slower than the other minor species and thus also represent the major emissions. At blowdown, NO accounts for 0.027%, OH for 0.003% of the cylinder gases by volume.

(v) CO and O formations maximize at about 0.022% but also show rapid dissociation rates during expansion. By blowdown, their volume percentages are only: 0.44×10^{-5} for CO and 0.9×10^{-5} for O.

(vi) The volume percentages of H_2 and H reach maxima of only 0.004 and 0.008 respectively, dropping to 0.27×10^{-5} and 0.24×10^{-7} at blowdown.

(vii) The volume percentage of CH_4 is vary small (in the order of 10^{-30}), hence, treated as zero.

Although the research program is not focused on exhaust gas analysis, emissions are of interest with respect to engine/fuel interaction studies. Further, in this chapter, proving the combustion model (i.e. equilibrium reactions, constants, calculations, etc.) is of interest. Now, based on the species concentrations at blowdown, a good evaluation of the combustion model can be made by matching conditions at blowdown and executing a complete combustion analysis. Thus, from the model, at 2200 RPM, full load with Fuel 1, the conditions are:

(i) Air/Fuel ratio = 21.9,

(ii) Total fuel injected, $M_t = 0.5247 \times 10^{-4}$ (Kg/cylinder/cycle),

(iii) Mass fraction: $X_1 = 0.0083$ for C_8H_{18},
$X_2 = 0.1810$ for C_6H_6,
$X_3 = 0.8107$ for $C_{12}H_{26}$,

(iv) Percent of fuel burned = 81 %.

Now, the chemical reaction for complete combustion is:

$$n_1C_8H_{18} + n_2C_6H_6 + n_3C_{12}H_{26} + n_4O_2 + n_5N_2$$

$$= n_6CO_2 + n_7H_2O + n_8O_2 + n_9N_2$$

Thus, the number of moles can be established:

Reactants:

$$n_1 = 0.81 \cdot X_1 \cdot M_t / W_{C_8H_{18}} = 3.089 \times 10^{-9}$$
$$n_2 = 0.81 \cdot X_2 \cdot M_t / W_{C_6H_6} = 9.850 \times 10^{-8}$$
$$n_3 = 0.81 \cdot X_3 \cdot M_t / W_{C_{12}H_{26}} = 2.023 \times 10^{-7}$$
$$n_4 = \frac{0.21 \cdot (A/F) \cdot M_t}{28.96} = 8.332 \times 10^{-5}$$
$$n_5 = \frac{0.79 \cdot (A/F) \cdot M_t}{28.96} = 3.135 \times 10^{-5}$$

Products:

$$n_6 = 8n_1 + 6n_2 + 12n_3 = 3.043 \times 10^{-6}$$
$$n_7 = 9n_1 + 3n_2 + 13n_3 = 2.953 \times 10^{-6}$$
$$n_8 = n_4 - n_6 - 0.5n_7 = 3.813 \times 10^{-6}$$
$$n_9 = n_5 = 31.316 \times 10^{-6}$$

Now, the total products are: $n_t = n_6 + n_7 + n_8 + n_9$ and the percent by volume of each product is n_i/n_t. Table 7–2 compares the equilibrium combustion results (model calculation) with the complete combustion approximation for the specified test point at blowdown. The major species correspond very well, the differences being due to the minor species and equilibrium, as opposed to complete combustion.

TABLE 7-2

COMPARISON OF SPECIES CONCENTRATIONS
BETWEEN EQUILIBRIUM AND COMPLETE COMBUSTION
(2200 RPM, FULL LOAD, FUEL 1 AT BLOWDOWN)

Calculation Procedure	SPECIES AND CONCENTRATION (% By Volume)										
	N_2	O_2	CO_2	H_2O	CO	O	H_2	H	OH	NO	CH_4
Equilibrium Combustion (model)	76.30	9.35	7.47	6.88	0.44 $\times 10^{-5}$	0.9 $\times 10^{-5}$	0.27 $\times 10^{-5}$	0.24 $\times 10^{-7}$	0.003	0.027	$\approx 10^{-30}$
Complete Combustion (approximation)	76.19	9.27	7.39	7.17	-	-	-	-	-	-	-

7.4 GENERAL ASSESSMENT

7.4.1 ENGINE MAP COMPARISONS

Engine indicated performance and combustion parameter mapping was introduced in the experimental program [48]. Not only was it shown that such parameters are mappable, but also that such maps provide a perspective and an insight into engine-fuel behavior not attainable from classical characteristic (maximum torque) plots. The maps provide, in a single plot, the behavior pattern of any parameter over the complete speed/load operating range of the engine for a given test fuel. Thus, engine-fuel trends become highly visible and extremum conditions (optimum or critical) can be located.

In the experimental program [48], for mapping purposes, an RPM-brake torque grid was used with approximately 154 test points plus the maximum torque curve. At each test point, approximately 64,000 data samples were taken (complete data set) or, for the maps, approximately 10,000,000 data per fuel tested. This data is reduced by the lab computer (HP 1000) and generates a map data matrix for each parameter (brake, indicated or combustion) of interest. The general mapping program, resident on the mainframe, expands the data matrix supplied to a 101 by 101 matrix, through interpolation, to increase map precision. From this 101×101 matrix, specified isocline values are searched and drawn and minimum/maximum values are located and printed.

Thus, the thermodynamic program was run over the same operating grid as used in the experimental program (speed: 1500–2800 with steps of 100 RPM; load: 100 ft.lbs–maximum brake torque with steps of 50 ft-lb.). This allows not only model parameter mapping but also direct comparison of all predicted maps with experimentally derived maps.

Figures 7.26 to 7.31 present the map comparisons. Two performance parameters (IHP and IMEP) and two combustion parameters (maximum cylinder pressure and maximum pressure rate), considered to be the most important assessment parameters,

are shown for each of the three test fuels. It should be noted that such comparisons are without precedent, for a model to simulate not only all engine speed/load settings but also different fuels is simply not expected.

In the opinion of the author, the results of the maps exceed expectation. Both the indicated performance and combustion parameter maps clearly show that the model is predicting accurate trends not only for the complete operating speed range of the engine, but also from fuel-to-fuel. Furthermore, the model does not possess or show any "quirks" for any of the fuels; thus, parametric studies can be expected to be reliable. Moreover, subtleties of the engine-fuel interaction or behavior are also reflected by the model; for example, Fuel 3 is predicted to give the lowest performance (IHP), Fuel 4 the highest, exactly as determined in the experimental program. Also, maximum pressure rates are predicted to occur at 200 ft.lbs. torque and low speed, again exactly as measured. Such subtleties, together with accurate trending, allow engine/fuel and pressure rate analyses to be conducted with confidence.

7.4.2 PARAMETER SENSITIVITY ANALYSIS

This chapter has been concerned with model evaluation through direct comparison with experimental data. Such comparisons validate the accuracy and predictive capability of a model; however, interpretation of the results requires an understanding of the behavior of the model itself. This can only be achieved through parameter sensitivity analyses.

Thus, parameter sensitivity studies were conducted in order to: (i) gain insight into the controlling variables of thermodynamic and combustion models, and (ii) to confirm that the established values of the parameters are reasonably located: i.e., $\pm$ variations of a parameter should show similar trends in the model response. Thus, the established parameter value together with $\pm 10\%$ variations of that value were run on

the general simulation program. All tests were run at full load, 2200 RPM with Fuel 1. The sensitivities of indicated horsepower, indicated thermal efficiency, maximum cylinder pressure, maximum pressure rate and ignition delay were evaluated against a range of model parameters. The results are presented in Table 7-3.

The first observation of interest is the overall model behavior and, in this regard, all trends are correct. For example, increased turbocharging (increased P_{ab}) results in higher engine performance and shorter ignition delays whereas intercooling (decreased T_{ab}) increases engine performance but also increases ignition delays, all of which are known to be true in practice. Likewise, similar arguments can be applied to all other parameters listed.

The second set of observations relates to the sensitivity and interaction of each parameter. From such observations, considerable insight into the model's behavior, and thus the engine's behavior, can be gained. Overall, it is clear that initial conditions have the greatest impact on both engine performance and ignition delay. However, ignition delay itself has the greatest impact on maximum pressure rates. This apparent paradox will be explained.

Of the initial conditions, charging efficiency is the most intriguing. While increased engine performance was expected, the impacts on ignition delay and pressure rates were not. However, an increase in charging efficiency translates directly into an increase in trapped mass at the end of scavenging or at the start of compression. Now, an increase in trapped mass (at a fixed volume) must be accompanied by a corresponding increase in pressure of the trapped gas or a decrease in its temperature. In the model, as one would expect to be the case of an operating engine, trapped gas pressure will not alter significantly. Thus, increased trapping efficiency correlates with decreased trapped gas temperature. The increased trapped mass readily explains the increase in engine performance and maximum cylinder pressure while the decrease in cylinder gas temperature correlates with the increase in ignition delay. Indeed, the model predicts

a decrease in the gas temperature at the start of injection from 969°K to 897°K due to increase in charging efficiency of 10%. Based on the earlier ignition delay study (Table 3–3 and Fig. 3.2), this 7.4% decrease in cylinder gas temperature will result in an increase of 29.8% in ignition delay, almost exactly as predicted. The difference is due to the slight variations in cylinder pressure and fuel/air ratio which also affect ignition delay. Also, the large change in ignition delay would be expected to give rise to much greater pressure rate changes than those predicted, as is indicated by the ignition delay parameter values of Table 7–3. This again is a direct result of reduced cylinder gas temperatures during early combustion and hence a reduced reaction rate.

The heat transfer results show that large variations in either the heat transfer coefficient or the cylinder wall temperatures do not have significant effects on either engine performance or the combustion parameters. This is very desirable in that uncertainty exists with respect to the values of both 'h' and 'T_{w_i}' as is evidenced from the literature.

Relative to the combustion variables, several points are of interest. Reaction rate has no affect on any of the parameters other than maximum pressure rate. Also, ignition delay within reasonable limits (eg.$\pm$ 1°CA) has an insignificant impact on engine performance and maximum cylinder pressure but is the key parameter affecting maximum pressure rates (i.e. rough combustion and knock in an actual engine). This correlates exactly with the behavior of the low cetane off-specification fuels as measured in the experimental program. Finally, improved fuel-air mixing rate results in improved engine performance (a direct result of more rapid combustion especially near TDC) and increased pressure rates due to an increase in prepared fuel at the end of the ignition delay period.

TABLE 7-3

PARAMETER SENSITIVITY ANALYSIS

EFFECT OF MODEL PARAMETERS ON

ENGINE PERFORMANCE AND COMBUSTION CHARACTERISTICS

(Tests Conducted at 2200 RPM, Full Load, Fuel #1)

	MODEL PARAMETER	CONDITION	IHP		η_{th} (%)		MAX.CYL.PRESSURE (psi)		MAX.PRES.RATE (psi/°CA)		IGNITION DELAY (°CA)	
			VALUE	DIF.(%)	VALUE	DIF.(%)	VALUE	DIF.(%)	VALUE	DIF.(%)	VALUE	DIF.(%).
INITIAL CONDITION	AIRBOX PRESSURE (P_{ab})	Standard	271.4	-	38.4	-	1760.8	-	110.0	-	7.99	-
		+10%	277.1	+2.1	39.2	+2.1	1826.2	+3.7	110.2	+0.2	7.59	-5.0
		-10%	264.9	-2.4	37.5	-2.3	1692.8	-3.9	109.2	-0.7	8.39	+5.0
	AIRBOX TEMPERATURE (T_{ab})	Standard	271.4	-	38.4	-	1760.8	-	110.0	-	7.99	-
		+10%	267.5	-1.4	37.9	-1.3	1743.9	-1.0	106.2	-3.5	7.60	-4.9
		-10%	275.2	+1.4	39.0	+1.6	1777.1	+0.9	113.3	+3.0	8.39	+5.0
	CHARGING EFFICIENCY (η_{ch})	Standard	271.4	-	38.4	-	1760.8	-	110.0	-	7.99	-
		+10%	291.9	+7.6	41.3	+7.6	1845.8	+4.8	131.8	+19.8	10.43	+30.5
		-10%	247.1	-9.0	35.0	-8.9	1654.8	-6.0	89.7	-18.5	5.79	-27.5
HEAT TRANSFER	HEAT TRANSFER COEFFICIENT (h)	Standard	271.4	-	38.4	-	1760.8	-	110.0	-	7.99	-
		+10%	268.6	-1.0	38.0	-1.0	1756.9	-0.6	112.9	+2.6	8.00	+0.1
		-10%	274.3	+1.1	38.8	+1.0	1765.5	+0.3	110.9	+0.8	7.97	-0.3
	CYLINDER WALL TEMPERATURE (T_{wi})	Standard	271.4	-	38.4	-	1760.8	-	110.0	-	7.99	-
		+10%	273.1	+0.6	38.7	+0.8	1771.3	+0.6	109.3	-0.6	7.80	-2.4
		-10%	269.7	-0.6	38.2	-0.5	1750.0	-0.6	110.5	-0.5	8.18	+2.4
COMBUSTION VARIABLE	FUEL/AIR MIXING RATE (MR)	Standard	271.4	-	38.4	-	1760.8	-	110.0	-	7.99	-
		+10%	279.7	+3.1	39.6	+3.1	1810.5	+2.8	117.8	+7.1	7.99	0.0
		-10%	261.4	-3.7	37.0	-3.6	1704.7	-3.2	102.2	-7.1	7.99	0.0
	FUEL/AIR REACTION RATE	Standard	271.4		38.4	-	1760.8	-	110.0	-	7.99	-
		+10%	271.5	0.0	38.4	0.0	1763.5	+0.2	116.5	+5.9	7.99	0.0
		-10%	271.3	0.0	38.4	0.0	1757.9	-0.2	103.5	-5.9	7.99	0.0
	IGNITION DELAY	Standard	271.4	-	38.4	-	1760.8	-	110.0	-	7.99	-
		+10%	271.8	+0.1	38.5	+0.01	1768.6	+0.4	145.0	+31.8	8.79	+10.0
		-10%	271.1	-0.1	38.4	0.0	1755.4	-0.3	84.5	-23.2	7.20	-10.0

7.5 CLOSURE

In this chapter an extensive evaluation of the thermodynamic and combustion model was conducted. Through a comparison with the extensive experimental data base [48] and the open literature, the model was shown to accurately predict 6V53T engine performance and combustion parameter data for all three test fuels and at all engine speed/load operating points. Thus, considerable confidence exists in using this model to study not only engine parametric effects but also the subtleties of engine-fuel interaction and off-specification fuel combustion control.

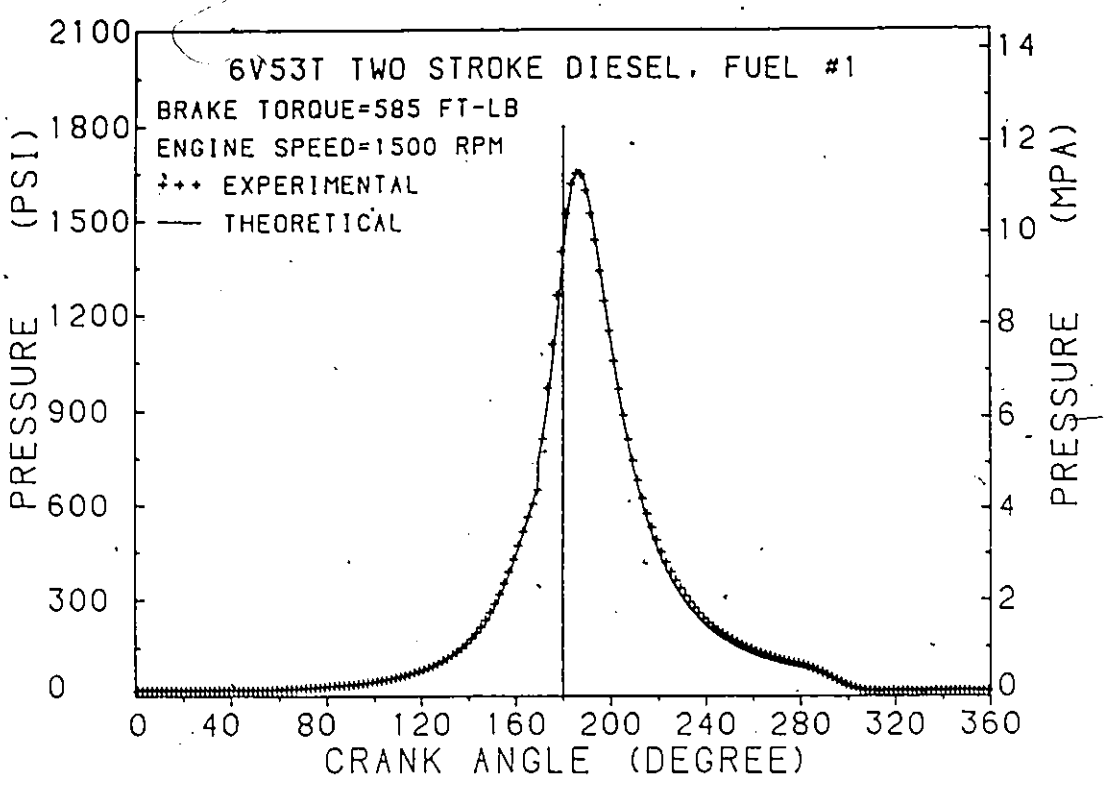

(a) Full Load

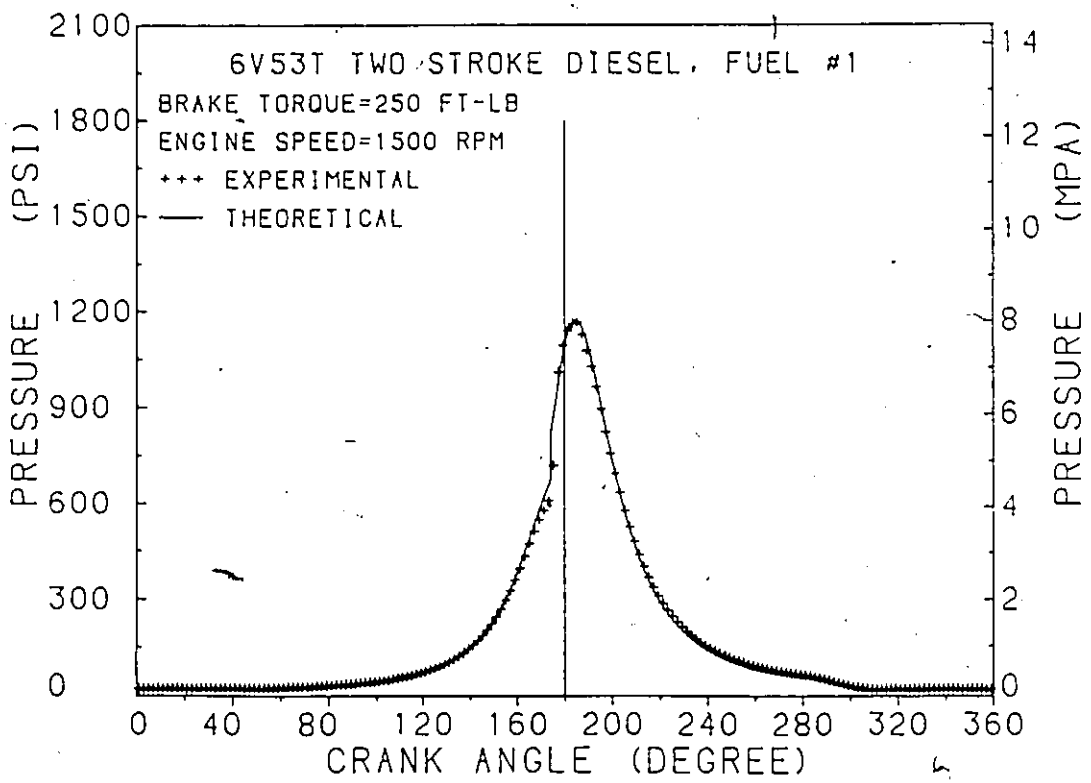

(b) Part Load

Fig. 7.1: Cylinder Pressure vs. Crank Angle and Comparison with Experimental Data, Fuel 1 @1500 RPM.

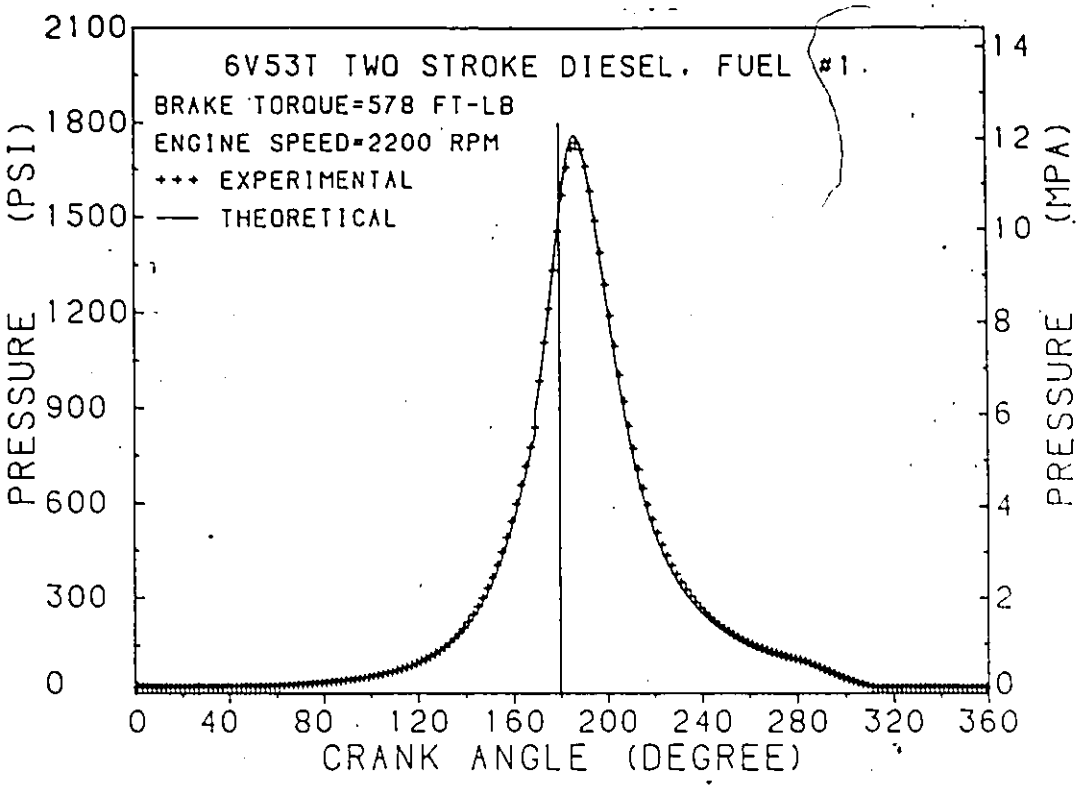

(a) Full Load

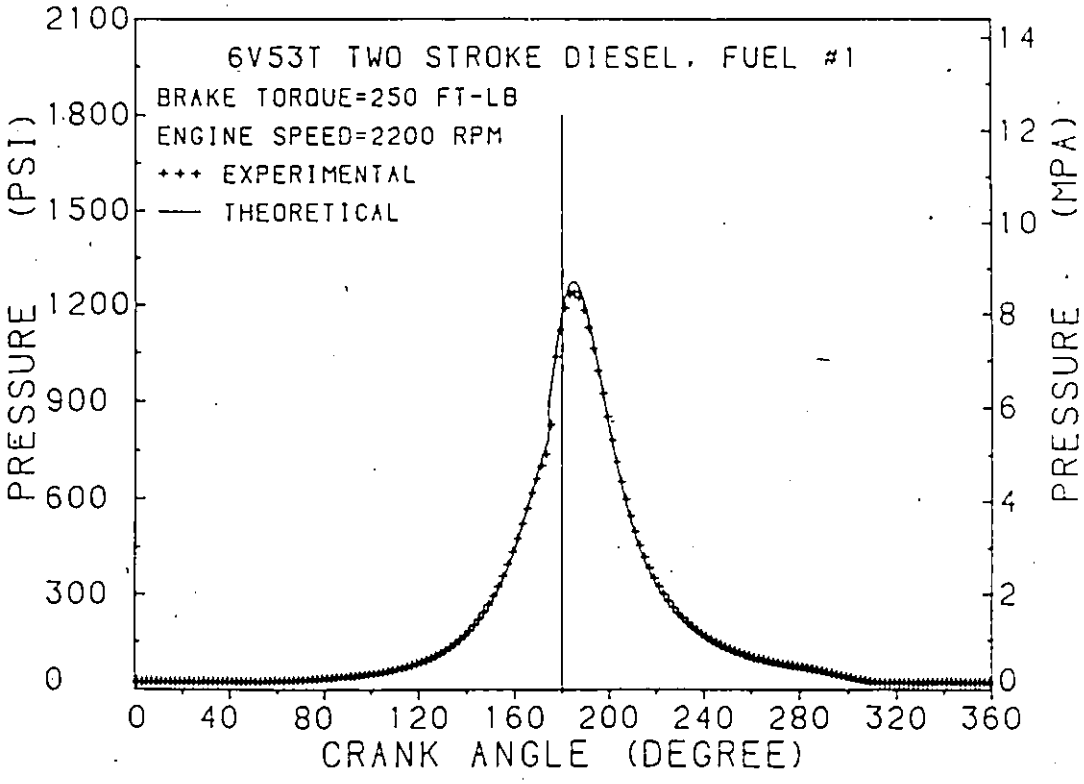

(b) Part Load

Fig. 7.2: Cylinder Pressure vs. Crank Angle and Comparison with Experimental Data, Fuel 1 @2200 RPM.

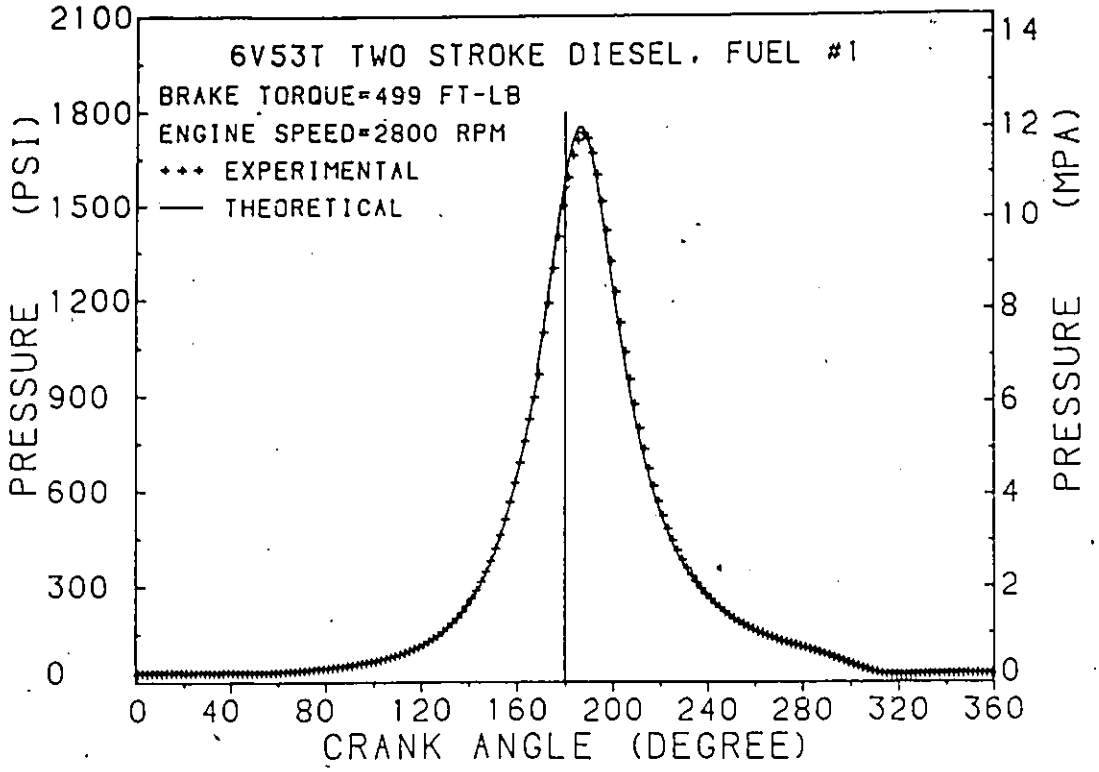

(a) Full Load

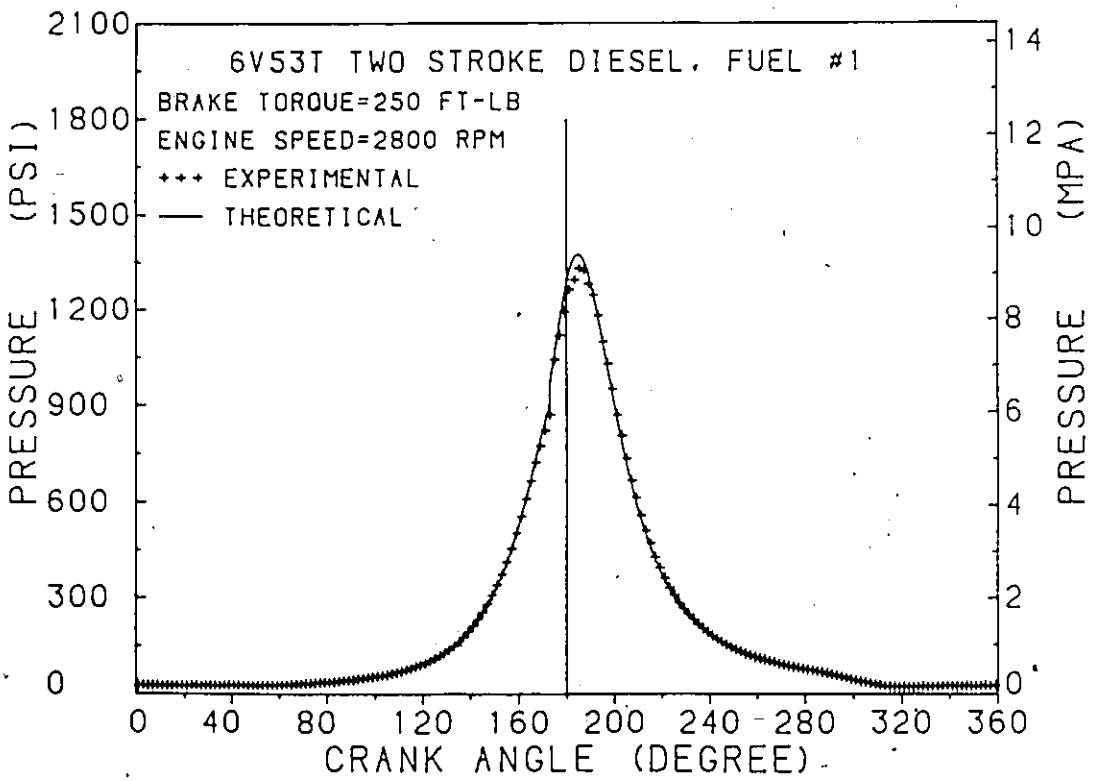

(b) Part Load

Fig. 7.3: Cylinder Pressure vs. Crank Angle and Comparison with Experimental Data, Fuel 1 @2800 RPM.

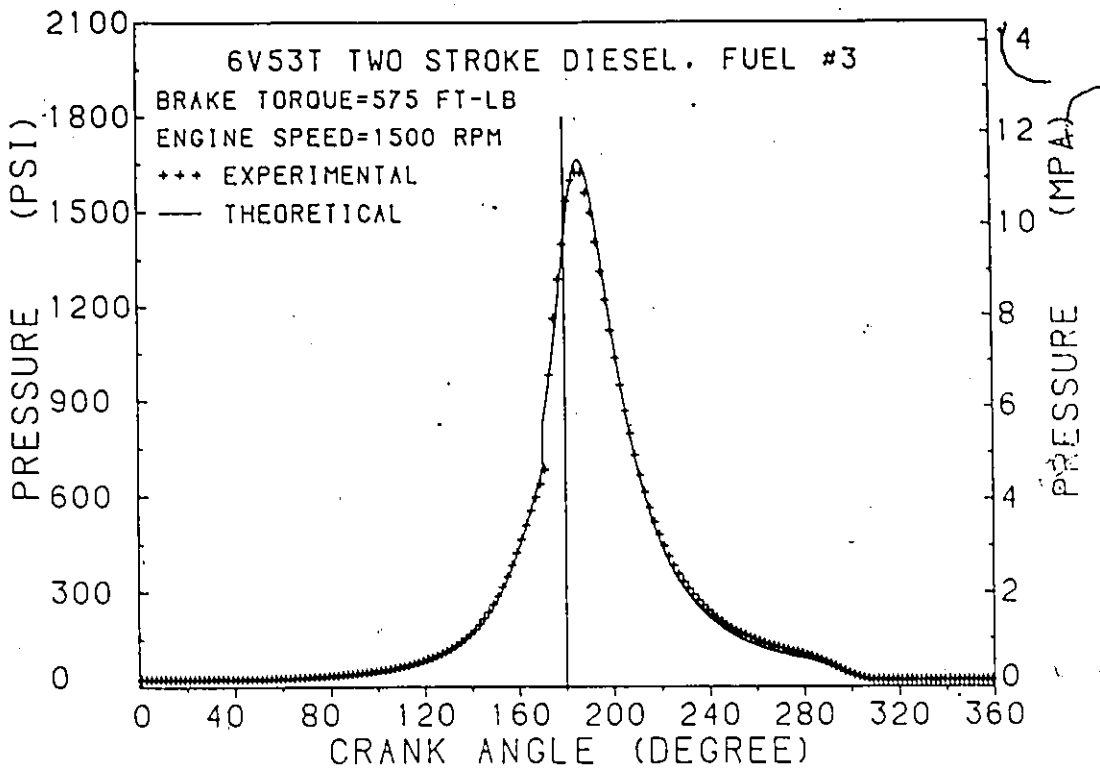

(a) Full Load

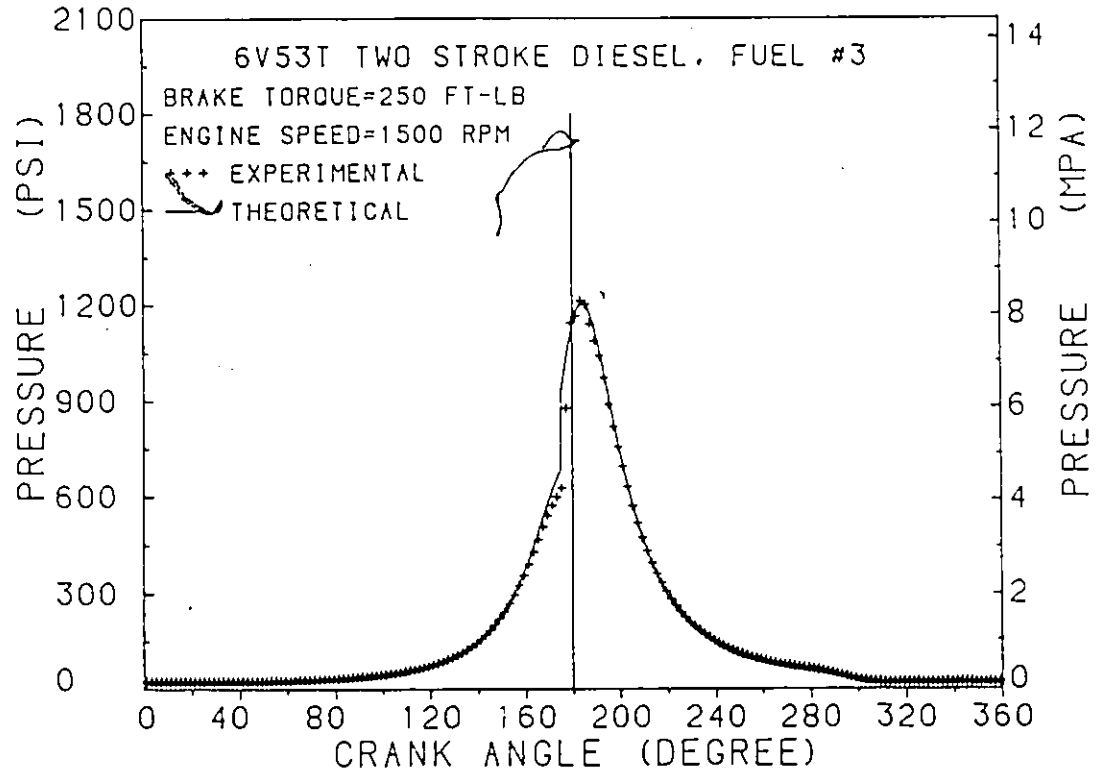

(b) Part Load

Fig. 7.4: Cylinder Pressure vs. Crank Angle and Comparison with Experimental Data, Fuel 3 @1500 RPM.

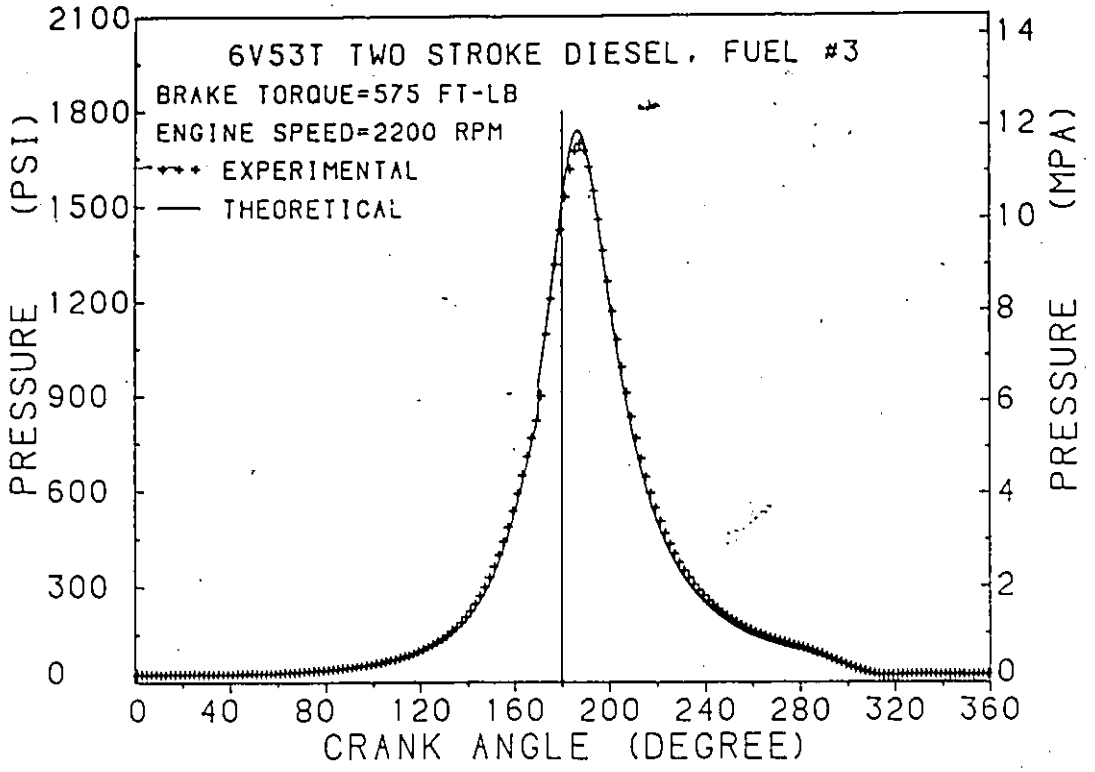

(a) Full Load

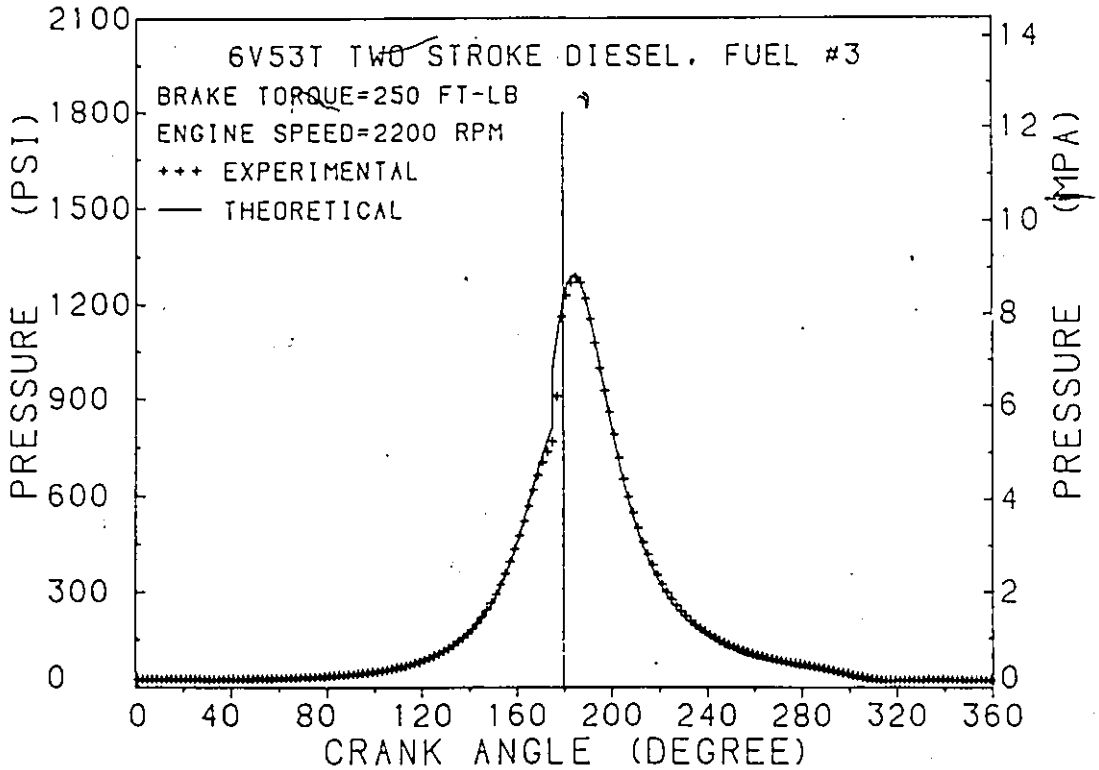

(b) Part Load

Fig. 7.5: Cylinder Pressure vs. Crank Angle and Comparison with Experimental Data, Fuel 3 @2200 RPM.

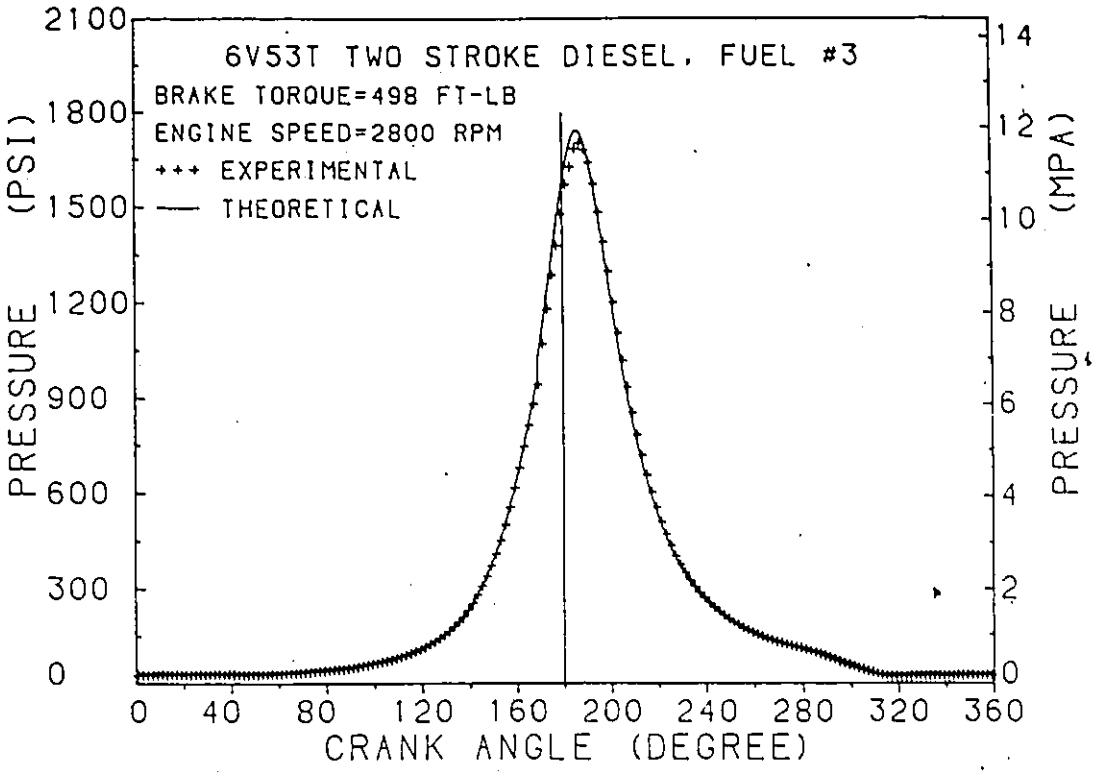

(a) Full Load

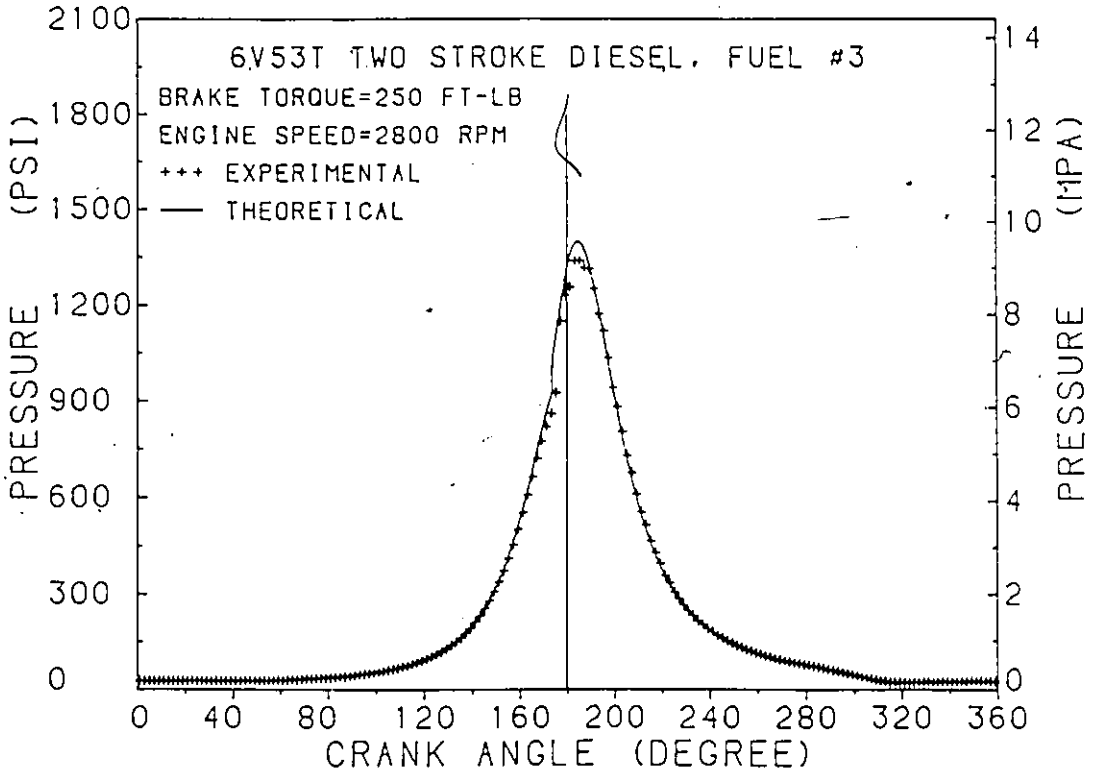

(b) Part Load

Fig. 7.6: Cylinder Pressure vs. Crank Angle and Comparison with Experimental Data, Fuel 3 @2800 RPM.

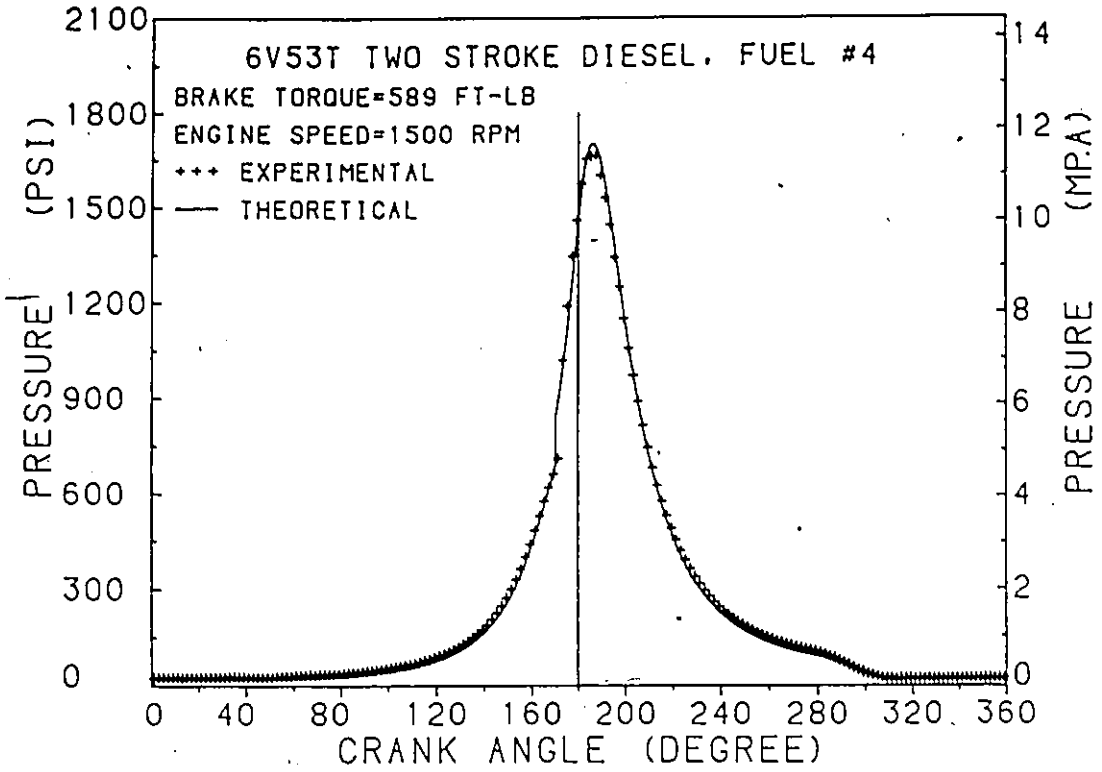

(a) Full Load

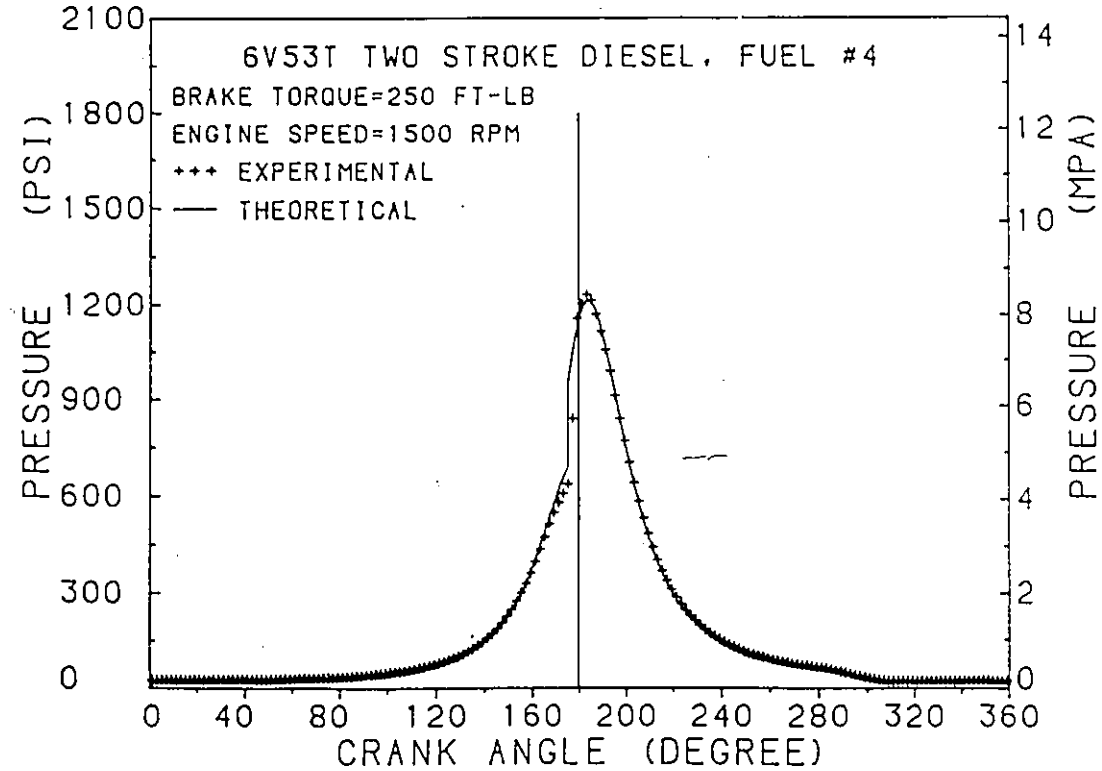

(b) Part Load

Fig. 7.7: Cylinder Pressure vs. Crank Angle and Comparison with Experimental Data, Fuel 4 @1500 RPM.

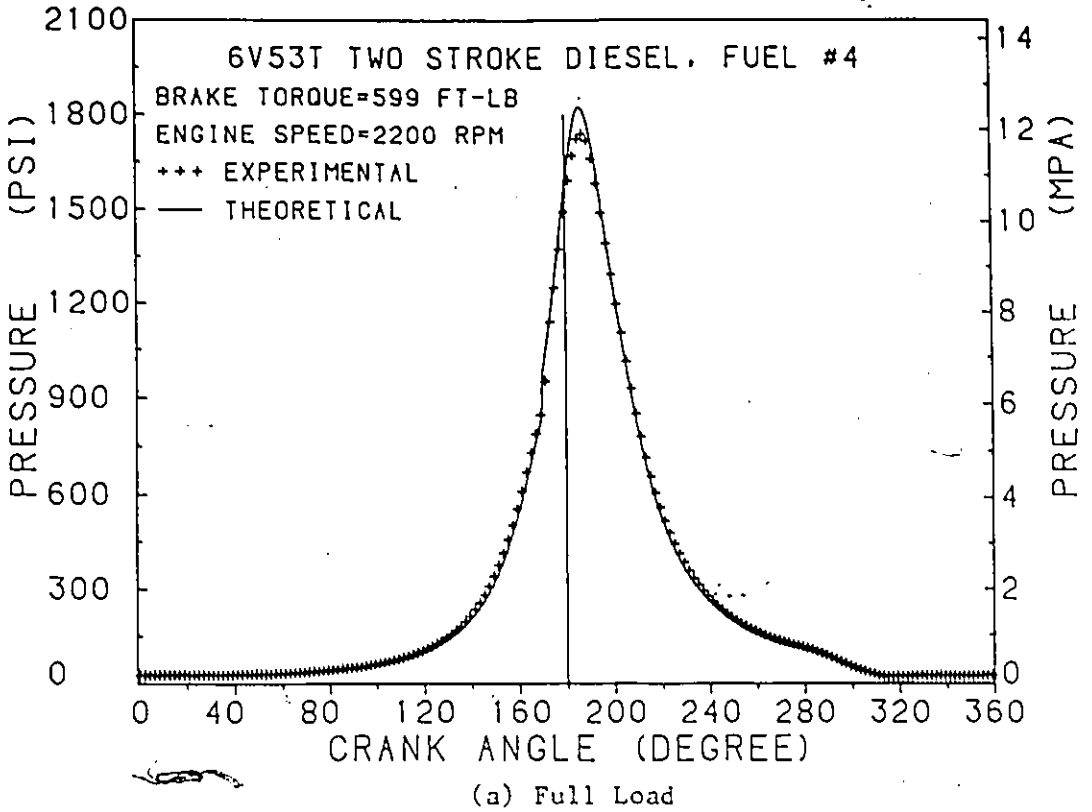

(a) Full Load

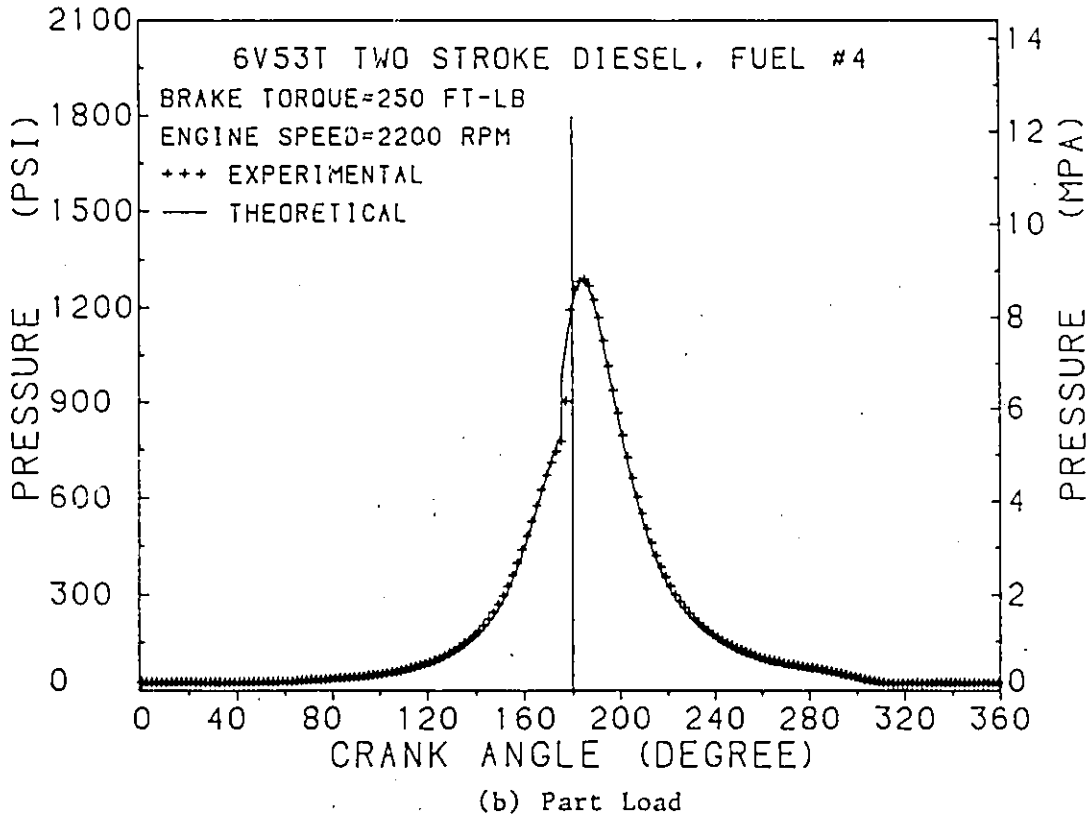

(b) Part Load

Fig. 7.8: Cylinder Pressure vs. Crank Angle and Comparison with Experimental Data, Fuel 4 @2200 RPM.

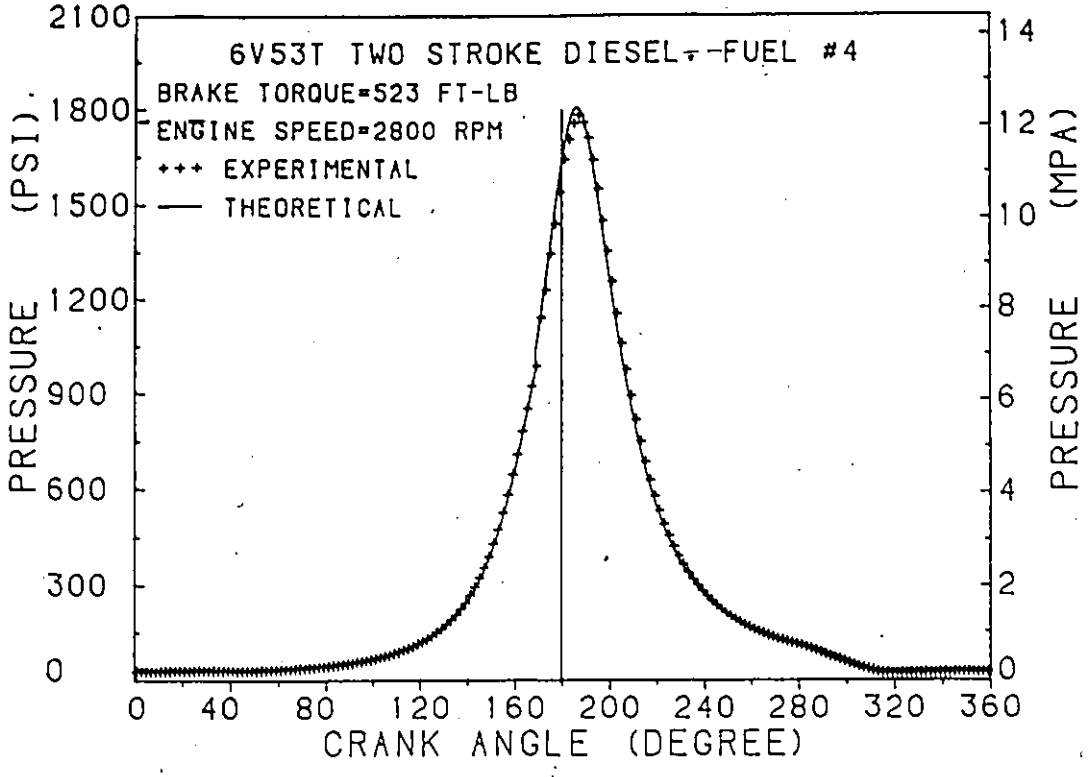

(a) Full Load

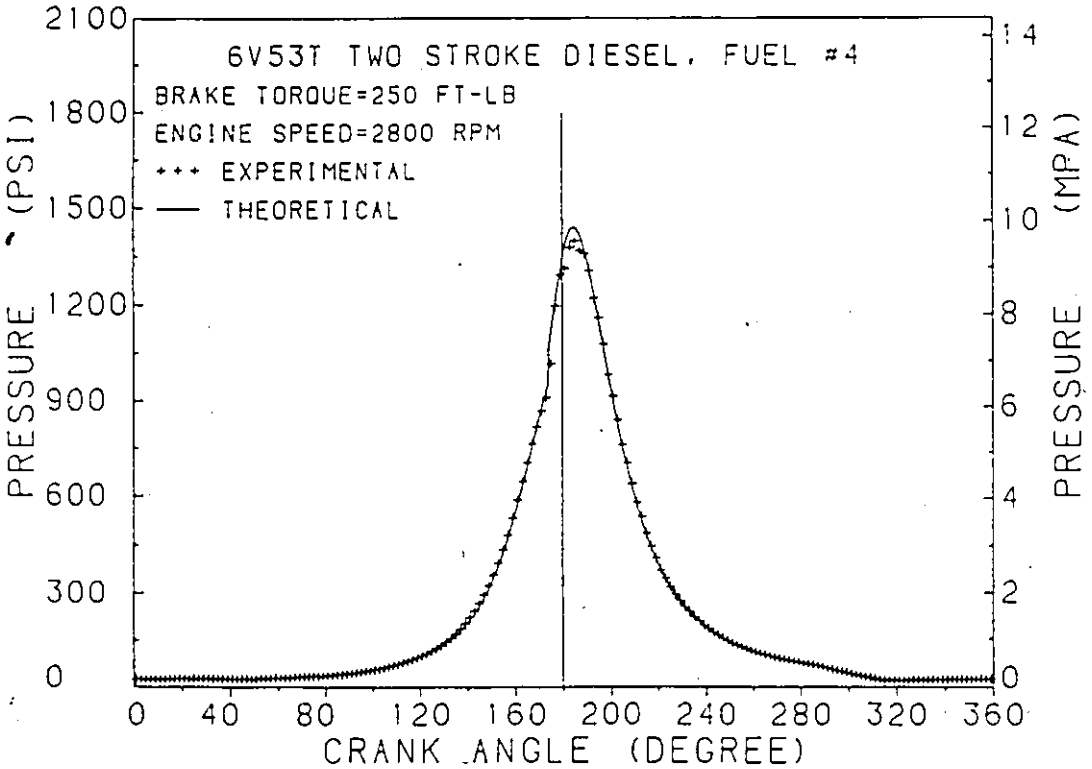

(b) Part Load

Fig. 7.9: Cylinder Pressure vs. Crank Angle and Comparison with Experimental Data, Fuel 4 @2800 RPM.

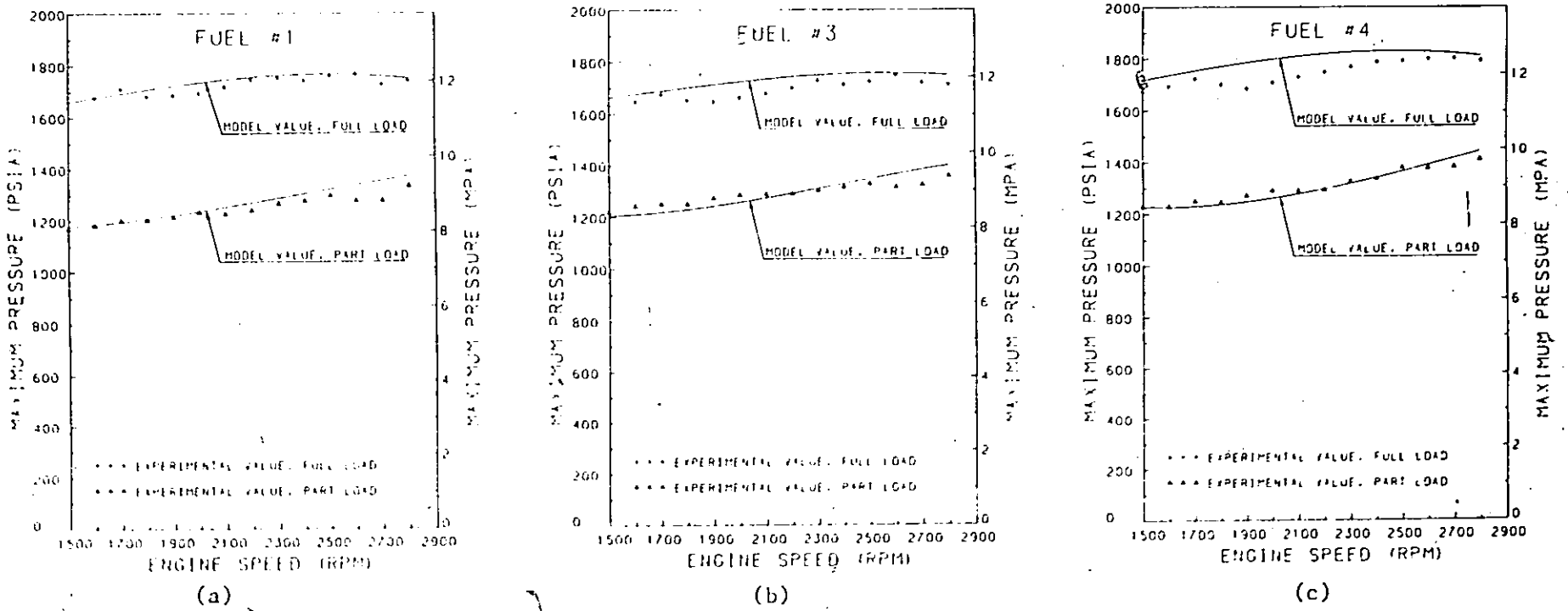

Fig. 7.10: Maximum Cylinder Pressure vs. Engine Speed and Comparison with Experimental Data: (a) Fuel 1, (b) Fuel 3, (c) Fuel 4.

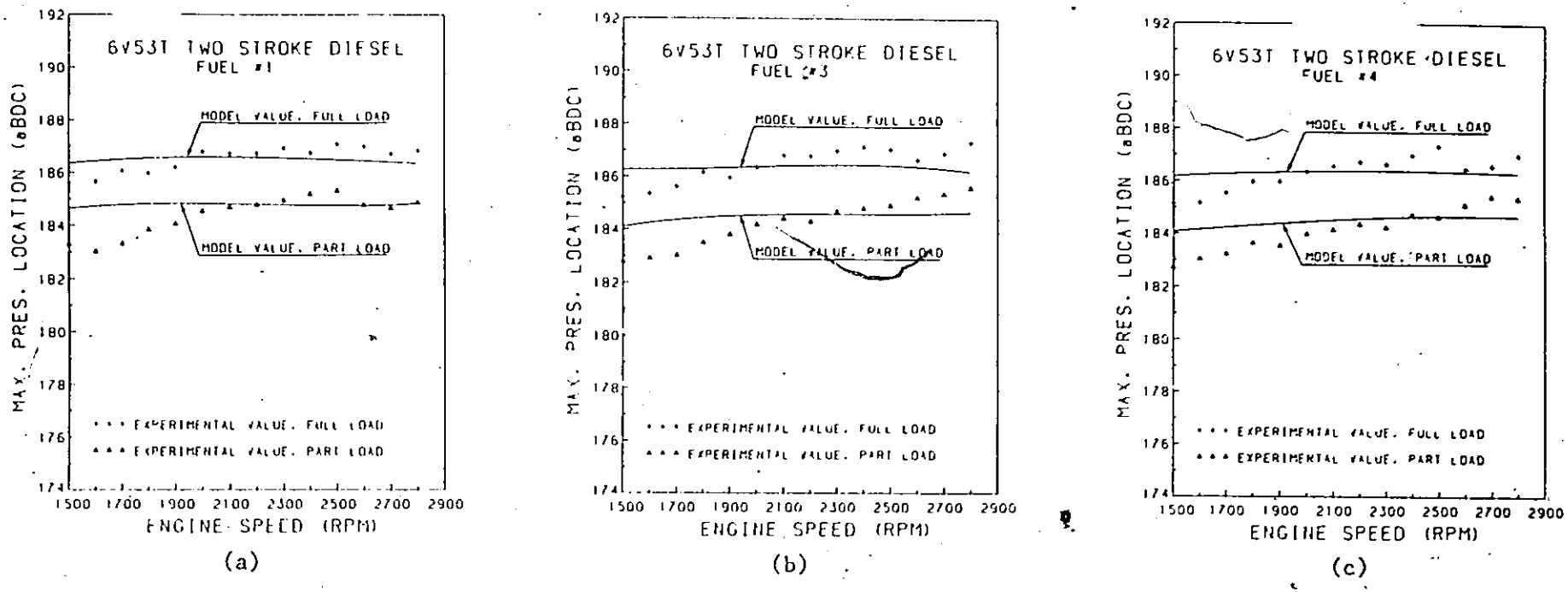

Fig. 7.11: Location of Maximum Cylinder Pressure vs. Engine Speed and Comparison with Experimental Data: (a) Fuel 1, (b) Fuel 3, (c) Fuel 4.

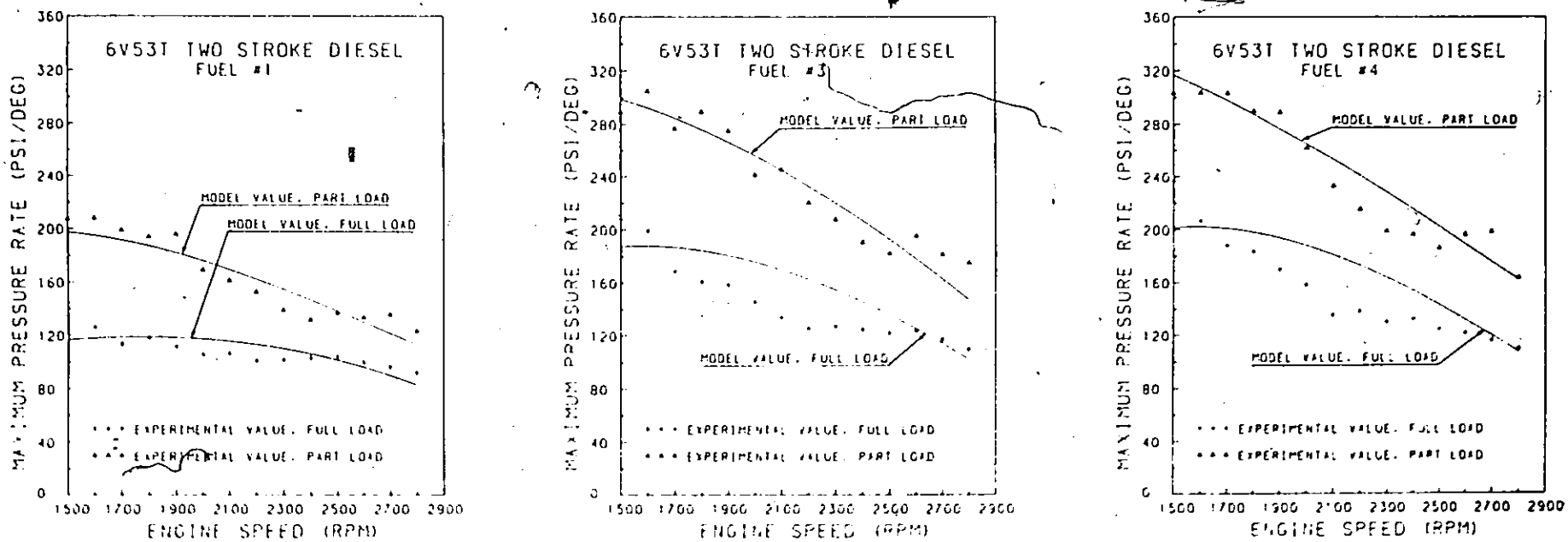

Fig. 7.12: Maximum Pressure Rate vs. Engine Speed and Comparison with Experimental Data: (a) Fuel 1, (b) Fuel 3, (c) Fuel 4.

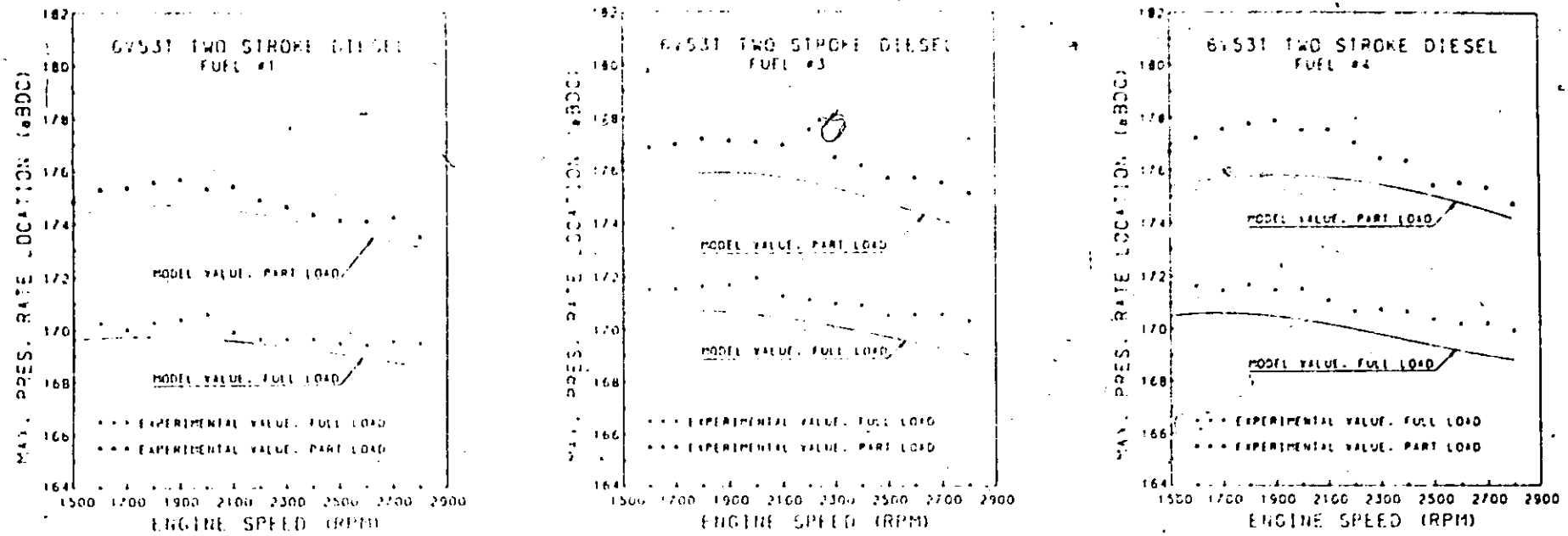

(a) (b) (c)

Fig. 7.13: Location of Maximum Pressure Rate vs. Engine Speed and Comparison with Experimental Data: (a) Fuel 1, (b) Fuel 3, (c) Fuel 4.

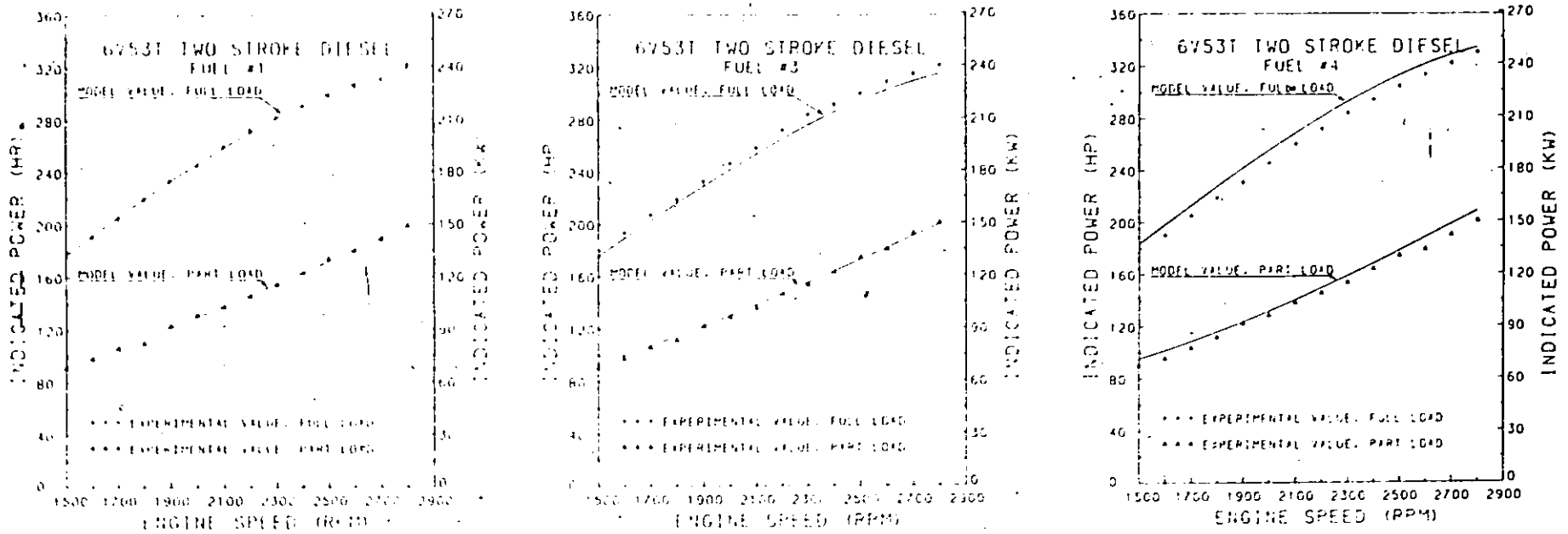

Fig. 7.14: Indicated Power vs. Engine Speed and Comparison with Experimental Data:
(a) Fuel 1, (b) Fuel 3, (c) Fuel 4.

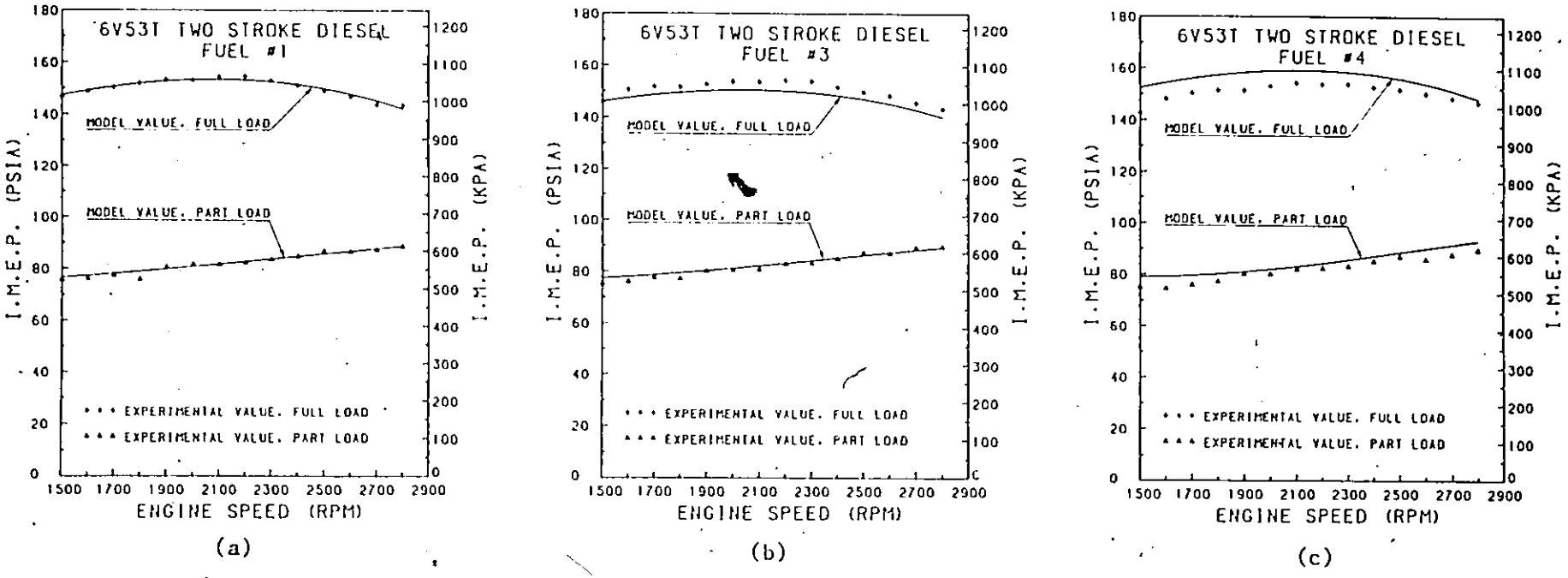

Fig. 7.15: Indicated Mean Effective Pressure vs. Engine Speed and Comparison with Experimental Data: (a) Fuel 1, (b) Fuel 3, (c) Fuel 4.

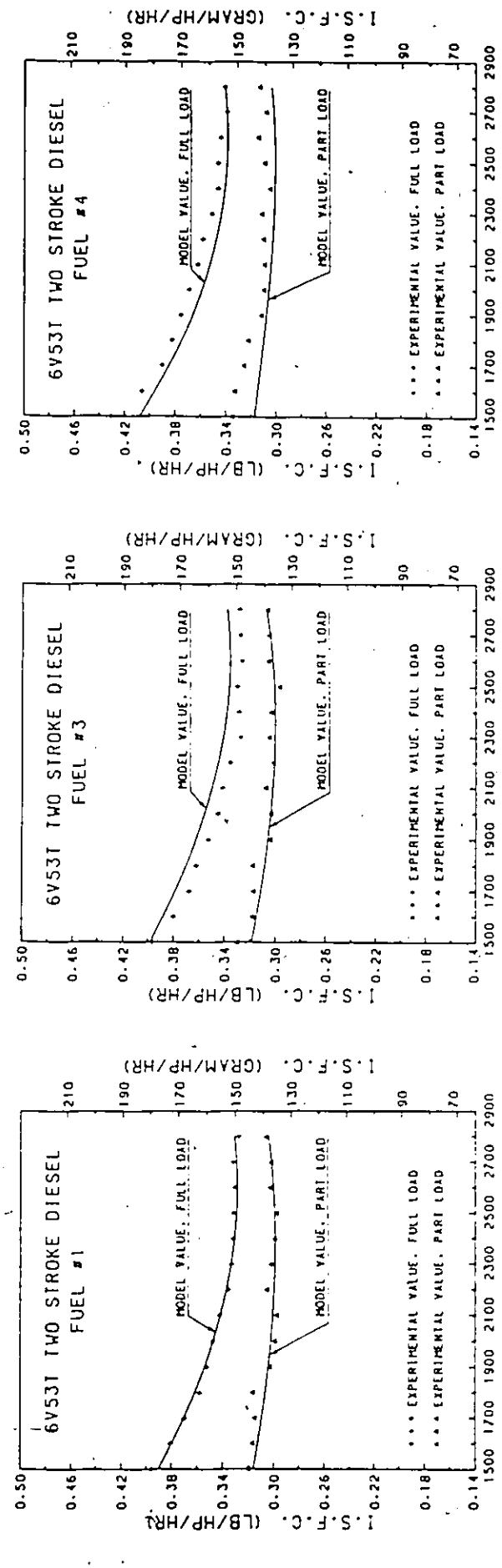

Fig. 7:16: Indicated Specific Fuel Consumption vs. Engine Speed and Comparison with Experimental Data:
(a) Fuel 1, (b) Fuel 3, (c) Fuel 4.

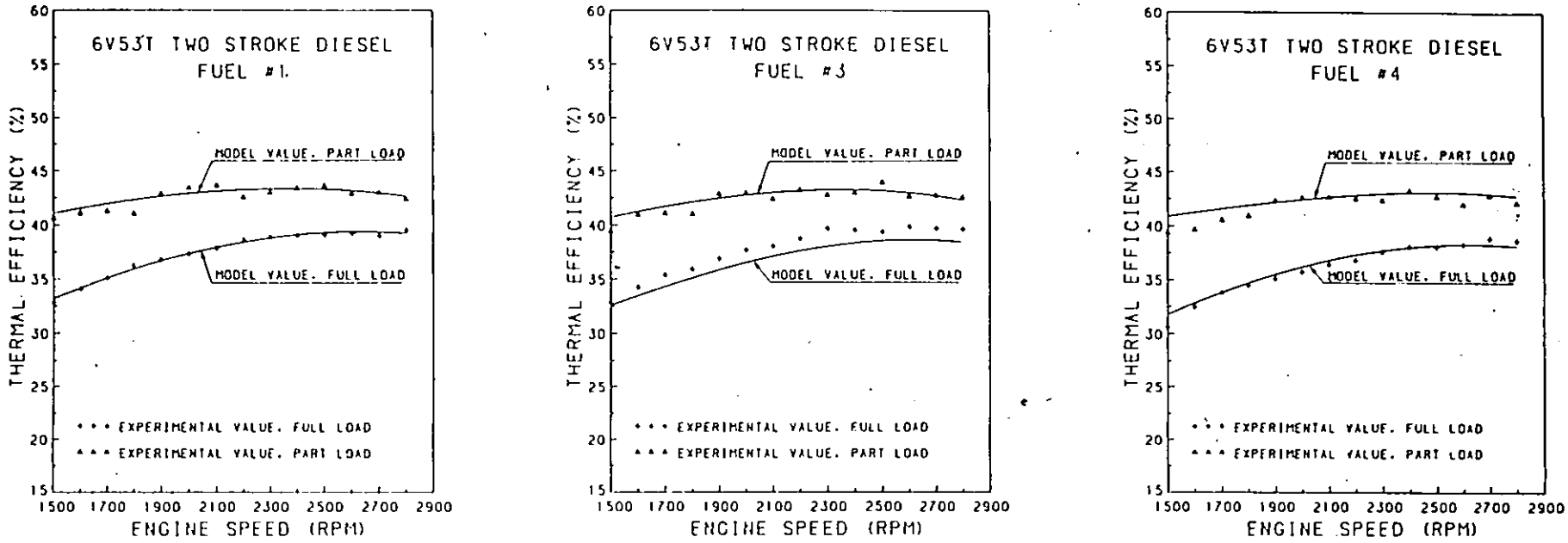

Fig. 7.17: Indicated Thermal Efficiency vs. Engine Speed and Comparison with Experimental Data: (a) Fuel 1, (b) Fuel 3, (c) Fuel 4.

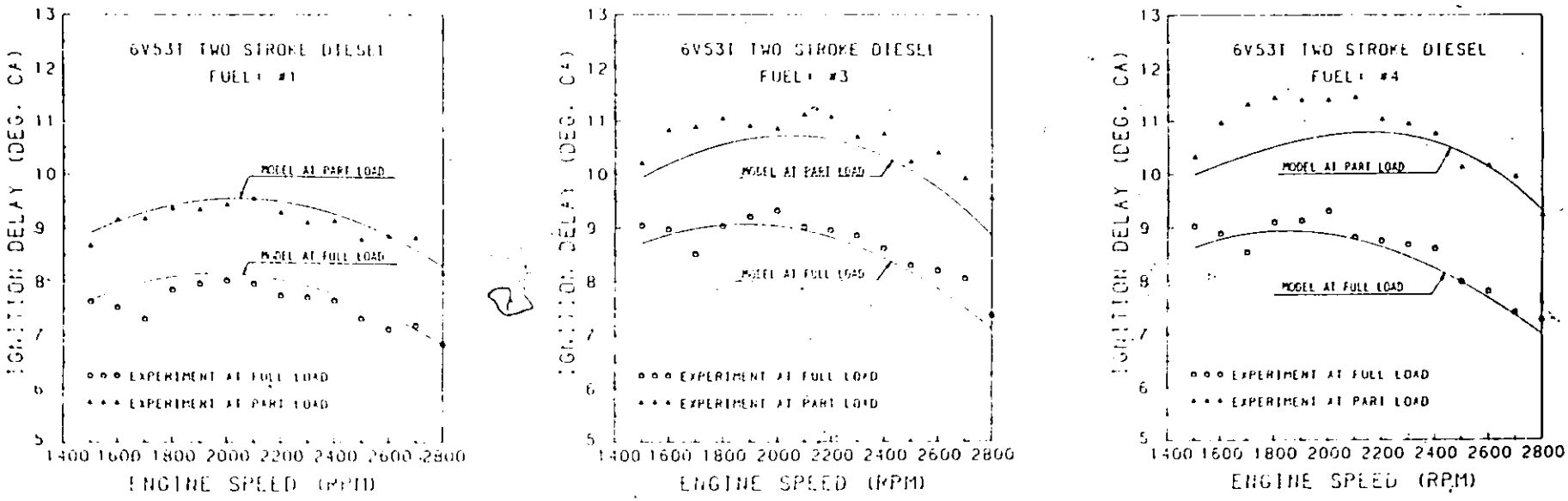

(a) (b) (c)

Fig. 7.18: Ignition Delay vs. Engine Speed and Comparison with Experimental Data: (a) Fuel 1, (b) Fuel 3, (c) Fuel 4.

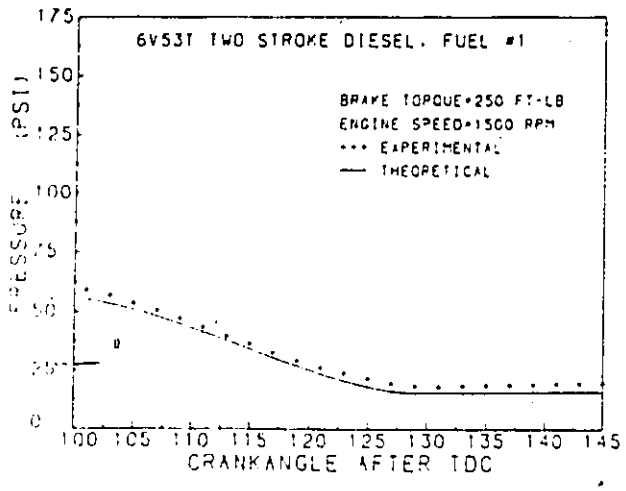

(a) 1500 RPM

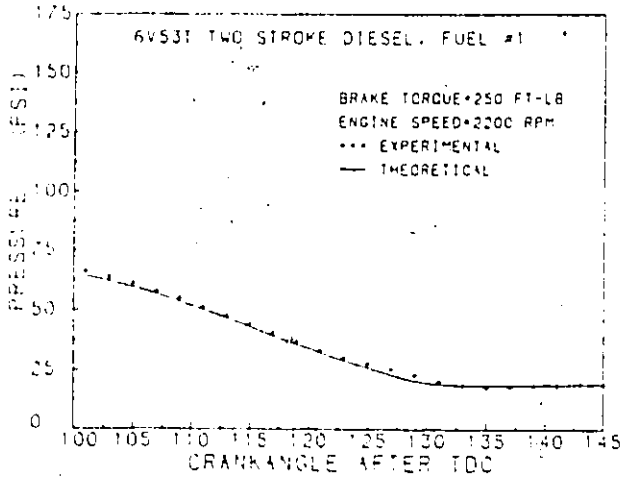

(b) 2200 RPM

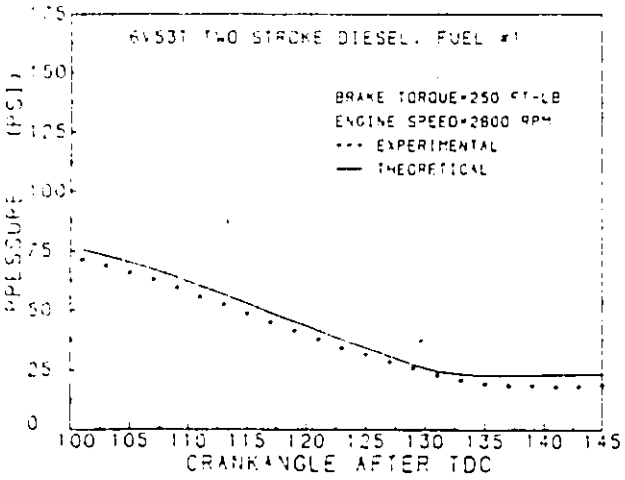

(c) 2800 RPM

Fig. 7.19: Blowdown Cylinder Pressure Prediction and Comparison with Experiment Data at Part Load.

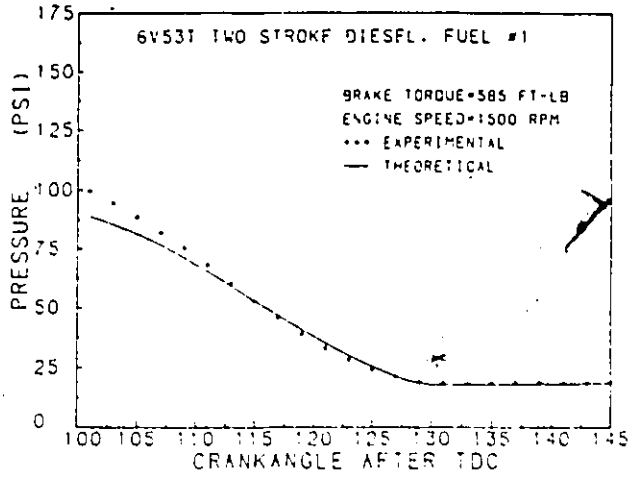

(a) 1500 RPM

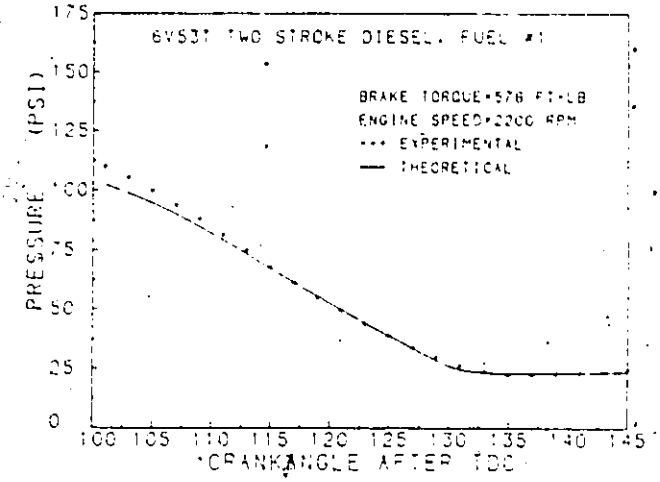

(b) 2200 RPM

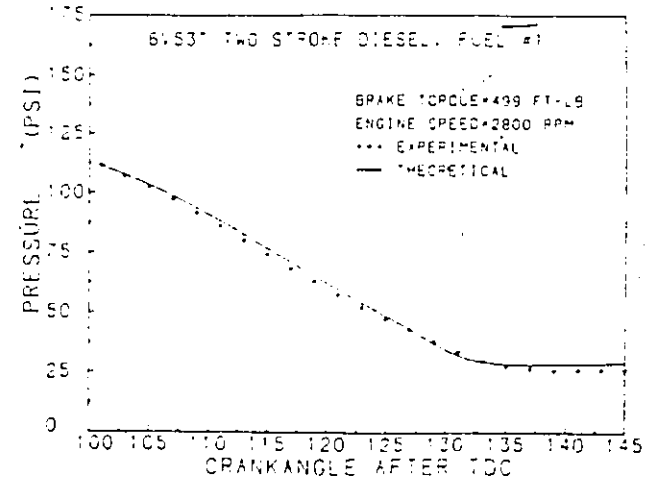

(c) 2800 RPM

Fig. 7.20: Blowdown Cylinder Pressure Prediction and Comparison with Experiment Data at Full Load.

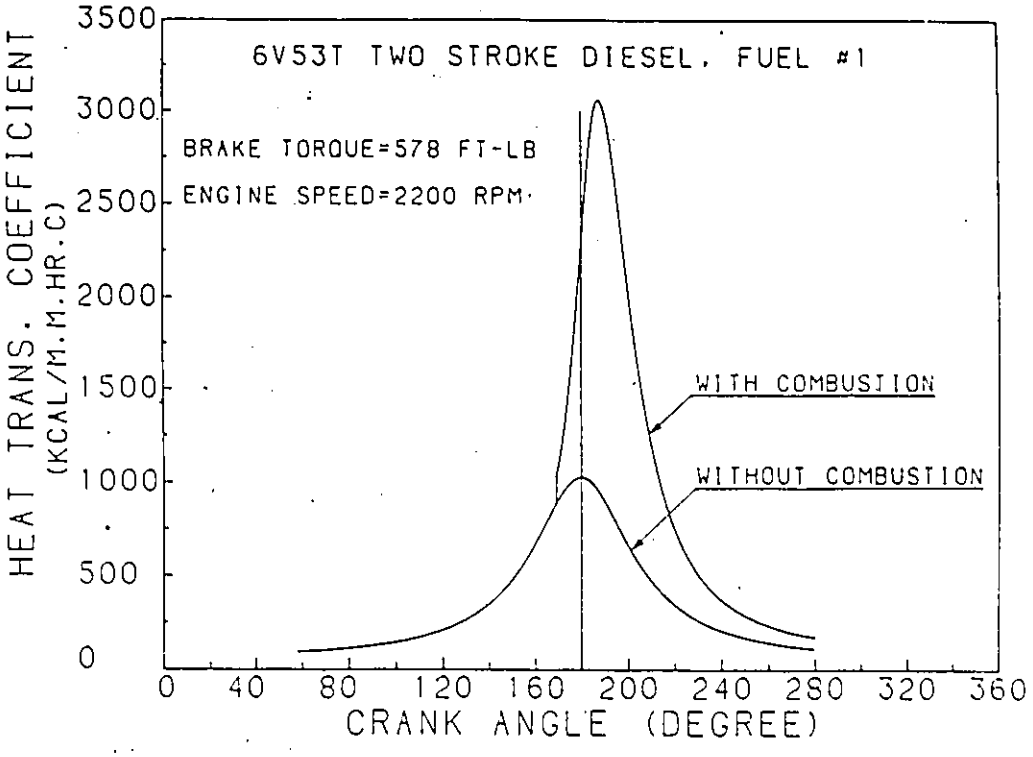

(a) Full Load

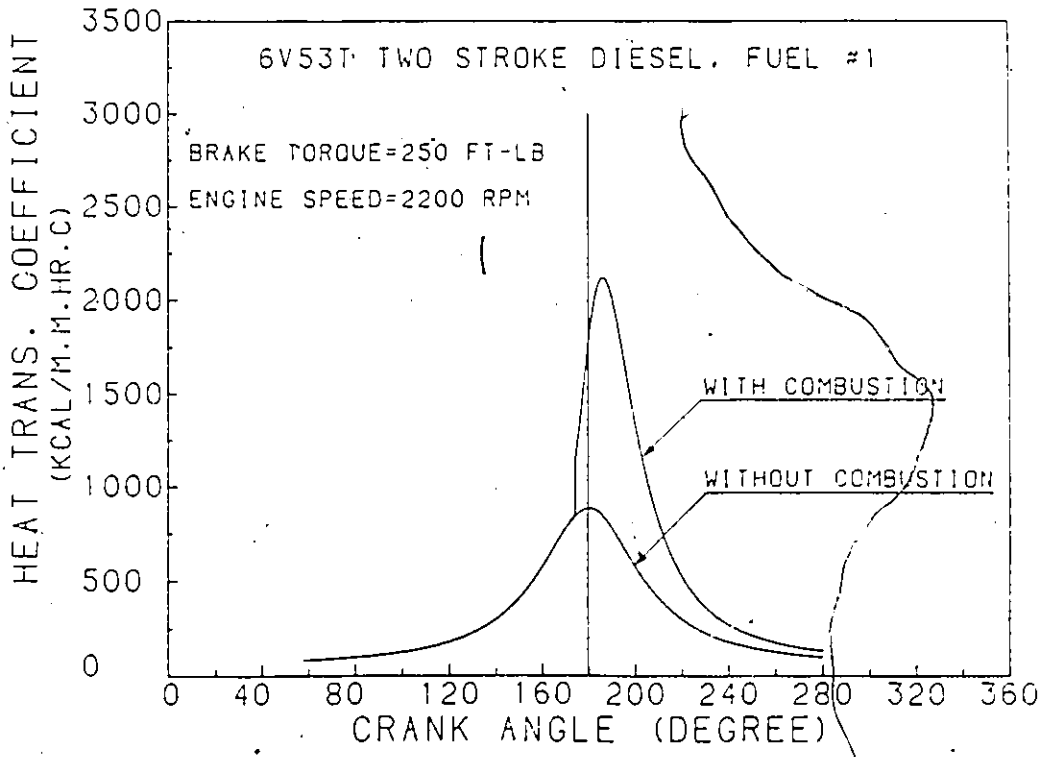

(b) Part Load

Fig. 7.21: Predicted Instantaneous Heat Transfer Coefficient at 2200 RPM.

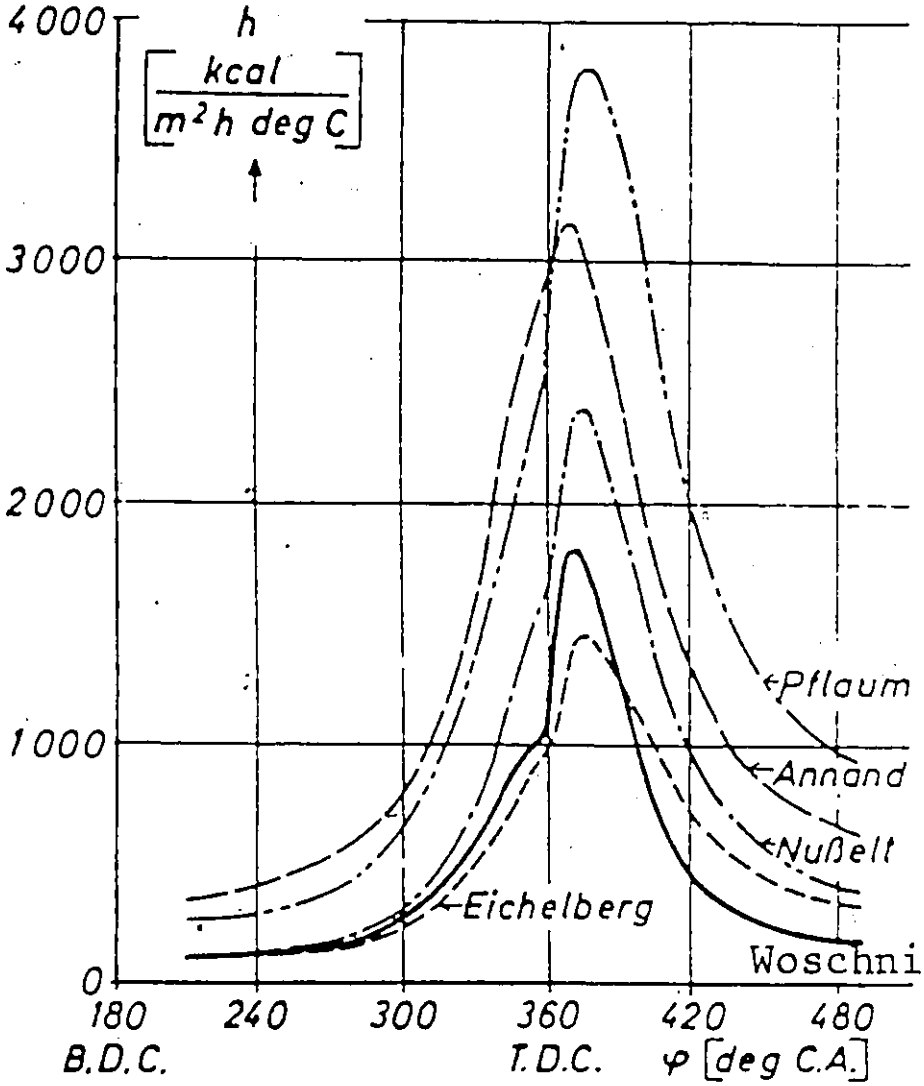

Fig. 7.22: Comparison of Heat Transfer Coefficient Calculated from Different Formulas.

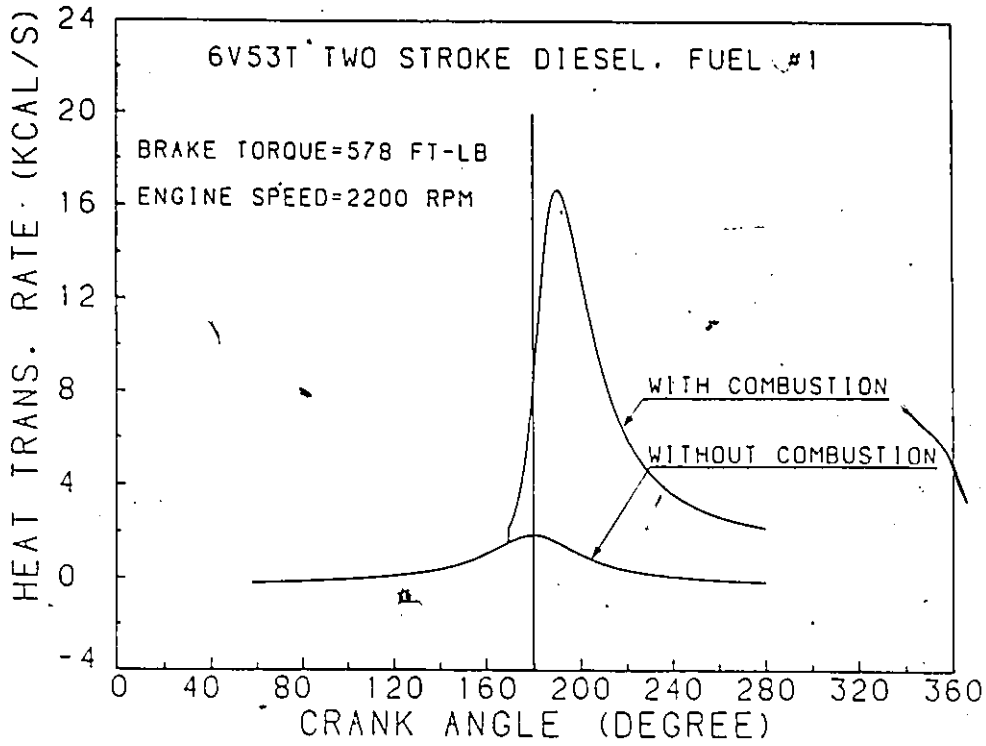

(a) Full Load

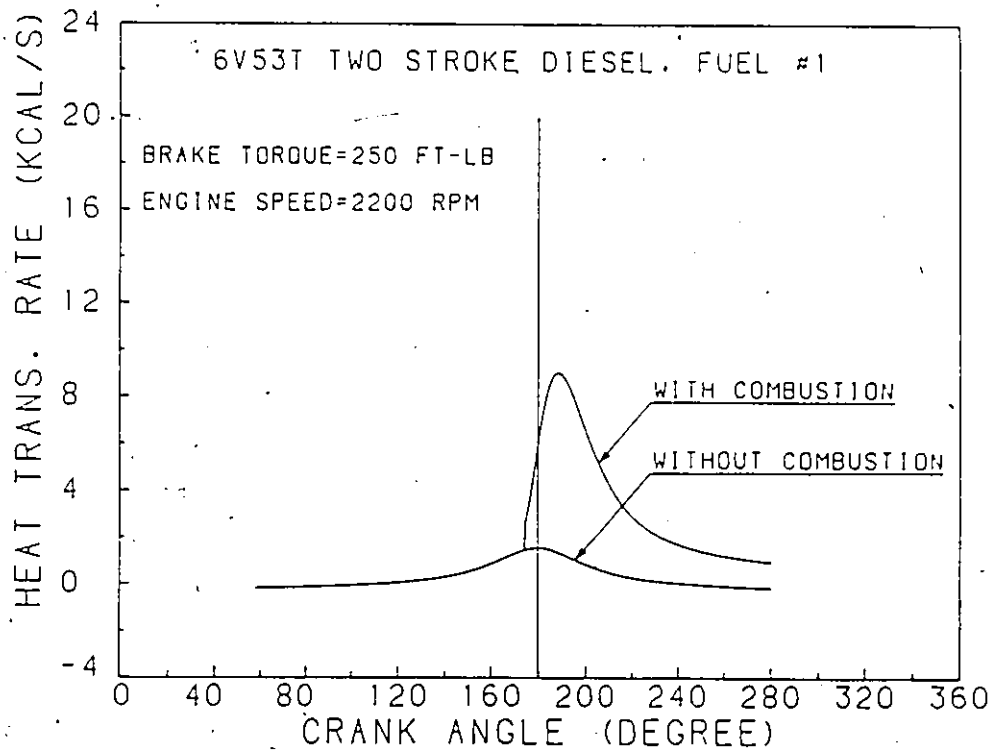

(b) Part Load

Fig. 7.23: Instantaneous Heat Transfer Rate (per Cylinder) Through Combustion Chamber Walls at 2200 RPM.

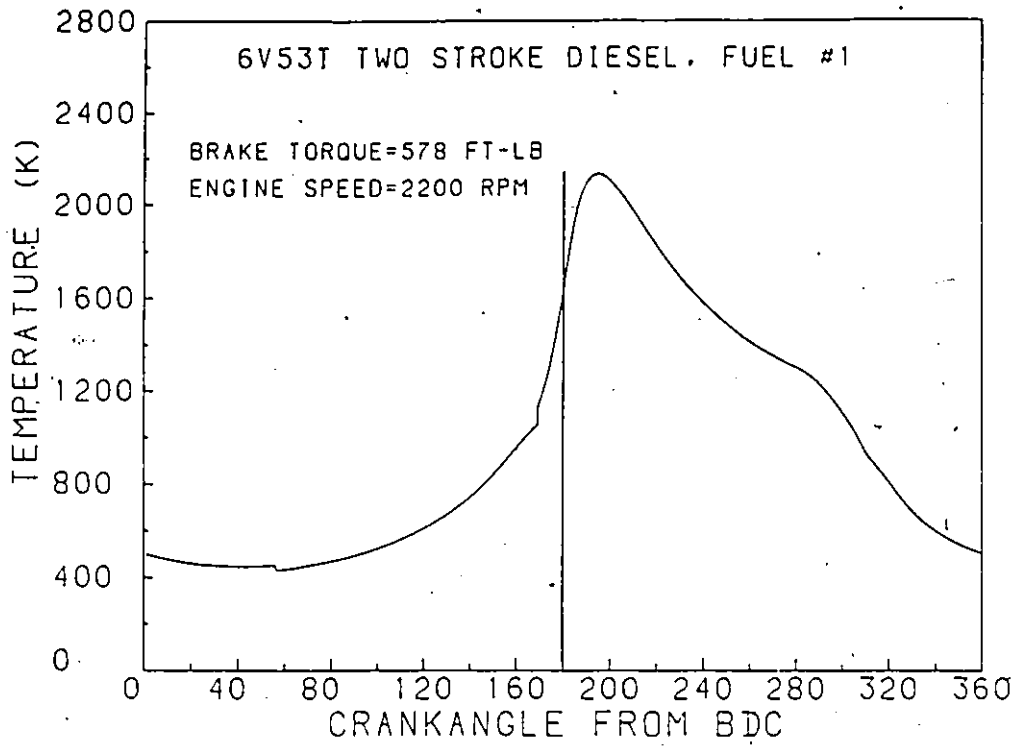

(a) Full Load

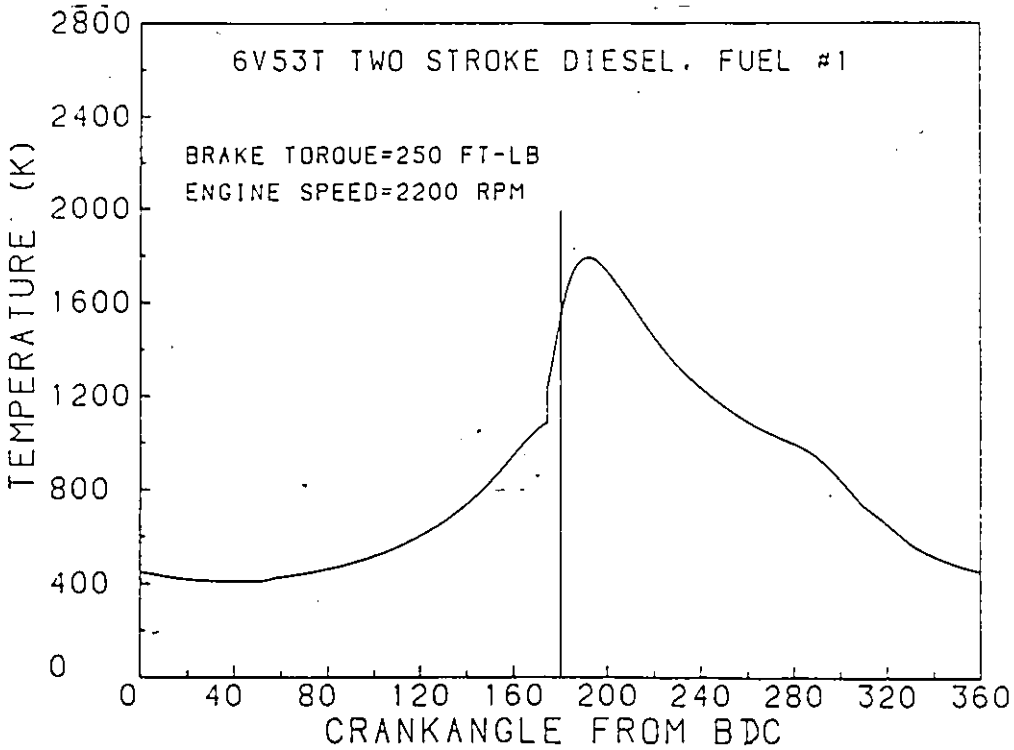

(b) Part Load

Fig. 7.24: Instantaneous Cylinder Gas Temperature vs. Crank Angle at 2200 RPM.

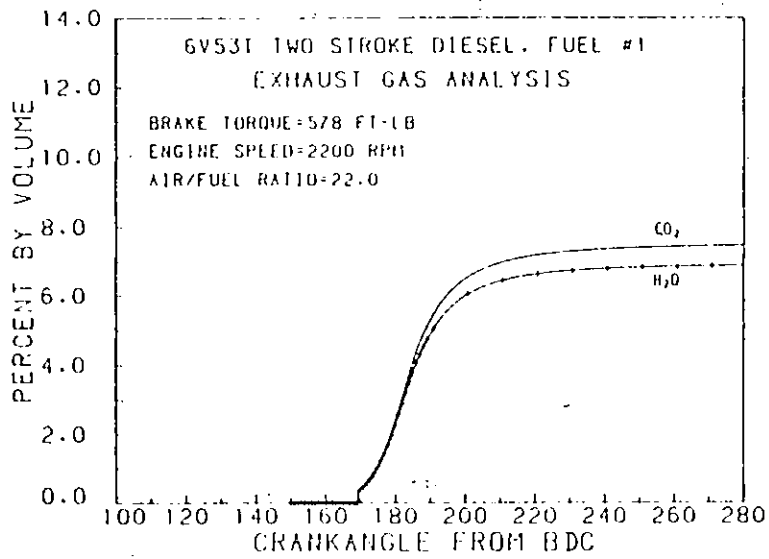

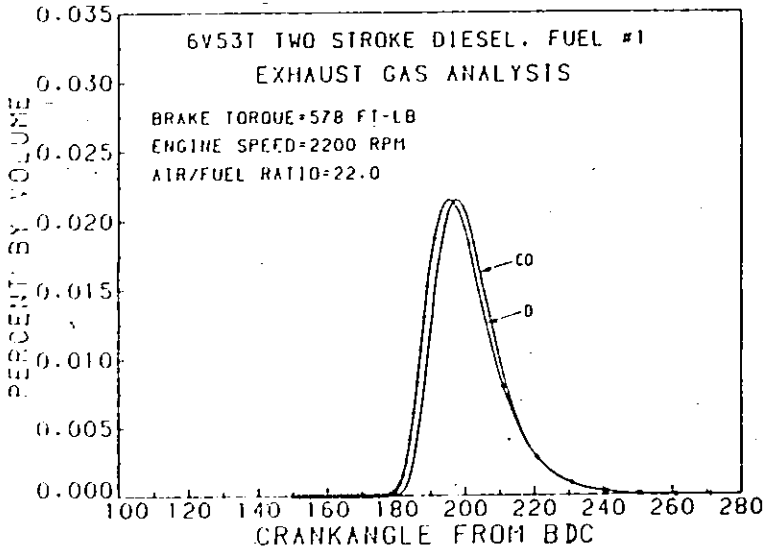

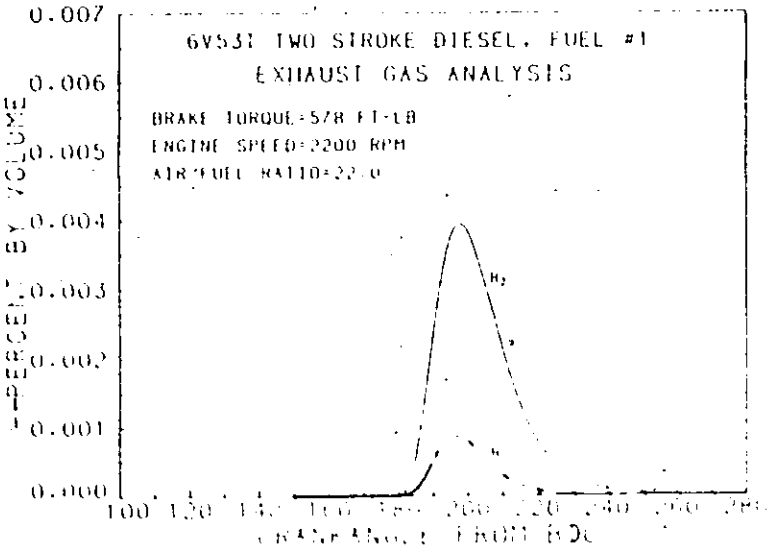

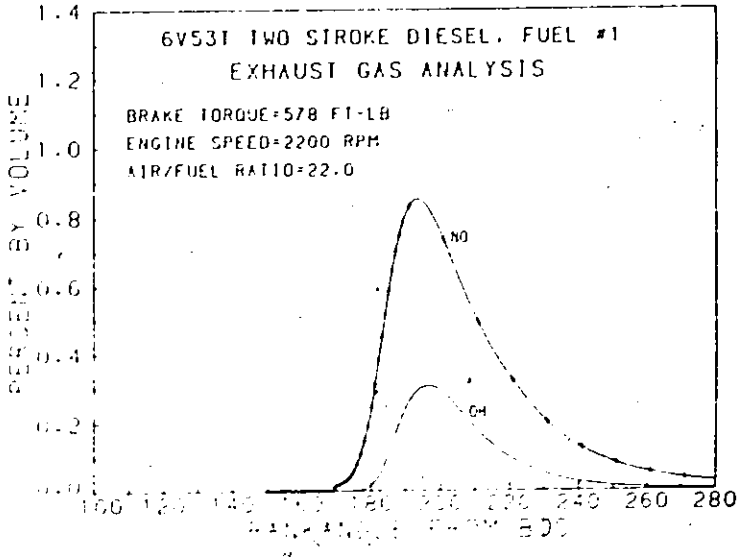

Fig. 7.25: Products of Combustion: Percent by Volume vs. Crank Angle (2200 RPM, Full Load, Fuel 1).

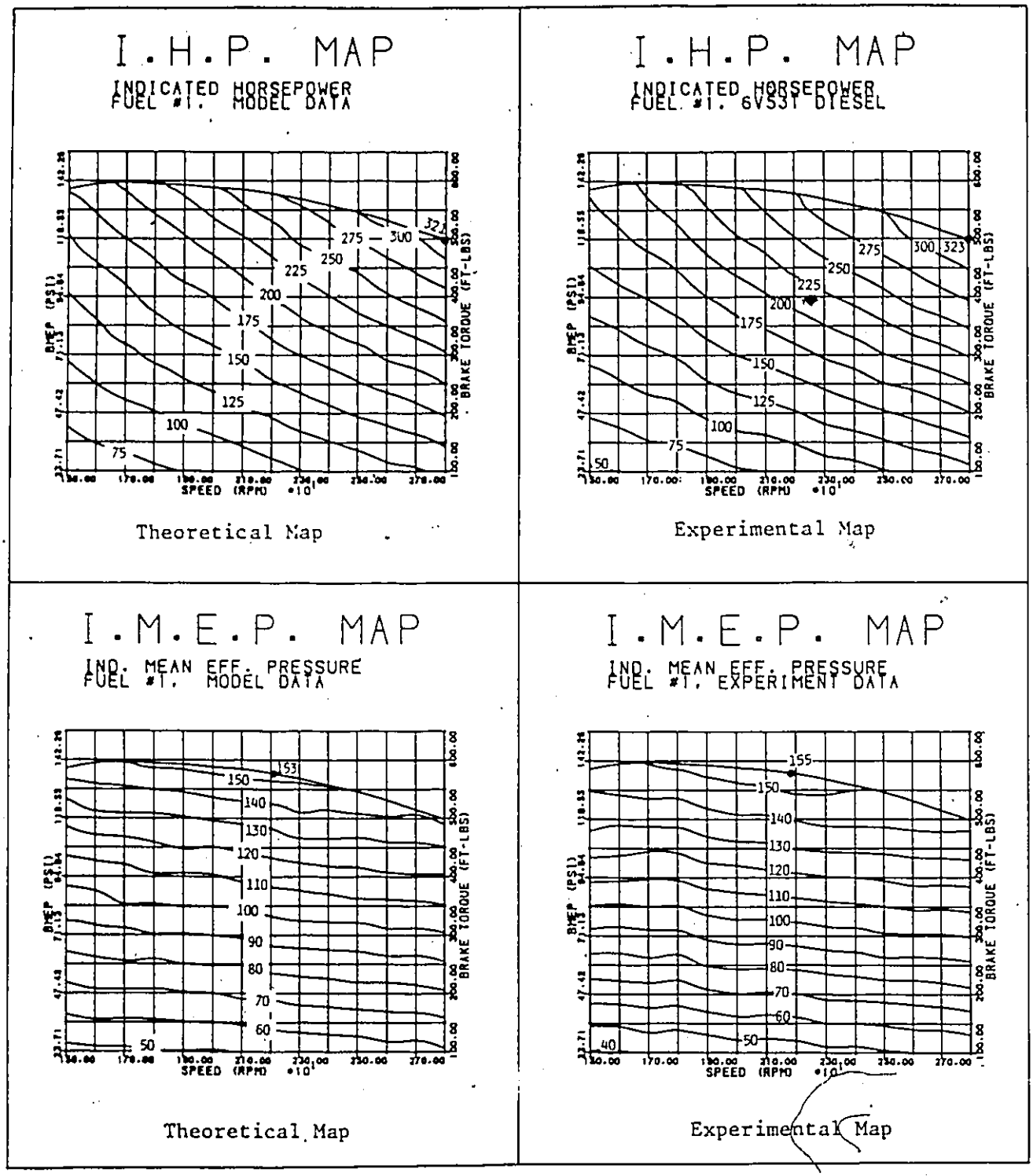

Fig. 7.26: Indicated Parameter Map Comparisons, Fuel 1
(IHP in HP, IMEP in psia)

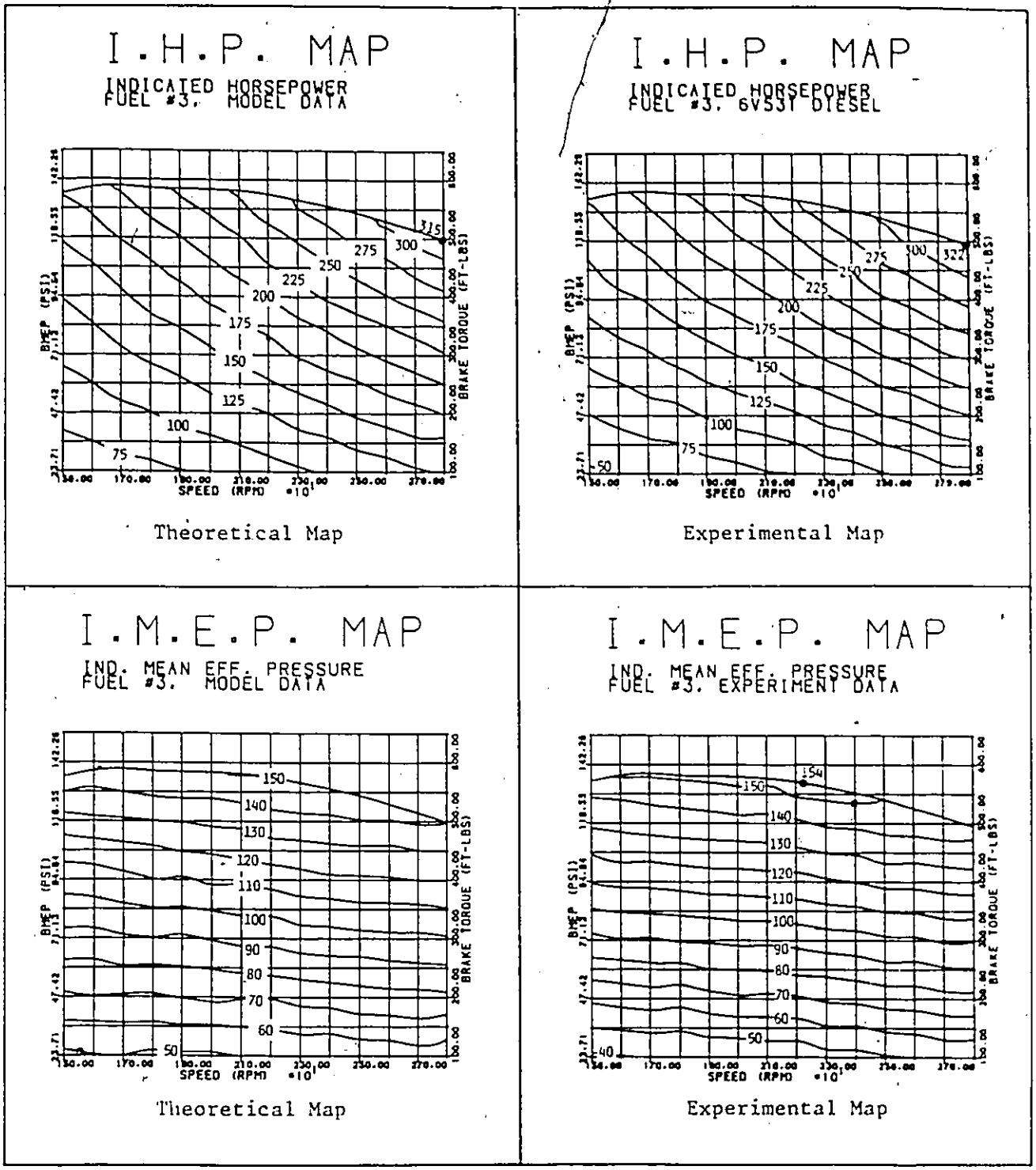

Fig. 7.27: Indicated Parameter Map Comparisons, Fuel 3
(IHP in HP, IMEP in psia)

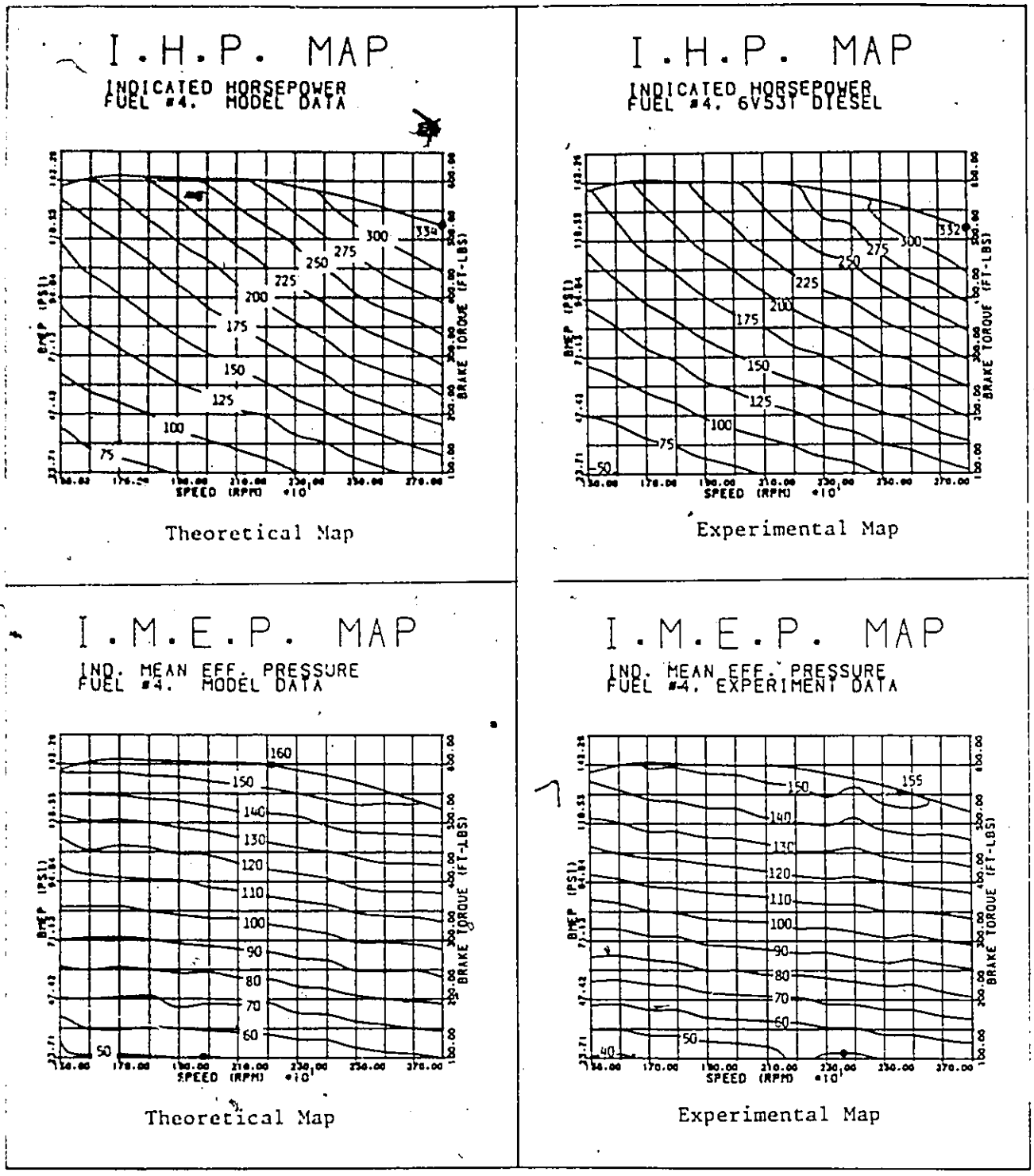

Fig. 7.28: Indicated Parameter Map Comparisons, Fuel 4
(IHP in HP, IMEP in psia)

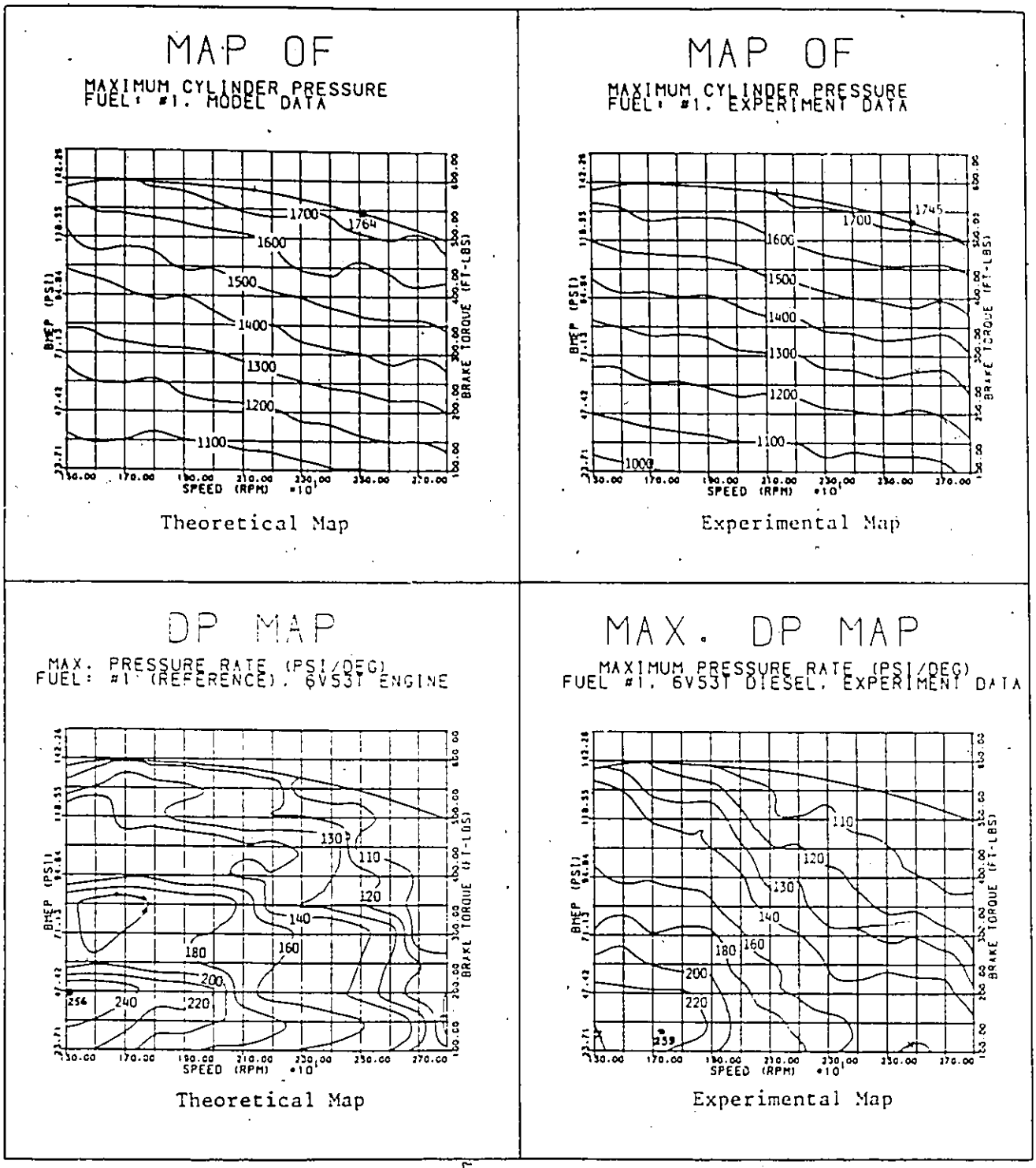

Fig. 7.29: Combustion Parameter Map Comparisons, Fuel 1
(Max. Pressure in psia, Max. DP in psi/°CA)

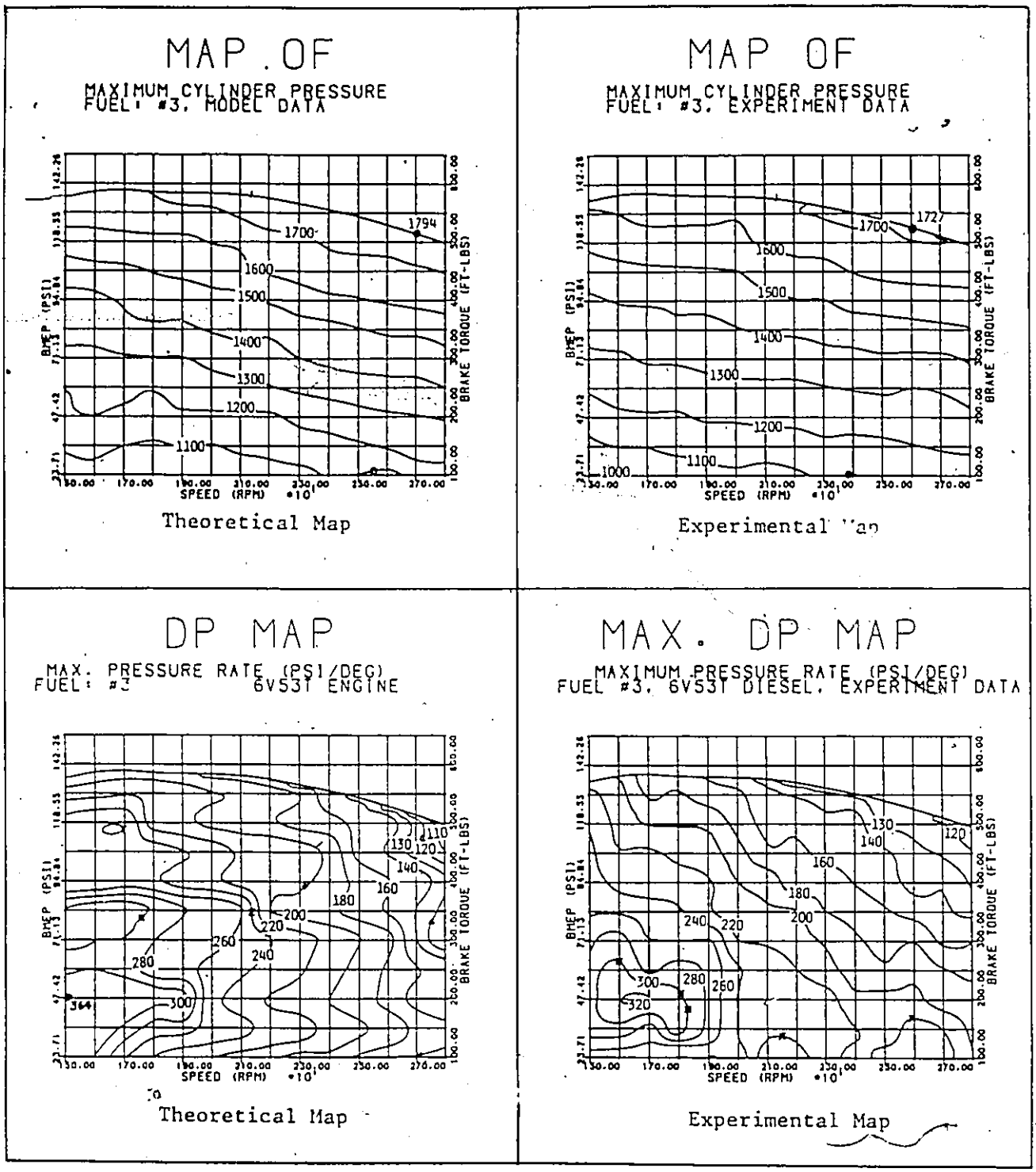

Fig. 7.30: Combustion Parameter Map Comparisons, Fuel 3
(Max. Pressure in psia, Max. DP in psi/°CA)

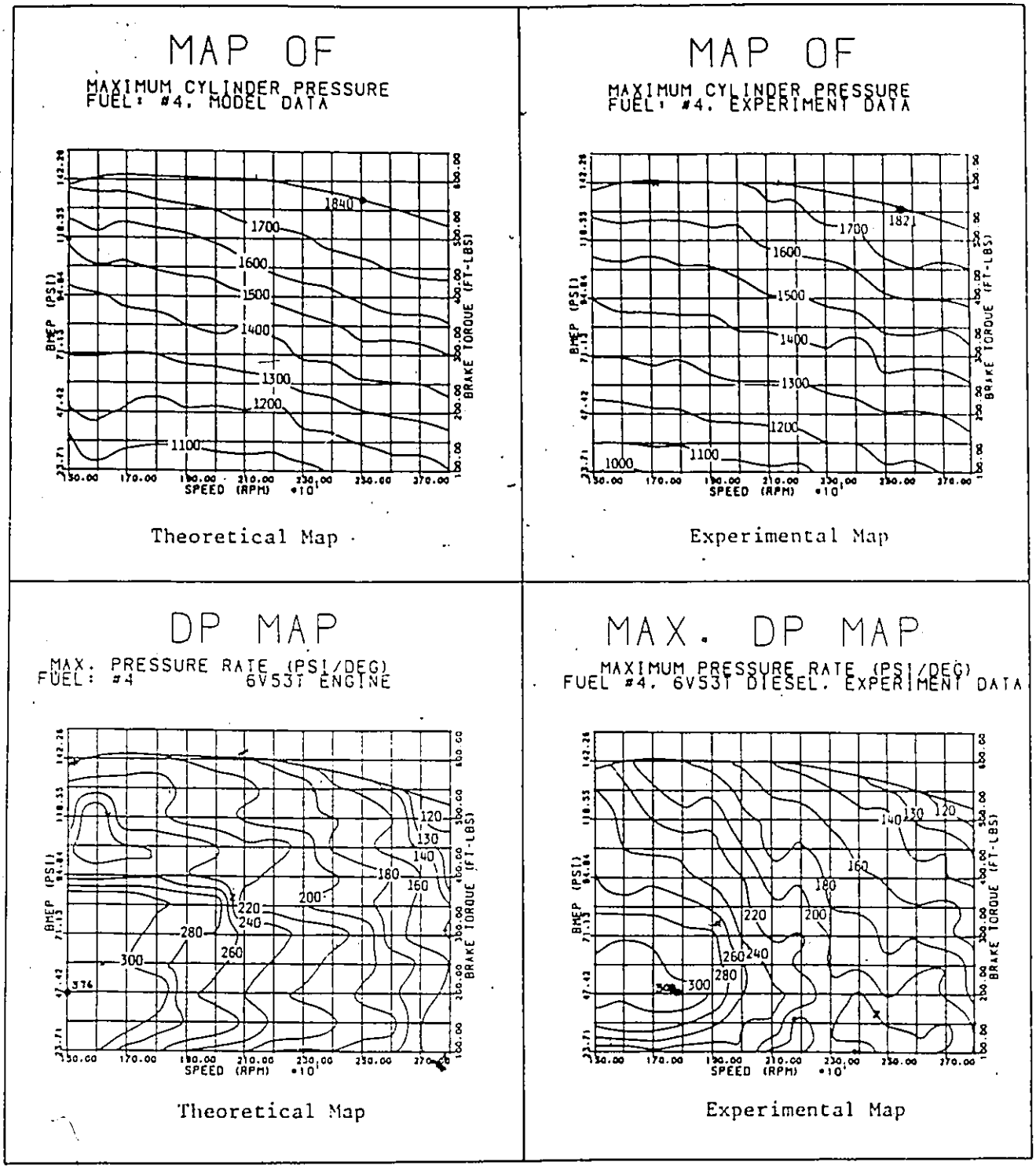

Fig. 7.31: Combustion Parameter Map Comparisons, Fuel 4
(Max. Pressure in psia, Max. DP in psi/°CA)

CHAPTER 8

CONCLUSIONS

In this volume a general thermodynamic and combustion simulation model was developed for a two-stroke diesel engine. Further, by incorporating fuel parameters into a number of submodels, particularly those pertaining to combustion, actual engine/fuel simulation was achieved.

While the theories for engine thermodynamic simulation are fairly well established, diesel engine combustion modeling is not and, in particular, combustion simulation with respect to fuel type is new. In this research program, the combustion process was established around four key submodels, namely: ignition delay, fuel-air mixing rate, fuel-air reaction rate and fundamental chemical equilibrium. There models, as developed, all reflect either explicitly or implicitly, fuel properties as well as engine speed and load settings.

The combustion philosophy reflects actual diesel engine combustion with an explicit ignition delay followed by the characteristic rapid combustion phase on into main and tail combustion. This sequence, though interactive with a number of submodels, is sequentially controlled by the ignition delay, reaction rate and mixing rate models respectively. Also of interest is the fuel simulation. Here, the test fuel is represented by a combination of pure fuels (in this work three pure fuels were used) through a correlation with the test fuels' specification data (in this work C/H ratio, aromatic content and fuel density were used). This allows fundamental chemical equilibrium analysis, rather than the usual "heat release" approach, when simulating combustion. Thus, both the combustion chemical reactions and products of combustion are correlated with diesel fuel specification data.

In summary, the salient features of the study are as follows:

(i) Diesel engine combustion has been successfully simulated and correlated

with fuel properties. This model should be applicable to other diesel engines with suitable fitting of parameters.

(ii) The general thermodynamic and combustion simulation model was fitted to the 6V53T engine and test fuels through a direct correlation with experimental data. This model should lend itself readily not only to other two-stroke diesel engines but also to four-stroke diesels by replacing the blowdown/scavenging and initial condition submodels.

(iii) Through an extensive evaluation study it was shown that:

— the model accurately simulates all engine trends not only for all engine speed/load settings but also for each of the test fuels,

— engine indicated performance and combustion parameters are accurately predicted, and that

— the early combustion period, in particular pressure rates as a function of fuel type, is correctly interpreted.

(iv) Parametric studies revealed a number of interesting insights into engine/fuel behavior including:

— ignition delay was seen to have the greatest affect on combustion pressure rates although maximum pressure rates themselves do not affect maximum cylinder pressures nor engine indicated performance,

— fuel cetane number was seen to have a direct correlation with ignition delay; however, cylinder gas temperature was seen to control or dominate the actual delay period, and

— initial conditions were seen to have the greatest impact on engine performance.

In general, it is believed that this model can be used not only for engine performance parametric studies but also for more subtle engine/fuel interaction analyses.

PART II

ENGINE/FUEL ANALYSIS

CHAPTER 9

INTRODUCTION

In Part I of this thesis, a broad literature survey of internal combustion engine modeling was executed together with the development and evaluation of a thermodynamic and combustion model for the two stroke GM6V53T diesel engine. Simulation focused on the development of several key models which affect interaction and combustion characteristics as well as simulation over the complete engine operating range and for each of the three test fuels. These include: i) ignition delay, ii) fuel-air mixing rate, iii) fuel-air reaction rate and iv) equilibrium chemical reaction or combustion. The model was extensively evaluated in Chapter 7 by direction comparison with the complete engine/fuel data base established in the companion engine/fuels testing program. The model was shown to correlate with experimental data for all test fuels and at all engine operating points. In particular, early diesel combustion was accurately simulated, thus suggesting that cylinder pressure rates (diesel knock) as well as engine performance could be investigated.

Further, since one of the R&D objectives was to gain insight into engine/fuel interaction, fuel parameters were incorporated into a number of the submodels. This feature appears to allow simulation of ignition delay, early combustion and main combustion not only between engine operating points but also from fuel-to-fuel. In the experimental program, the only difficulty found when burning the off-specification fuels was the high pressure rates encountered during early combustion. Theoretical analysis can provide considerable insight and understanding of the early combustion process which is a complex interaction of a number of parameters, including cylinder thermodynamic state, fuel injection schedule, ignition delay, reaction rate controlled and diffusion rate controlled combustion phases, etc. Thus, searching for possible solutions of reducing the pressure rate while maintaining engine output and thermal efficiency can only be reasonably approached through theoretical analyses.

In Chapter 10, engine/fuel interaction studies are conducted at 2200 RPM, full and part load, for each of the three test fuels. In particular: i) cylinder pressure and temperature; ii) pressure rate and fuel mass burning rate; iii) ignition delay and iv) cylinder thermodynamic state at the start of fuel injection are investigated. The study of these parameters help to explain the subtle engine/fuel behavior noted in the experimental measurements.

An engine performance study is conducted in Chapter 11 at 2800 RPM, full load with Fuel 1. In this study, the variation of engine power, thermal efficiency, maximum cylinder pressures, maximum pressure rates and ignition delay are evaluated subject to changes in: i) injection timing; ii) airbox temperature (intercooler); iii) airbox pressure (turbocharger boost) and iv) engine compression ratio.

In Chapter 12, a combustion knock and control study is presented. Both experimental measurement and theoretical modeling have shown that high cylinder pressure rates occur in the low engine speed and load region. Thus, a pilot injection system was studied at 1600 RPM, 200 ft-lb. brake torque operating condition. An optimized pilot injection profile was established by studying the overall affects of: i) start of pilot injection; ii) start of main injection, and iii) mass of fuel in the pilot. This dual injection principle was also tested at maximum engine speed and torque (2800 RPM, full load) conditions. The predicted results for all three fuels are very encouraging and show that engine performance and combustion characteristics can both be improved.

CHAPTER 10

ENGINE/FUEL INTERACTION

10.1 OVERVIEW

One of the R&D objectives was to predict and analyze engine performance and combustion characteristics when operating on the off–specification, tar-sands derived fuels. Thus, the submodels in the simulation program were developed to represent both engine and fuel properties. Although the physical and chemical processes occurring in an engine cylinder are too complex to model exactly, the simulation program does reflect a number of key parameters such as gas temperature and pressure, mass of air, availability of air and fuel, fuel composition, cetane number and density, etc., and thus allows fuel-to-fuel comparisons to be made. Such comparisons provide a first significant step towards understanding some of the subtleties of engine/fuel interaction.

In this chapter, comparison of a number of thermodynamic and combustion parameters, as a function of the three test fuels, are presented.

10.2 COMBUSTION PHASE ANALYSIS

During the cycle, simulation of compression, expansion and the gas exchange processes are only indirectly related to fuel properties. Basically, engine/fuel interaction directly occurs only from the start of fuel injection to the end of combustion. However, as was shown in Part I, maximum cylinder pressure rates or combustion knock occurs during the onset of combustion while main combustion controls engine performance. For this study, engine operating conditions were chosen at nominal settings of 2200 RPM, full load and 2200 RPM, 200 ft.lbs. brake torque. The initial conditions

used in the simulations are based on actual experimental data for each fuel and engine operating point.

10.2.1 CYLINDER TEMPERATURE AND PRESSURE CORRELATION

Comprehensive insight into engine/fuel interaction can be gained from a direct comparison of cylinder temperature and pressure for each of the three fuels under the same initial operating conditions. Figure 10.1 plots cylinder temperature and pressure for the three fuels at full load operating conditions. It could be noted that the discontinuities in the curves correlate with the period of rapid (early or onset-of) combustion. For Fuel 4, onset of combustion occurs between Fuels 1 and 3, contrary to their cetane number order. However, Fuel 4 does result in the highest cylinder temperatures and pressures. Further, while temperatures remain ordered, the pressure curves of Fuels 1 and 3 cross during main combustion. On the other hand, at part load (Fig. 10.2), Fuels 3 and 4 are almost indistinguishable and remain ordered throughout the cycle. Some of these subtle differences can also be noted in the experimental data.

10.2.2 PRESSURE RATE AND MASS BURNING RATE CORRELATION

Predicted cylinder pressure rates for the three fuels at 2200 RPM are shown in Figure 10.3 for full load and part load operation. These figures show the instantaneous pressure rate calculated every $1°CA$ over the complete compression and expansion cycle. Without combustion, the motored rate curves are near symmetric about TDC. With combustion, the pressure rates show a similar character in that the maximum peak occurs immediately after ignition. Comparisons from fuel to fuel show that the maximum rates are significantly higher with lower cetane fuels at the same operating loads. Likewise, rates are significantly higher at part load for all fuels tested.

Fuel mass burning rates calculated by the simulation program at the corresponding operating conditions are presented in Figure 10.4. Though similar to cylinder pressure rates, they do represent a more fundamental form of data. Both at full and part load operation, mass burning rates have two peaks. The first peak starts at the start of ignition and rapidly increases to its maximum value due to the initial reaction rate controlled combustion. It also drops quickly when the premixed fuel/air mixture, which accumulated during the ignition delay period, is consumed by the reaction. The main body, incorporating the second peak, is diffusion controlled combustion. It is clear that reaction rate controlled combustion affects cylinder pressure rates or combustion knock while fuel-air diffusion rate affects maximum cylinder pressures and engine performance.

At a given operating point, the mass burning rates for all fuels are remarkably similar with the low cetane fuels giving slightly higher initial peaks which correspond with the higher pressure rates encountered. However, comparing with Figure 10.3, it is clear that the correlation between mass burning rate and cylinder pressure rate is not linear and further, high mass burning rates during main combustion (diffusion controlled) do not give rise to high cylinder pressure rates.

Low load operation, when compared with full load, always gives higher reaction rate controlled peaks with low diffusion rate controlled peaks. This is opposite to that desired for good combustion characteristics and thermal efficiency. In general, it is desirable to have low initial peaks and high diffusion controlled mass burning rate peaks with a minimum of tail combustion.

10.2.3 IGNITION DELAY CORRELATION

The ignition delay model was developed and evaluated in Chapter 3 together with an investigation of the controlling parameters (Fig. 3.2 and Table 3–3). Thus far

in this section, fuel-to-fuel comparisons of the cylinder gas temperature and pressure, pressure rates and mass burning rates have been made. The cause of many of the differences has not been explained but can be related to ignition delay itself. Figure 10.5 plots ignition delay for the three fuels at full and part operation. As was noted earlier (and also from the experimental data), Fuel 4 produces shorter ignition delays than Fuel 3 at full load, contrary to their cetane numbers. Also, part load operation gives rise to significantly longer delay periods and thus higher initial mass burning rates resulting in a 'rougher' combustion.

Table 10–1 lists the ignition delay and numerical values of the controlling parameters. This data, together with the sensitivity study conducted in Chapter 3, allows interpretation of the ignition delay behavior.

TABLE 10-1

IGNITION DELAY AND CONTROLLING PARAMETERS
2200 RPM, FULL AND PART LOADS

OPERATING CONDITION	FUELS	EFFECTING PARAMETER				IGNITION DELAY (°CA)
		CETANE NUMBER	CYL. PRESSURE AT INJECTION (ATM, abs.)	CYL. TEMPERATURE AT INJECTION (°K)	F/A RATIO	
FULL LOAD 2200 RPM	FUEL 1	46.7	38.8	968.8	0.0456	8.0
	FUEL 3	36.9	38.3	979.4	0.0468	8.9
	FUEL 4	35.9	39.3	982.3	0.0488	8.6
PART LOAD 2200 RPM	FUEL 1	46.7	37.8	1003.9	0.0266	9.5
	FUEL 3	36.9	38.2	1007.2	0.0263	10.7
	FUEL 4	35.9	37.8	1007.9	0.0272	10.8

Table 10–1 shows that at full load, it is the fuel/air ratio, not temperature, pressure or cetane number, which dominates the relative ignition delay periods between Fuels 3 and 4. Likewise, at part load, it is again the fuel/air ratio which accounts for the longer delay periods over full load operation. It is also interesting to view the temperature and pressure trends, at the start of injection, for the three fuels. Figures 10.6 and 10.7 plot this data as a function of engine speed for full and part loads.

10.3 PRODUCTS OF COMBUSTION

The hydrocarbon fuel combustion model was developed in Chapter 5. Mass and energy conservation equations were applied together with seven equilibrium reactions resulting in eleven products of combustion. Including excess air, they are classified as major products: O_2, N_2, CO_2, H_2O, and minor products: CO, H_2, OH, O, H, NO, CH_4, according to their mole concentrations. Equilibrium state was assumed at each calculation step in order to determine the mole concentrations for each chemical species at the instantaneous cylinder temperature and pressure. The concept of total enthalpy was used instead of heating value, together with heat transfer and work energy, to balance the total energy in the system before and after chemical reaction. This feature enables the model to predict combustion products as a function of not only thermodynamic state (gas temperature and pressure), but also hydrocarbon fuel properties such as the hydrogen/carbon ratio and density.

This preliminary study is performed at 2200 RPM, full load operating conditions for the three fuels. During the combustion period, i.e. from start of ignition to exhaust valve opening, the volume percentages of each product are calculated for the three fuels under the same initial conditions. Figure 10.8 shows the calculated volume percentages of the reaction products versus crank angle position for the three fuels.

The major combustion products, CO_2 and H_2O, accumulate while the hydro-

carbon fuel is consumed and reach their maximum values at the point of blowdown. On the other hand, the minor species: CO, H_2, OH, O, H and NO reach a maximum at about $15°CA$ aTDC in accord with cylinder gas temperatures. Based on the assumed chemical equilibrium throughout the cycle, dissociation of the minor species occurs during expansion to the point of blowdown. Of the minor species, NO has the highest volume percentage followed by OH, CO, O, H_2, and H. The concentration of CH_4 was determined to be in the order of 10^{-30}. Also, Fuel 4 produces the highest concentrations of minor species in the exhaust gases, followed by Fuel 3 and Fuel 1.

Tables 10-2 and 10-3 present the maximum values reached and the values at blowdown of the product concentrations in the cylinder respectively (again, CH_4 is neglected and excess air, O_2 and N_2, is not of interest). The maximum volume percentage values of Fuel 3 minor products increased by $4 - 18\%$ relative to Fuel 1 while those of Fuel 4 increased substantially by $15 - 70\%$. This is, in part, due to the higher cylinder temperatures of Fuel 3 ($2152°K$) and Fuel 4 ($2196°K$) compared with that of Fuel 1 ($2134°K$). At blowdown, the volume percentages of Fuel 3 minor products increased by 9–33% relative to that of Fuel 1 while those of Fuel 4 increased by 31–176%. Again, temperatures at blowdown are: Fuel 1 ($1199°K$), Fuel 3 ($1312°K$) and Fuel 4 ($1344°K$).

10.4 EFFICIENCY AND FUEL CONSUMPTION

Indicated thermal efficiency (η_t) and indicated specific fuel consumption (ISFC) are two parameters that can be used to assess diesel engine performance regardless of engine size and type. The general simulation program was used to predict these two parameters over the complete engine operating range. Figures 10.9 and 10.10 plot the maps for each of the fuels.

From fuel to fuel, the maps do not show any significant difference since η_t

and ISFC basically depend on the main combustion process which is similar for each of the fuels. As analyzed in previous sections, fuel properties strongly affect the early combustion phase such as ignition delay and pressure rates, however, the early combustion period does not significantly affect engine performance even if very high pressure rates are encountered.

TABLE 10-2

COMPARISON OF THE MAXIMUM CONCENTRATION OF COMBUSTION PRODUCTS FOR THE THREE FUELS (2200 RPM, Full Load)

CONSTITUENT	MAXIMUM SPECIES CONCENTRATION				
	FUEL 1	FUEL 3		FUEL 4	
	Value (% by Volume)	Value (% by Volume)	Relative to Fuel 1 (%)	Value (% by Volume)	Relative to Fuel 1 (%)
CO_2	7.744	7.745	0	8.067	+4.2
H_2O	6.884	6.448	-6.3	6.669	-3.1
CO	0.0215	0.0254	+18.1	0.0363	+68.8
H_2	0.00394	0.00415	+5.3	0.00564	+43.1
OH	0.305	0.316	+3.6	0.369	+21.0
O	0.0215	0.0240	+11.6	0.0294	+36.7
H	0.867×10^{-3}	0.991×10^{-3}	+14.3	0.146×10^{-2}	+68.4
NO	0.850	0.891	+4.8	0.982	+15.5

TABLE 10-3

COMPARISON OF THE CONCENTRATION OF

COMBUSTION PRODUCTS AT BLOWDOWN FOR THE THREE FUELS

(2200 RPM, Full Load)

CONSTITUENT	SPECIES CONCENTRATION AT BLOWDOWN				
	FUEL 1	FUEL 3		FUEL 4	
	Value (% by Volume)	Value (% by Volume)	Relative to Fuel 1 (%)	Value (% by Volume)	Relative to Fuel 1 (%)
CO_2	7.744	7.745	0	8.067	+4.2
H_2O	6.884	6.448	-6.3	6.669	-3.1
CO	0.440×10^{-5}	0.587×10^{-5}	+33.4	0.111×10^{-4}	+152.3
H_2	0.275×10^{-5}	0.321×10^{-5}	+16.7	0.559×10^{-5}	+103.3
OH	0.00291	0.00322	+10.7	0.00436	+49.8
O	0.896×10^{-5}	0.111×10^{-4}	+23.9	0.177×10^{-4}	+97.5
H	0.244×10^{-7}	0.324×10^{-7}	+32.8	0.675×10^{-7}	+176.6
NO	0.0271	0.0296	+9.2	0.0355	+31.0

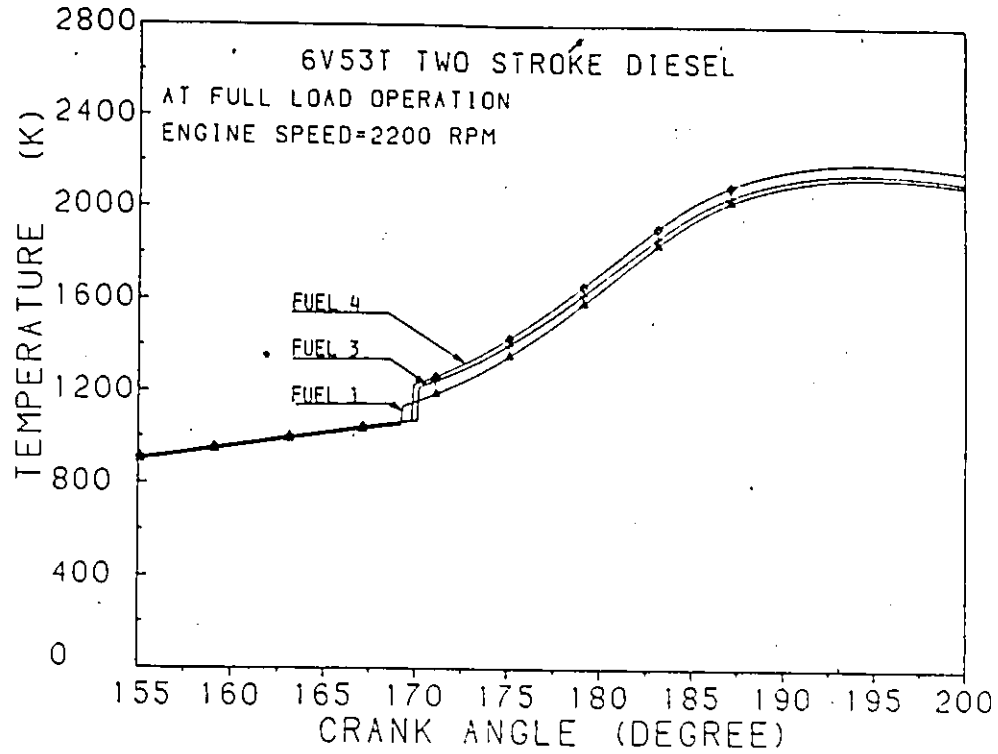

(a) Temperature Comparison

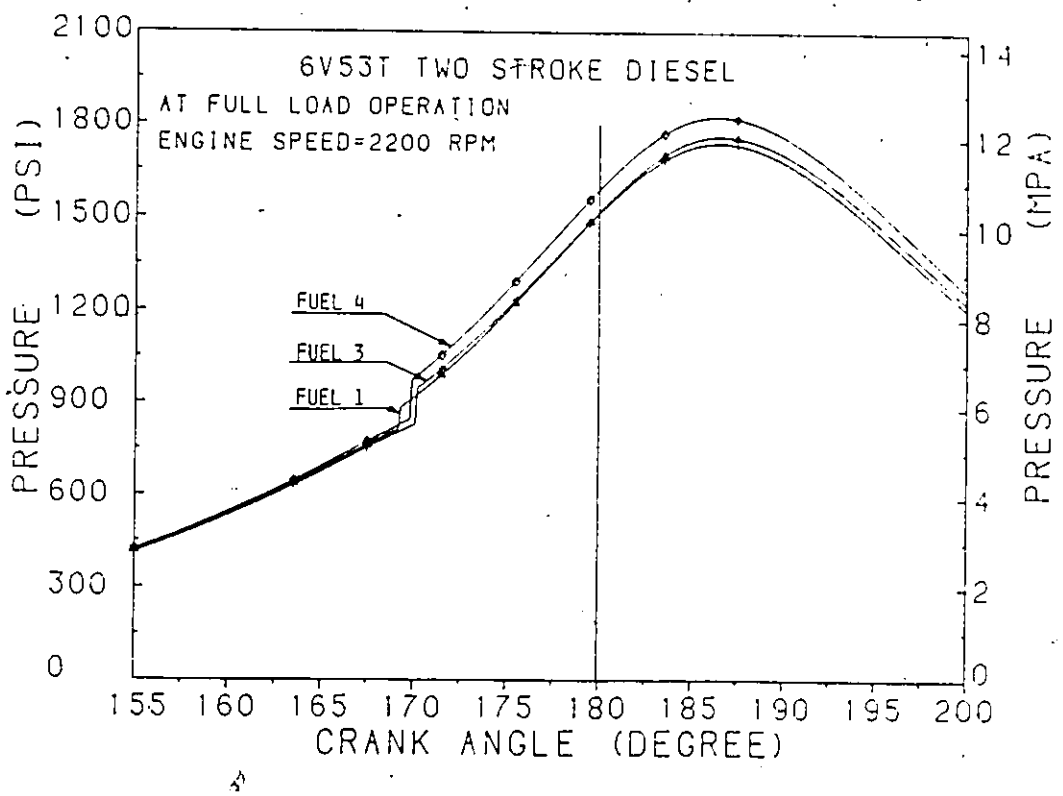

(b) Pressure Comparison

Fig. 10.1: Predicted Cylinder Temperature and Pressure Comparison for the Three Test Fuels at 2200 RPM, Full Load

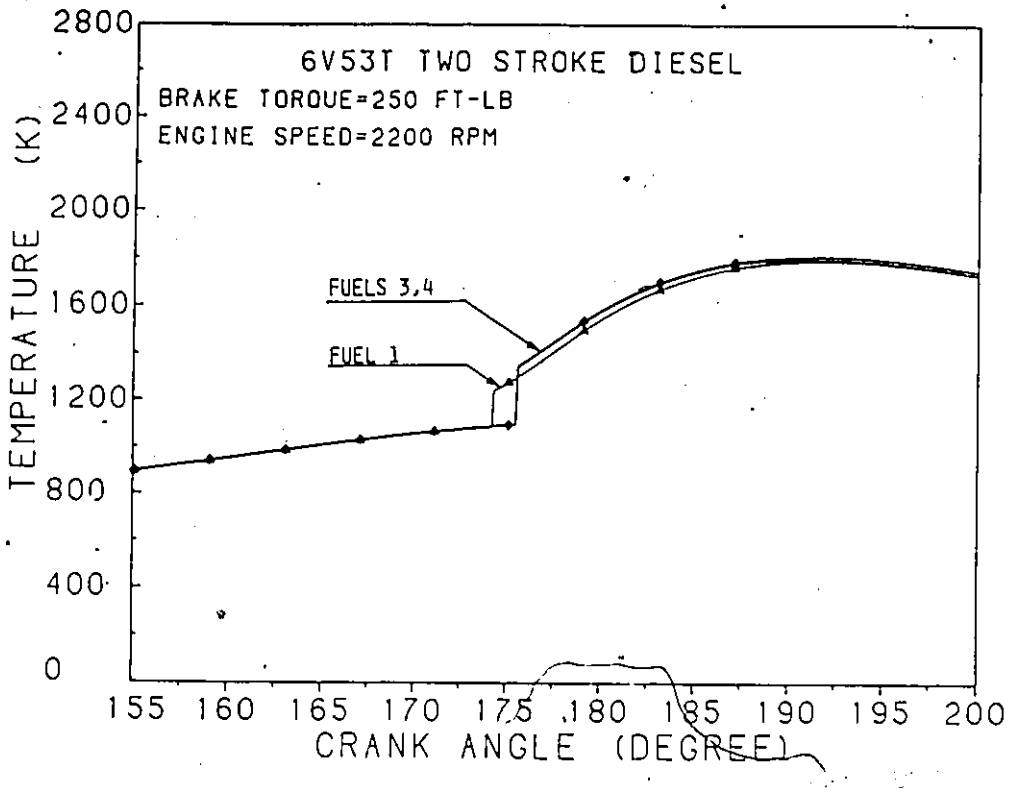

(a) Temperature Comparison

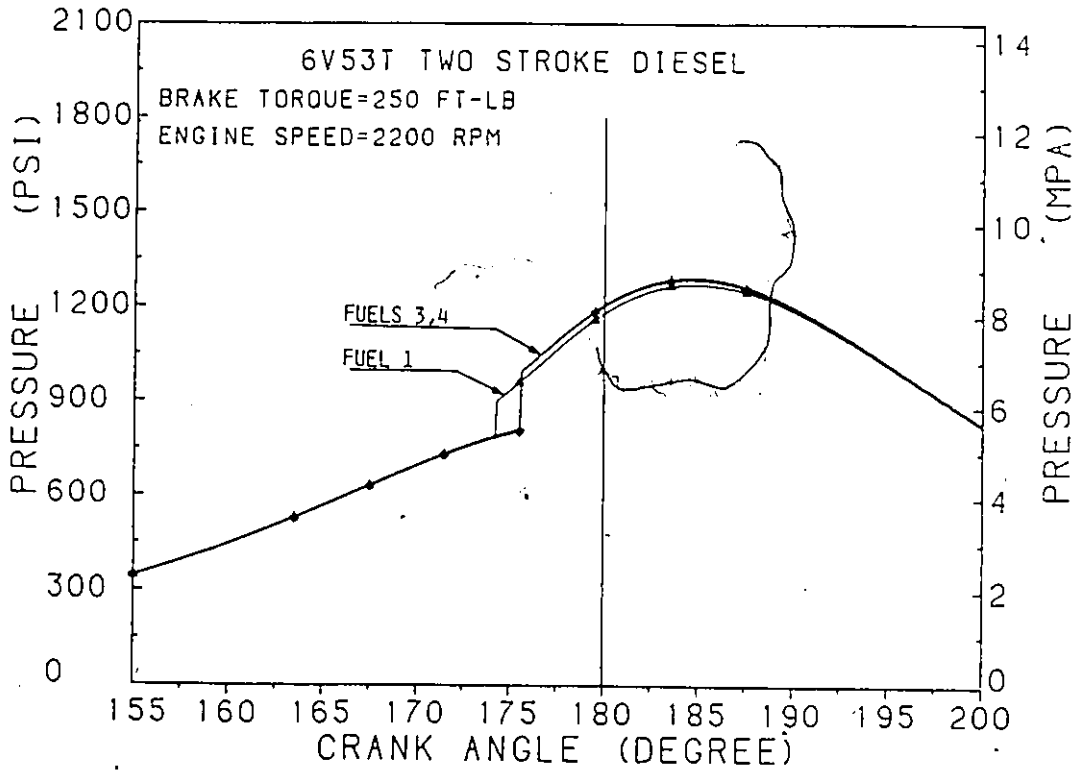

(b) Pressure Comparison

Fig. 10.2: Predicted Cylinder Temperature and Pressure Comparison for the Three Test Fuels at 2200 RPM, Part Load

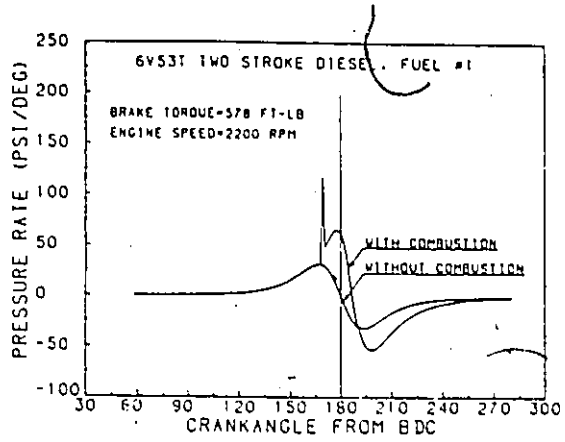

Fuel 1

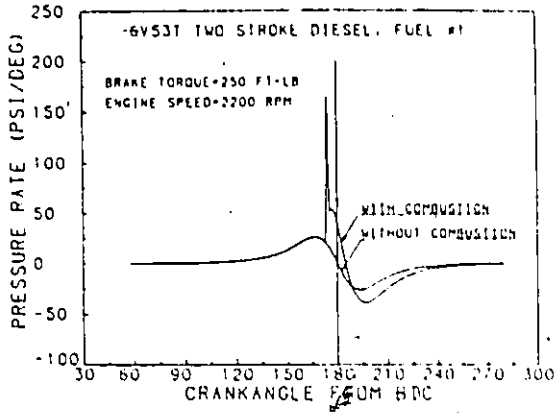

Fuel 1

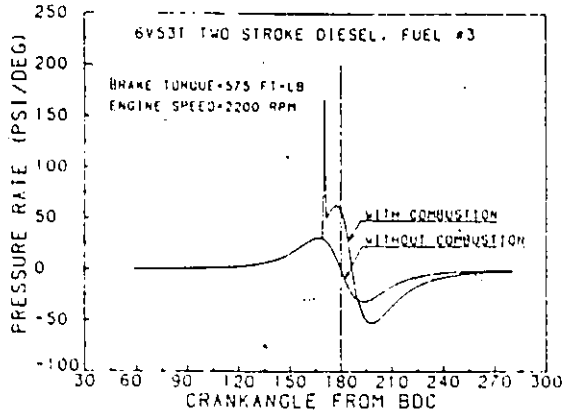

Fuel 3

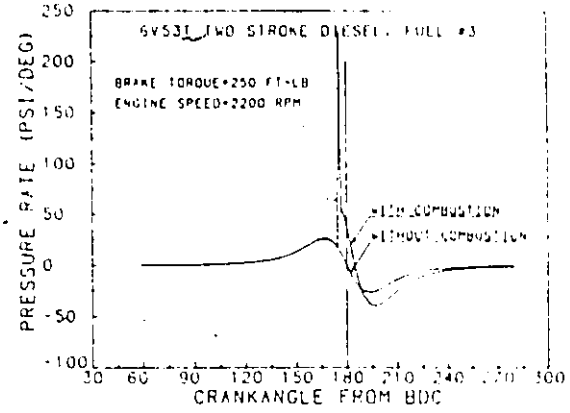

Fuel 3

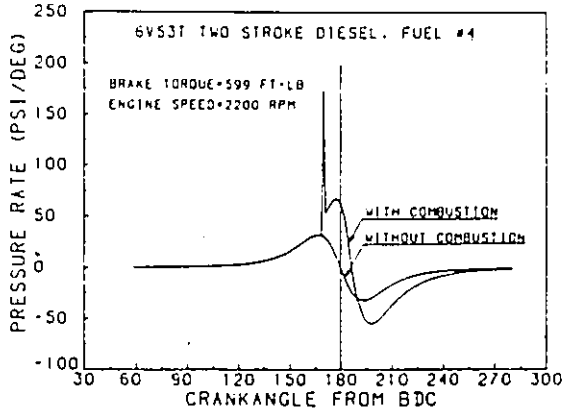

Fuel 4

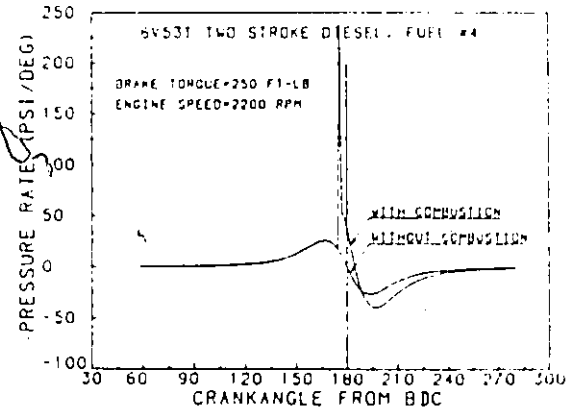

Fuel 4

(a) Full Load Operation

(b) Part Load Operation

Fig. 10.3: Predicted Cylinder Pressure Rate at 2200 RPM, Full Load and Part Load Operating Conditions for the Three Test Fuels

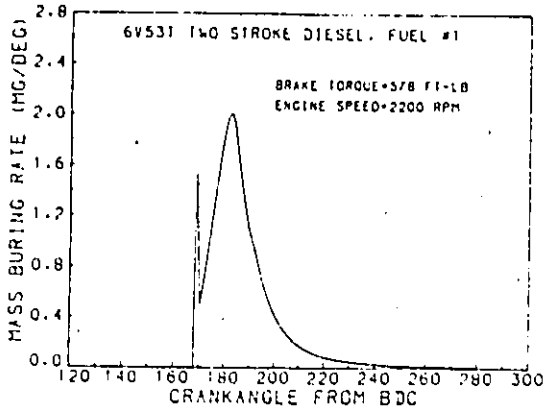

Fuel 1

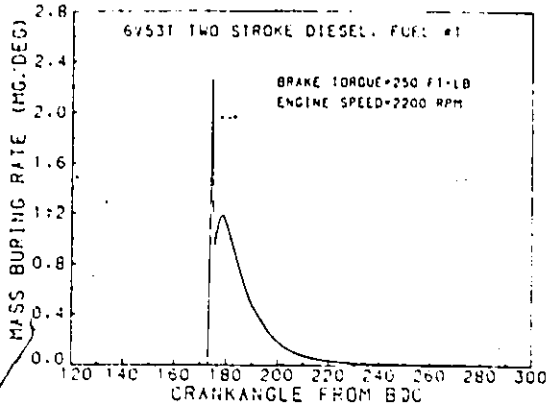

Fuel 1

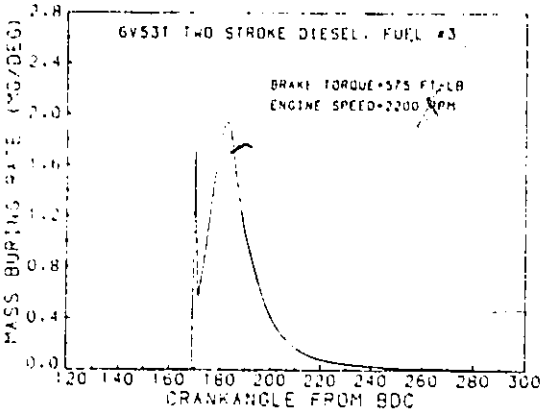

Fuel 3

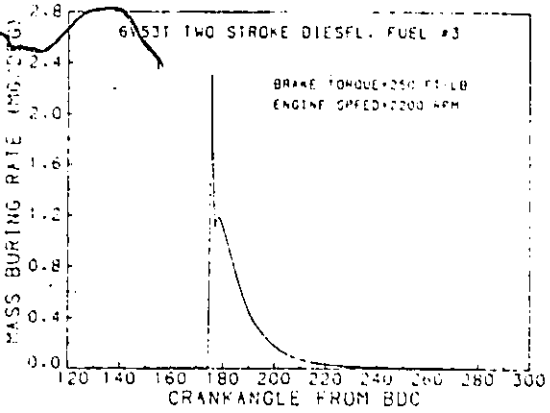

Fuel 3

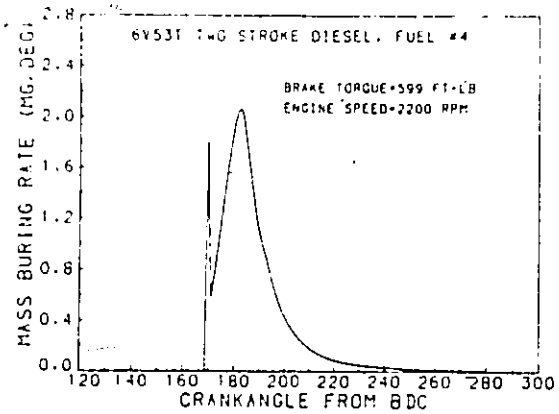

Fuel 4

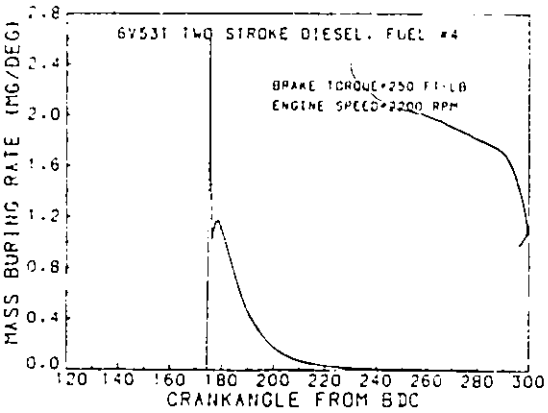

Fuel 4

(a) Full Load Operation

(b) Part Load Operation

Fig. 10.4: Predicted Fuel Mass Burning Rate at 2200 RPM, Full Load and Part Load Operating Conditions for the Three Test Fuels

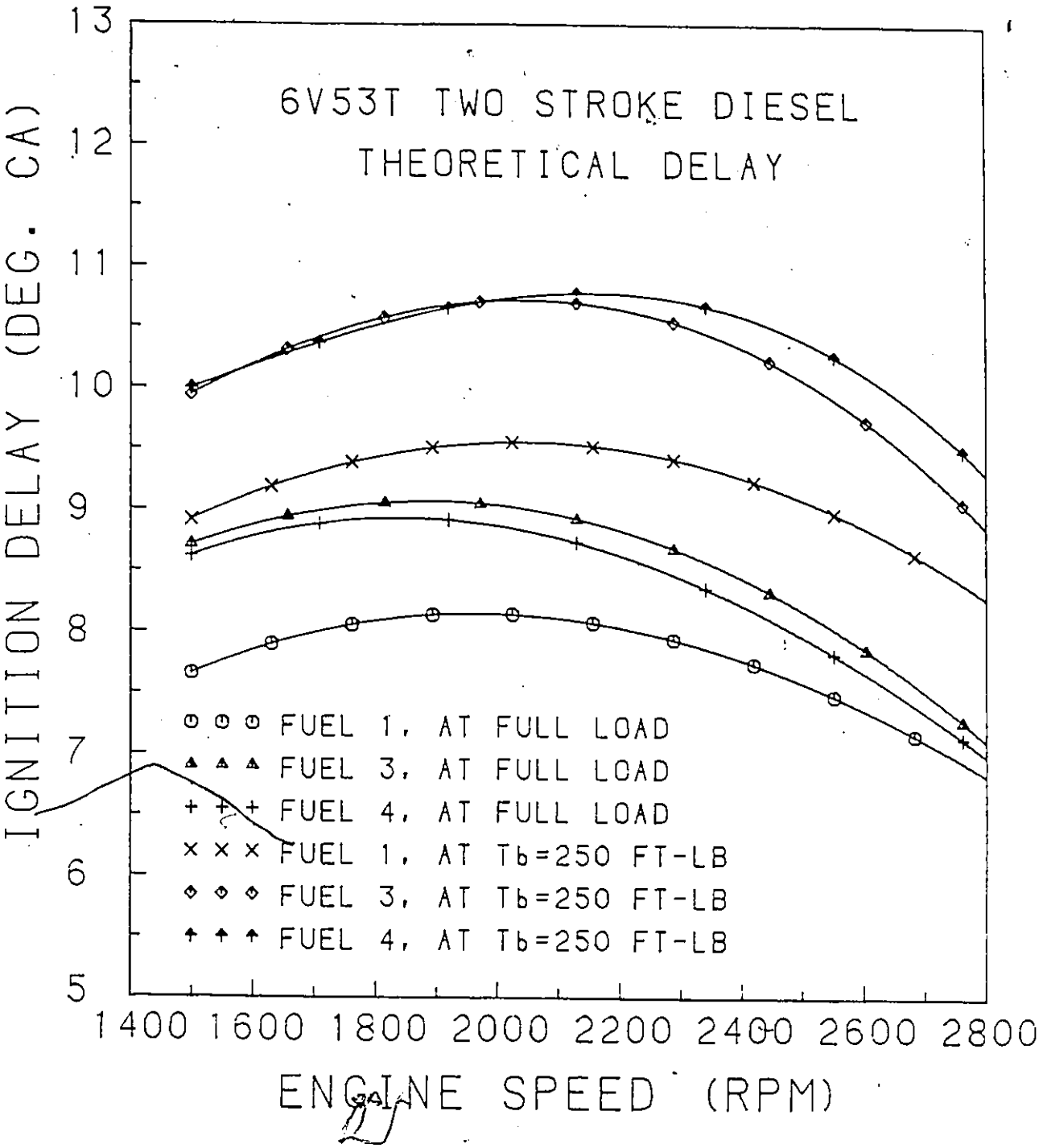

Fig. 10.5: Predicted Ignition Delay for the Three Fuels at Full Load and Part Load Operation

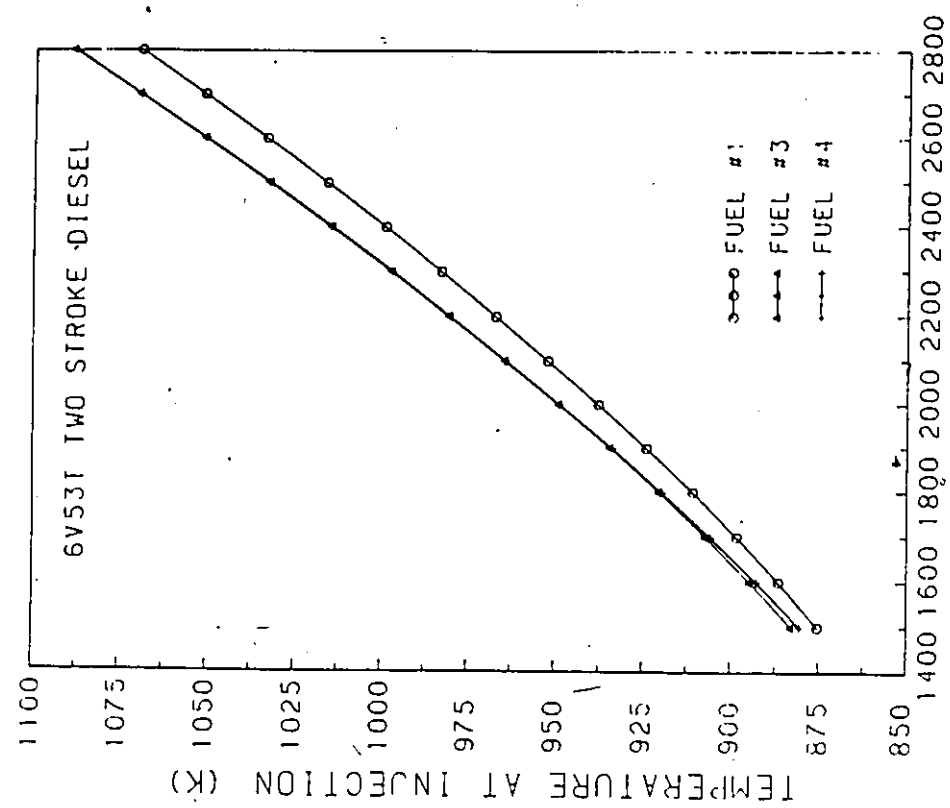

(b) Temperature

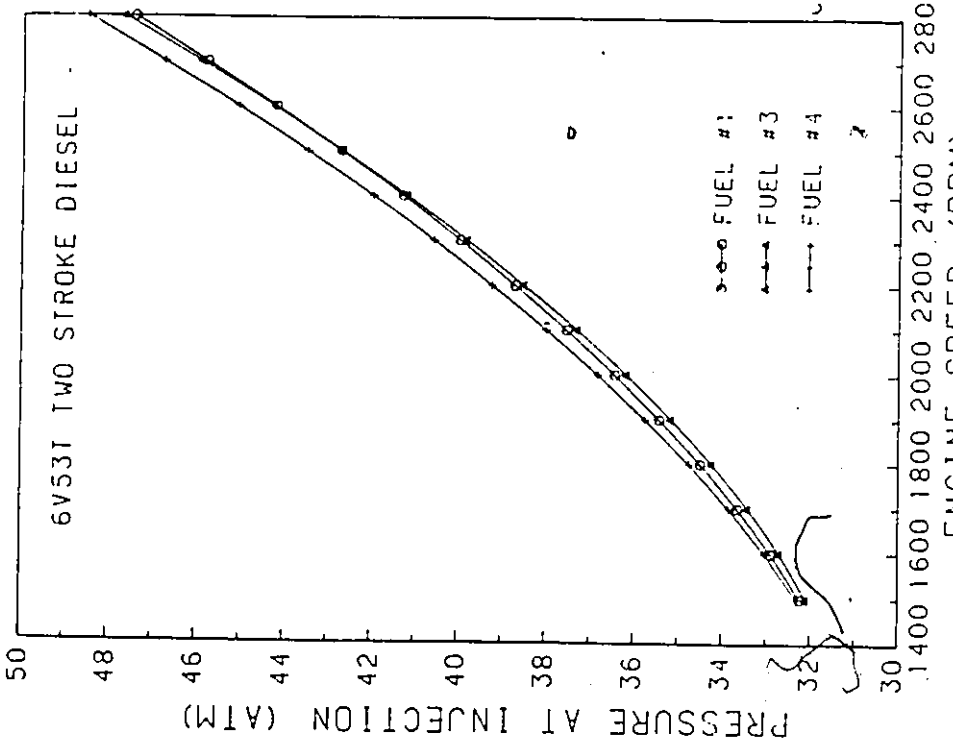

(a) Pressure

Fig. 10.6: Cylinder Pressure and Temperature at Start of Injection, Full Load

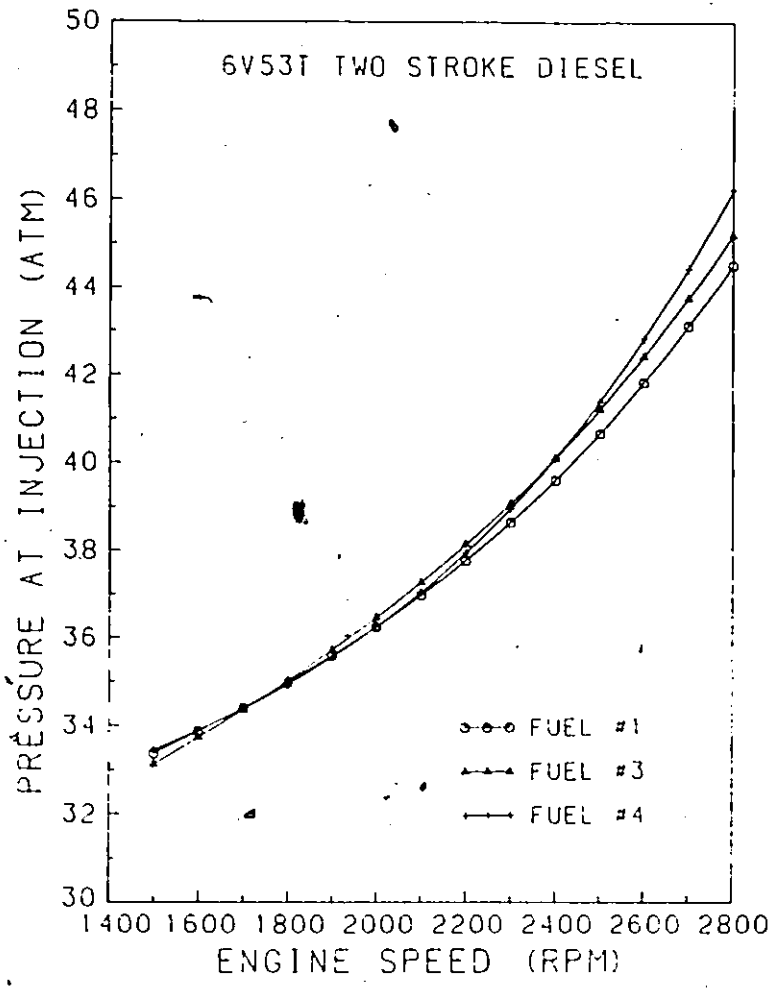

(a) Pressure

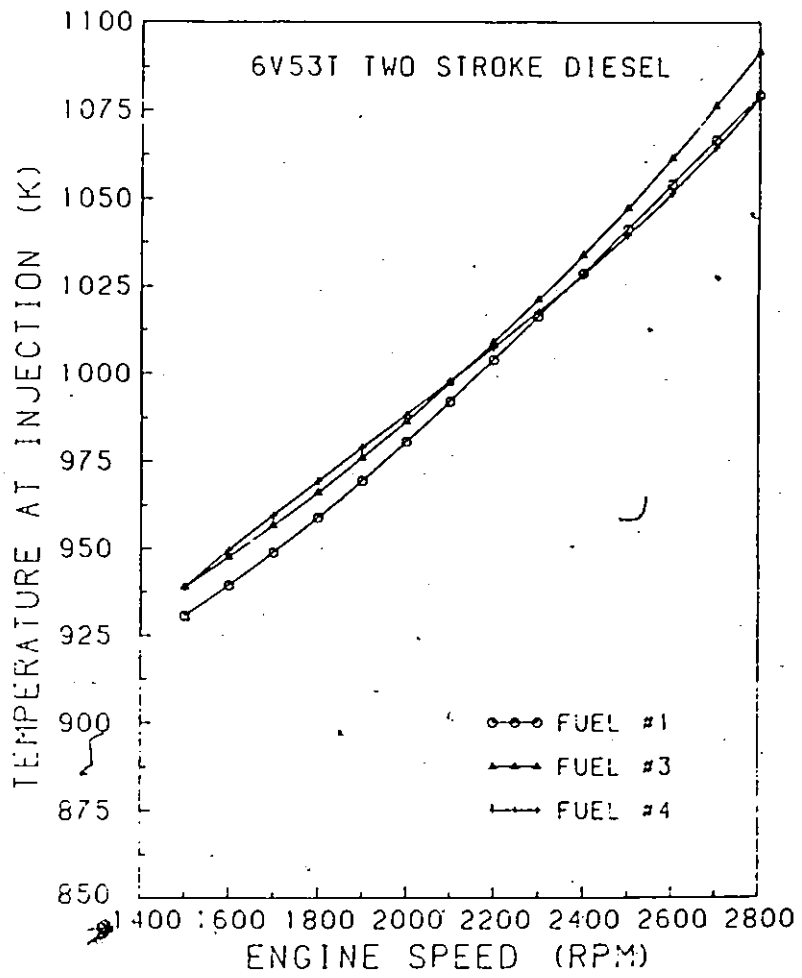

(b) Temperature

Fig. 10.7: Cylinder Pressure and Temperature at Start of Injection, Part Load

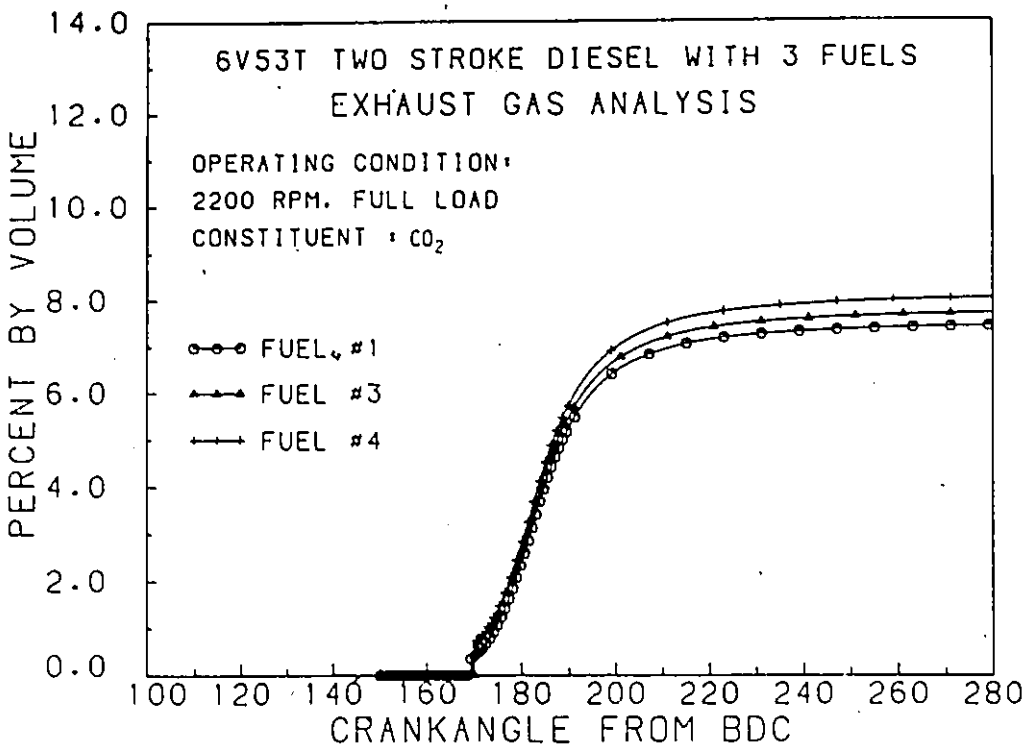

(a) Constituent: CO_2

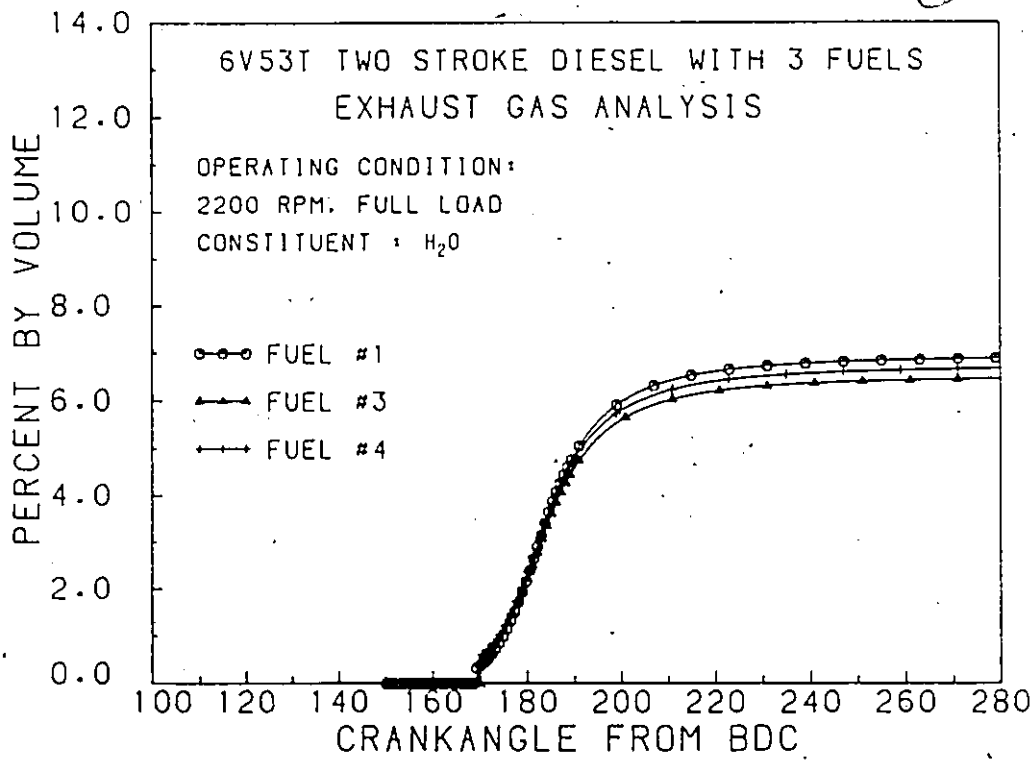

(b) Constituent: H_2O

Fig. 10.8: Predicted Combustion Products by Volume Percent for the Three Fuels

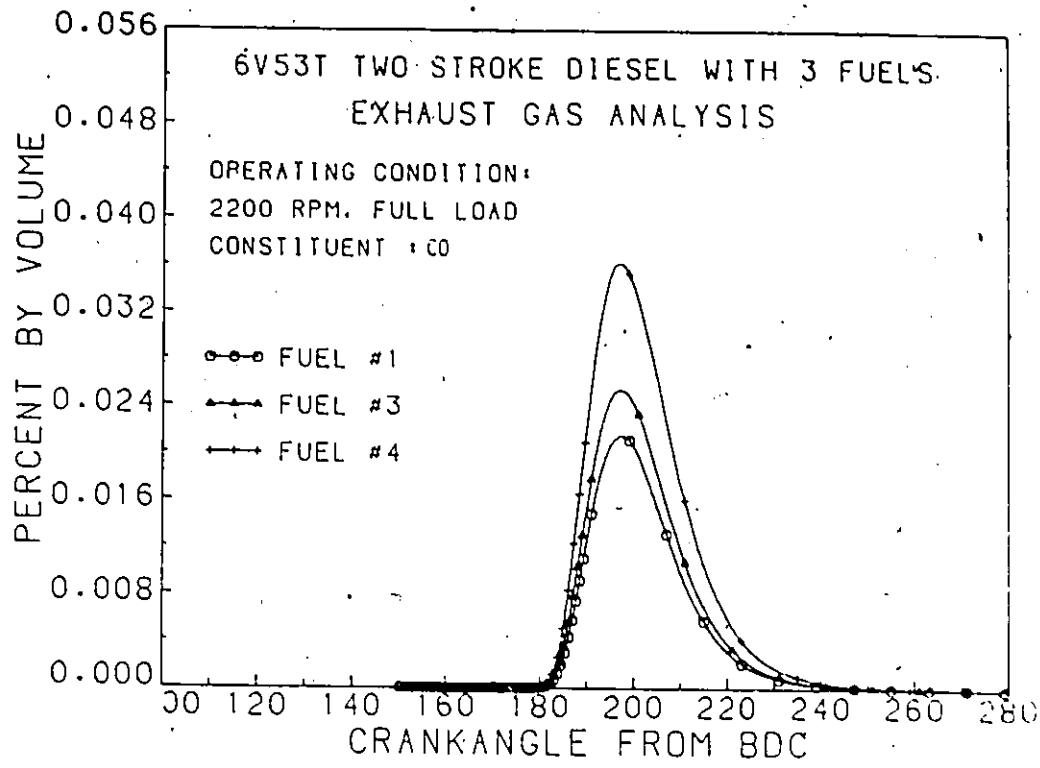

(c) Constituent: CO

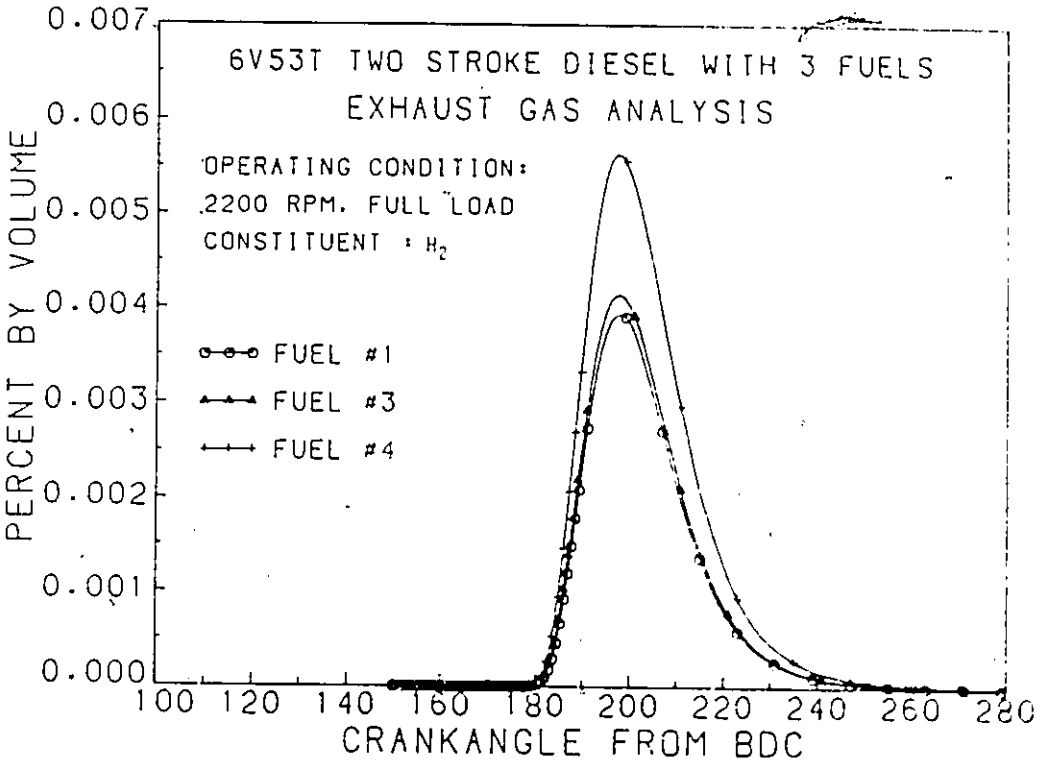

(d) Constituent: H_2

Fig. 10.8: continued

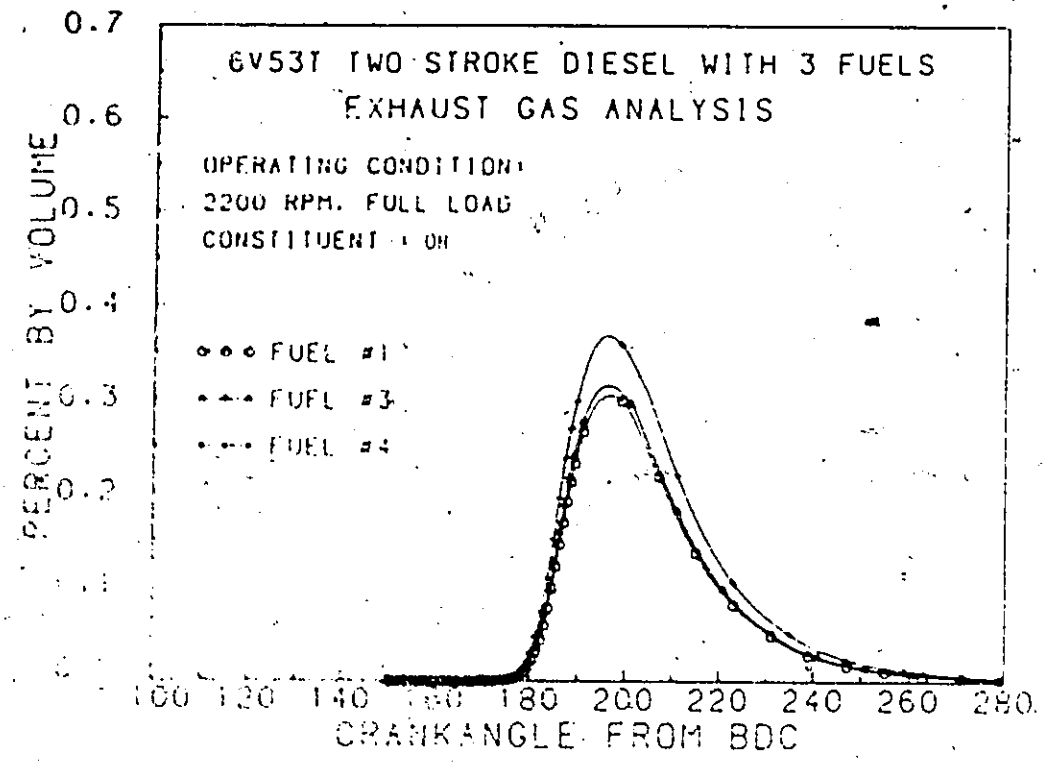

(e) Constituent: OH

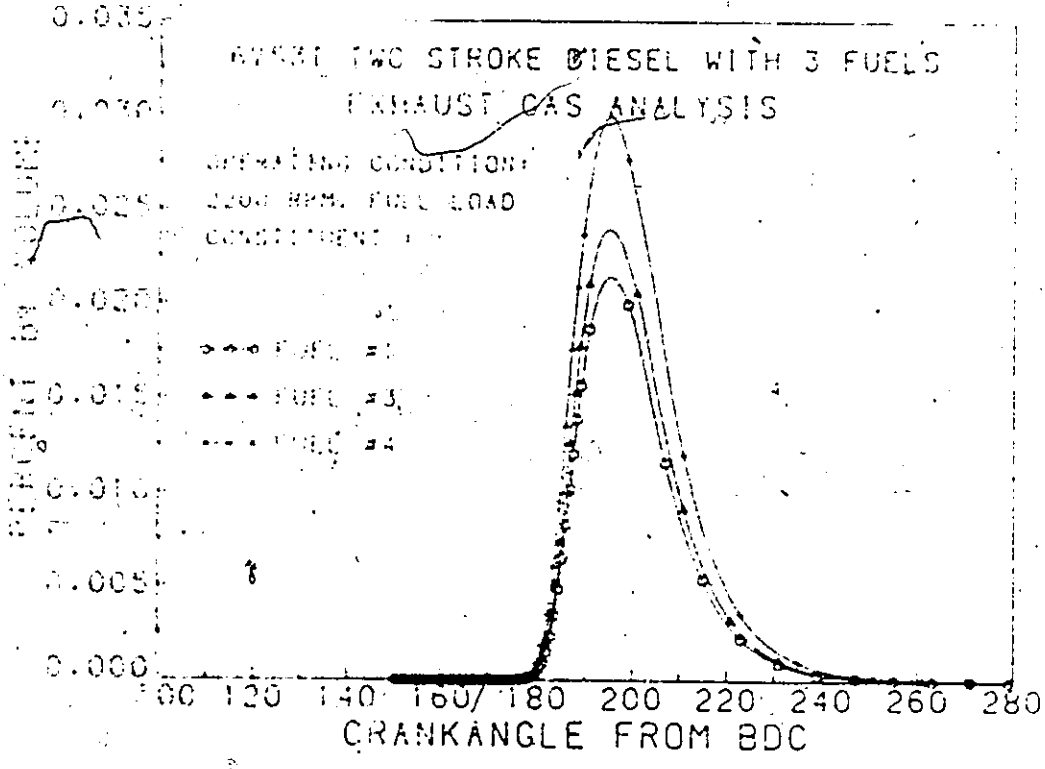

(E) Constituent: O

Fig. 10.8: continued

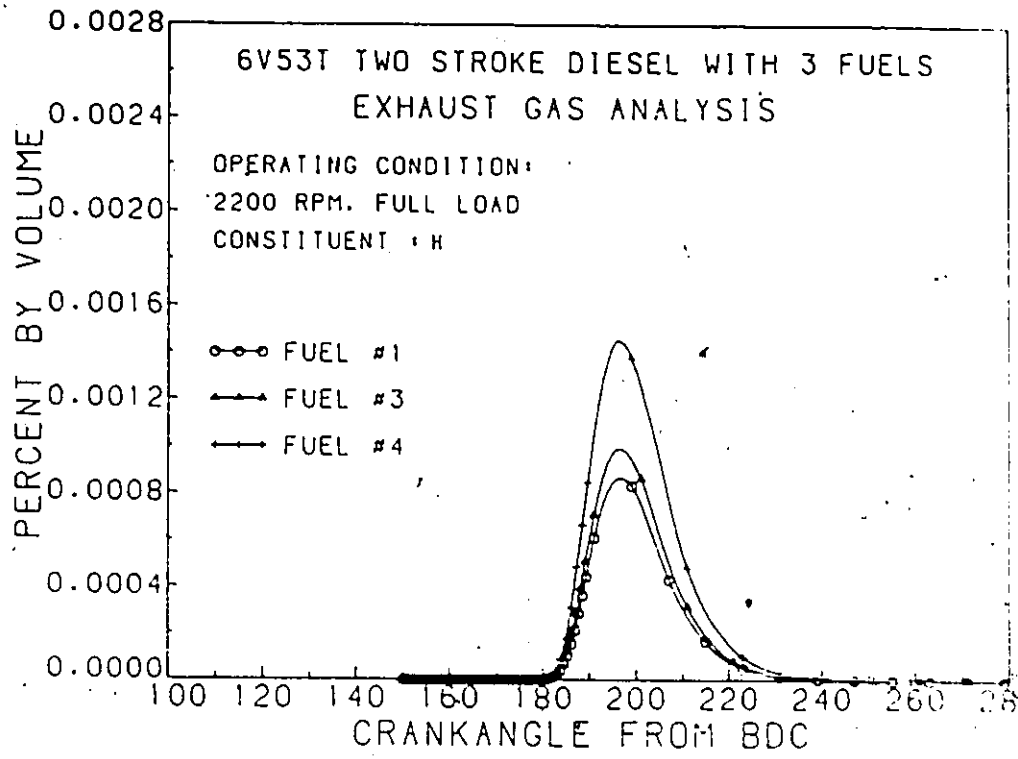

(g) Constituent: H

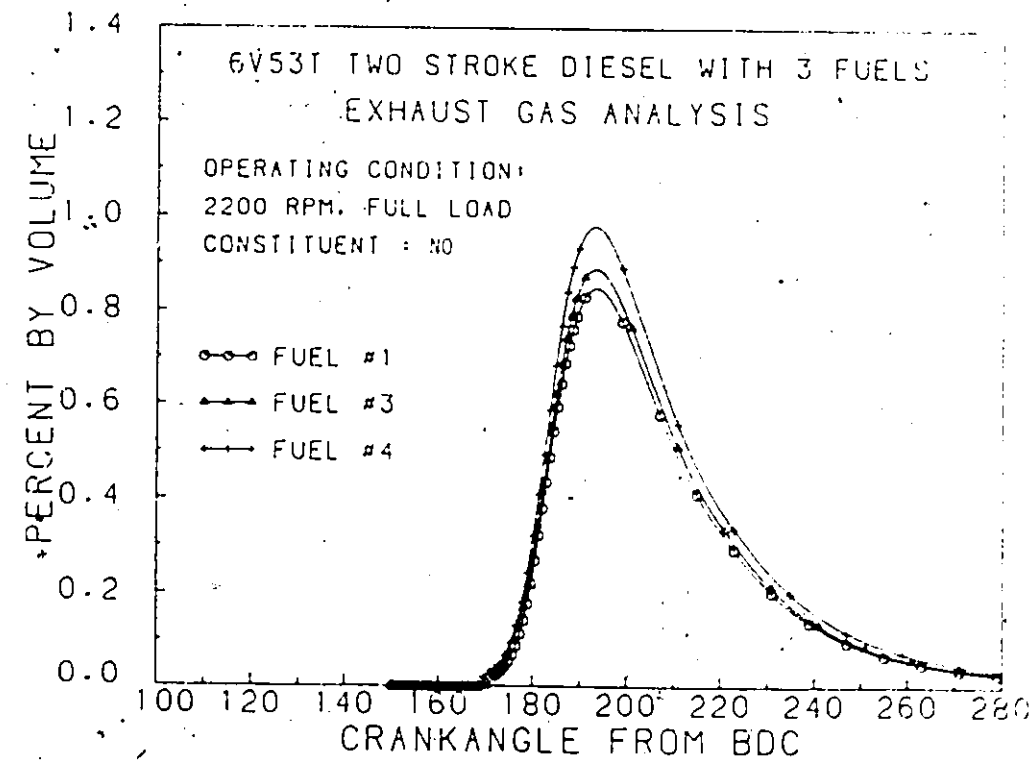

(h): Constituent: NO

(Fig. 10.8: continued

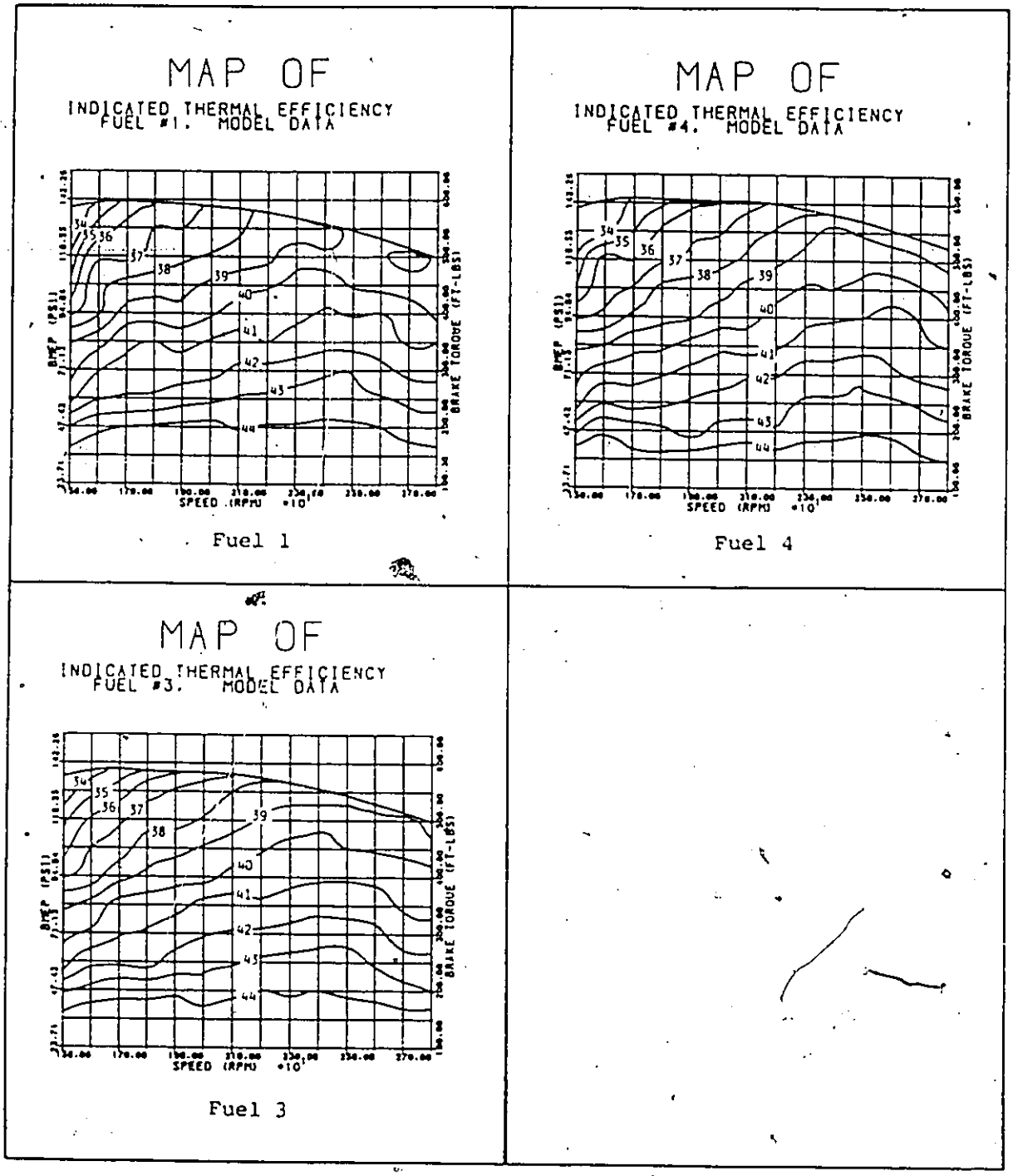

Fig. 10.9: Maps of Indicated Thermal Efficiency for the Three Fuels

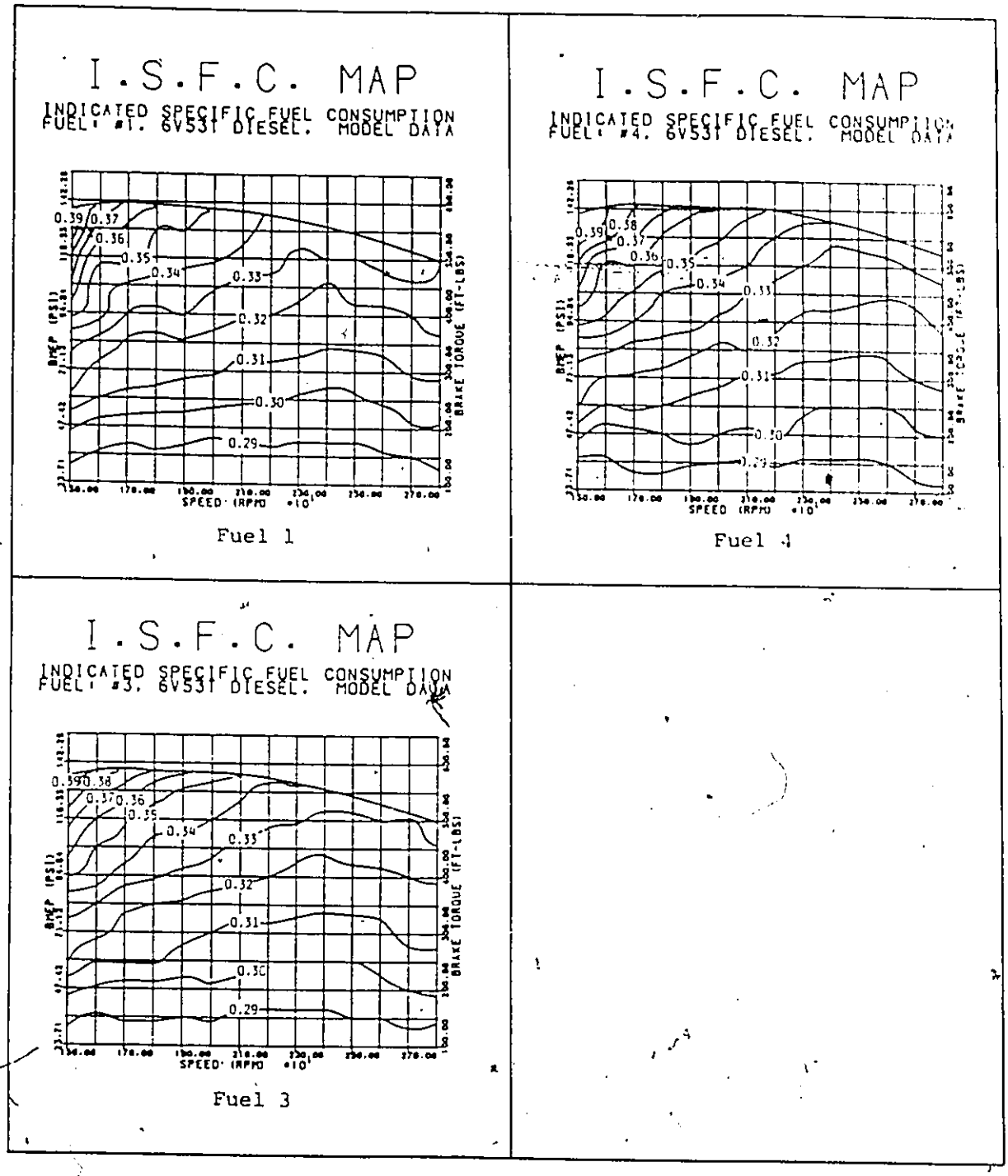

Fig. 10.10: Maps of Indicated Specific Fuel Consumption for the Three Fuels

CHAPTER 11

ENGINE PERFORMANCE

11.1 OVERVIEW

The thermodynamic and combustion model, developed in Part I, was shown to simulate performance, combustion characteristics and trends of the 6V53T engine with considerable accuracy. Thus, the simulation program can play an important role in assessing the effects of basic engine design modifications and in guiding experimental investigations. Such parametric studies can not only save considerable time and costs for research and development but also quickly identify possible solutions as well as possible problems that could arise from engine design modifications. Thus, optimal solutions can be searched analytically which would not likely be found experimentally.

In this chapter, an engine performance study is conducted. Standard engine parameters are varied so as to assess their effect on engine rated power. The study is conducted at 2800 RPM, full load using Fuel 1.

11.2 INDIVIDUAL PARAMETER EFFECTS

Five basic design parameters were studied so as to see their effects on the 6V53T engine power output and their corresponding effects on the combustion characteristics (cylinder pressure and pressure rate). The parameters are: i) engine design related: fuel injection timing (t_{fi}) and compression ratio (CR); ii) initial charge related: airbox temperature (T_{ab}) or intercooler effects and airbox pressure (P_{ab}) or turbo-boost effects and iii) fuel property related: fuel cetane number (CN). In general, it is of interest to increase both engine rated power and thermal efficiency while maintaining acceptable

levels of pressure rate and cylinder pressure.

11.2.1 ENGINE DESIGN PARAMETERS

At 2800 RPM, full load, the nominal start of fuel injection is at 18.4°CA before TDC. Keeping the fuel injection profile unchanged together with all operating conditions (i.e., P_{ab}, T_{ab}, CR, FA, etc.), injection timing was varied by ±6°CA about the nominal setting. Figure 11.1 plots the effect of injection timing on engine power and thermal efficiency and on maximum cylinder gas pressure and pressure rate.

As expected, all parameters increase with earlier injection timing. Though not linear, increases are approximately in the order of: 2.8 $HP/°CA$ for IHP, 0.33%/°CA for η_t, 42 $psi/°CA$ for P_{max} and 6 $psi/°CA$ for DP_{max}. It could be noted that at high speed, high load operation, pressure rates are not a problem, thus an increase in rated engine performance is limited by maximum cylinder pressures. Assuming cylinder pressures can be pushed to about 1900 psia, then injection timing can be shifted to 22°CA before TDC with a corresponding increase in IHP of 9.5 HP ($\simeq$ 3%).

The effect of engine compression ratio on the parameters of interest is shown in Figure 11.2. All parameters increase with increasing compression ratio. Again, assuming a maximum cylinder pressure of 1900 psia, CR can be increased to about 18.6 with a corresponding increase in IHP of 7.0 HP ($\simeq$ 2.2%).

11.2.2 INITIAL CHARGE PARAMETERS

Variation of airbox temperature (T_{ab}) can be considered as an intercooler effect on the engine parameters. As is well established, intercooling has a significant effect on engine performance while only slightly increasing cylinder pressures (Fig. 11.3).

Indeed, for the temperature range studied (T_{ab} reduced by 40 °C to 96 °C), engine IHP increases by about 12.0 HP ($\simeq$ 3.5%) with maximum cylinder pressures remaining below 1800 *psia*.

Figure 11.4 shows the effect of turboboost or airbox pressure (P_{ab}) on the engine parameters. As with decreasing airbox temperature, increasing airbox pressure has the effect of increasing cylinder trapped air mass. However, increasing airbox pressure is clearly not as effective as intercooling in that cylinder pressures are increasing more quickly relative to engine power. Indeed, only about 3 IHP can be gained below cylinder pressures of 1800 psia whereas intercooling will yield over a 12 IHP increase.

11.2.3 FUEL CETANE NUMBER

The fuel parameter of particular interest is that of cetane number (CN). Figure 11.5 shows the effect of CN on the engine parameters. The plot clearly shows that fuel cetane number has little effect on engine performance or maximum cylinder pressure in that only pressure rate shows significant variation. This behavior was also documented experimentally. It is also clear that low cetane fuels can be used in diesel engines provided the high pressure rates encountered during initial or onset of combustion can be either tolerated or controlled.

11.3 INTEGRATED PARAMETER EFFECTS

In this section, the integrated effects of injection timing, intercooler temperature, turbo-boost pressure, and compression ratio on the 6V53T engine indicated horsepower IHP, indicated thermal efficiency η_t, ignition delay t_i, maximum cylinder pressure P_{max} and maximum pressure rate DP_{max} are studied. Again, the operating condition

was chosen at engine rated output, 2800 RPM, full load, with Fuel 1.

11.3.1 INJECTION TIMING AND INTERCOOLER

At 2800 RPM, full load, the nominal start of injection is 18.4 degrees before TDC and airbox temperature is 136°C for Fuel 1. Injection timing and airbox temperature are varied about these nominal values and the integrated effect on engine performance is plotted in Figure 11.6 (a and b) while Figure 11.7 (a,b and c) shows their effect on the combustion parameters.

From a study of the plots, engine performance can be improved by reducing airbox temperature together with earlier injection timing. Again, using a maximum cylinder pressure of 1900 psia, from Figure 11.7b, injection timing could be set at 21.1°CA bTDC with $T_{ab} = 96°C$. By so doing, from Figure 11.6a, power could be increased by about 20 IHP or about 6.3%.

11.3.2 INJECTION TIMING AND TURBO-BOOST

The combined effects of injection timing and turbo-boost or airbox pressure on engine performance and cylinder thermodynamic state are presented in Figures 11.8 (a and b) and 11.9 (a,b and c). A study of the plots reveals that the combination of injection timing and turbo-boost offers little or no advantage over turbo-boost alone, the latter having the advantage of lower pressure rates. Again, using a 1900 psia ceiling, the maximum engine power increase that can be gained by any combination of the two variables is less than 10 IHP ($\simeq 3.1\%$).

11.3.3 INJECTION TIMING AND COMPRESSION RATIO

Figures 11.10 (a and b) and 11.11 (a,b and c) show the combined effects of injection timing and compression ratio on the engine parameters. As with timing and turbo-boost, timing and compression ratio do not provide any integrated positive effects. Again, power improvements are limited to about 10 IHP and this is best achieved through earlier injection timing alone.

11.3.4 MASS OF FUEL INJECTED AND INTERCOOLER

It could be noted that intercooling or lowering T_{ab} increases the mass of air trapped in the cylinder. Thus, it follows that more fuel could also be injected concurrent with intercooling and yet retain the thermal efficiencies of the engine. This combination is presented in Figures 11.12 and 11.13. For the study, increases in fuel mass was accomplished through increases in injection rate, both timing and injection duration were held constant.

From the figures, it is clear that this is a very effective combination for increasing engine rated power. Indeed, it is projected that by reducing airbox temperature by $40°C$ (from $136°C$ to $96°C$) and increasing fuel mass by about 12% to 63.9 mm^3/cylinder would result in an engine output of about 360 IHP ($\simeq$ 12% increase) without any loss in thermal efficiency. Further, maximum cylinder pressures only increase marginally to about 1837 *psia*. Allowing one percentage drop in efficiency (from 39.3% to ~~38.3%~~), engine power can be boosted to just over 375 IHP with maximum cylinder pressures in the order of 1863 *psia*.

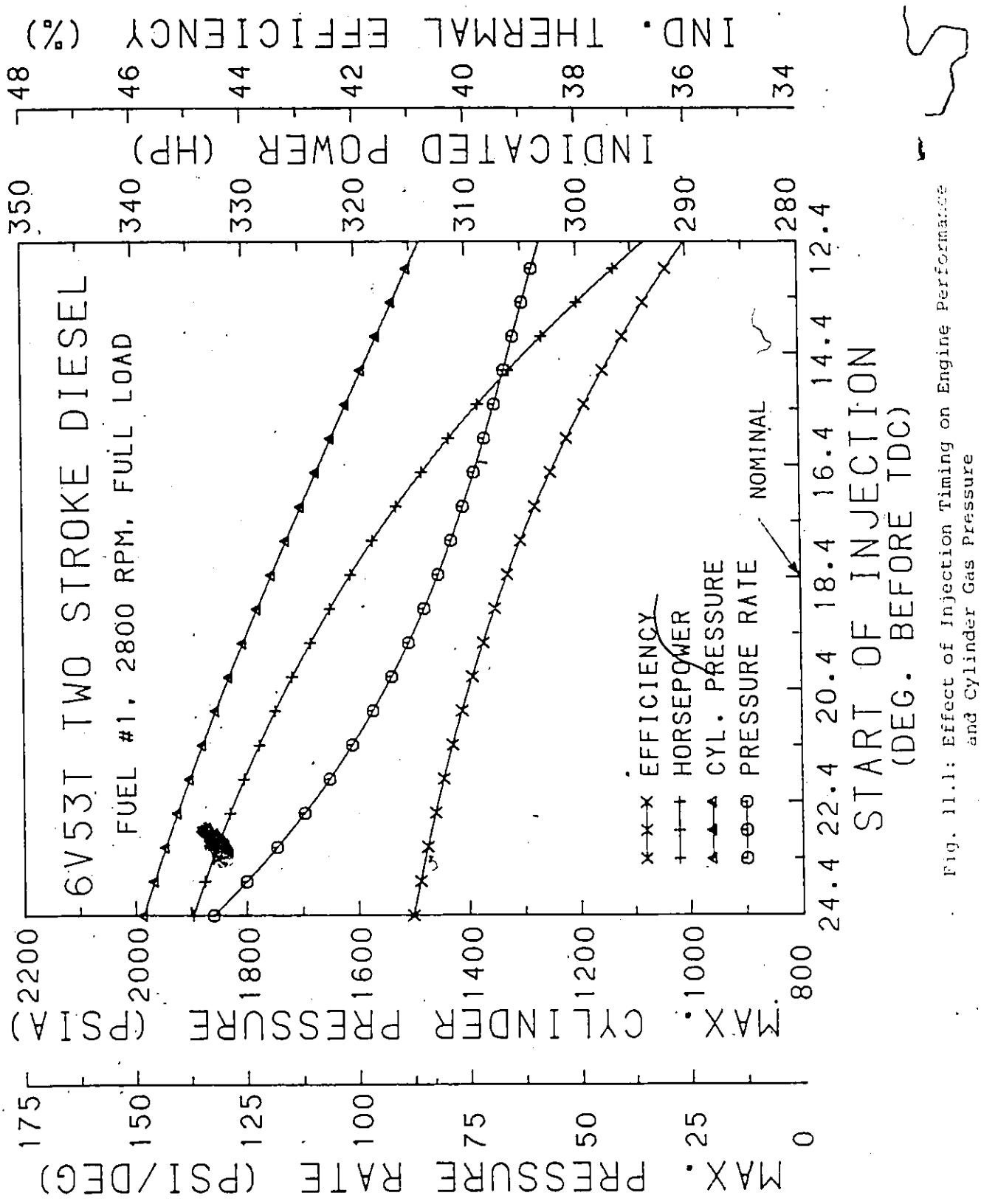

Fig. 11.1: Effect of Injection Timing on Engine Performance and Cylinder Gas Pressure

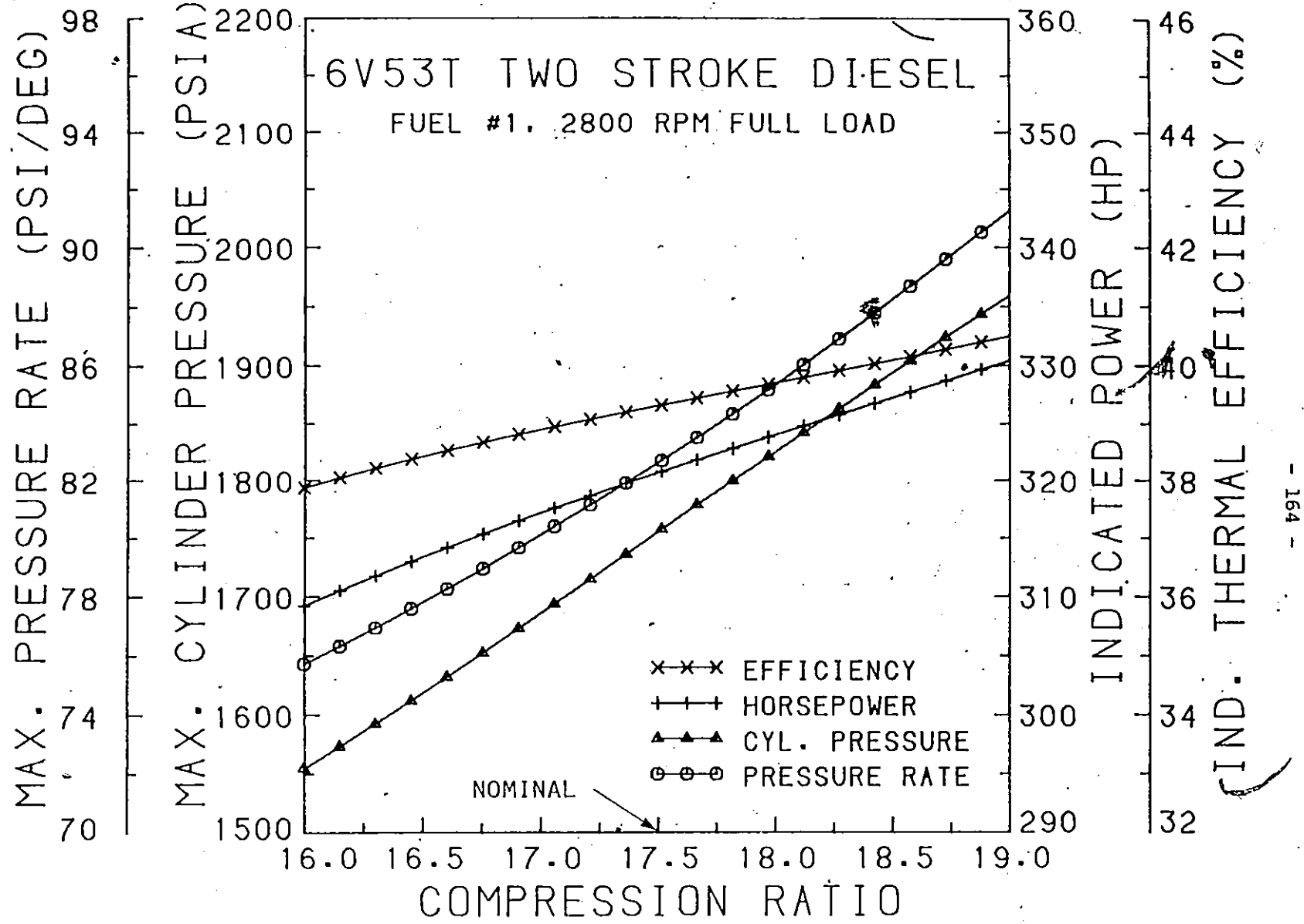

Fig. 11.2: Effect of Compression Ratio on Engine Performance and Cylinder Gas Pressure

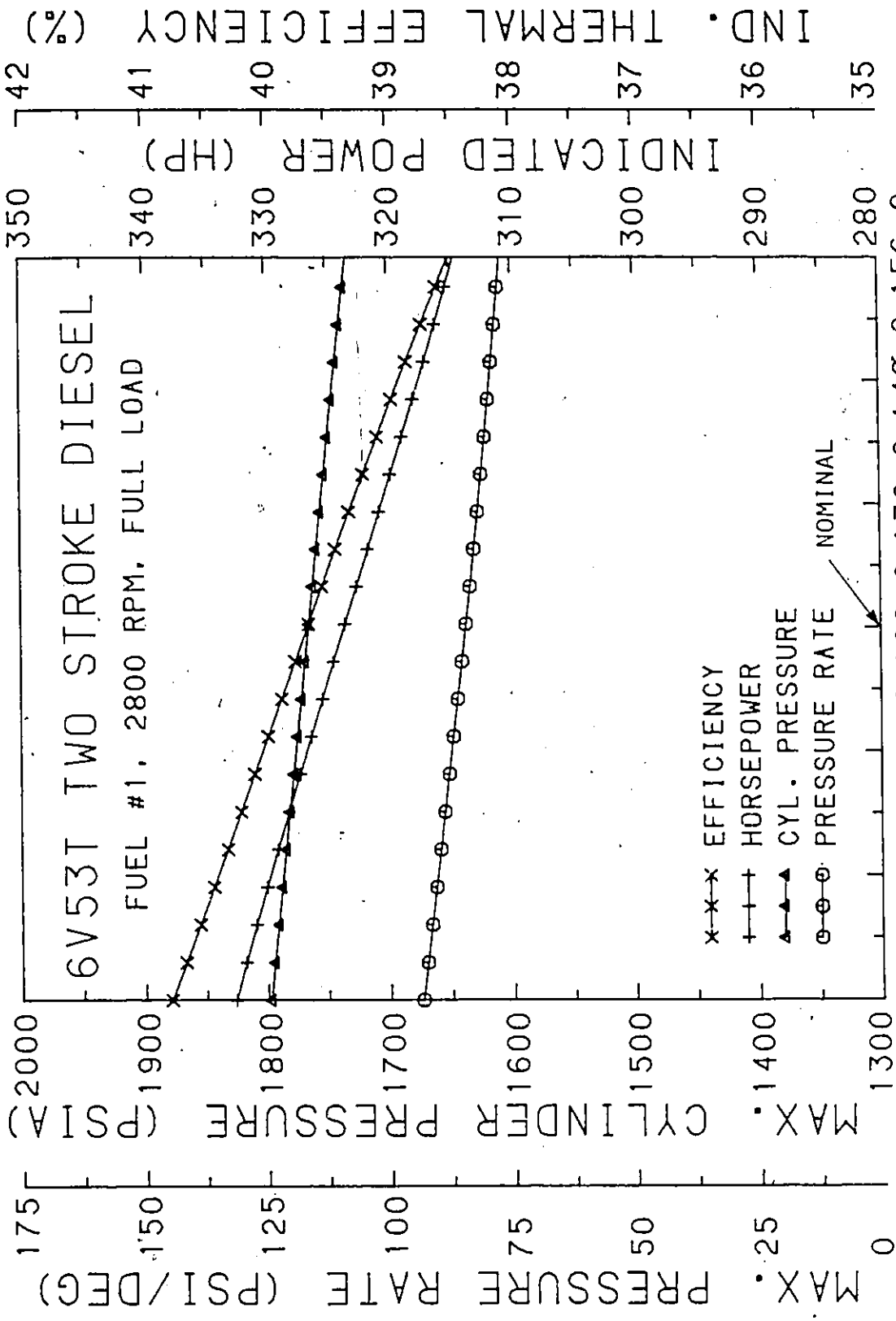

Fig. 11.3: Effect of Intercooler Temperature on Engine Performance and Cylinder Gas Pressure

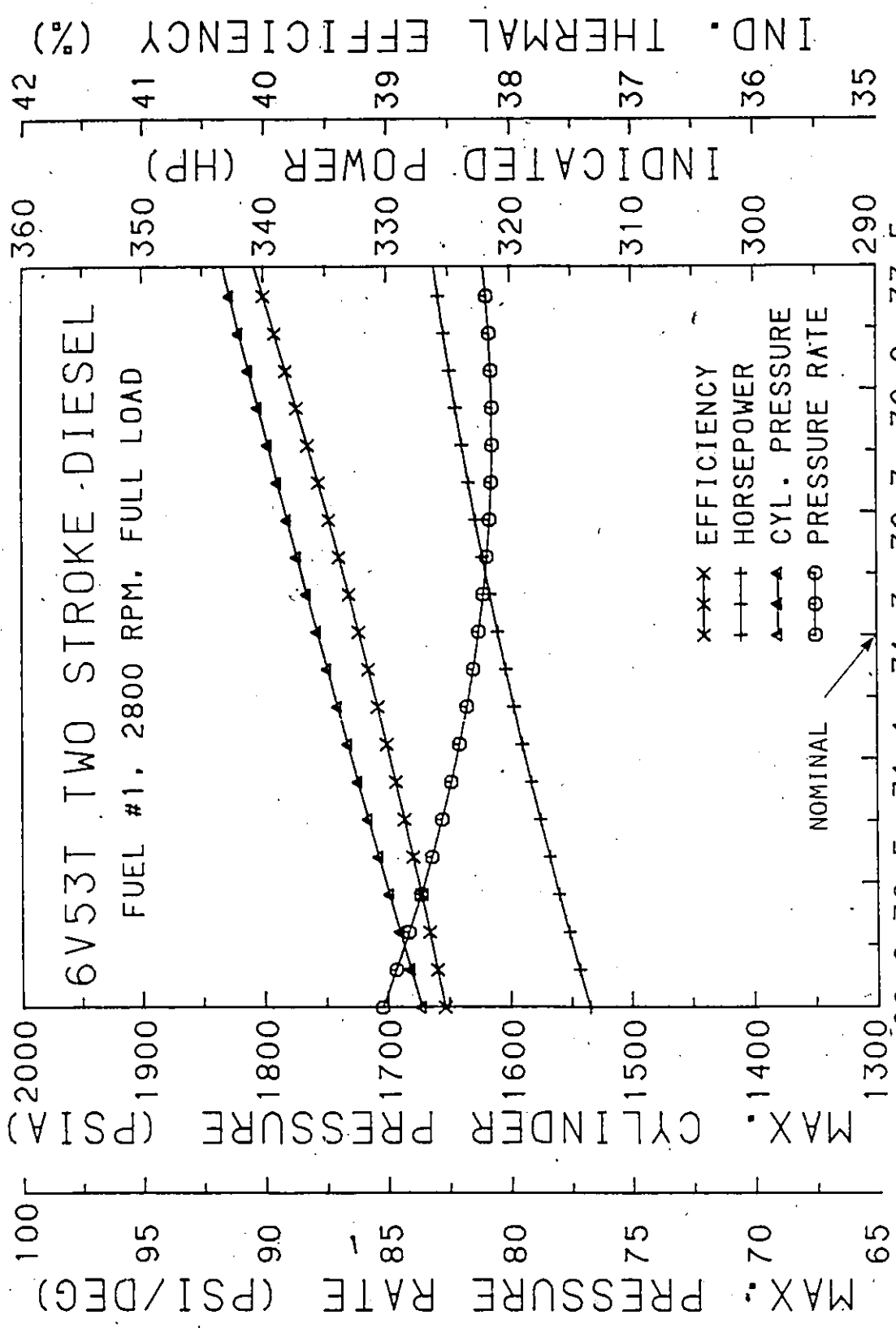

Fig. 11.4: Effect of Turbo-Boost Pressure on Engine Performance and Cylinder Gas Pressure

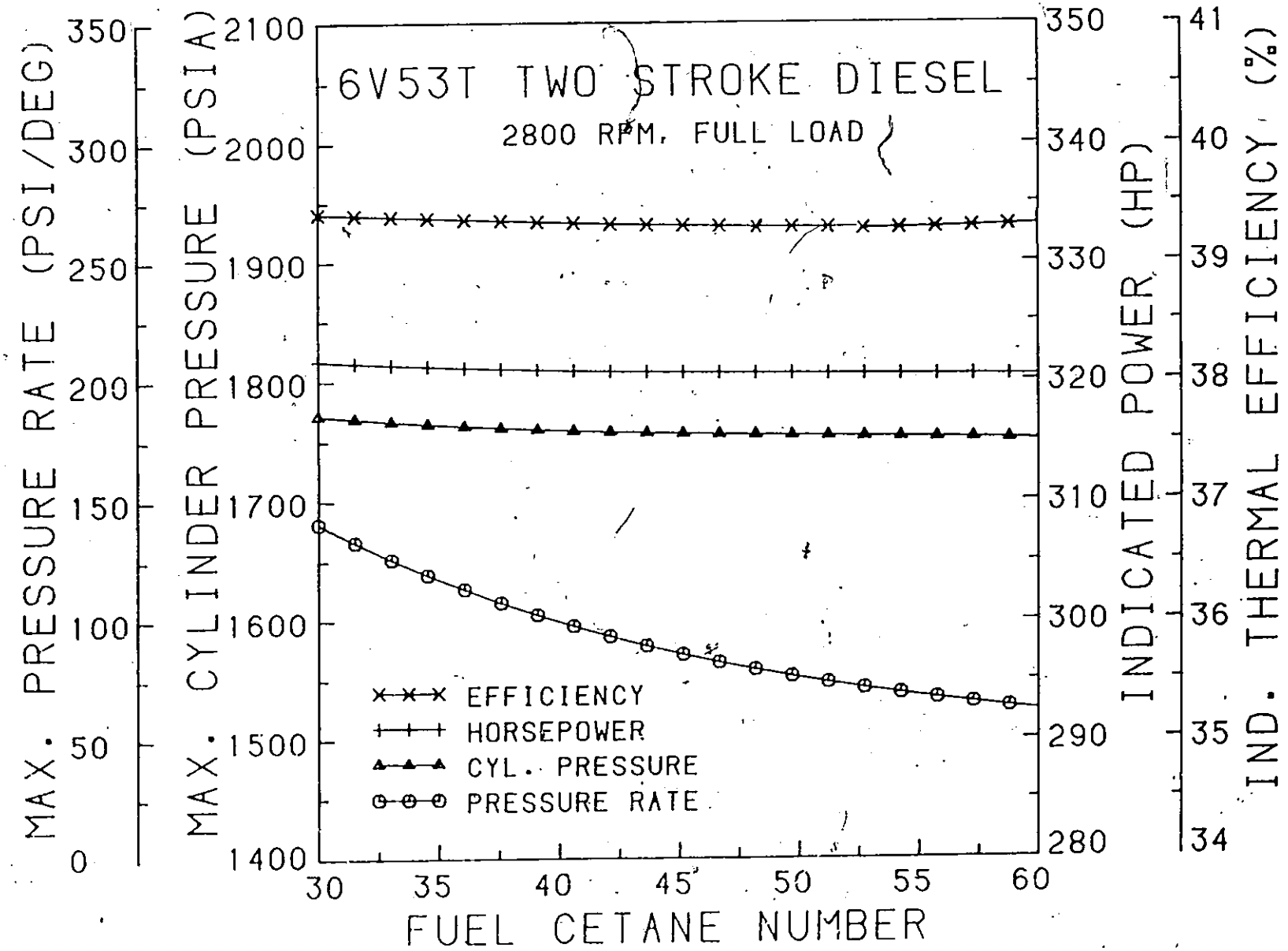

Fig. II.1: Effect of Fuel Cetane Number [illegible]
and Cylinder Gas Pressure

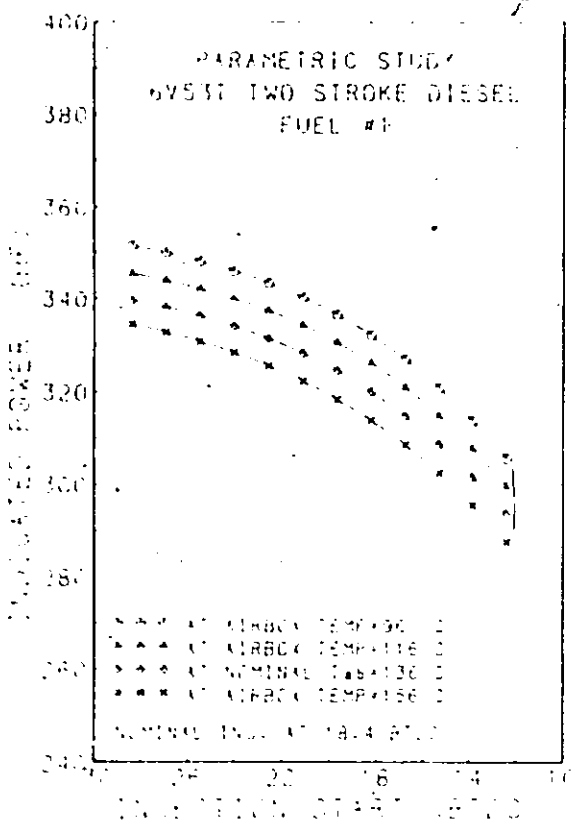

(a)

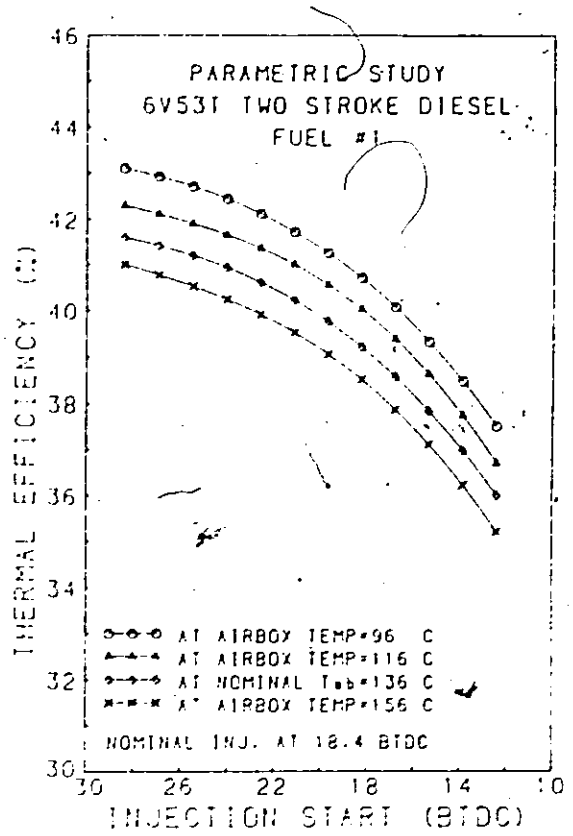

(b)

Fig. 11.6: Integrated Effects of Injection Timing and Airbox Temperature on Engine Performance

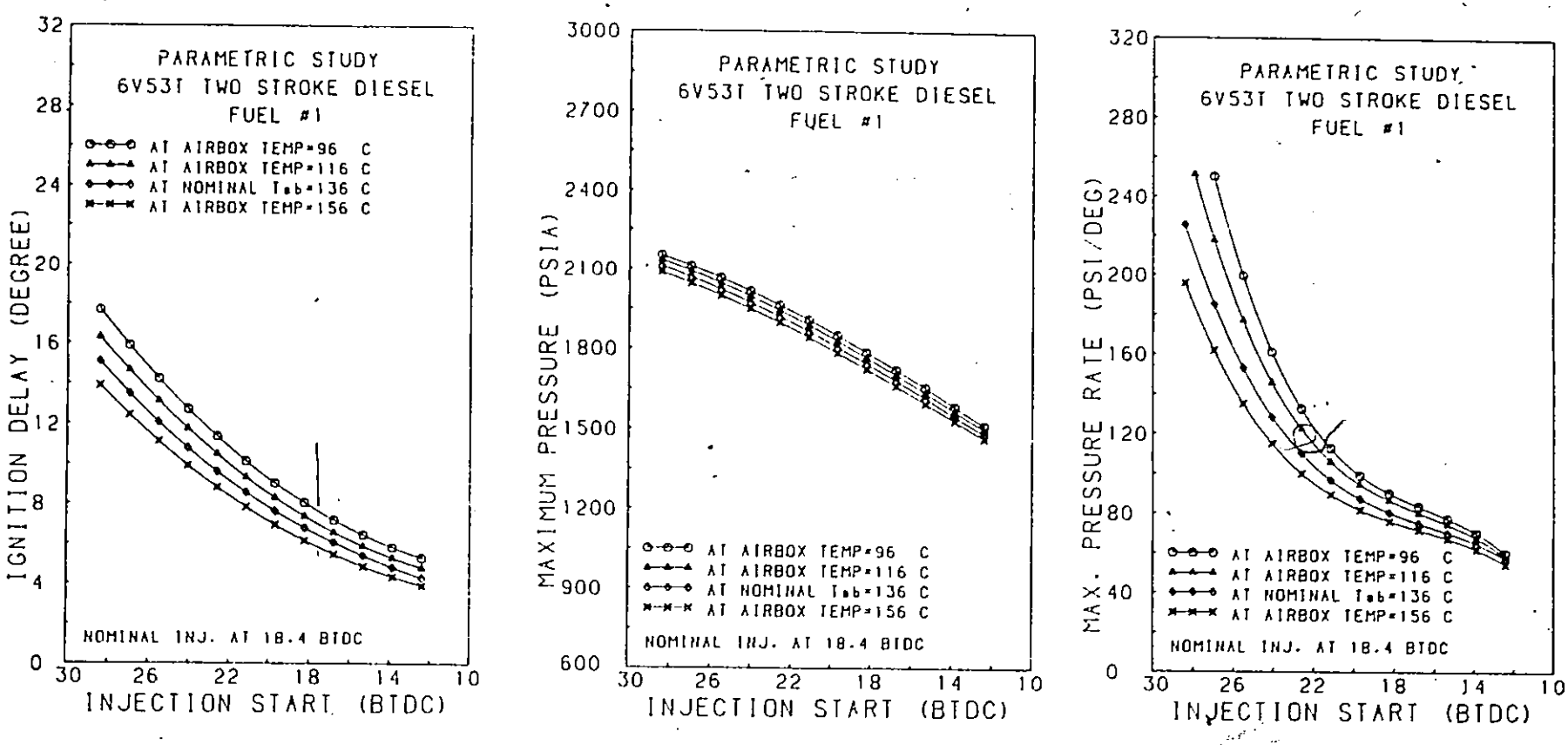

Fig. 11.7: Integrated Effects of Injection Timing and Airbox Temperature on Combustion Parameters

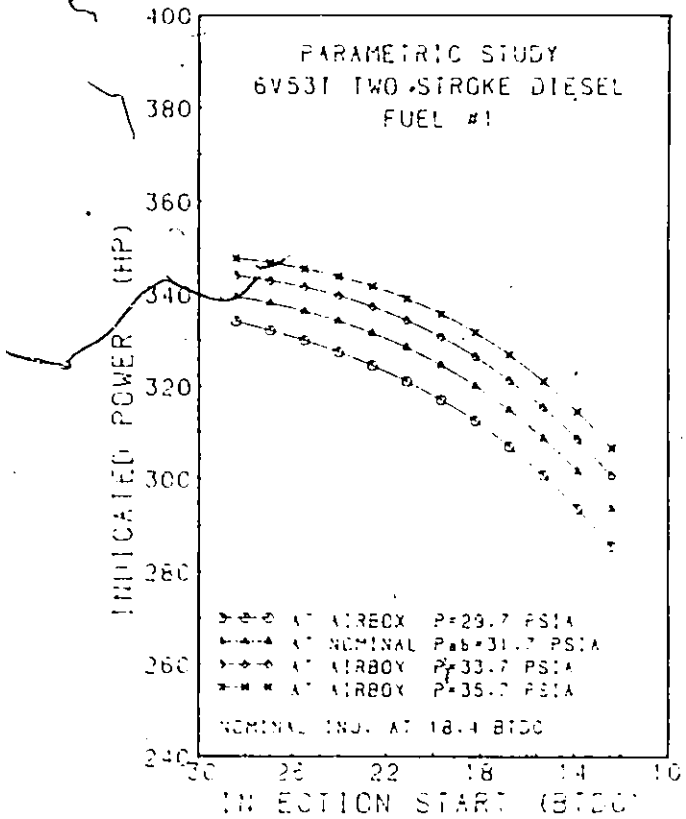

(a)

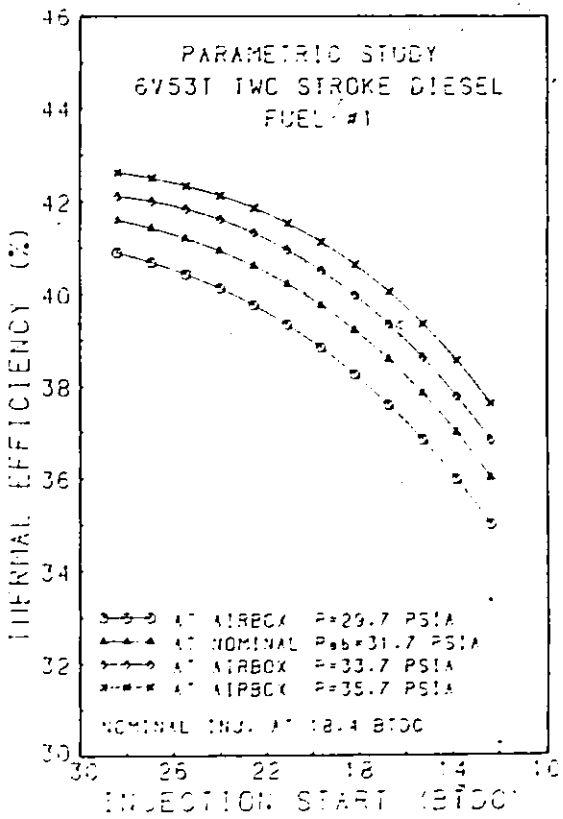

(b)

Fig. 11.8: Integrated Effects of Injection Timing and Airbox Pressure on Engine Performance

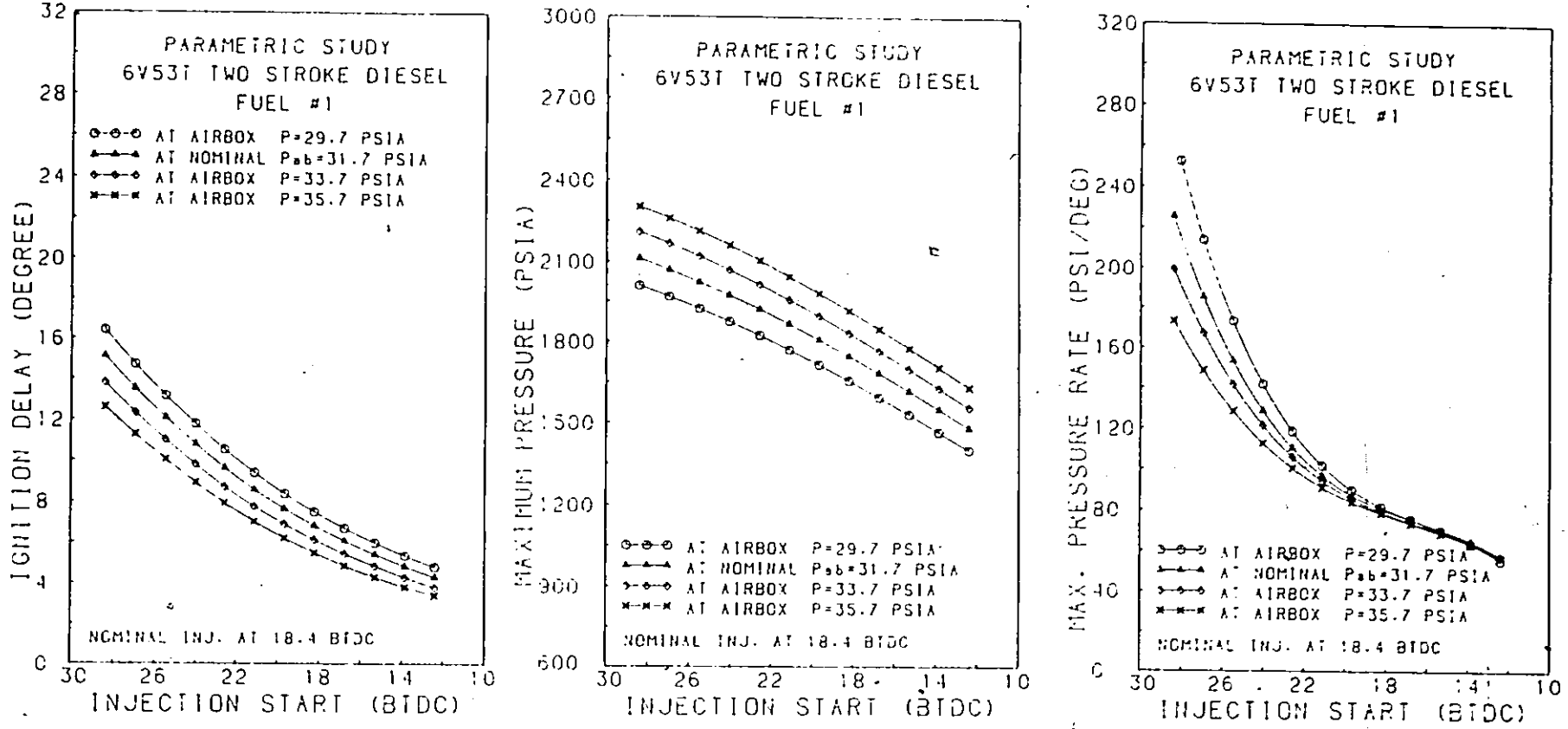

Fig. 11.9: Integrated Effects of Injection Timing and Airbox Pressure on Combustion Parameters

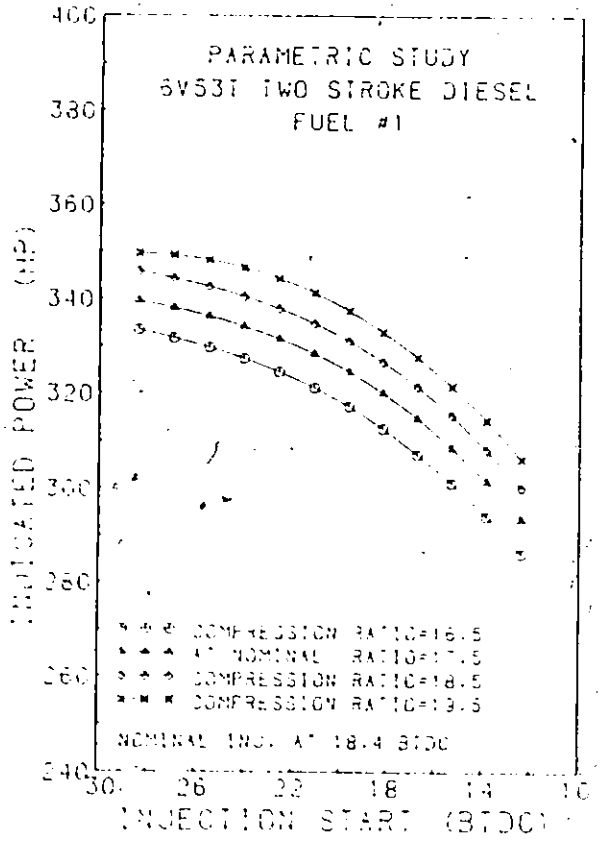

(a)

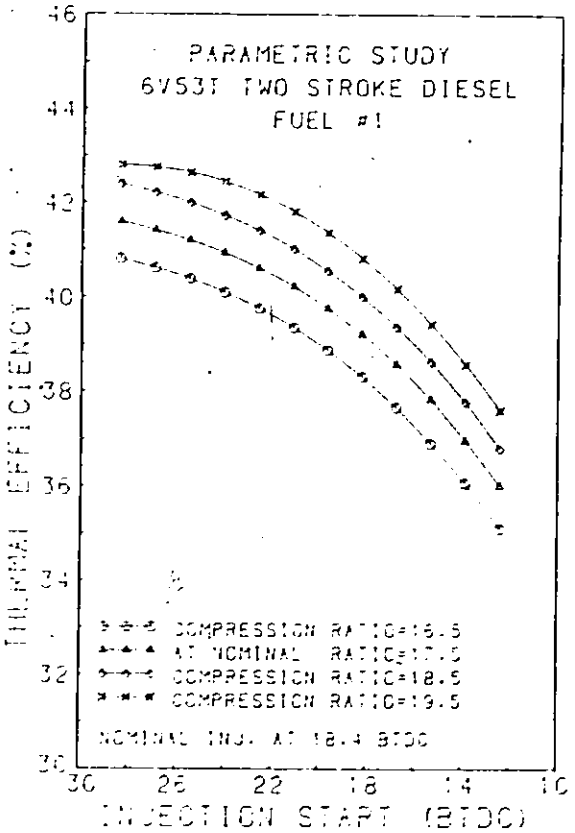

(b)

Fig. 11.10: Integrated Effects of Injection Timing and Compression Ratio on Engine Performance

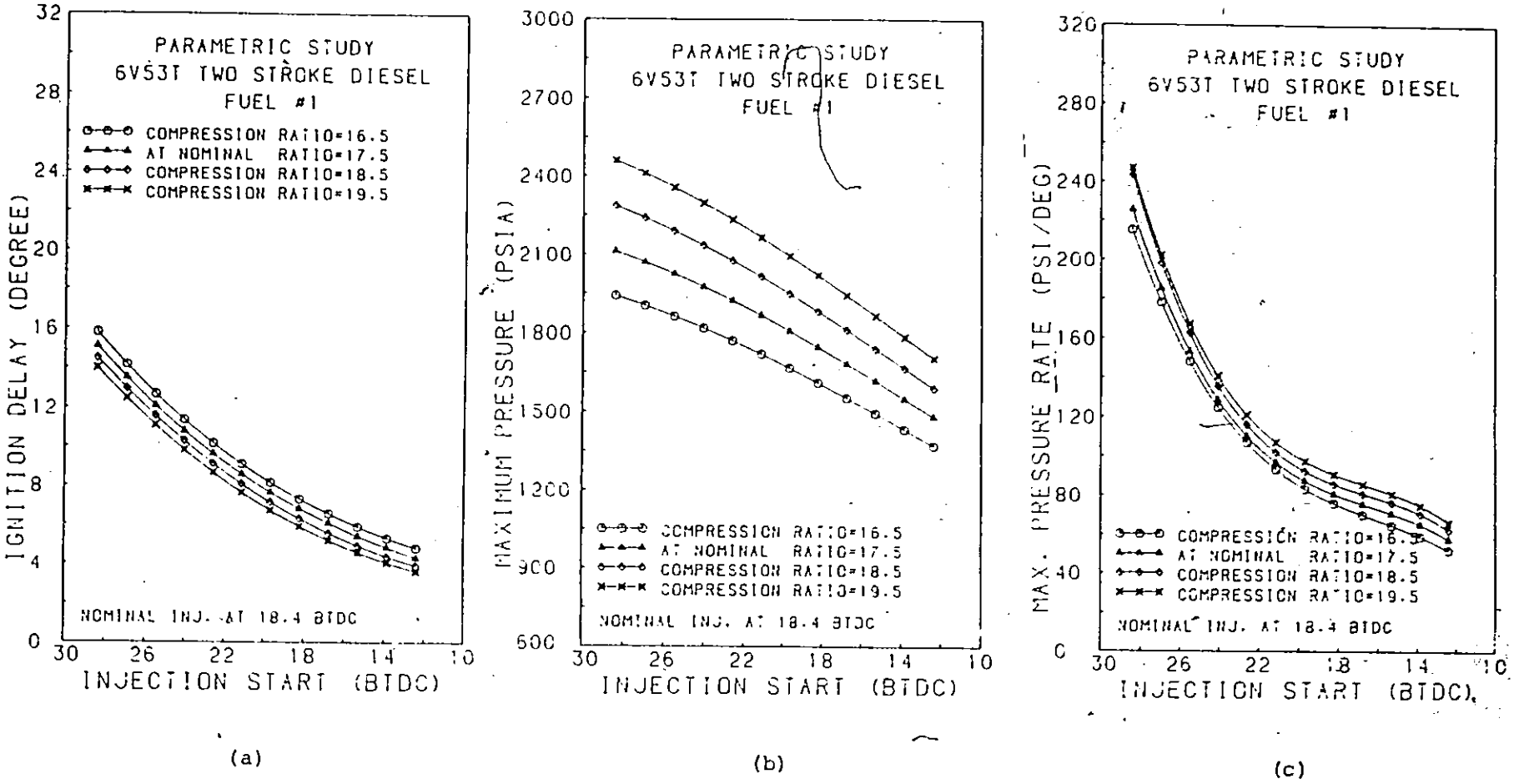

Fig. 11.11: Integrated Effects of Injection Timing and Compression Ratio on Combustion Parameters

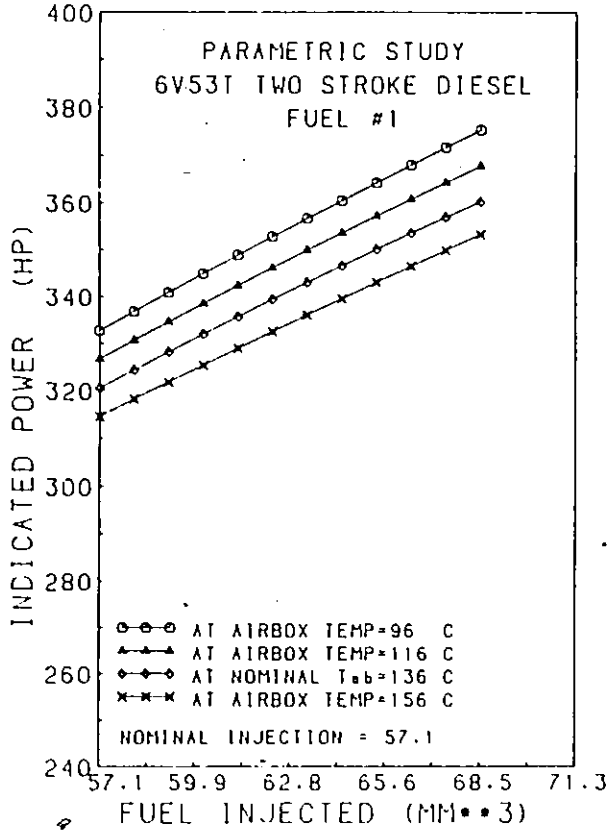

(a)

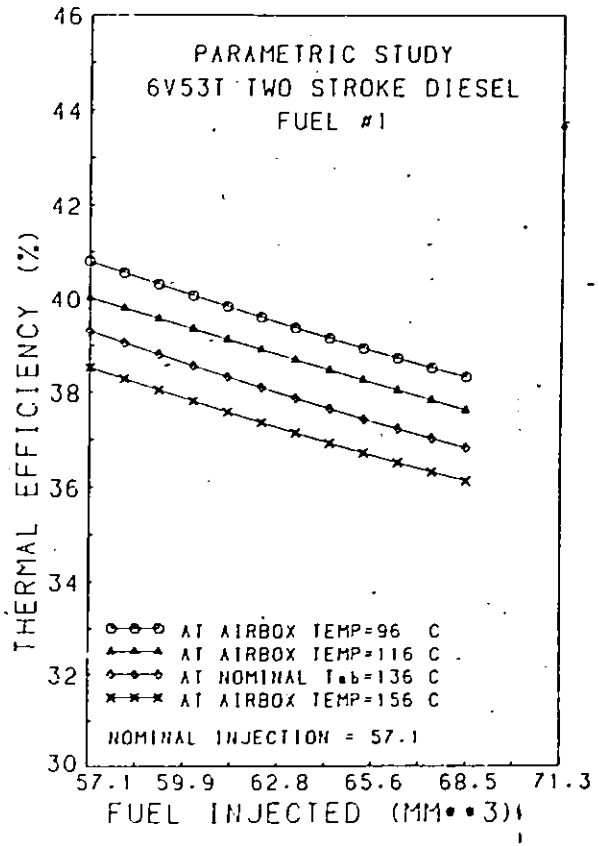

(b)

Fig. 11.12: Integrated Effects of Fuel Mass and Intercooling on Engine Performance

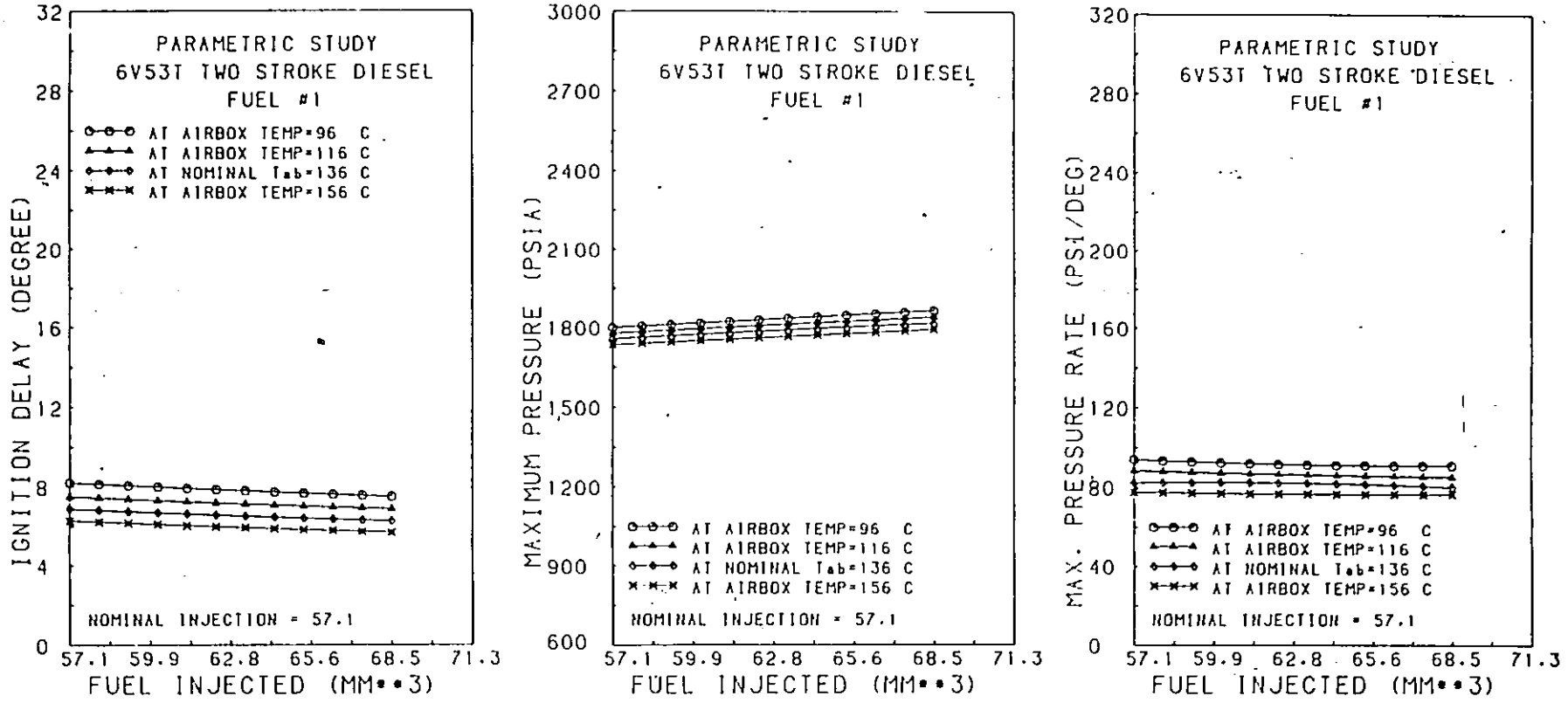

Fig. 11.13: Integrated Effects of Fuel Mass and Intercooling on Combustion Parameters

CHAPTER 12

COMBUSTION KNOCK AND CONTROL

12.1 OVERVIEW

One of the key objectives of this current research project is to search for possible solutions for the 6V53T engine when operating on the low cetane, tar sands derived fuels. Experimentally, it was shown that these fuels give rise to diesel knock, i.e. very high pressure rates during onset or early combustion. This in turn gives rise to cylinder gas vibrations (5000-6000 Hz) and, more importantly, engine noise and component vibrational stressing (0-2000 Hz range) were shown to correlate with pressure rates.

The simulation program developed is unique in that it reflects, with considerable numerical accuracy, the pressure rates encountered during early combustion. Moreover, pressure rate trends for each of the three fuels over the complete operating range of the engine were shown to correlate with the experimental data. In general, the critical pressure rate region occurs at low speed, low load operation. For this study, 1600 RPM, 200 ft.lbs. brake torque is used and acceptable levels of pressure rate are taken to be those measured with high quality diesel fuel, namely, Fuel 1.

In this chapter, pressure rate control when using Fuels 3 and 4 will be studied. Initially, standard engine variables will be examined followed by a study of 'staged' fuel injection.

12.2 ANALYSIS WITH STANDARD ENGINE PARAMETERS

Pressure rate control using the standard engine variables, namely: compression ratio, injection timing, airbox temperature and airbox pressure is shown in Figures 12.1 through 12.4 respectively, together with their corresponding effects on engine performance, for each of the three fuels. At the test point (1600 RPM, 200 ft.lbs. brake torque), the nominal values of the variables, from experimental data, are:

compression ratio — 17.5
injection timing — 13.2°CA bTDC
airbox temperature — 44.9°C
airbox pressure — 17.7 *psia*.

In this critical operating region, pressure rates encountered at the nominal settings are for Fuel 1 = 254 $psi/°CA$, Fuel 3 = 355 $psi/°CA$ and Fuel 4= 367 $psi/°CA$. Thus, the objective is to bring the rates for Fuels 3 & 4 in the order of 250 $psi/°CA$ as for Fuel 1.

From a study of the figures, it is clear that within reasonable ranges of the variables, only compression ratio and injection timing hold the potential of reducing the pressure rates of Fuels 3 & 4 to Fuel 1 levels. In this regard, it is projected that either a compression ratio in the order of 16 or delayed injection timing to about 8°CA bTDC will accomplish the pressure rate objective. However, both alterations are accompanied by significant losses in engine indicated thermal efficiency.

Of the two approaches, injection timing is the most attractive, especially if electronic injectors and combustion knock sensing is used. In this way, performance losses could be minimized in the high pressure rate operating region together with performance improvements outside this region as recorded in Section 11.2.1. Further, knock sensing would improve the multi-fuel capability of the engine since changes to the timing logic should not be required for different cetane fuels.

It could also be noted that intercooling does produce a desirable effect in this region. While engine power and efficiency increase with decreasing airbox temperature, cylinder pressures and pressure rates remain largely unchanged. This insensitivity of pressure rate to airbox temperature was not expected. Thus, a set of experiments were run on the engine using Fuel 3 (in cylinder No. 1 only). While the experiments were conducted at 1600 RPM, 200 ft.lbs. brake torque, they did not exactly duplicate the model simulation. However, for a 20°C reduction in airbox temperature, pressure rates increased by only 19$psi/°CA$ on average although the standard deviation at both temperatures was in the order of 30$psi/°CA$. Likewise, the difference of the average maximum cylinder pressure was also within the standard deviation. Thus, the predicted insensitivity of pressure rates and maximum cylinder pressures in this operating region is clearly confirmed. In Chapter 11, intercooling was also found to be the single most desirable variable for engine performance improvements.

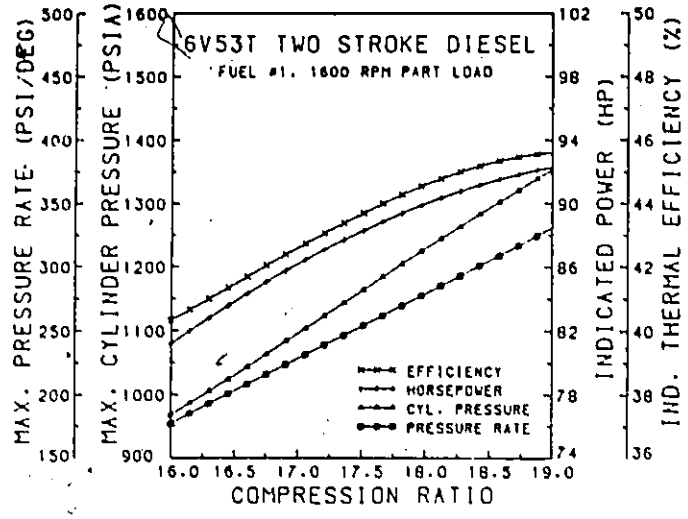

Fuel 1

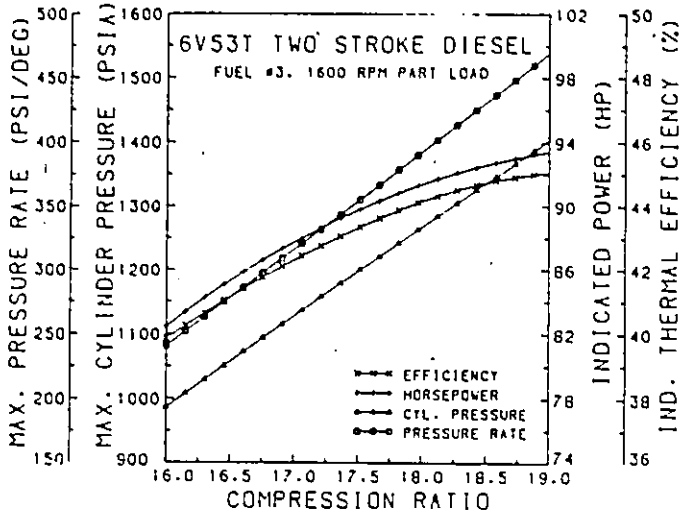

Fuel 3

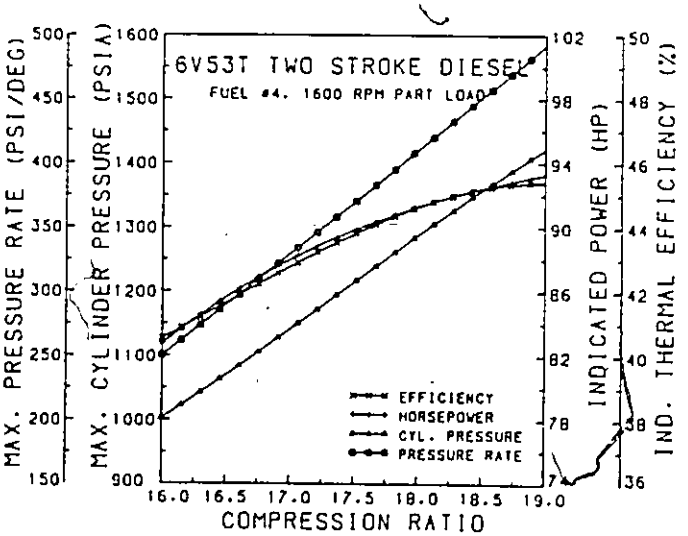

Fuel 4

Fig. 12.1: Effect of Compression Ratio on Engine Performance and Combustion Parameters

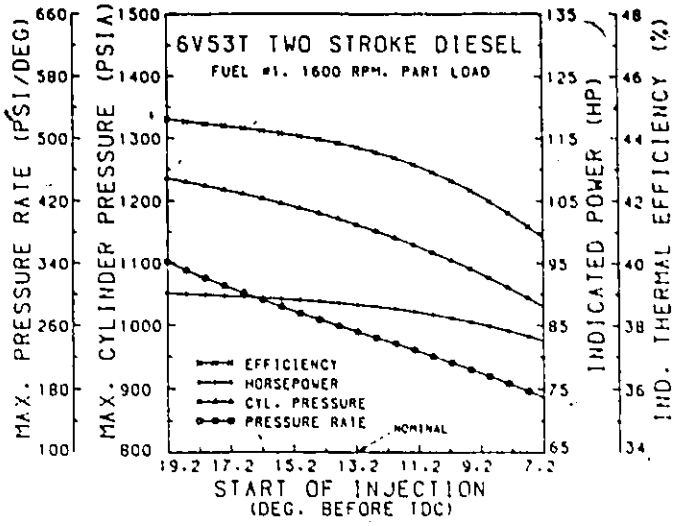

Fuel 1

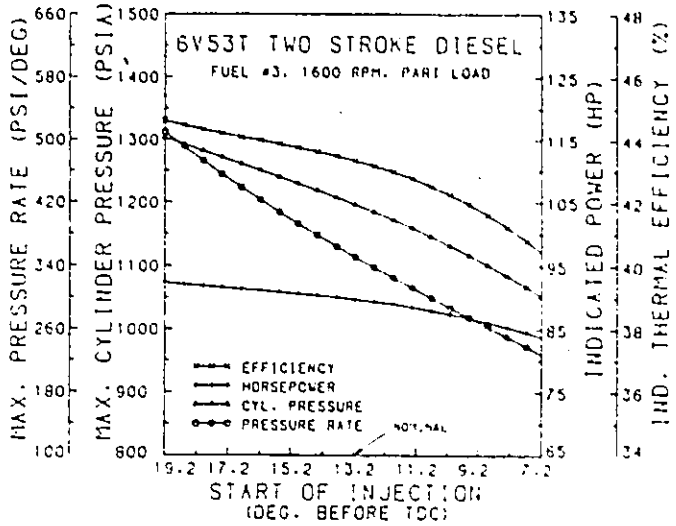

Fuel 3

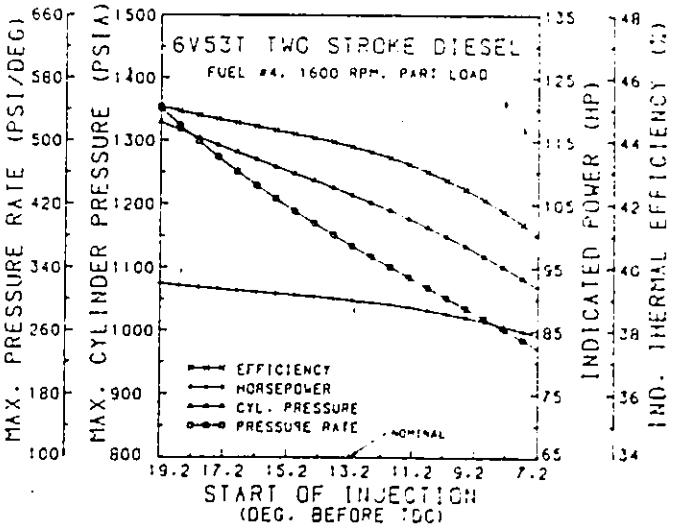

Fuel 4

Fig. 12.2: Effect of Injection Timing on Engine Performance and Combustion Parameters

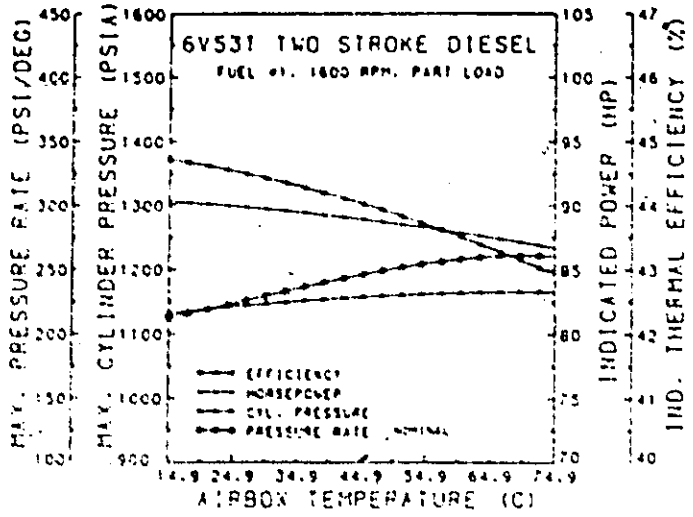

Fuel 1

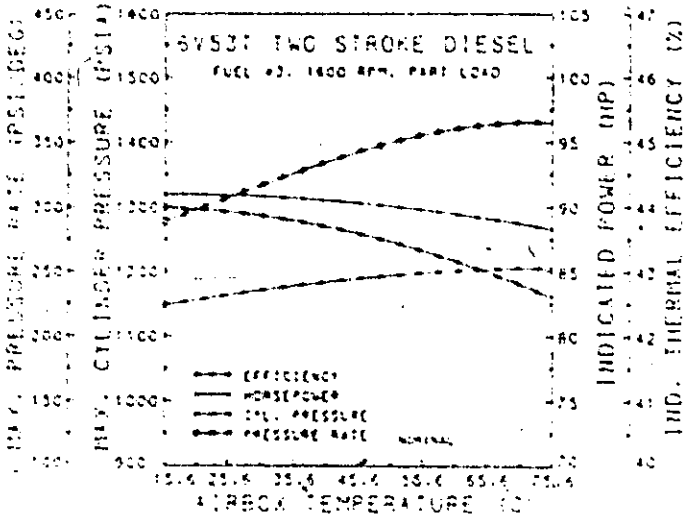

Fuel 3

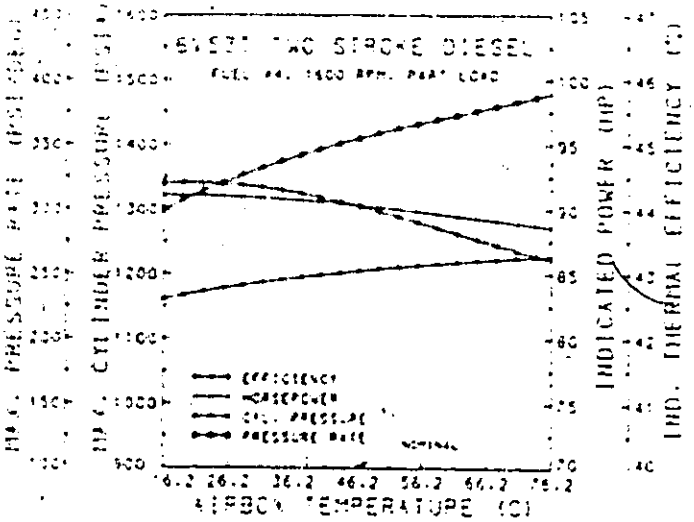

Fuel 4

Fig. 12.3: Effect of Airbox Temperature on Engine Performance and Combustion Parameters

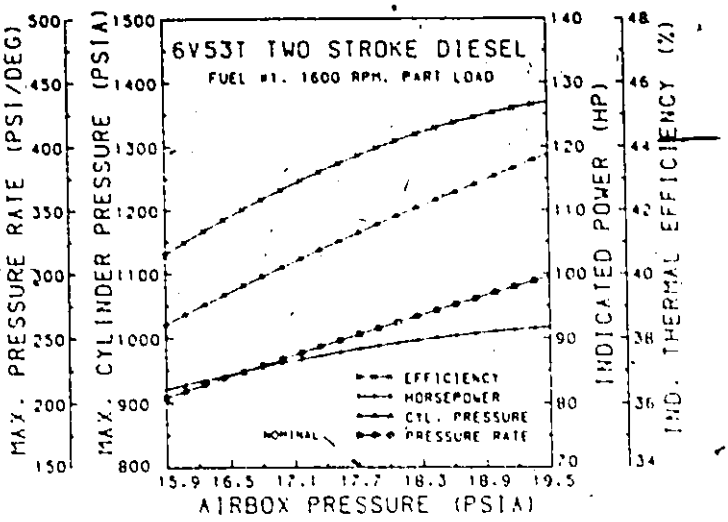

Fuel 1

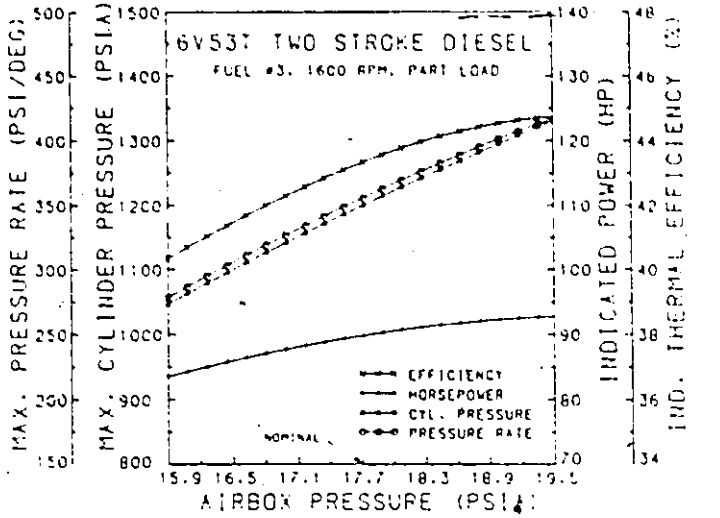

Fuel 3

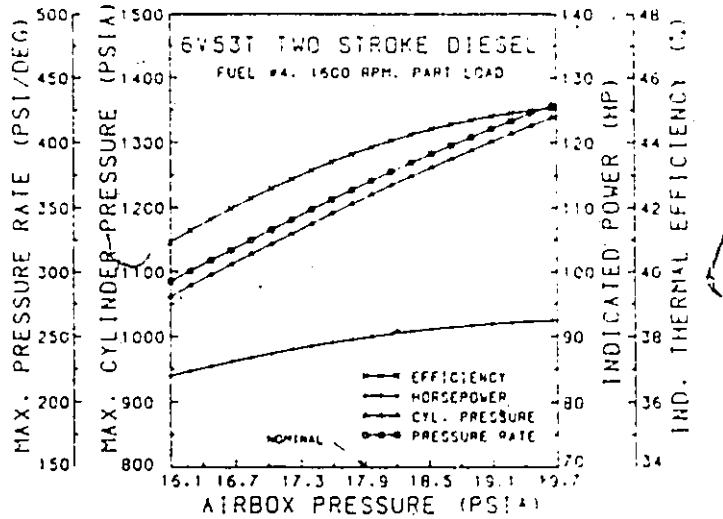

Fuel 4

Fig. 12.4: Effect of Airbox Pressure on Engine Performance and Combustion Parameters

12.3 ANALYSIS WITH STAGED INJECTION

12.3.1 OVERVIEW

Combustion knock and high pressure rates, as interpreted by the model, are a direct result of the chemical reaction rate and mass of the accumulated fuel/air mixture in the cylinder at the start of combustion. These, in turn, are a function of a number of parameters, significant among which are gas temperature, fuel quality and the rate of fuel injection. Logically, the most direct way to control the mass of accumulated fuel is to control the rate of fuel injection. In practice, fuel injection rate control is difficult to achieve; however, multiple or staged injection can provide rate control together with easier implementation.

In this study, a two stage injection profile (pilot plus main) is evaluated. The objective is to optimize the timing, fuel masses and rates of the profile so as to achieve acceptable pressure rates with Fuels 3 & 4 without loss of engine efficiency or rated engine performance. As before, the 1600 RPM, 200 ft.lbs. brake torque test point is used for pressure rate evaluation while 2800 RPM, full torque is used to evaluate engine rated power. All parameters at the test points are held identical to the standard equipment test, including the total mass of fuel injected, the only variable being the injection rate profile itself.

12.3.2 PROFILE EVALUATION

Figure 12.5 shows a typical two-stage injection profile. For the analytical study, a computer subroutine was used to vary the profile while maintaining the total mass of fuel injected. The variables are:

a) start point of pilot injection,

b) duration and rate of the pilot injection,

c) start point of main injection, and

d) the maximum rate of main injection.

Further, during main injection the increase in rate was set at 1.6 $mm^3/°CA$.

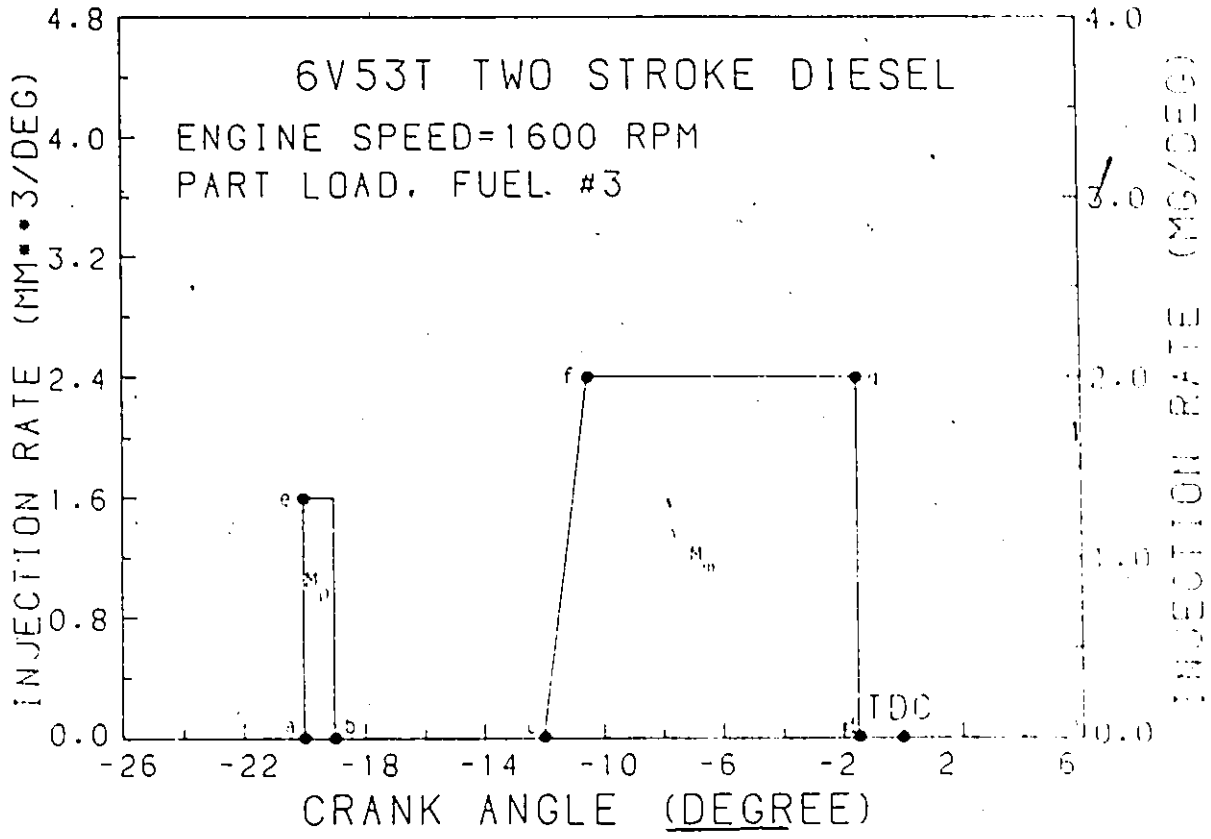

Fig. 12.5: Typical Two Stage Injection Profile

At 1600 RPM, Part Load.

Figures 12.6, 12.7 and 12.8 are typical and show the effect of pilot injection timing, main injection timing and mass of fuel in the pilot on the engine performance and combustion parameters. These plots are based on the profile shown in Fig. 12.5 where, for Figure 12.6 only pilot timing is varied, for Figure 12.7 only main injection timing is varied and for Figure 12.8 – only profile durations are varied. From the plots, it is clear that two stage injection can reduce pressure rates to very low values but not without an attendant loss in engine power or thermal efficiency.

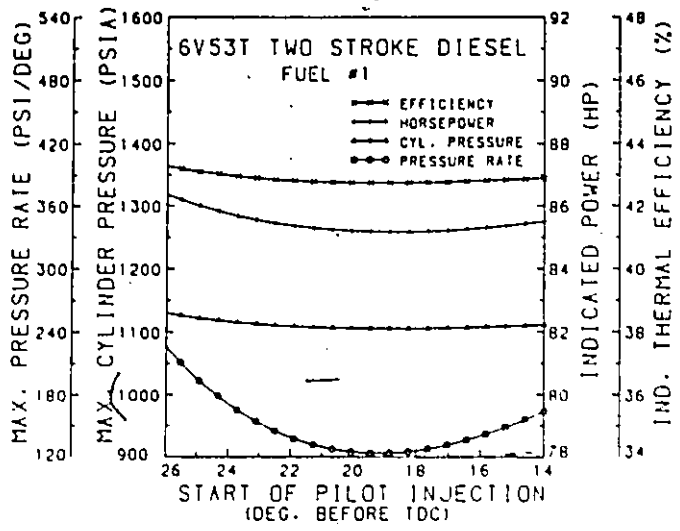

(a) Fuel 1

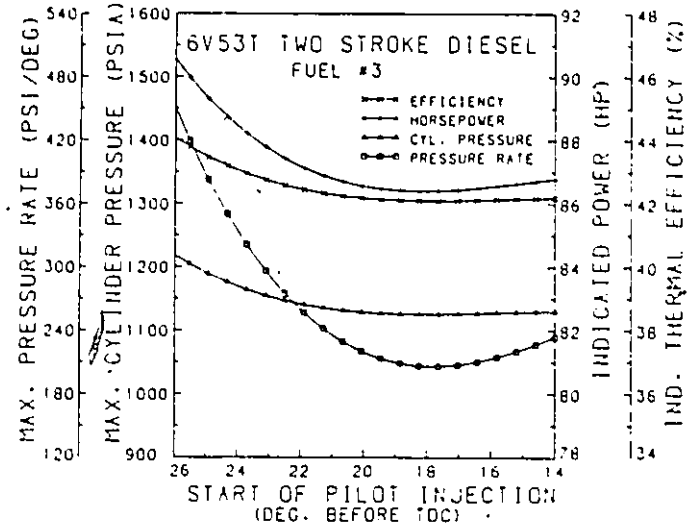

(b) Fuel 3

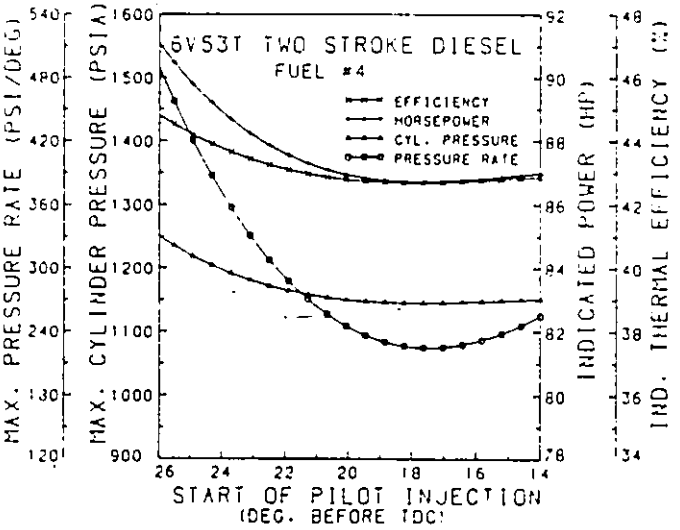

(c) Fuel 4

Fig. 12.6: Effect of Pilot Injection Timing on Engine Parameters

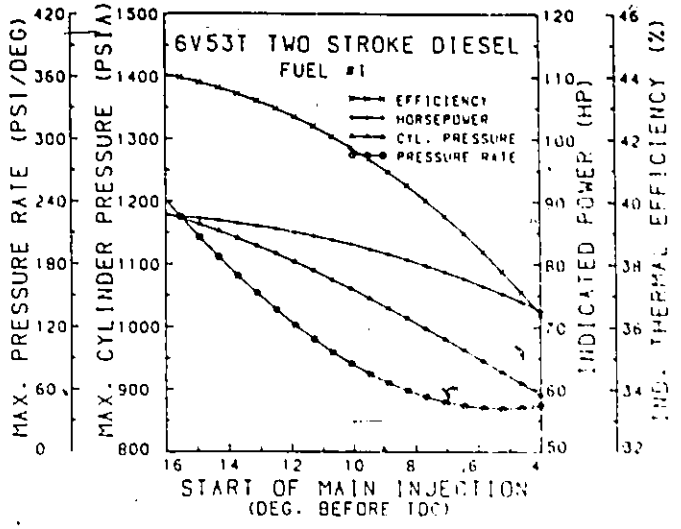

(a) Fuel 1

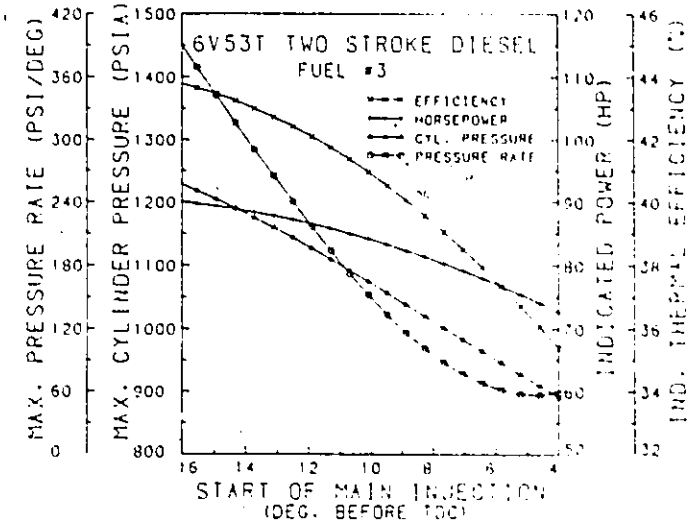

(b) Fuel 3

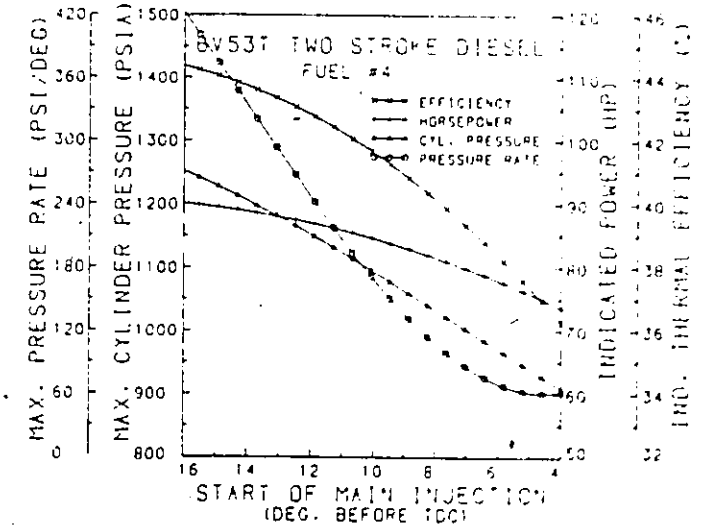

(c) Fuel 4

Fig. 12.7: Effect of Main Injection Timing on Engine Parameters

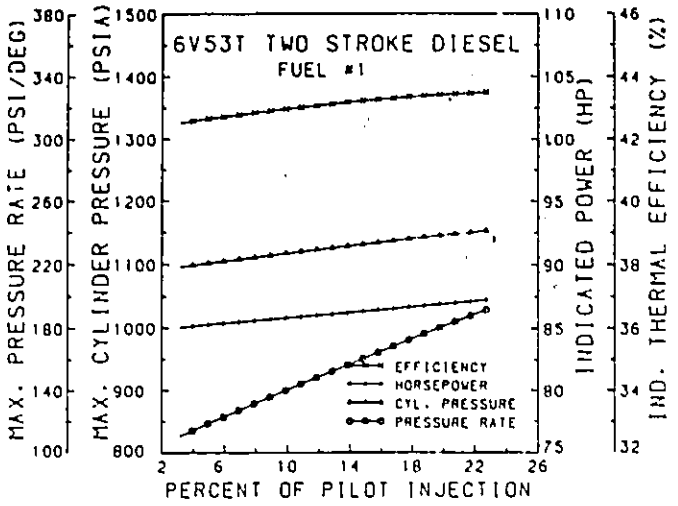

(a) Fuel 1

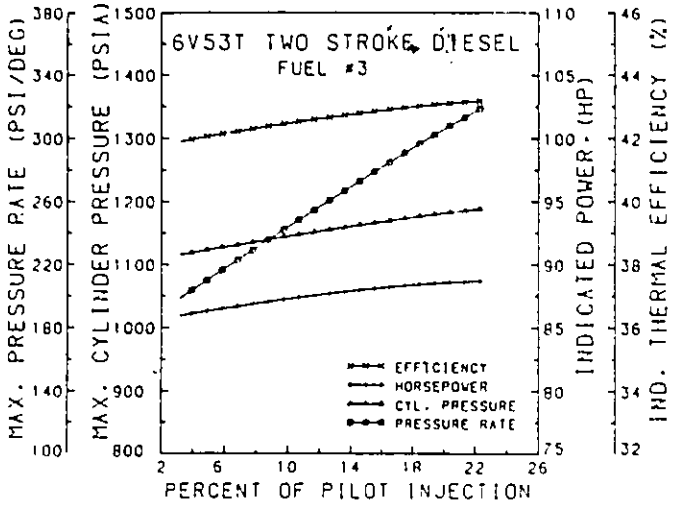

(b) Fuel 3

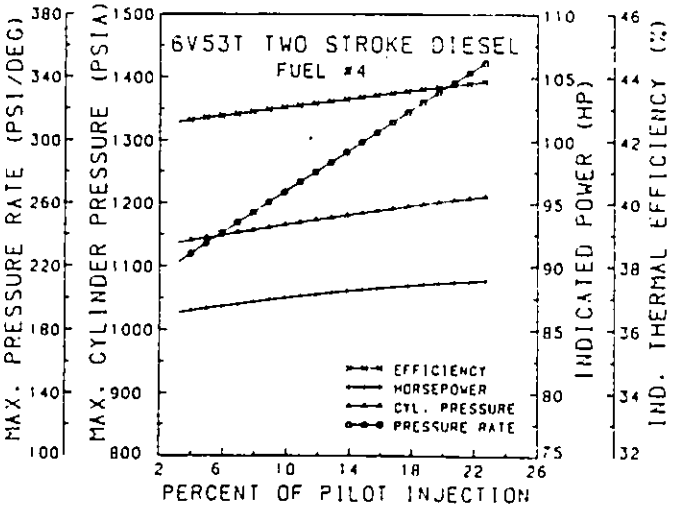

(c) Fuel 4

Fig. 12.8: Effect of Fuel Mass in the Pilot on Engine Parameters

Thus, it is desirable not to reduce pressure rates below that associated with Fuel 1. From all data, the profile selected is as follows:

i) Start of Pilot Injection — $20°CA$ bTDC

ii) Duration of Pilot Injection — $1°CA$

iii) Rate of Pilot Injection — $1.6\ mm^3/°CA$

iv) Start of Main Injection — $12°CA$ bTDC

v) Rate of Main Injection — $2.4\ mm^3/°CA$ (similar to the mechanical injector)

This profile reduces the pressure rate of Fuel 3 to slightly lower than that of Fuel 1 (standard equipment). Further, the study was repeated with Fuel 4 without any significant variations in results.

12.4 EFFECT ON ENGINE PERFORMANCE

12.4.1 INJECTION PROFILE AT RATED POWER

To evaluate the effect two-stage injection may have on engine rated power, the above study was repeated, for all three fuels, at 2800 RPM, full load. Figure 12.9 gives the injection profile while Figures 12.10, 12.11 and 12.12 show the effect of pilot injection timing, main injection timing and pilot fuel mass on the engine parameters.

From Fig. 12.10, pilot injection timing has virtually no effect on engine power, thermal efficiency or maximum cylinder pressure at 2800 RPM, full load. Although pressure rates at this engine setting are low, smoother combustion does result at a pilot injection timing of about $22°CA$ bTDC. Main injection timing (Fig. 12.11) is established by maximum cylinder pressure; here, to hold pressures in the order of 1800 psia, main injection timing was selected at $14°CA$ bTDC. The mass of fuel in the pilot is not a critical parameter (Fig. 12.12). Thus, it was taken identical to that

established in the above pressure rate control study.

Comparing Figures 12.5 and 12.9 it is interesting to note, for these two extreme operating positions of the engine, that the pilot can be held constant. That is, its rate and duration (i.e. pilot fuel mass) and its relative location to main injection timing remain unchanged. Alternatively, since the pilot timing was not critical at 2800 RPM, pilot timing could be held constant at 20°CA bTDC. This should simplify the design of a dual injection system. Also, main injection timing has changed very little (2°CA earlier at 2800 RPM).

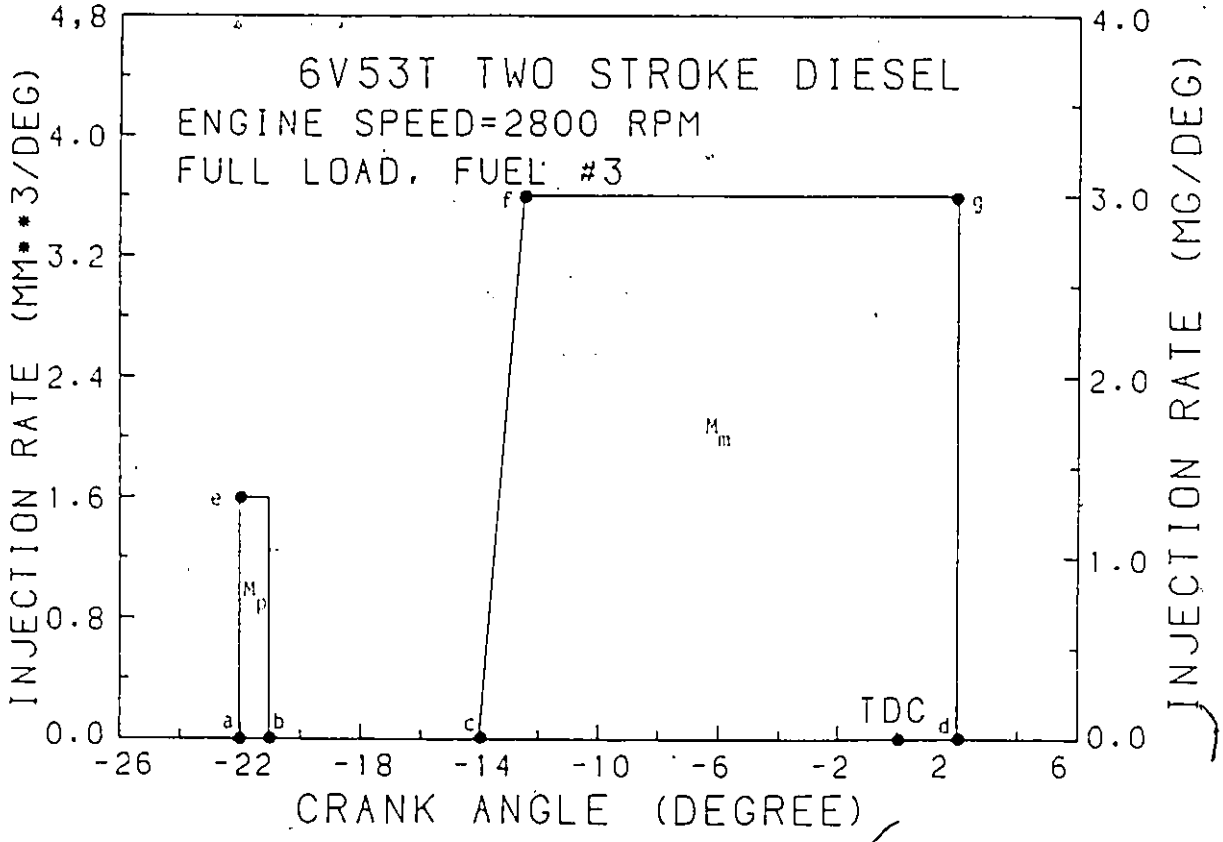

Fig. 12.9: Typical Two Stage Injection Profile
At 2800 RPM, Full Load.

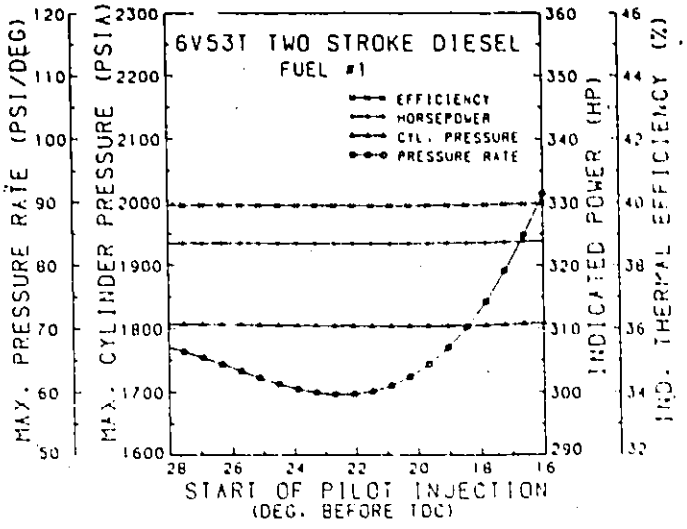

(a) Fuel 1

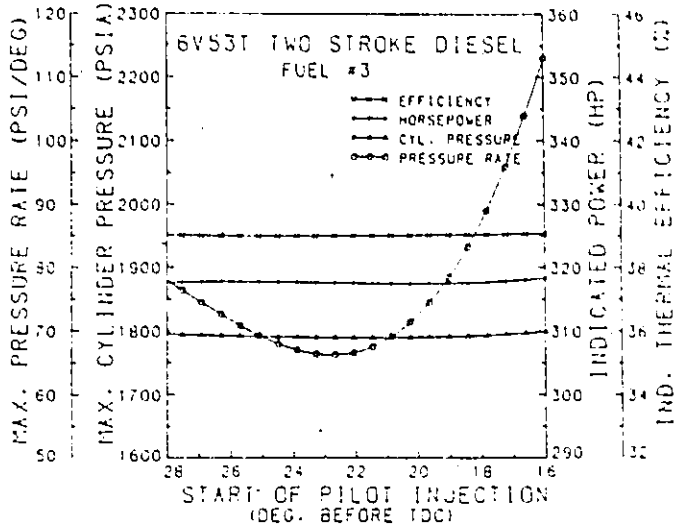

(b) Fuel 3

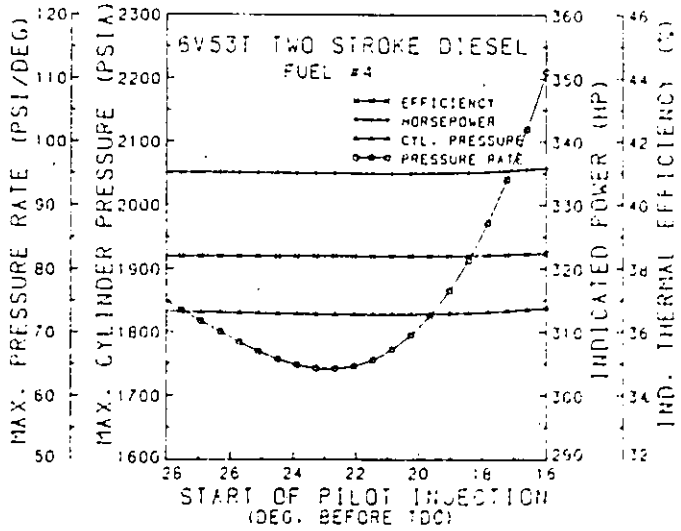

(c) Fuel 4

Fig. 12.10: Effect of Pilot Injection Timing on the Engine Parameters, 2800 RPM

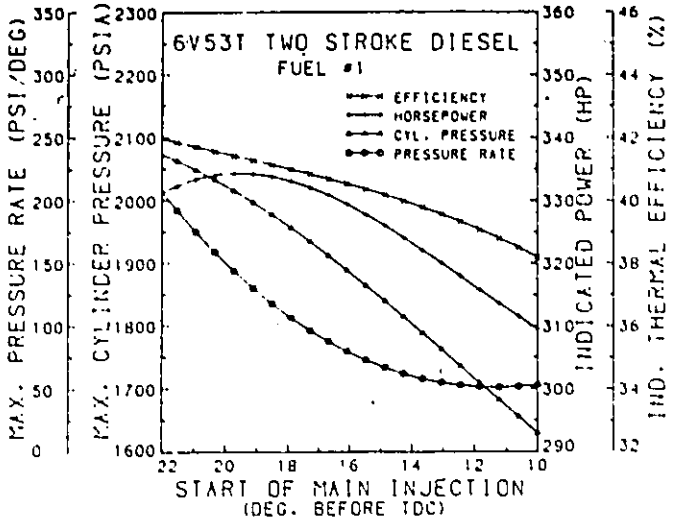

(a) Fuel 1

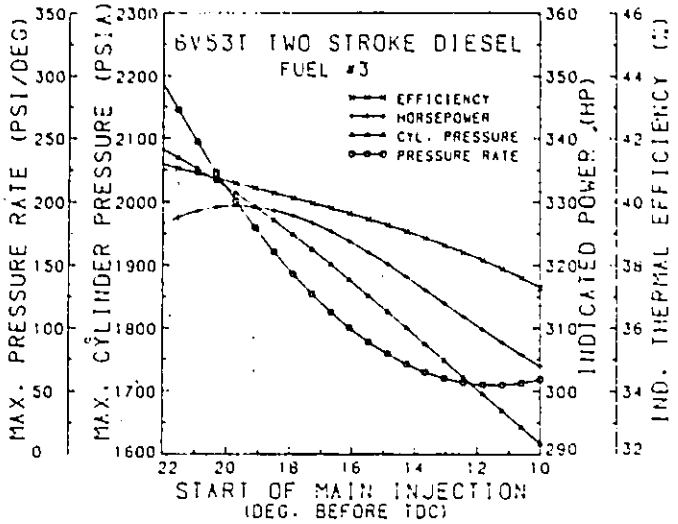

(b) Fuel 3

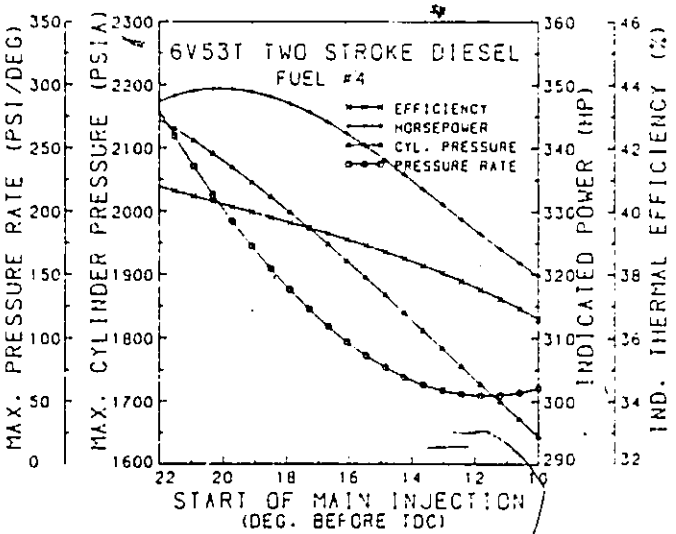

(c) Fuel 4

Fig. 12.11: Effect of Main Injection Timing on the Engine Parameters, 2800 RPM

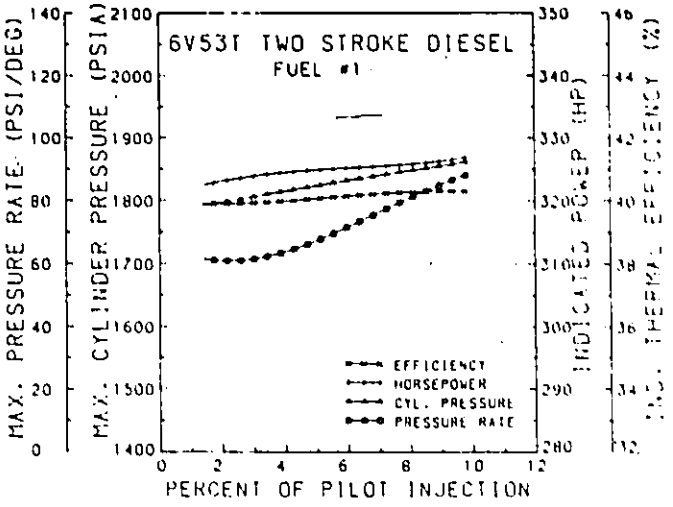

(a) Fuel 1

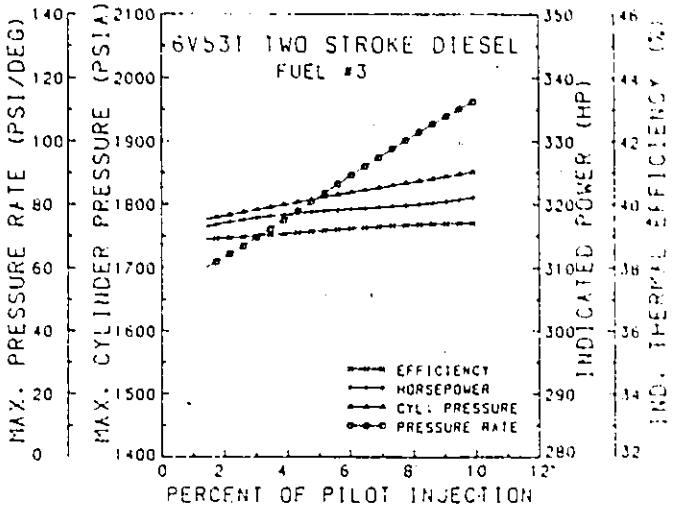

(b) Fuel 3

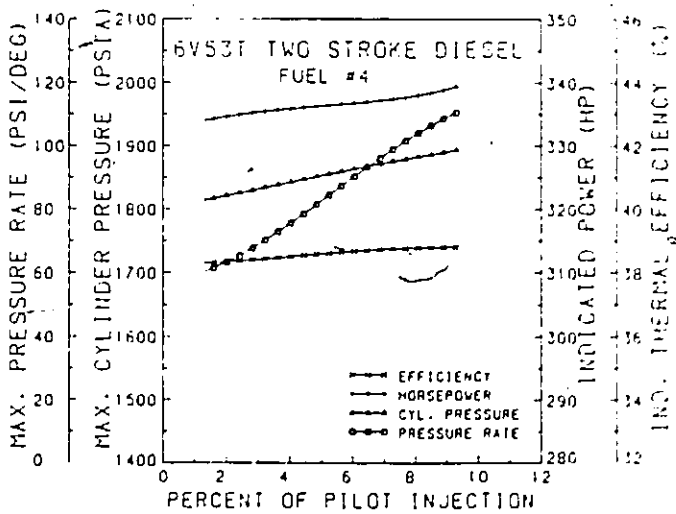

(c) Fuel 4

Fig. 12.12: Effect of Fuel Mass in the Pilot on Engine Parameters

12.4.2 PERFORMANCE COMPARISON

Using the fuel injection profiles determined for 1600 RPM, 200 ft.lb. torque and for 2800 RPM, full load, the thermodynamic and combustion model was used to simulate the 6V53T engine performance and combustion characteristics with the three fuels. These two particular engine operating points, as stated above, are the two extremes for combustion knock and engine performance respectively. To numerically examine the engine- fuel interaction, the cylinder gas thermodynamic state (maximum pressure rate and maximum pressure) and the engine output performance (indicated horsepower and thermal efficiency) were generated from both fuel injection profiles, namely, the proposed dual injection profile and the standard GM injection profile. The results are presented in Table 12.1.

From the tabulated data, it appears that the dual injection system devised can reduce the pressure rates for the low cetane Fuels 3 & 4 to within that measured with Fuel 1 (standard injection system). Further, the dual injection system should retain rated engine power without any significant increases in maximum cylinder pressures.

TABLE 12-1

PREDICTION AND COMPARISON OF COMBUSTION KNOCK AND ENGINE PERFORMANCE FROM PROPOSED AND STANDARD FUEL INJECTION SYSTEMS

OPER. CONDIT.	FUEL	MAX. PRES. RATE psi/°CA			MAX. CYL. PRESSURE psia			INDICATED POWER HP			IND. THER. EFFICIENCY %		
		S	P	%	S	P	%	S	P	%	S	P	%
1600 RPM 200 ft-lb	1	254.6	124.7	-51.0	1163.0	1106.2	-4.9	88.3	85.2	-3.5	43.7	42.8	-2.1
	3	355.1	220.0	-38.0	1198.5	1129.9	-5.7	89.8	86.6	-3.6	43.3	42.2	-2.3
	4	367.4	245.8	-33.1	1214.8	1151.9	-5.2	89.8	87.0	-3.1	43.8	42.8	-2.3
2800 RPM, FULL LOAD	1	82.0	62.0	-24.4	1754.9	1804.5	+2.8	320.6	323.5	+1.0	39.3	39.9	+1.5
	3	102.7	67.4	-34.4	1742.5	1789.6	+2.7	314.6	317.5	+1.0	38.4	39.0	+1.6
	4	107.1	65.8	-38.6	1807.3	1828.2	+1.2	333.7	335.0	+0.4	38.0	38.4	+1.1

S - Standard injection system by GM.

P - Proposed pilot injection system.

% - Relative variation of pilot injection results to that of standard injection in percentage.

CHAPTER 13

CONCLUSIONS

The Part II of this thesis focused on the analytical investigation of the 6V53T engine burning off-specification low cetane fuels using the simulation model developed in Part I. As such, the results should be seen not as absolute truths, although accuracy of the simulation was shown in Chapter 7, but rather as a direction and focus for experimental investigation.

The engine/fuel interaction studies provided considerable insight into the behavior of the off-specification fuels. Interpreting engine/fuel behavior and in particular ignition delay and combustion in general provided a foundation for the performance and pressure rate analyses that followed. From these analyses, the salient conclusions reached are as follows:

1. Heating the intake air in the high pressure rate region (i.e. low speed, low load) does not produce the desired effect of improving combustion and hence reducing pressure rates. Indeed, from the simulation program, the integrated effect of trapped air mass, ignition delay, fuel-air mixing rate and reaction rate resulting from heating intake air leaves pressure rates and maximum cylinder pressures largely unchanged. Hence, it is recommended that this planned experimental program not be executed.

2. Tuned injection timing was seen to be more effective than increasing compression ratio or turbo-boost for improving engine performance. However, intercooling was seen as the single most promising parameter for improved engine performance. Moderately significant gains (est. at 12 IHP) can be had without significant increases in maximum cylinder pressures. Also, intercooling was seen to provide positive benefits in the high pressure rate engine operating region. Further, intercooling combined with increased fuel injection was seen to be very attractive

providing possible increases in the order of 40–55 IHP with cylinder pressures in the order of 1840–1860 psia. This could be readily accomplished with an electronic injector.

3. Of the standard engine variables, injection timing was seen to be the most attractive approach for controlling the high pressure rates associated with the off-specification low-cetane fuels. In this regard, it was projected that retarding injection timing to about 8°*CA* bTDC in the 1600 RPM, 200 ft.lbs. operating region would reduce the pressure rates of Fuels 3 & 4 to the level of Fuel 1. However, losses in engine performance and thermal efficiency also result. Implementing this approach with electronic injection and a combustion knock sensor would minimize losses in the high pressure rate region and should result in gains outside this region. Also, it would considerably improve the multi-fuel capability of the engine.

4. Dual injection was seen to offer the best solution to burning the off-specification fuels. It was projected that pressure rates could be reduced to equal or better than that of high quality fuel (Fuel 1) without any significant losses in thermal efficiency. Further, engine performance and rated engine power should not suffer and indeed may increase slightly. Also, the optimized dual injection profile established allows for easy implementation in that the "pilot" remains fixed relative to "main" injection.

Based on this analysis, it is recommended that the experimental program focus on injection timing, dual injection and intercooling.

BIBLIOGRAPHY

1. Personal discussions with Dr. R.B. Whyte, Director, NRC-Fuels and Lubricants Laboratory, Ottawa, Canada.

2. Obert, E.F., "Internal Combustion Engines and Air Pollution", Third Edition 1973.

3. Wark, K., "Thermodynamics", Third Edition 1977.

4. Eastop, T.D. and McConkey, A., "Applied Thermodynamics", Third Edition,1978.

5. Benson, R.S. and Whitehouse N.D., "Internal Combustion Engines", Pergamon Press 1979.

6. Nusselt, W., "Die Warmeubergang in den Gasmaschinen", ZVDI 361, 414, 459 (1914).

7. Nusselt, W., "Die Warmeubergang in den Verbrennungs-kraftmaschinen", ZVDI 67, 692 (1923).

8. Eichelberg, G., "Temperaturverlauf und Warmespannung in Verbrennungs-motoren", Forsch. Ing. Wes. 263 (1923).

9. Eichelberg, G., "Some New Investigations on old Combustion Engine Problems", Engineering 149, 463, 547 (1939).

10. Oguri, T., "On the Coefficients of Heat Transfer Between Gases and Cylinder Walls of the Spark Ignition Engine", Bull, Jap. Soc. Mech. Engrs. 2, 384 (1959).

11. Pflaum, W., "Heat Transfer in Internal Combustion Engines", La Termotecnica N4 (April), Italy, (1963).

12. Annand, W.J.D., "Heat Transfer in the Cylinders of Reciprocating Internal Combustion Engines", Proc. Instn. Mech. Engrs. 177, 973 (1963).

13. Woschni, G., "A Universally Applicable Equation for Instantaneous Heat Transfer

in the Internal Combustion Engine", SAE Paper 670931 (1967).

14. Wolfer, H.H.; "Ignition Lag in the Diesel Engine", VDI–Forschungsheft No. 392, 1938, Trans. by Royal Aircraft Establishment, Farnborough Library No. 358, August 1959, U.D.C. No: 621-436.047.

15. Rogener, H.; "Entzundung von Kohlenwasserstoff- Luft-Gemischen durch Adiabatische Verdichtung", Zeitschrift fur Elecktro-chemie, Vol. 53, No. 6 (1949), PP. 389-397.

16. Sitkei, G.; "Uber den dieselmotorischen Zundverzug (On the Ignition Delay in Diesel Engines)" MTZ, Vol. 24, No. 6 (1963), p. 190.

17. Henein, N.A. and Bolt, J.A.; "Ignition Delay in Diesel Engines", SAE Paper 670007.

18. Henein, N.A. and Bolt, J.A.; "Correlation of Air Charge Temperature and Ignition Delay for Several Fuels in a Diesel Engine", SAE Paper 690252.

19. Faeth, G.M. and Olson, D.R.; "The Ignition of Hydrocarbon Fuel Droplets in Air", SAE Paper 680465.

20. Hardenberg, H.O. and Hase, F.W.; "An Empirical Formula for Computing the Pressure Rise Delay of a Fuel From Its Cetane Number and From the Relevant Parameters of Direct -Injection Diesel Engines", SAE Paper 790493.

21. Pedersen, P.S., and Qvale, B.; "A Model for the Physical Part of the Ignition Delay in a Diesel Engine", SAE Paper 740716.

22. Schweitzer, P., " The Tangent Method Analysis of Indicator Cards of Internal Combustion Engines", Bulletin No. 35. Pennsylvania,State Univ., September 1926.

23. Obert, E.F., "Internal Combustion Engines", International Textbook Co. Scranton, Pennsylvania, PP. 610-612, 1968.

24. Amann, C.A., "Classical Combustion Diagnostics for Engine Research", SAE Paper 850395.

25. Foster, D.E., "An Overview of Zero-Dimensional Thermodynamic Models for IC Engine Data Analysis" SAE Paper 852070.

26. Blumberg, P.N., "The Applicability of Combustion Modeling and Diagnostics- Observations, Issues and Outlook",SAE Paper 850397.

27. Austen, A.E.W. and Lyn, W.T.; "Relation Between Fuel Injection and Heat Release in a Direct-Injection Engine and the Nature of the Combustion Processes", Proc. 1. Mech. E.(A.D.), No. 1, pp.47-62,1960-61.

28. Krieger, R.B. and Borman, G.L., "The Computation of Apparent Heat Release for Internal Combustion Engines", ASME Paper No. 66-WA/DGP-4, 1966.

29. Gupta, C.P. and Sharma, C.P., "Computer Calculation of Heat Release Rata in a Diesel Engine From Experimental Pressure- Time Diagram".IE (I) Journal-ME, Vol. 57, January, 1977.

30. Austen, A.E.W. and Lyn, W.T., "The Application of Heat Release Analysis to Engine Combustion Study", 1067, CIMAC (1962).

31. Whitehouse, N.D. and Way, R.J.B., "Rata of Heat Release in Diesel Engines and its Correlation with Fuel Injection Data", Proc. Instn. Mech. Engrs. 184, Part 3J, 17 (1969-70).

32. Whitehouse,N.D.and Way,R.J.B.,"A Simple Method for the Calculation of Heat Release Rates in Diesel Engines Based on the Fuel Injection Rate",SAE Paper 710134(1971).

33. Whitehouse,N.D.and Sareen,B.K.,"Prediction of Heat Release in a Quiescent Chamber Diesel Allowing for Fuel Air Mixing", SAE Paper 740084 (1974).

34. Whitehouse, N.D. and Abughres, S.M., "Calculation for Fuel/Air Mixing in a Diesel Engine With Swirl for the Purpose of Heat Release Prediction", in Combustion in Engines, PP. 147, Inst. of Mech. Eng. London and New York, 1975.

35. Shahed, S.M., Chiu, W.S. and Lyn, W.T., "A Mathematical Model of Diesel Combustion, in Combustion in Engines", p. 119, Institution of Mechanical Engineers, 1975.

36. Hodgetts,D.and Shroff,H.D.,"More on the Formation of Nitric Oxide in a Diesel Engine in Combustion in Engines",Institution of Mechanical Engineers,1975.

37. Bedran, E.C. and Beretta, G.P.; "General Thermodynamic Analysis for Engine Combustion Modeling", SAE Paper 850205.

38. Amsden, A.A., Butler, T.D., O'Rourke, P.J. and Ramshaw, J.D., "KIVD-A Comprehensive Model for 2-D and 3-D Engine Simulations", Paper 850554.

39. General Motors, DDA Division; Personal Discussions and Data Exchange With R.C. Flanagan. April 21, 1981.

40. Webster, G.D., Chiappetta, S.J. and Ho, J.; "Tar Sands Derived Fuels Tested in an Air Cooled High Speed Diesel", SAE Paper 831206.

41. Steiger, A. and Aue, G.K.; "The Influence of the Thermal Loading Criterion on the Design of Turbocharged Two-Stroke Diesel Engines", Proc. Instn. Mech. Engrs. 179, Par 3C, 68(1964-5).

42. General Mortors, DDA Division; Personal Data Exchange, March, 1985.

43. Kanury, A.M.; "Introduction to Combustion Phenomena", Second Printing, May 1977, Gordon and Breach, New York.

44. Dixon, L.C.W.; "Nonlinear Optimization", Crane, Russak and Company, Inc. 1972.

45. Flanagan, R.C., and Menard, L.; "Effects of Fuel Quality on the Performance of a High Speed Diesel Engine: Brake and Indicated Characteristics", SAE p-155, pp. 89-102, March 1985, presented at the ATD-CCM Meeting, Detroit.

46. Menard, L. and Flanagan, R.C.; "Effects of Fuel Quality on the Performance of a High Speed Diesel Engine: Combustion Parameter Characteristics", SAE p-155, pp. 103-117, March 1985, presented at the ATD-CCM Meeting, Detroit.

47. Flanagan, R.C. and Menard, L.; "Combustion Characteristics of Tar Sands Derived Fuels in a Two-Strok Turbocharged Diesel", Proceedings: Future Diesel Fuels, Their Analysis and Correlations with Engine Performance and Combustion, Ottawa, Canada, Oct. 1984, 22 pp.

48. Flanagan, R.C. and Menard, L.; "A Study of Wide Boiing Range Fuel-Engine Interaction: Engine Performence and Combustion Monitor Tests", Contract Report 2SU81-00088, Technical Report No. UOME-EP-8403-1, Department of National Defence, DREO, Ottawa, Canada, 1984, 199 pp.

49. Flanagan, R.C., Salcudean, M., Xia, Y.Q. and Carapanayotis, A.; "A Study of Wide Boiling Range Fuel-Engine Interaction: Thermodynamic and Multidimensional Modeling", Contract Report 2SU82-000396, Technical Report No. UOME-EP-8404-1, Department of National Defence, DREO, Ottawa, Canada, 1984, 195 pp.

50. Flanagan, R.C. and Xia, Y.Q.; "Development and Evaluation of a Diesel Engine Thermodynamic Model", Proceedings, IASTED Int. Conf. ASM '86, Vancouver, Canada, June 1986.

51. Flanagan, R.C., Carapanayotis, A. and Xia, Y.Q; "Thermodynamic Simulation of a Two-Stroke Direct Injected Turbocharged Diesel", Proceedings, IASTED International Conference: Applied Simulation and Modeling, Montreal, Canada, June, 5 pp.

52. Flanagan, R. C., Xia, Y.Q., Menard, L. and Carapanayotis, A.; "Indicated Performance Comparisons Between Thermodynamic Model Predictions and Experimental Measurement on a Two-Stroke Turbocharged Diesel", Proceedings IASTED International Confrence: Applied Simulation and Modeling, Montreal, Canada, June 1985, 5 pp.

53. Xia, Y.Q. and Flanagan, R.C., "Ignition Delay – A General Engine/Fuel Model", 1987 SAE International Congress & Exposition, Detroit. SAE paper, 870591.

54. Westbook, C.K. and Dryer, F.l., "Simplified Reaction Mechanisms For The Oxidation Of Hydrocarbon Fuels In Flames", Combustion Science And Technology, 1981, Vol. 27, pp.34-43.

APPENDIX A

LITERATURE SURVEY OF IGNITION DELAY MODELS

A number of papers have been published on ignition delay in compression ignition engines. The following is a list of the models investigated .

1) Model of Wolfer [14] :

$$\text{Delay} = 6N \times 10^{-3}\left\{0.44\exp(\tfrac{4650}{T})/P^{1.19}\right\} \ , \qquad (^{\circ}CA)$$

T — Temperature at start of injection (K)

P — Pressure at start of injection (atm)

N — Engine speed (RPM)

2) Model of Rogener [15] :

$$\text{Delay} = 6N \times 10^{-3}\{8.1 \times 10^{-9}\exp(15100/T)/P^{0.66} + 0.5 \times 10^{3}\exp(-1400/T)/P^{1.82}\} \ , \qquad (^{\circ}CA)$$

T — Temperature at start of injection (K)

P — Pressure at start of injection (atm)

N — Engine speed (RPM)

3) Model of Sitkei [16] :

$$\text{Delay} = 6N \times 10^{-3}\{0.5 + 0.135\exp(\tfrac{7800}{RT})\cdot P^{-0.7} + 4.8\exp(\tfrac{7800}{RT})P^{-1.8}\} \ , \qquad (^{\circ}CA)$$

T — Temperature at start of injection (K)

P — Pressure at start of injection (atm)

N — Engine speed (RPM)

R — Universal gas constant ($R = 8.314 \ \ Kj/Kg - mole\ ^{\circ}K$)

4) Model of Henein and Bolt [17] :

$$\text{Delay} = 6N \times 10^{-3}\{C/P^n\} \ , \qquad (^\circ CA)$$

P — Pressure at start of injection (psia)

N — Engine speed (RPM)

n — 0.271 when $C = 8.85$ for West engine

n — 0.411 when $C = 32.4$ for Tsao engine

5) Model of Faeth and Olson [19] :

$$\text{Delay} = 6N \times 10^{-15}\{0.916P^{-2.57}\phi^{-1.04}\exp(\tfrac{58320}{T})\} \ , \qquad (^\circ CA)$$

T — Temperature at start of injection (R)

P — Pressure at start of injection (atm)

N — Engine speed (RPM)

ϕ — Equivalence ratio

6) Model of Hardenberg and Hase [20] :

$$\text{Delay} = (0.36 + 0.22MPS) \cdot \exp\left\{E_A(\tfrac{1}{R \cdot T_m \cdot CR^{c-1}} - \tfrac{1}{17190}) + (\tfrac{21.2}{P_m \cdot CR^c - 12.4})^{0.63}\right\} \ , \qquad (^\circ CA)$$

E_A — $\frac{618840}{CN+25}$ (J/mole)

MPS — Mean piston speed (m/s)

T_m — Absolute temperature in intake manifold (K)

P_m — Absolute pressure in intake manifold (bar)

CR — Compression ratio

R — Universal gas constant ($R = 8314 J/mole\ ^\circ K$)

c — Polytropic exponent of compression

7) Model of Pederson and Qvale [21] :

$$\text{Delay} = 0.00642 \cdot \exp\left[\frac{3.53 \cdot T_{A,ref}}{T_A}\right] \cdot \left[\frac{0.22 \cdot P_A}{P_{A,ref}} + 0.78\right] \cdot \left[\frac{d}{d_{ref}}\right]^{1.77} \cdot \left[1.74 - \frac{0.74 \cdot T_F}{T_{F,ref}}\right] \cdot \left[\frac{W}{W_{ref}}\right]^{-0.17}$$

Delay	—	Physical ignition delay (ms)
T_A	—	Air temperature (K)
P_A	—	Air pressure (abs. atm)
T_F	—	Fuel droplet initial temprature (K)
W	—	Droplet initial velocity (m/s)
d	—	Droplet diameter (μm)
$T_{A,ref}$	—	823 K
$P_{A,ref}$	—	34 abs. atm
d_{ref}	—	25 μm
W_{ref}	—	200 m/s
$T_{F,ref}$	—	293 K